Physical Aging in Strongly Interacting Blends

Abdelsallam Ebrahim Abdelsallam Youssef

A Thesis submitted for the degree of Doctor of Philosophy

Heriot-Watt University

<School of Engineering & Physical Sciences /Institute of Chemical Sciences>

<July> <2013>

ABSTRACT

Physical aging is the general term used to describe changes in the properties of glassy materials as a function of storage time, at a temperature below the glass transition, T_g. Extensive studies have been carried out on homopolymers and copolymers but fewer investigations have dealt with aging in polymer blends. This Thesis reports a detailed study of physical aging in polymer-polymer mixtures where strong intermolecular interactions are active between components.

Miscible blends incorporating poly(4-hydroxystyrene) (P4HS) or styrene-co-4-hydroxystyrene (SHS) and poly(ethyl methacrylate) , poly(ethylene oxide) , poly(4-vinylpyridine) and poly(methyl methacrylate) were prepared. Fourier transform infrared spectroscopy was used to extract qualitative and quantitative information on the strength and number of hydrogen bonds. The effect of temperature and dilution of the hydrogen bonding sites is discussed and a comparison made between different systems.

Enthalpic relaxation data for a series of homopolymers and copolymers, including poly(methyl methacrylate-co-ethyl methacrylate), and blends incorporating P4HS and SHS were collected and analysed using Cowie-Ferguson relaxation model. It is found that the enthalpic relaxation for all P4HS and SHS blends increases upon increasing hydrogen bonding strength between the components. The relaxation rate also increases with increasing strength of interaction as well as chain rigidity.

Average activation energies were calculated of all homopolymers, copolymers and blends under study. This parameter is shown to be correlated to polymer structure and polymer-polymer interactions and it is therefore useful to compare the aging behaviour of different systems.

Table of Contents

Chapter 1 Introduction

1.1 Physical aging of polymer blends

1.1.1 Definition of physical aging

Physical aging is the term used to describe the observed changes in properties of glassy materials as a function of storage time at a temperature below the T_g [1].

Cooling of an amorphous polymer from the melt to a temperature, T_a, below its glass transition leads to incomplete relaxation of the polymer chains, i.e. the polymer chains do not relax to their lowest energy configuration [2]. Instead, a glass is formed that is not in equilibrium with its surrounding. The non-equilibrium glass state has an excess of volume, enthalpy and entropy and, as a result of annealing at a temperature below its T_g (i.e. T_a), it will lose these excess quantities in an attempt to achieve its thermodynamic equilibrium state. *"This it can do through a variety of localised molecular relaxation processes, which collectively are called physical aging"* [1, 2].

Physical aging should not be confused with other non-reversible aging processes such as chemical aging (thermal degradation, photo-oxidation etc.). When a glassy material is heated above the T_g, any previous physical aging that has occurred will be erased. This behaviour is in contrast to chemical or biological aging, where the changes in properties of the material are accompanied by irreversible changes in structure involving permanent, chemical modification [3].

Now the question present itself why should one study physical aging?
The difficulty that arises when studying physical aging is that the enthalpy relaxation seems strictly limited by temperature: nothing relevant will appear at any temperature lower than 35 K below T_g, at least within a decade. Therefore, chemists and engineers regard physical aging as a matter of only academic interest, with little applicability. Certainly the same has been said of many other subjects in the past, and in the mass of these cases things have proved otherwise. In demonstration of this fact we may recall that atomic energy was once thought to be impossible to use, that copper oxide catalysts could not have industrial application and that liquid crystal polymers had pleasant colours and elegant properties but naught more. However, all these communal sense-based declarations have become misplaced with time and maybe the labelling of

physical aging as a purely academic problem will prove to be another case of scientific misjudgement.

Physical aging is the most important feature, as it occurs in every glass, irrespective of its polymeric, monomeric, organic or inorganic nature [4]. Therefore, physical aging is a general phenomenon of the glassy state, as the melting point is a phenomenon for the crystalline state, and consequently, it has to be taken into account. The range of temperature in which physical aging can be reasonably significant, the so-called aging range, has always been thought to be limited to a small interval below T_g; however, there is experimental evidence that the aging range is generally not restricted to such a narrow band, but falls between T_g and first secondary transitions, T_β [5]. It follows that a number of thermoplastic materials have an aging range which includes temperatures of practical interest. It is also worthy of note that very low temperature physical aging processes have been described [6], since the effects differ significantly from those observed during T_g annealing.

Polymers have been increasingly used in many fields, including high precision technology. One of the most important requirements for such applications is dimensional stability. Common factors affecting the dimensions of glassy thermoplastics are: (1) chemical degradation, (2) absorption of liquids, (3) the variation in temperature; all of these can obviously affect the dimensions of unfilled thermoplastics. As temperature is under control, volume expansions or contractions can be kept within tolerance limits. Only recently has physical aging been added to the list and it is now well proven that relaxation of glasses can modify their dimensions sufficiently to make the material unsuitable for the specific purpose it was intended for. Thus, knowledge of these variations with time is clearly necessary to define the length of time the shaped material can be used without a problem arising.

Physical aging is also relevant in other sectors. If a manufactured article has to be stored for a long period- say, in the order of years- at a constant temperature, the engineering designer should be aware of how the material properties may change during that time, under service conditions. This becomes quite important if the piece itself is not easily accessible for inspection or replacement. Metals and their alloys have very high time stability, but due to their unfavourable weight-performance ratio, they have been widely substituted by plastic-based materials, i.e. copolymers and composites.

Being in their glassy state, the mechanical response, e.g. creep and strength behaviour, of these polymer based materials varies with time. Therefore, long-term physical aging effects must be taken into account; otherwise, the product may fail, regardless of whether in the short term the item seems to be adequately designed.

The final result, that is the difference between the predicted and the real performance, depends on these data and on how accurate the theoretical model is. Hence, the entire process relies on the understanding of short-term phenomena, the development of a reliable theoretical interpretation for them and the use of such an approach to forecast long-term phenomena. Above all, time will reveal the success of the third step, and not only in the literal sense of the words.

1.1.2 Experimental measurements of physical aging

The most widely used methods to follow the aging relaxation process is by measuring the rate of evolution of thermodynamic properties such as enthalpy and volume, or the changes in the stress relaxation and creep compliance over time. Other methods that have been adopted to follow physical aging are spectroscopic and scattering methods. Here, we will describe in more detail the measurement of enthalpy relaxation. A comprehensive description of other methods has been given by Hutchinson [7].

1.1.2.1 Enthalpy relaxation

The availability of high precision calorimeters and the simplicity of the experimental procedure have meant that most investigations into physical aging have focused on enthalpy relaxation, with measurements carried out using differential scanning calorimetry (DSC). Hutchinson [7] points out that enthalpy relaxation *"compares unfavourably with volume relaxation"* because instead of being measured directly by DSC, enthalpy is obtained by integration of heat capacity, C_p, curves, and these are calculated from the DSC output signal. However, reliable and informative data can be obtained via enthalpy relaxation, with careful experimental procedure [8], enthalpy relaxation can yield data which are both reliable and informative.

The enthalpy relaxation process is shown schematically in Figure 1.1 (a). The amorphous polymer, on cooling through T_g , arrives at point A. Annealing at this aging temperature, T_a, for a given period of time (aging time, t_a), results in a loss of enthalpy. During annealing, the system moves to point B. Following this, the polymer is cooled to T_1 and heated immediately to T_2, at a constant rate, in the DSC instrument. The corresponding C_p curve obtained from the DSC trace is shown in Figure 1.1 (b): the characteristic C_p overshoot for an aged material can clearly be seen superimposed on the T_g step. Cooling the polymer to T_1, without annealing and heating back to T_2 yields the more familiar DSC trace, exhibiting the usual C_p step at T_g (Figure 1 (b)).

The enthalpy lost in aging is equivalent to the difference between the areas of these two C_p curves, or, in equation form,

$$\Delta H(T_a, t_a) = \int_{T_\alpha}^{T_\beta} \left[C_p(aged) - C_p(unaged)\right] dT \qquad (1.1)$$

where T_α and T_β are arbitrary integration limits.

One or two features of the enthalpy relaxation process are worthy of note. It can be seen that the enthalpy lost on annealing is not recovered gradually as the T_g is approached. In fact, there is virtually no recovery until the extrapolated liquid enthalpy curve is reached. Subsequently, between this point and the equilibrium liquid state immediately after T_g, all the enthalpy lost is regained. The peak in the DSC trace of the aged material is a direct consequence of this. To understand this behaviour, it is important to realise that the structure of the glass is frozen-in once the system departs from equilibrium at T_g [7]; the structures of the materials at T_g and at point A, therefore, are identical. Annealing to B changes the structure, which will now remain constant until the equilibrium liquid enthalpy line is crossed. Therefore, none of the enthalpy lost during aging is recovered up to this point. Beyond this, however, the T_g is being approached, and so the polymer chains are beginning to gain enough thermal energy to start segmental motion. Thus, all the enthalpy lost is essentially regained during the transition period, when the chains have sufficient energy to move.

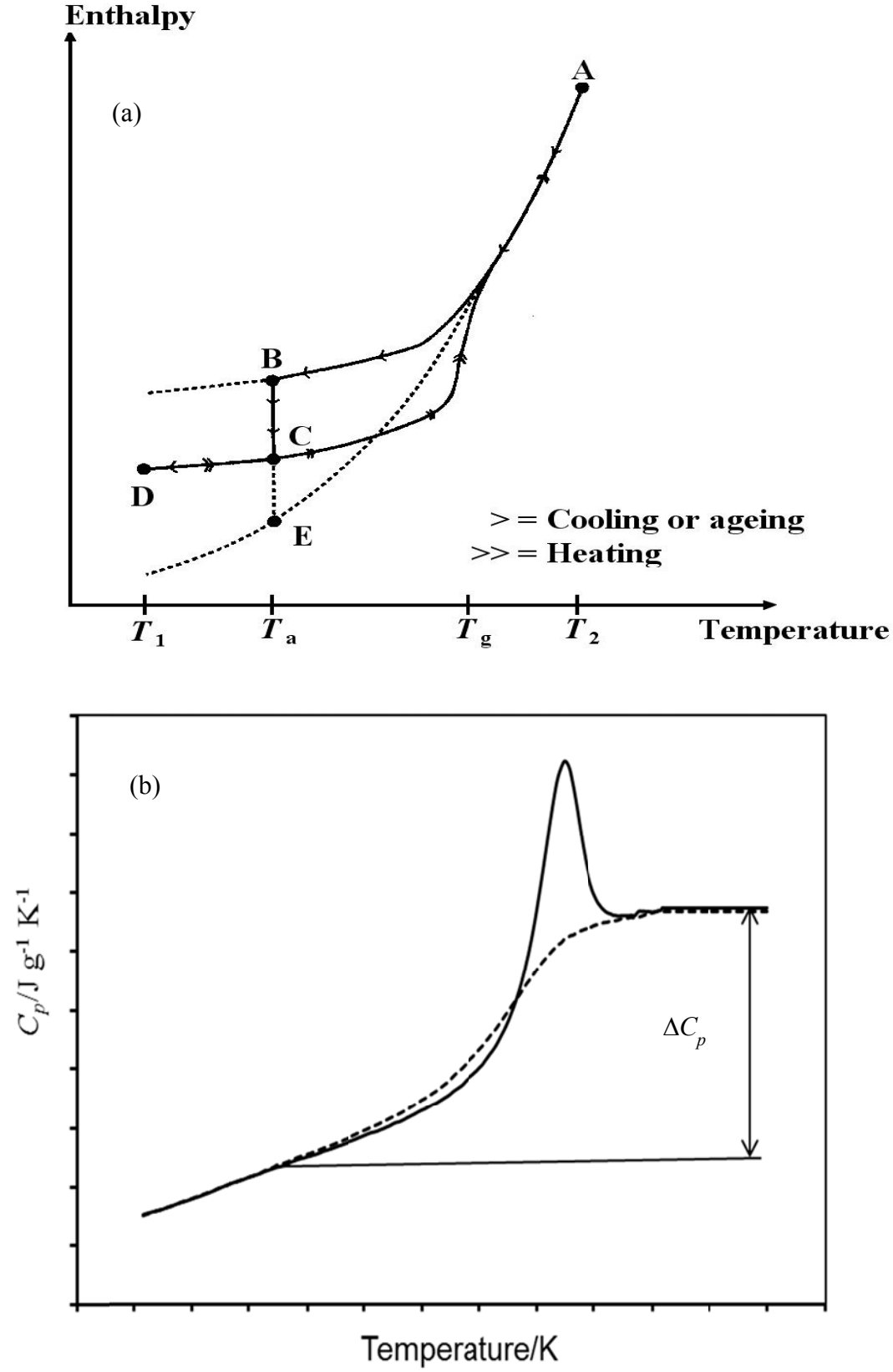

Figure 1.1 (a) Cooling, aging, and heating cycles use a fixed thermal history; (b) DSC curves for aged (solid line) and unaged (dashed line) polymer sample. (From Cowie et al. [9])

1.1.3 The multiparameter phenomenological models to describe enthalpy relaxation

There have been many attempts to develop quantitative models which describe the physical aging process. In order to quantify the behaviour below the glass transition, the models have to be able to predict the complicated behaviour displayed by polymers. The effects of experimental rate [10], asymmetry [11], non-linearity [11], non-exponentiality [11] and memory [4] have to be considered and adequately reproduced.

The approaches developed roughly fall under the following categories: the single parameter (SP) or free volume models; the multi-parameter (MP) models, including the Narayanaswamy - Moynihan (NM) [12] and Kovacs - Aklonis - Hutchinson - Ramos (KAHR) [13] models, as well as the semi-empirical models, the main example of which is the Cowie-Ferguson (CF) model [3].

1.1.3.1 Single parameter (SP) models

In glassy polymers, it is necessary to introduce additional ordering parameters, other than temperature and pressure, to define the non-equilibrium state. The SP models use one ordering parameter, free volume, to describe the non-equilibrium state of the material. Equations derived by Kovacs to describe isobaric volume recovery [13] and the Doolittle equation, relating viscosity to free volume [14], lead to descriptions of volume relaxation time and free volume.

SP models are not without limitations. Firstly, it is unlikely that such models can adequately describe the thermodynamic state of a glassy material. Struik [4] has shown that the free volume models each have their limitations but are nevertheless useful qualitatively. Unless a quantity of the free volume, V_F, can be defined, the theory cannot work quantitatively. Free volume holes are known to exist with a distribution of sizes [15], and, as such, give rise to a distribution of molecular environments. Consequently, a distribution of relaxation times would be expected; it is therefore necessary to be able to measure the free volume hole and distribution size. Techniques such as positron annihilation lifetime spectroscopy (PALS) have enabled such information to be obtained [15-17].

1.1.3.2 Multi-parameter (MP) models

The MP models were introduced to explain the four main features of physical aging (non-linearity, non-exponentiality, asymmetry and memory effects) that have been noted in multiple temperature jump experiments. The non-linearity aspect is addressed by expressing the average relaxation time as a function of the departure from equilibrium, which is measured using the fictive temperature (T_f). The differential scanning calorimetry (DSC) data are treated as a series of infinitesimal temperature jumps (ΔT) in the NM model [12]. T_f is defined as

$$T_f(T) = T_2 + \int_{T_2}^{T} \left\{ 1 - exp\left[-\left(\int_{T'}^{T} \frac{dT''}{Q_{\tau_0}} \right)^{\beta} \right] \right\} dT' \qquad (1.2)$$

where T_2 is a temperature above T_g, T' and T'' are dummy variables, Q is the heating/cooling rate and β defines the width of relaxation rates, such that $0 < \beta \leq 1$. The parameter, β also incorporates non-exponentiality into the model. When $\beta = 1$ the function is exponential and when β is close to zero, the function is highly non-exponential, with a broad distribution of relaxation times. The relaxation time (τ_0) is defined as

$$\tau_0 = A\, exp\left[\frac{x\Delta h^*}{RT} + \frac{(1-x)\Delta h^*}{RT_f} \right] \qquad (1.3)$$

where Δh^* is the activation energy for the relaxation process; x is a structural parameter such that it partitions τ_0 into a temperature-dependent part ($x\Delta h^*/RT$) and a structure dependent part ((1 - x) $\Delta h^*/RT$); A is the pre-exponential factor. The equations are solved by numerical integration.

Experimental heat capacity data are used to calculate the T_f:

$$\frac{dT_f}{dT} = \left[\frac{C_p(T) - C_{p(glass)}(T)}{C_{p(liquid)}(T_f) - C_{p(glass)}(T_f)} \right] \qquad (1.4)$$

Four parameters, Δh^*, β, ln A and x, are ultimately calculated, which are used to predict the response of the material as it is heated through the glass transition region. The model considers the entire thermal history and not only the aging behaviour.

Another MP model is the KAHR model [13] which resembles the NM model, except that a discrete distribution of relaxation times is introduced instead of a continuous distribution. This allows the distribution of free volume to be determined at any stage.

The MP models, by introducing a T independent shape parameter, assume that the shape of the relaxation function is independent of temperature. This concept has been questioned in the light of experimental data that suggests that β does, in fact, vary with temperature [18, 19]. The MP models also fail to predict the enthalpy lost upon aging to the equilibrium state, and they assume that the state reached after infinite aging time is the same as the equilibrium liquid state extrapolated into the glassy region. However, it has been suggested that this is not the case [20] and that the experimentally observed $\Delta H_\infty(T_a)$ value, where T_a is the aging temperature, is less than the calculated value. Also, the parameters tend not to be the so-called material parameters, since they vary with both aging time (t_a) and temperature. Semi-empirical models like the CF model discussed below represent an attempt to address these issues.

1.1.4 Semi-empirical models – The Cowie-Ferguson model

The Cowie-Ferguson model can be described as a "semi-empirical" model. The model attempts to predict the enthalpy lost on annealing to equilibrium ($\Delta H_\infty(T_a)$) by curve-fitting to the experimental enthalpy data accumulated at various aging temperatures after a range of aging times ($\Delta H(T_a, t_a)$). These values are determined from experimental C_p data obtained from DSC measurements. The approach of the system to equilibrium on annealing at T_a is shown schematically in Figure 1.2.

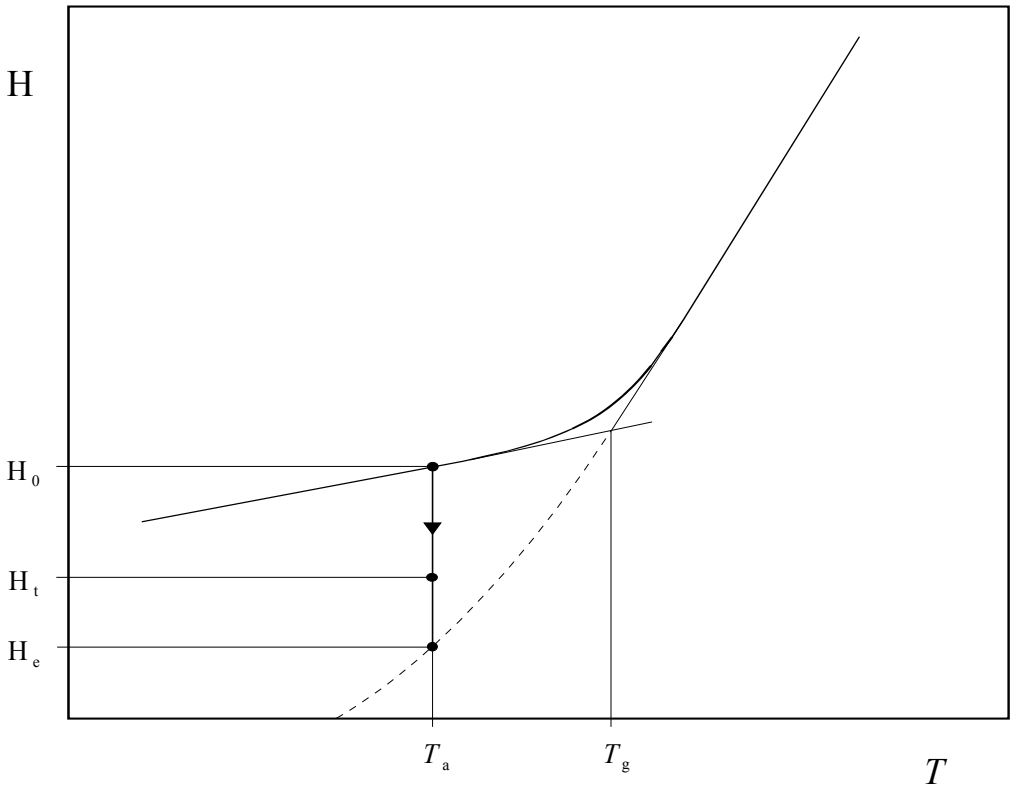

Figure 1.2 Schematic diagrams indicating the loss of enthalpy on annealing at T_a. H_0 is the initial enthalpy at an aging temperature, H_t is the enthalpy at an aging temperature for period of time, t_a, and H_e is the equilibrium enthalpy.

The relaxation function, $\Phi(t)$, describes the progression of the system towards equilibrium, such that

$$\Phi(t) = \frac{H_t - H_e}{H_0 - H_e} \qquad (1.5)$$

$\Delta H(T_a, t_a)$ can be described by the following empirical equation:

$$\Delta H(T_a, t_a) = \Delta H_\infty(T_a)[1 - \Phi(t_a)] \qquad (1.6)$$

where

$$\Phi(t) = exp\left[-(t_a/t_c)^\beta\right] \qquad (1.7)$$

β is the shape parameter, as discussed earlier, and t_a is an aging time, whereas t_c is a characteristic time and $(\Phi(t_c) = 1/e)$ is a kinetic parameter. The parameters $\Delta H_\infty(T_a)$,

β and log(t_c) are obtained from a curve-fitting procedure. The model has been used to study the aging of a number of polymeric systems, including plasticised PVC [21], PMMA [22], poly(vinyl acetate) (PVAc) [19] and several *para*-substituted polystyrenes.

1.2 Polymer blends

At this point it seems valuable to clarify, even briefly, some concepts related to polymers, such as miscibility and glass transition temperature, and the factors affecting them.

1.2.1 Miscibility of polymer blends

Polymer blends are physical mixtures of at least two polymers or copolymers [23]. Polymer-polymer mixtures can form a homogeneous single- phase, in which case the blend is said to be miscible or exist as heterogeneous phase-separated systems (immiscible blends) [23]. However, most miscible polymer blends (single-phase) tend to phase separate as temperature is raised. This type of behaviour is known as lower critical solution de-mixing and occurs at the lower critical solution temperature (LCST). It is frequently noticed in miscible blends [24]. Some miscible polymer systems, such as polyolefins, also exhibit phase separation at low temperatures. This behaviour is known as upper critical solution temperature (UCST) behaviour and the observation of UCST in polymer blends of high-molecular weight components is rare [25-27]. Both LCST and UCST behaviour are shown in Figure 1.3.

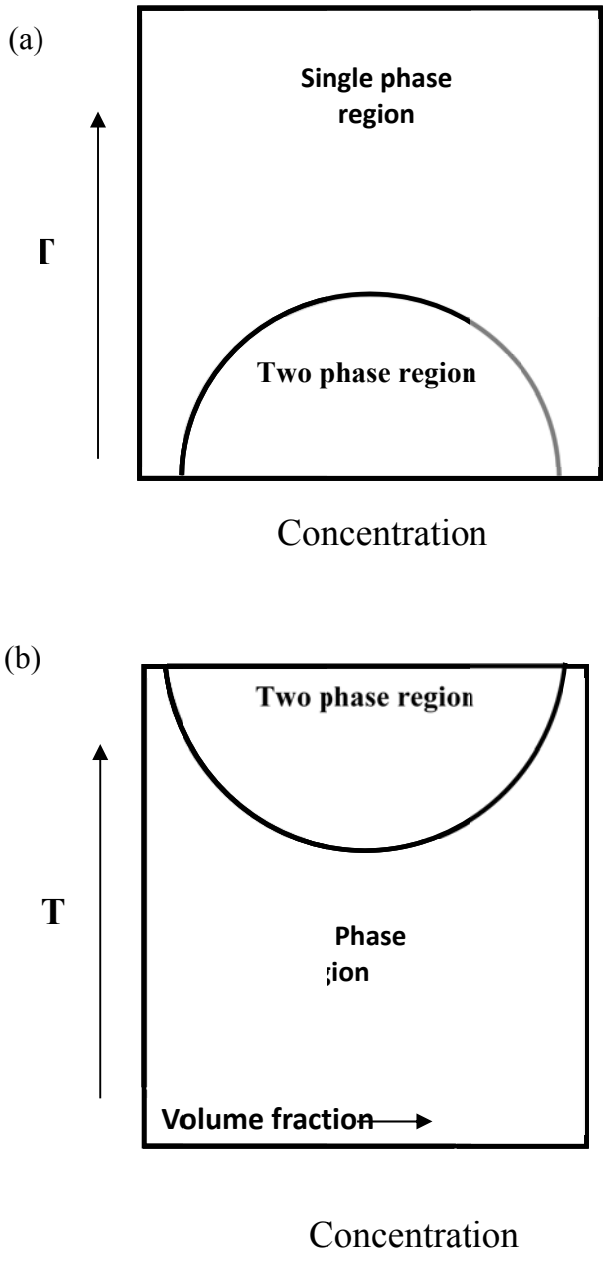

Figure 1.3 Schematic diagram showing (a) upper critical solution temperature (UCST): (b) lower critical solution temperature (LCST).The diagram was adapted from Figure 2.1 in ref [28].

The state of miscibility of a polymer-polymer mixture is controlled via the Gibbs free energy of mixing, ΔG_m, which is defined as:

$$\Delta G_m = \Delta H_m - T\Delta S_m \qquad (1.8)$$

where ΔH_m and ΔS_m are the enthalpy and entropy of mixing, respectively.

According to the second law of thermodynamics, a blend is miscible only if the Gibbs free energy of mixing is negative:

$$\Delta G_m < 0 \qquad (1.9)$$

1.2.2 Methods for determination of polymer-polymer miscibility

The miscibility of polymer blends can be detected by different methods, which can be divided into three groups [29]:

a) Phase equilibrium methods: this group includes turbidity measurements, light scattering methods, small angle X-ray scattering (SAXS) and small angle neutron scattering (SANS), fluorescence techniques and ultrasonic velocity.

b) Indirect methods include glass transition temperature, nuclear magnetic resonance, infrared spectroscopic methods, and microscopy.

c) Measurements of polymer/polymer interaction parameters: this group include direct methods such as the depression of the melting point and ternary-solution methods.

However, brief descriptions will be given of glass transition temperature and infrared spectroscopic methods that are used for the determination of polymer/polymer miscibility, as these methods are more common in studying the miscibility of polymer blends and this study depends on these methods. More descriptions of the other methods are included in reference [30].

1.2.2.1 The Glass Transition of Polymer Blends

The glass transition temperature, T_g, is known as the temperature at which an amorphous polymer changes from hard and relatively fragile to viscous and rubbery

[31]. At this point, the physical properties, such as the heat capacity, refractive index, and specific volume, drastically change. The measurement of T_g is the most widely accepted method to establish polymer blend miscibility [32]. Recently, Lodge and McLeish [33] have proposed that the effective glass transition temperature $T_{\mathrm{g}}^{eff}(\Phi)$ of each blend component can be calculated via the following equation:

$$T_{\mathrm{g}}^{eff}(\Phi) = T_{\mathrm{g}}(\Phi_{eff}) \qquad (1.10)$$

where Φ is the bulk concentration of polymer segments and Φ_{eff} is the effective local concentration.

The glass transition temperature T_g is often determined by means of differential scanning calorimetry (DSC) (Figure 1.4). T_g determines the onset of molecular motion and it depends, among other factors, on the polymer chain environment [23]. Thus, a miscible blend has a single T_g intermediate between those of the individual pure components (Figure 1.4 (a)), while an immiscible blend displays two glass transition temperatures equal to those of the pure components (Figure 1.4 (d)). However, when the blend is partially miscible, either multiple T_{g}s shifted closer together in temperature (Figure 1.4 (b)), or a broadening of the transition region is observed (Figure 1.4 (c)).

Experimental techniques that can be used to determine T_{g} include differential scanning calorimetry, dynamic mechanical thermal analysis and dielectric relaxation spectroscopy.

The glass transition temperature of a polymer blend is depended on the blend composition. The available equations to describe the dependence of the glass transition temperature on blend composition will be discussed later in the results chapters.

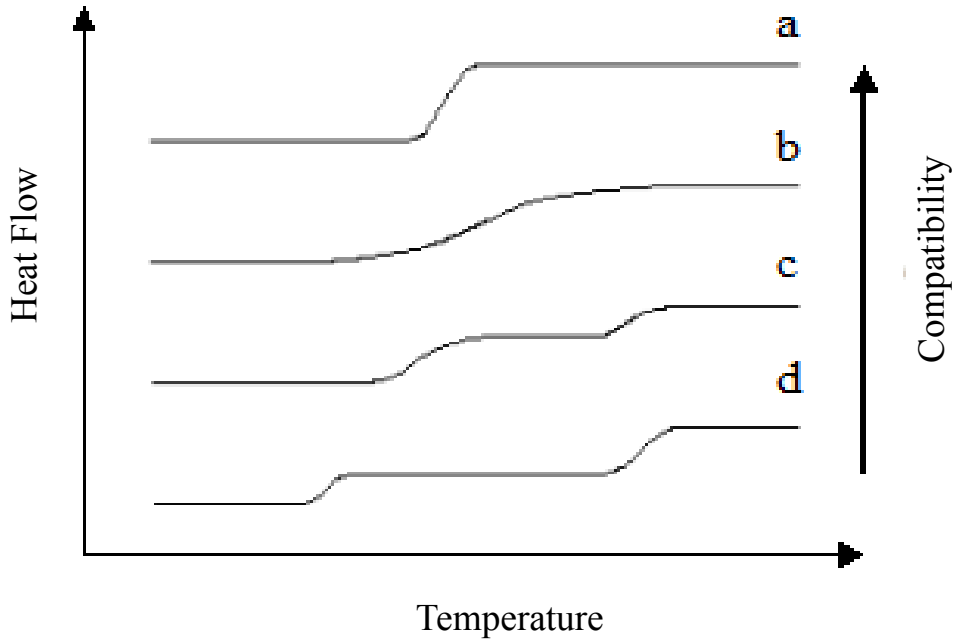

Figure 1.4 Typical DSC thermograms for (a) a miscible blend, (b) miscible blend close to phase separation, (c) partially miscible blend close to complete immiscibility and (d) immiscible blend [30].

1.2.2.2 Infrared spectroscopy

Among the spectroscopic techniques used to characterise the miscibility of polymer blends, Fourier transform infrared spectroscopy (FTIR) has been shwon to be one of the most powerful in examining the phase behaviour and intermolecular interactions in polymer blends [34-36]. Moreover, the miscibility between the component polymers in the blends often disturbs the environment of their molecular chains, causing variation of intensities and/ or shifts in their characteristic absorption in IR spectra. Thus, the infrared spectrum of a blend will be affected by whether the components are miscible or immiscible [37]. In an immiscible blend, the two individual polymers will act independently. However, in a miscible blend of A and B polymers, a single phase is involved, with the polymers closely mixed. Thus, the spectrum of the

blend will be very different from the spectrum of the two components, due to frequency shifts and band broadening from intermolecular interactions and changes in polymer chain conformation. The comparison of the blend spectrum with spectra of the two components can give an insight into those spectral features which are due to intermolecular interactions. Additionally, FTIR can help to identify the interaction mechanism between the components in the blend [30]. For instance, in a PS/PVME blend, the change in miscibility behaviour between PS and PVME can be detected by monitoring the changes occurring in the position and intensity of C-H out-of-plane vibration of the phenyl ring at 698 cm^{-1} and the $COCH_3$ vibration of PVME (at 1085 and 1107 cm^{-1}) [38, 39] .

FTIR measurements of polymer blends are excellent ways to investigate the presence and strength of the interactions occurring between the components [34-36]. For example, FTIR measurements of poly(4-hydroxystyrene), P4HS, blends have provided excellent proof of the capacity of FTIR to investigate the presence and strength of hydrogen bond interactions in these blends [40-46]. Moreover, FTIR studies of the effect of hydrogen bonding interactions in P4HS blends on the carbonyl (1650-1800 cm^{-1}) and hydroxyl (3100-3700 cm^{-1}) regions of the IR spectra give accurate information on the contribution of free, intra, and inter-association hydrogen bond vibration [42]. The effect of temperature on the miscibility of polymer blends has also studied using FTIR [34, 43, 47]. Serman and co-workers [43] used FTIR to calculate the hydrogen bonding fraction at different temperatures for P4HS/poly(n-alkyl methacrylate) blends. The results indicated that, for all blend compositions of P4HS/poly(methyl, ethyl, and propyl methacrylate) blends, the fraction of hydrogen bonding carbonyl groups obtained at different temperatures in the range from 25 to 200 ^{o}C were within 1%, well within the margin of experimental error, reflecting the fact that the blends are completely miscible in that temperature range. In marked contrast, the results of the calculation of the fraction of hydrogen bonding of P4HS/poly(butyl methacrylate), P4HS/PBMA, blends demonstrated that over 15% of the original hydrogen bonding carbonyl groups were lost upon heating to 200 ^{o}C, suggesting phase separation (immiscibility) in P4HS/PBMA blends at elevated temperatures.

1.2.3 The effect of interactions on the miscibility

Polymer-polymer interactions can be exploited to enhance polymer miscibility. For example, the interactions in PS/PVME are weak van der Waals interactions between the methoxyl group of PVME and the PS phenyl ring [48-50]. Nevertheless, there are some factors which can change the PS/PVME blend from a miscible to an immiscible blend. The most effective of these is the tacticity. Beaucage and co-workers [51] finding that a atactic PS is less miscible with isotactic PVME than heterotactic PVME. However, styrene-co-4-hydroxystyrene (SHS) or poly(4-hydroxy styrene) (P4HS), which has similar chemical structure to PS (except for the substitution of a hydrogen atom on the para position of phenyl ring with a hydroxyl function) has been reported to be miscible with PVME over the whole composition range [52-56].

Polystyrene PS is immiscible with PMMA [57], but miscible with P4HS [41-43, 58]. However, when PS is modified to contain around 4 % or more of HS as a co-monomer, the free energy change caused by the hydrogen bonding interaction between the hydroxyl and carbonyl groups promotes miscibility [58, 59].

Poly ethylene oxide (PEO) is reported to be immiscible with PS [60]. However, P4HS or SHS copolymers are reported to be miscible with PEO over the whole composition range [54, 55, 61-68], due to the presence of hydrogen bonds between the ether oxygen of PEO and hydroxyl groups of the other polymer.

According to the above brief review, miscibility of polymer blends can be achieved via selecting systems in which the components can interact with one another. Several specific group interactions have been identified that contribute to a negative free energy of mixing and are therefore able to enhance polymer-polymer miscibility [69]. In fact, four classes of specific interactions have been identified:

(1) Ion-Ion interactions: if one polymer involves a specific group that has a negative charge and the other polymer involves a specific group that has a positive charge then there is a probability for ion-ion interactions, as shown in Figure 1.5 (a).

(2) Hydrogen bonding: The most common strong interaction in polymers, and one that is central to the properties and phase behaviour of a range of important materials, is hydrogen bonding. It is one of the most influential interactions to enhance miscibility. As shown in Figure 1.5 (b), hydrogen bonding occurs between a proton accepting group

and a proton donating group [70-80]. This interaction has been used many times to produce miscible blends and thus all the blends in this thesis interact via hydrogen bonding. Further information on the hydrogen bonding interaction is presented in a separate section (1.2.3.1).

(3) Other interactions: these include dipole-dipole and ion-dipole interactions that are illustrated in Figure 1.5 (c). Those interactions are also responsible for polymer miscibility [23, 81].

(4) Dispersive interactions: a good example to understand this type of reaction is that between two molecules of benzene. An instantaneous dipole of one benzene molecule induces a dipole of another one at a particular time t_1. When the dipole of one benzene molecule changes, the other changes automatically at t_2, these variations are known as dispersive interactions (Figure 1.5 (d)) [82].

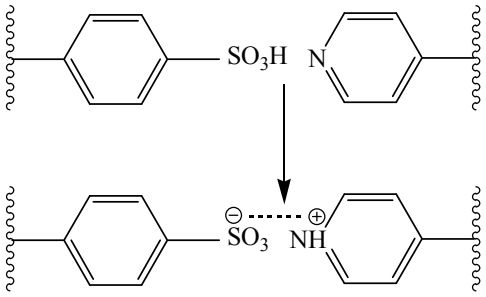

(a) Ionic interactions between two polymeric chains

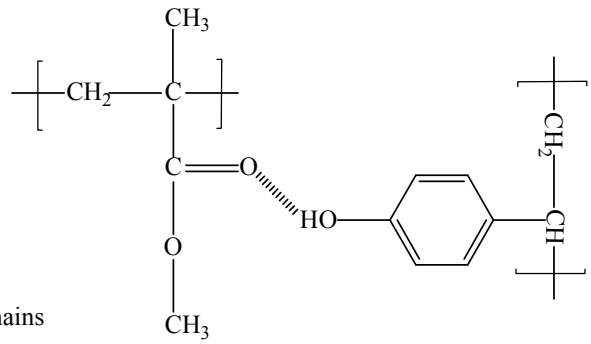

(b) Hydrogen bonding between two polymeric chains

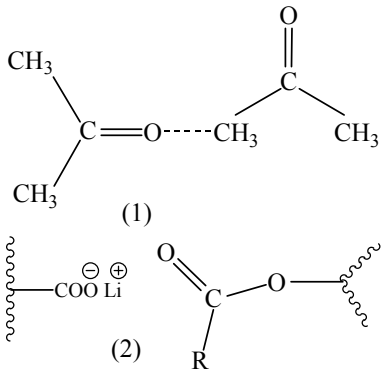

(c) Other interactions (1) dipole-dipole interaction (2) ion-dipole interaction

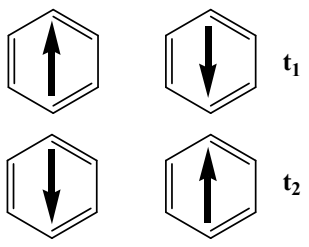

(d) Instantaneous dipoles of two benzene molecules at time $\mathbf{t_1}$ and $\mathbf{t_2}$

Figure 1.5 Specific interaction in polymer blends.

1.2.3.1 Hydrogen bonding interactions

The hydrogen bonding interaction has been defined in two ways; by Coleman et al. [34], according to the effect of the hydrogen bond on the physical properties of a material and by Pimental [83], based on its molecular characterisations.

The strength of hydrogen bonds most often lies in the range 1 -10 kcal/mol, which is between the covalent bonds which have strength of the order of 50 kcal/mol, and the van der Waals attraction which is of the order of 0.2 kcal/mol. Thus, at room temperature, materials in the non-crystalline state, above their T_g , are in a dynamic situation, with hydrogen bonds breaking and reforming. For interaction strengths of 3 kcal/mol, about 1% of interacting units could dissociate at a particular moment. The hydrogen bond is dynamic, with the number present dependent on temperature and composition. They do not behave like covalent crosslinks [34].

The other definition was introduced by Pimental [83] as follows: hydrogen bonds exist between a functional group A-H and atom or a group of atoms B in the same or different molecules when there is evidence

a) of bond formation (association or chelation)
b) that this new bond linking A-H and B specifically involves the hydrogen atom already bonded to A.

The hydrogen bond is linear: A and B are usually only strongly electronegative atoms i.e. O, N & F. The nature of the molecules involved can also affect the strength of hydrogen bonds.

Characterisation of hydrogen bonds can be difficult, as the position of the proton is hard to find by X-ray diffraction and many materials do not form single crystals, particularly polymers. Other techniques which can be used are infrared [40-46] and Raman spectroscopy [84, 85], and proton NMR [86, 87]. This last technique is used to examine the effect of hydrogen bond formation on the chemical shift of the A-H proton. The most sensitive of these techniques is infrared spectroscopy and this has been used

widely to investigate hydrogen bonding in different materials, including polymers [40-46].

1.2.3.2 Hydrogen bonding studies using infrared spectroscopy

The FTIR spectrum of a miscible blend usually differs from the spectrum of the blend components [37]: band broadening and frequency shifts can be observed due to intermolecular interactions and changes in polymer chain conformation [88].

In miscible blends that have accessible carbonyl groups, the carbonyl stretching vibration shifts to lower frequency and broadens. This effect is shown in a range of blends [89], such as polyester blends with polyvinyl chloride (PVC) styrene/acrylonitrile copolymers, polybis phenol A carbonate, polyhydroxyether of bisphenol A and poly(4-hydroxystyrene). This is normally accepted to be as a result of specific interactions, including the carbonyl-hydroxyl bond, which enhance miscibility in the blend. Shifts to lower frequencies are often considered to be indicative of the formation of a hydrogen bond but the shifts observed will depend on the extent of self-association in the original components, relative to interactions in the mixture [89].

The size of this frequency shift is a measure of the hydrogen bonding strength. An example of this is the study of Li and Brisson into hydrogen bonding in poly(methyl methacrylate) (PMMA)/ P4HS blends [90]. These authors reported a strong absorption peak at 3460 cm^{-1}corresponding to hydrogen bonding of OH to carbonyl groups, with an absence of free OH shoulder at 3530 cm^{-1}. As the temperature is increased, the areas of the free OH groups increase and the areas of OH hydrogen-bonded to carbonyls decrease. A further example of shifts in OH peaks is given in the spectroscopic characterisation of hydrogen bonding in P4HS/PVME carried out by Zhang and co-workers [91]. The spectrum of P4HS had a band at 3360cm^{-1} corresponding to associated OH moieties and a shoulder at about 3530cm^{-1}, which corresponds to non-associated OH stretch. The lower frequency band, at 3320cm^{-1}, increased in intensity with increasing PVME concentration, and this decreased in intensity with increasing temperature. These bands are associated with the OH stretch, hydrogen bonded to ether oxygen in PVME.

Wang et al. [92] reported shifts to lower frequencies of ($\Delta\nu \cong 202cm^{-1}$) in the OH stretching frequencies relative to the free hydroxyl of hydrogen bond between P4HS with nitrogen in poly (4-vinylpyridine) (P4VP). There was also a decrease of both the intensities of free and self-bonded hydroxyl groups. This provides evidence that intermolecular hydrogen bonding in P4HS/P4VP is stronger than the intra-molecular association in P4HS.

Recently, Zhang and co-workers [53] used FTIR to measure the extent of inter- and intra-molecular interactions in styrene-co-4-hydroxystyrene (SHS)/poly(vinyl ethyl ether) (PVEE) blends. Their results have detected that the intermolecular hydrogen bond in the blends, with $\Delta\nu$ of $225cm^{-1}$, is much stronger than the intra-molecular one of P4HS ($\Delta\nu \cong 95cm^{-1}$). Moreover, the intermolecular hydrogen bonds of P4HS and SHS with PVEE have the same strength, due to similar chain structure and the same proton-donating group of P4HS and SHS.

To summarise, hydrogen bonding is evidenced by a frequency shift to lower wave number values than those observed if the group was free, however, depend on the level of self-association in original materials relative to the blend and the size of shift gives a measure of the strength of the bonds. The dynamic nature of hydrogen bonding means that the peak shifts seen are affected by raising the temperature of the system.

1.3. Physical aging studies of polymers and blends

1.3.1 Poly (4-hydroxystyrene)

P4HS is quite important polymer due to firs the hydroxyl groups of P4HS can act as proton donor form strong interactions with other proton acceptor polymers; and second, the hydroxyl group in P4HS can act as both proton donor and acceptor, forming self-associated hydrogen bonds between either two P4HS repeat units of the same chain (intra-chains) or two adjacent ones (inter-chain). Recently, Tang and co-workers [93] have made brief mention to the application of P4HS as a valuable material in semiconductor and photoresistant applications [93]. More recently, an interesting paper

has been published on the application of P4HS [94]. Using of an ultrathin insulating polymeric layer of P4HS as interfacial layer between the polymer, fullerene photoactive layer, and the Al electrode led to enhanced power conversion efficiency (PCE) in a bulk-heterojunction of organic photovoltaic cells.

Although those applications described above require long-term stability. However, there are just two publications have been focused on the prediction of long-term thermal stability of P4HS homopolymer[18, 95]. Enthalpy relaxation results by Yoshida et al. [95] indicate that the "enthalpy relaxation is caused by restriction of segmental motion of the main chain", and the difference in enthalpy relaxation between P4HS and PS could be attributed to the presence of hydrogen bonds in P4HS, which should interrupt the thermal motion of the chain and thus hinder relaxation [95]. On the other hand Brunacci et al. [18] suggest that enthalpy relaxation is dependent on the rearrangement of chain segments, during that the hydrogen bonds are disrupted; however due to the high hydroxyl group density the same number of hydrogen bonds are again formed, leading to an increase in the barrier energy and thus an increase in enthalpy relaxation values in comparison with those of PS. Regarding relaxation times, these results indicated that P4HS relaxes faster than PS, which contradicts the general belief that the hydrogen bond interactions dominate molecular motion. Assuming that the relaxation rate increases with increasing of repulsive energy originated by unfavourable positions of hydroxyl groups; it is justified to expect a faster relaxation rate in the case of strong interaction.

1.3.2 Polyethylene oxide

Polyethylene oxide, PEO, is semi-crystalline polymer that has been used as retention aid in newsprint mills [96] and also for medical applications, such as a tablet binder for direct compression, a thickening agent, a tablet coater, and mucosal bio-adhesive [97]. The retention efficiency of PEO is maximized by adding phenolic compounds that appear to interact strongly with PEO and allow it to bridge between the adjacent solid materials [97].

Although most of the applications described above require long-term stability; amorphous and partially amorphous polymers are not in thermodynamic equilibrium

and usually undergo physical aging. This is shown in both volume and enthalpy relaxation, leading to serious structural changes in the materials [7].

Physical aging studies of some PEO blends have been conducted [68, 98-101], physical aging study of pure PEO are rare [102, 103]. The first study of PEO relaxation was carried out using broadband dielectric spectroscopy [102]. This study focused on the relaxation of the crystal-amorphous interphase that exists between the disordered amorphous phase and the ordered crystalline lamella. The other study focused on monitoring the decrease and increase of the life time as a function of storage time. The results of that paper indicated that the mean free volume hole decreases with increasing crystallinity, and so there is a lack of space for molecules to move into, hindering the polymer's move towards equilibrium and therefore reducing the effect of aging [103]. In other words, the relaxation time decreases with increasing polymer crystallinity.

1.3.3 Poly(ethyl methacrylate)

Physical aging studies of poly(ethyl methacrylate) (PEMA) are also rare [104]. Beiner et al. have studied the effect of physical aging on the dynamic shear modulus near the onset of the α-relaxation in the splitting region (α+β) of PEMA. The results indicated that annealing leads to a shift of the α-relaxation towards equilibrium, which means longer relaxation times with increasing aging time. However, at very low aging temperature (below T_g-20), equilibrium cannot be reached in practicable aging times (t_a< 1200min) [104].

1.3.4 Poly (4-vinylpyridine)

Although to date there is no physical aging publication on poly (4-vinylpyridine) (P4VPy), enthalpy relaxation data are available for poly(2-vinylpyridine) (P2VPy) [105] which differs from P4VPy only in the placement of the nitrogen atoms in the pyridine ring. Enthalpy relaxation results indicate that the aging time required for P2VPy to reach the equilibrium state is dependent on aging temperature as expected: where $T_a = T_g$-20, the polymer reached equilibrium after 100h; however, at $T_a = T_g$-10 the required aging time to reach to equilibrium state was just 5 h.

1.3.5 Polymer blends

The first comprehensive study of physical aging in a miscible blend was supported by Cowie and Ferguson [106] using enthalpy relaxation as a function of physical aging of PS/PVME. Their results indicated that the PS/PVME blend relaxes more slowly than PVME. Furthermore, the lower T_g component (PVME) appears to be responsible for most of the aging effects measured, whereas PS, which has higher T_g, provides only a minor contribution to aging. Values of segmental activation energy, $\langle E_a \rangle$, for the blends were slightly higher than those of PVME, while for PS, those values were much higher, which indicates PVME dominates the aging process [2]. Another system subject to enthalpy relaxation studies is the PVC/PMMA blend [107]. It was found that the enthalpy relaxation values of the PVC/PMMA blend were approximately in between those of PVC and PMMA. Although interactions in PVC/PMMA are similar to those of a PS/PVME blend, the enthalpy relaxation results of PVC/PMMA are in conflict with those of PS/PVME. This is likely due to small differences between the glass transition temperature of PVC and PMMA compared with the big difference in the glass transition of PS and PVME [108].

Few reports of the effect of hydrogen bonding on the physical aging of polymer blends have been published. Most of those studies have come from Cowie and co-workers, who examined the enthalpy relaxation of blends [109, 110] and copolymers [17] with a group of varying hydrogen bond strengths. The enthalpy relaxation study by Arrighi et al. of P4HS/PVME blends at different compositions [110] is a perfect example of the effect of interactions on physical aging. It was mentioned previously that the hydrogen bond strength in P4HS/PVME increases with increasing PVME content. Moreover, positron annihilation lifetime spectroscopy, PALS, [110] suggests that at the ideal blend composition of 59/41 mole% P4HS/PVME, the free volume is a minimum, for both components. This indicates a close-packed blend structure which is the result of strongly interactive components. The authors report average relaxation times, derived from enthalpy relaxation using CF parameters, and the results indicated that the

relaxation time rate increases with the increasing the strength of hydrogen bonding in the blend. Thus, the slowest relaxation rate is measured at 59/41 blend composition, where the free volume is minimized and the hydrogen bonding is at maximum.

Another system blend which has been the subject of an enthalpy relaxation study is the P4HS/PMMA blend [109]. The results of that study have indicated that the P4HS/PMMA blend relaxed more slowly than PMMA, but faster than pure P4HS. These results for P4HS were in contrast to those published by Brunacci et al. [18]. However, we will leave the discussion here, but it will form part of the results chapters in this thesis.

P4HS/PEMA blends are also other system of P4HS; however most of the studies published have focussed on blend miscibility, such as the effect of temperature [43] or the effect of blend composition on miscibility [111].

Recently, Zhang et al. [112] demonstrated that for all blends compositions a single α-process founded in the temperature range where α and β relaxation are separated. This confirms the P4HS/PEMA blend is a miscible system in the composition range. This study also provided other important information on P4HS/PEMA blends, where, although hydrogen bonding increase the ΔC_p and intermolecular coupling. However, the present of hydrogen bonding between P4HS and PEMA has no effect on relaxation behaviour. Moreover, the correlation between fragility and thermodynamic properties is invalid in hydrogen bonded P4HS/PEMA blends.

The prediction of long term thermal stability of P4HS/PEMA blends is also quite an important property; however, to date, there is no aging study on P4HS/PEMA blends.

P4HS/PEO blends are one of the phenolic blends as well, and are a perfect example to show the effect of hydrogen bonding interactions on miscibility. Physical mixing of PEO with P4HS or –HS copolymers will cause hydrogen bonding between the oxygen atoms in PEO and the hydroxyl groups of –HS copolymers or the P4HS neat polymer. These bonds have been reported to be stronger than the self-association of hydroxyl groups (Figure 1.6). Most previous studies of this system have concentrated

on the effect of hydrogen bonding interactions on miscibility behaviour [54, 66, 113, 114]. The effect of hydrogen bonds on the rheological behaviour has also been studied [63]. However, although P4HS/PEO blends are used as a retention aid in newsprint mills [96], and applications like this requires long-term stability no physical aging study is recorded in the literature up to date.

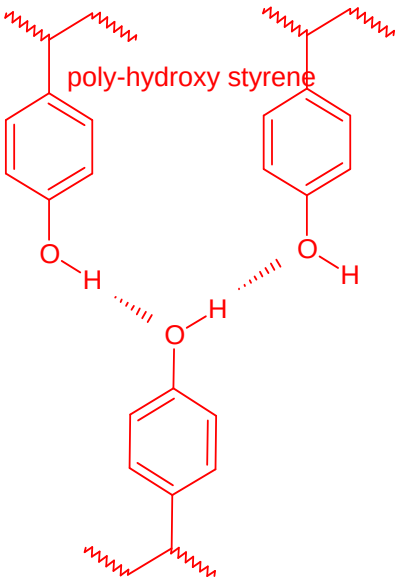

(a) Self-association (intra-and inter chain)

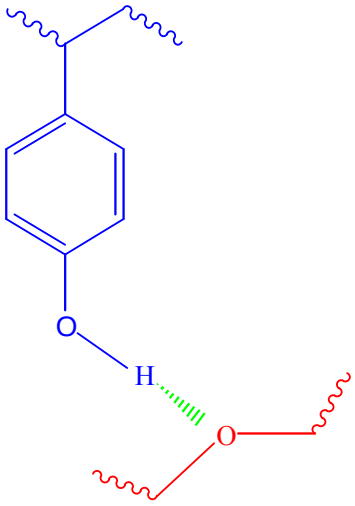

(b) Inter-molecular association (major interaction)

Figure 1.6 Interaction in P4HS/PEO blends

P4HS/P4VPy blends are other different system of P4HS interactions. The miscibility has been studied earlier by Meftahi and co-workers [115]. DSC measurements demonstrated that P4HS/P4VPy blends are miscible over the entire range of composition as result of single glass transition temperature. The interaction strength between P4HS and P4VPy has also been studied using X-ray photoelectron spectroscopy [116]. The results confirmed that the interactions in the P4HS/P4VPy blend are stronger than those in P4HS.

Recently, Wang and co-workers have reported that when the T_gs of the two constituent components are too close and the difference is less than 10°C, as with P4HS and P4VPy, it is impossible to identify whether there are two or one T_g in the blend. Therefore, the miscibility cannot be judged for such systems. They thus used ^{13}C solid-

state nuclear magnetic resonance (NMR) for investigating the scale of miscibility of P4HS/P4VPy [92].

All studies have focused on the effect of hydrogen bonding strength on miscibility and phase behaviour of P4HS/P4VPy blends. To date no publication has been submitted on the physical aging of these blends.

1.4 Objective and scope of this thesis

This thesis reports physical aging studies as a function of both aging temperature and blend composition for a series of miscible systems (i.e. P4HS/PEMA, P4HS/PEO, P4HS/P4VP, SHS/PMMA, SHS/PEMA, SHS/PVME, and SHS/PEO). Measurements of enthalpy relaxation are also carried out on P4HS, PEMA and P4VPy homopolymers. One reason for re-measuring the enthalpy relaxation of P4HS is that to date there have been only two papers that report enthalpy relaxation data of P4HS [18, 95]. However, there is a discrepancy between the results of these two papers, as mentioned in section 1.3.2.2. Thus it was necessary to carry out enthalpy relaxation measurements in an attempt to confirm the situation. Results are discussed in Chapter 3 in addition to the effect of dilution of hydrogen bonds (i.e. SHS copolymers) on the enthalpy relaxation process.

Chapter 4 deals with the behaviour of P4HS/PEO and P4HS/PEMA blends. First, the effect of composition on hydrogen bond strength, secondly is discussed, followed by a discussion of the effect of temperature on the strength of the hydrogen bonding, and finally, the effect of hydrogen bond strength on the relaxation process in a polymer blend. Moreover, in that chapter physical aging measurements of a stronger hydrogen bonding system (i.e. P4HS/P4VP blends) are reported. The interesting feature of P4HS/P4VP complexes is that the glass transition temperature of polymer complexes is significantly higher than the T_g of the pure components [92, 115, 117]. Thus, that chapter will report measurement of enthalpy relaxation of a 1:1 molar ratio P4HS/P4VP blend, in an attempt to investigate aging when the blend has maximum number of coupling pairs of the hydrogen bonds.

The fifth chapter will discuss the physical aging of SHS/PEO, SHS/PVME, SHS/PMMA, and SHS/PEMA blends. One reason for choosing these systems is to investigate the effect of dilution of hydrogen bonds between hydroxyl groups of P4HS by styrene units.

The second reason for choosing these systems was for comparison with the enthalpy relaxation work carried out on P4HS/PEO and P4HS/PEMA in Chapter 4 and with work carried out on P4HS/PMMA and P4HS/PVME previously in our laboratory [109, 110] .

Regarding the experimental part, this research will try to synthesise partially deuterated P4HS polymer (d-P4HS, deuterated in the aromatic ring), that would be to use in neutron scattering measurements to investigate the dynamic behaviour of H-bonded blends, particularly changes in PEO dynamics in blends with P4HS. The idea is to synthesise d-P4HS from PS-d according to the published papers of Nasrullah et al. [118] and Deokar et al. [119], who used PS to synthesise hydrogenated P4HS.

Chapter 2 Experimental technique and sample preparation

2.1 Instrumentation

2.1.1 Differential scanning calorimetry (DSC)

The initial polymer glass transition, T_g was determined using a TA Instruments DSC 2010 Differential Scanning Calorimeter. Nitrogen was used as the purge gas, liquid nitrogen and air as coolants. Sample sizes ranged from 7 – 15 mg and a heating rate of 20 K/min was usually employed. The reported T_g (midpoint) values were usually the average values based on the second and third runs. However there are some exemptions such as P4HS that took many runs (up 10 runs) to reach constant T_g (midpoint) value.

Glass transition values and enthalpic relaxation data of the pure polymers, copolymers and blends were obtained using a Perkin-Elmer Pyris 1 DSC. For these measurements nitrogen was used as a purge gas and a water coolant system was in place. Sample sizes ranged from 8 - 15 mg, a heating rate of 20 K/min and cooling rate of 40 K/min were used throughout. The Pyris 1 DSC was interfaced to a PC, which was used to control the DSC instrument as well as to process and analyse the data. Data collection and analysis was achieved using software developed by Dr Roderick Ferguson.

A series of three scans were recorded in order to determine T_g values. The reported T_g values were obtained from an average of the last two scans. The procedure of Richardson and Savill [120] was used in this work to calculate T_g. The C_p curves were transformed into enthalpy curves and the point of intersection of the liquid and glassy enthalpy lines extrapolated into the transition region was taken as the T_g (mid-point). This value is independent of the scanning rate and is deemed more accurate.

The signal produced by the DSC corresponds to the differential power, usually expressed in mJs^{-1}, required to keep a sample and a reference at the same temperature while they are heated or cooled at fixed rate. The signal produced by the DSC is of similar shape to the C_p-temperature curve of the sample but the units in which it is expressed need to be transformed into $Jg^{-1}K^{-1}$. To do this, the signal of a standard with a known C_p is compared within the same range of temperature. Sapphire is the most common C_p reference and it was used throughout this work as a result of its high

reproducibility and thermal stability. Moreover, Indium was also used here for temperature calibration. Since there are several other contributions to the shape of the experimental curves, a baseline scan is subtracted from both sample and sapphire scans. The baseline gives different contributions, mostly depending on the temperature range, but in the ideal it should be an almost flat line. The sample C_p is calculated using the following equation:

$$C_{p\ sample} = \frac{D_{sample} m_{sapphire} C_{psapphire}}{m_{sample} D_{sapphire}} \qquad (2.1)$$

where D_i is the DSC deflection after subtracting the baseline and m_i is the weight in grams of sample and sapphire.

2.1.1.1 Defining an aging profile

Identical automated thermal treatments were applied to each sample and a typical aging profile is described below, where T_2 is T_g + 50K and T_1 is T_g – 60 K. This is shown schematically in Figure 2.1.

1. Heat to T_2 at 320 K /min.
2. Hold at T_2 for 10 min.
3. Cool from T_2 to T_a at 40 K /min.
4. Hold at T_a for 10 min.
5. Cool from T_a to T_1 at 40 K/min.
6. Hold at T_1 for 5 min.
7. Heat from T_1 to T_2 at 20 K/min.
8. Hold at T_2 for 2 min.
9. Hold at T_2 for 10 min.
10. Cool from T_2 to T_1 at 40 K/min.
11. Hold at T_1 for 5 min.
12. Heat from T_1 to T_2 at 20 K/min.
13. Hold at T_2 for 2 min.
14. Hold at T_2 for 10 min.

In essence, steps 1 and 2 remove all previous thermal history in the samples. Steps 3 to 8 produce the aging of the sample and the resulting aged scan. Finally, steps 9 to 14 result in the recording of the unaged (reference) scan. The same sample was used for aging in all cases.

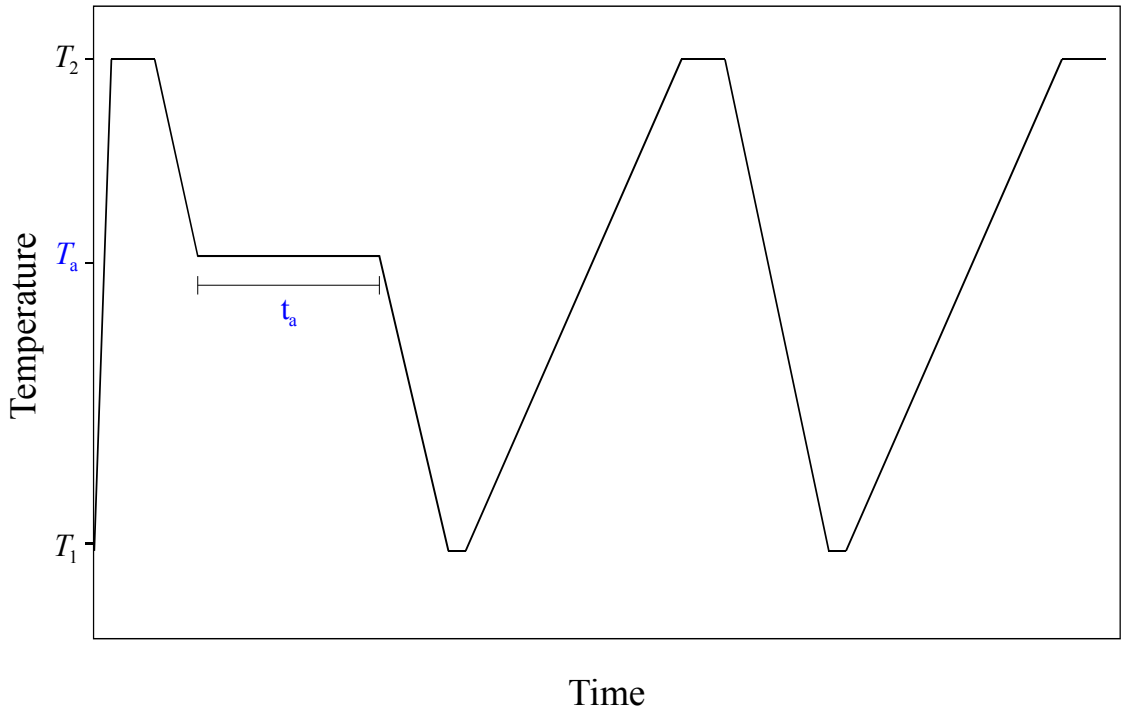

Figure 2.1 Schematic of thermal history used in aging experiments (See page 31), t_a is an aging time.

2.1.1.2 Processing of aging data

Several programs were developed during the course of the project by Dr Roderick Ferguson in order to process the aging data collected using the Pyris instrument. The enthalpic T_g (T_g (mid-point)) is determined using the !average- C_p program, which is also used to calculate ΔT and ΔC_p. The heat capacity files can be viewed with !Plot_C*p*, and the enthalpy lost at each aging time in an experiment ($\Delta H(T_a, t_a)$) is determined using !Int_ΔC_p. Once all the enthalpy values have been calculated at a particular T_a, the data are curve-fitted to the Cowie-Ferguson enthalpy relaxation model using the !Sci_Model program. The resulting data set plus the model curve can be displayed graphically by using! Sci_Graph.

The determination of $\Delta H(T_a, t_a)$ using !Int_C_p involves selecting an aging C_p file and its complementary unaged file, and dropping these onto the !Int_Cp icon. The program first plots the two files as a C_p difference plot (ΔC_p), which is shown schematically in Figure 2.2. It then asks for temperature limits for data smoothing, which is useful at short aging times when the Cp difference is smallest. Next the lower and upper integration limits (T_α and T_β) should be defined before performing the integration. The integration was performed three times and an average taken.

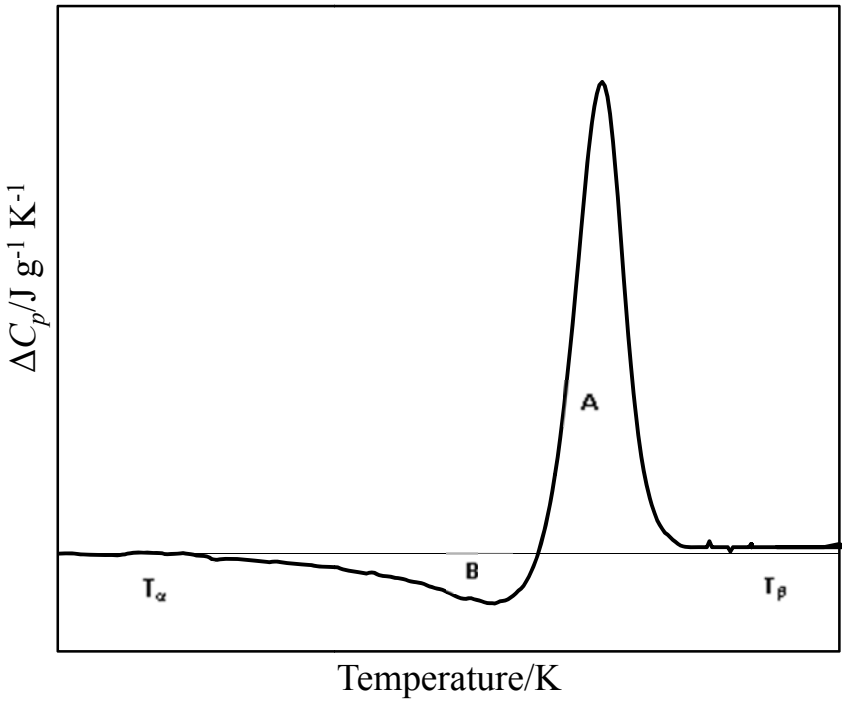

Figure 2.2 Heat capacity difference (ΔC_p) plot

2.1.2 Gel permeation chromatography (GPC)

The molar mass and molar mass distribution (PDI) of the polymers in this study was measured using Gel Permeation Chromatography (GPC). The GPC arrangement used consisted of a Waters 590 pump fitted with ultra-gel columns (normal pore size 10Å) and a Waters 410 Differential Refractometer. The instrument was calibrated using a series of standard polystyrene samples with narrow molecular weight distribution. Consequently, molecular weights expressed are with respect to polystyrene.

The polymer samples were dissolved in out-gassed tetrahydrofuran (0.2 % w/v solution) and filtered through 0.45 μm disposable syringe filters. The flow-rate of the mobile phase was 1.0 mL/min.

2.1.3 Fourier transform infrared spectroscopy (FTIR)

All infrared spectra were recorded on a Perkin Elmer RX FTIR spectrometer. The polymer was dissolved in a suitable solvent, such as tetrahydrofuran, cast on a NaCl disk and allowed to dry under a high power lamp to provide a thin film. Resolution of the instrument was set at 2 cm^{-1} and a minimum of 64 scans were taken. Spectra at elevated temperature (50 to 150 ^{o}C) were collected by using a SPECAC high-temperature cell, mounted in the spectrometer, with an accuracy of ± 2 ^{o}C.

2.1.4 ^{1}H Nuclear magnetic resonance (NMR) spectrometry

Proton NMR spectra were recorded on a Bruker WP-200SY FTNMR spectrometer at a frequency of 200 MHz. The instrument was operated in its standard mode. Chemical shifts were measured in ppm on a micro scale downfield from tetramethylsilane as an internal standard. Deuterated chloroform and DMSO-d6 were used as the solvents for the styrene-4-tert-butoxystyrene (StBuS) and SHS copolymers, respectively. Deuterated chloroform was used for the PMEMA copolymers.

2.2 List of chemicals

Standard laboratory chemicals were used for all syntheses and sample preparations. The source and purity of these chemicals are given below.

α, α-azobisisobutyronitrile (AIBN)	Sigma Aldrich (98%)
4-tert-butoxystyrene	Sigma Aldrich (99%)
Styrene	Sigma Aldrich (>99%)
Sodium hydroxide	BDH Laboratory Supplies
Anhydrous $MgSO_4$	BDH Laboratory Supplies
Xylene	Sigma Aldrich (>98.5%)
Oxygen free N_2 gas	BDH Laboratory Supplies
Liquid N_2	BDH Laboratory Supplies
Methanol	Fisher Scientific (99.5%)

Tetrahydrofuran (THF)	BDH Laboratory Supplies
Hydrochloric acid (HCl)	Sigma Aldrich (>36%)
Dimethyl sulfoxide-d_6 (DMSO)	BDH Laboratory Supplies
Acetone for HPLC grade	Sigma Aldrich (>36%)
Hexane for HPLC	BDH Laboratory Supplies
Chloroform	BDH Laboratory Supplies
Chloroform-d	BDH Laboratory Supplies
Ethyl methacrylate	Sigma Aldrich (99%)
Methyl methacrylate	Sigma Aldrich (99%)
Poly(4-hydroxystyrene) (P4HS)	Polysciences, Inc.
Polyethylene oxide (PEO)	Sigma Aldrich
Methyl ethyl ketone (MEK)	BDH Laboratory Supplies
Poly(methyl methacrylate)	Sigma Aldrich
Poly(ethyl methacrylate)	Sigma Aldrich

2.3 Synthesis of styrene-co-4-hydroxystyrene (SHS) copolymers

2.3.1 Synthesis of styrene-co-4-tert-butoxystyrene (StBuS) copolymers

Styrene and 4-tert-butoxystyrene monomers were first washed with 0.1M NaOH solution to remove the phenolic inhibitor and then with distilled water. Both monomers were then dried over anhydrous $MgSO_4$.

Solutions of styrene, 4-tert-butoxystyrene (tBuS) and 2,2'-azo-bis-isobutyronitrile (AIBN) in ~ 10 mL of xylene and with an initiator concentration of approximately 1.56 mole % relative to total monomer content, were placed in a

polymerisation vessel and degassed by three freeze-pump-thaw cycles. They were subsequently heated *in vacuo* at 60 ^{0}C for up to 4 hours in a thermostatically controlled water-bath. A total monomer weight of approximately 10 g was used.

The monomer and initiator contents are given in *Table 2.1*. This produced monomer feed ratios of 0.30 (StBuS 1), 0.50 (StBuS 2), and 0.70 (StBuS3) in mole fraction of tBuS.

Table 2.1: Quantities of reactants used in the preparation of StBuS copolymers

	StBuS1		StBuS2		StBuS3	
	Mass (g)	m moles	Mass (g)	m moles	Mass (g)	m moles
tBuS	3.804	21.58	6.365	36.10	8.876	50.36
S	5.239	50.30	3.727	35.80	2.245	21.56
AIBN	0.184	1.12	0.184	1.12	0.184	1.12

Following polymerisation, each solution was precipitated drop-wise into ~300 mL of methanol. The resulting solid polymers were re-precipitated from chloroform into methanol. They were dried under vacuum 85 °C for 24 hours to provide the copolymer as a white solid (1.2 g, 12% conversion).

FTIR: 1365/1388 (tert-butyl bands), 1236 (ph-O stretch), 1162, cm^{-1} (tBu-O stretch). ^{1}H NMR ($CDCl_3$, 200 MHz): δ =1.1–1.6 (broad s, backbone CH_2), 1.6–2.2 (broad s, backbone CH), 6.2–6.85 (broad s, 3H, Ar), 6.85–7.2 (m, 1.5H, p-S), 9.00 (s, 0.5H, ph–OH) (for proton assignments refer to Figure 2.4).

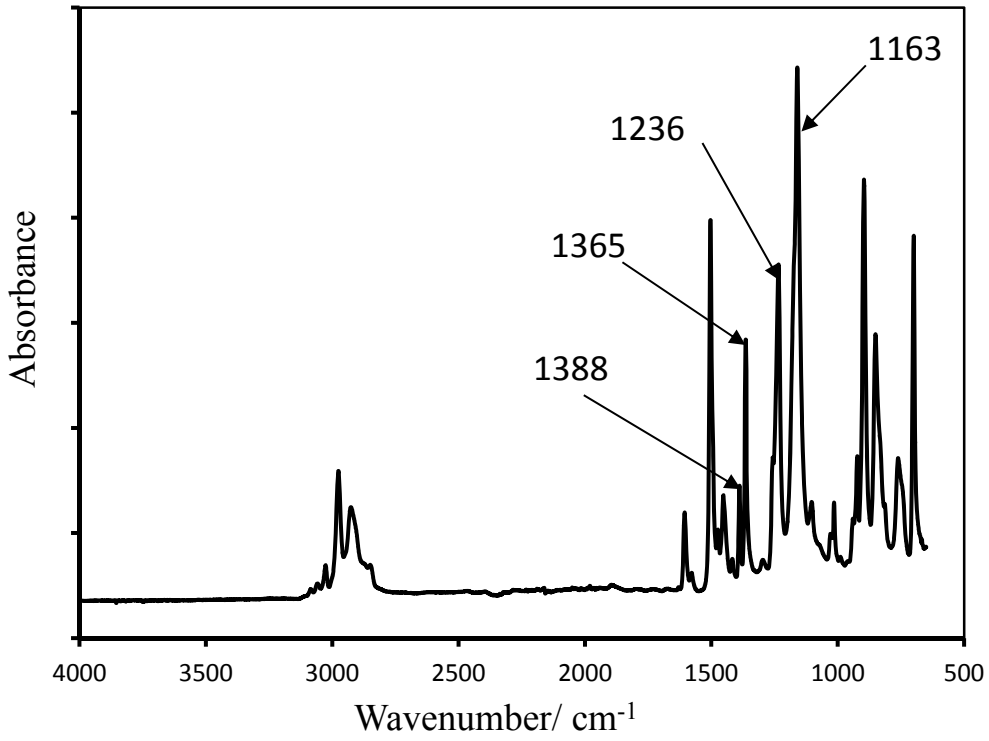

Figure 2.3 FTIR spectrum of poly(4-tert-butoxystyrene-co-styrene) with 70 mole-% tBuS in the feed.

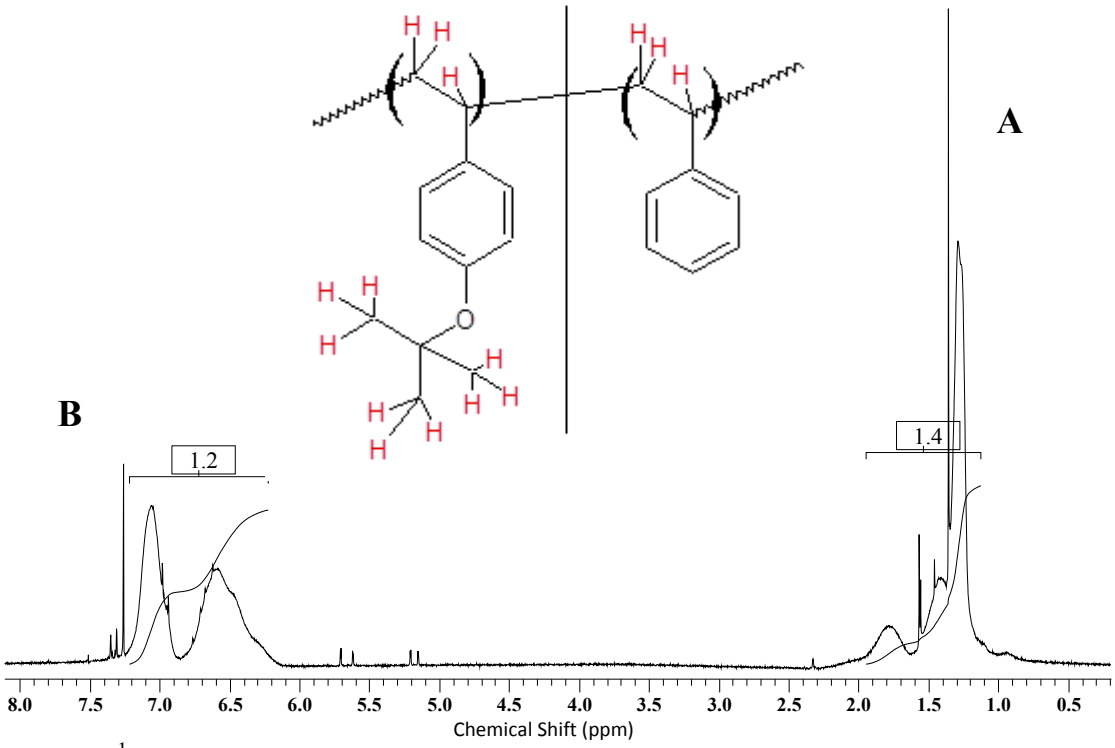

Figure 2.4 ^{1}H NMR spectrum of poly(4-tert-butoxystyrene-co-styrene) with 30 mole-% tBuS in the feed.

where A corresponds to aliphatic protons and B corresponds to aromatic protons.

StBuS copolymer compositions were determined using ^{1}H NMR spectra following the method described by Xu et al.[121] Copolymer compositions (F_{tBuS}) listed in *Table 2.2* are almost identical to the monomer feed ratios (f_{tBuS}).

Table 2.2: StBuS copolymer compositions determined from ^{1}H NMR spectra.

Copolymer	f_{tBuS}	F_{tBuS} ^{1}H NMR	Mw	PDI
StBuS1	0.30	0.28	79,606	1.62
StBuS2	0.50	0.51	88,832	1.50
StBuS3	0.70	0.73	67,638	1.55

2.3.2 Hydrolysis of styrene-co-4-tert-butoxystyrene copolymers

Several procedures have been used in order to convert StBuS to SHS copolymers as described below.

Procedure 1

The hydrolysis reaction was carried out in THF using conc. HCl as the hydrolytic agent [122]. For 1.3g StBuS 20 ml THF solvent and 2 ml conc. HCl were used. The reaction was allowed to proceed for up to 20 hours at reflux temperature (Schematic 2.1).

The reactions were monitored by following the disappearance of tert-butyl bands at 1365 and 1388 cm^{-1} in the FTIR spectrum (Figure 2.5). Following complete hydrolysis, each copolymer solution was concentrated to approximately 7ml and precipitated drop-wise into 10% HCl aqueous solution (~166ml) the resultant polymer was re-dissolved in THF and re-precipitated into 10% HCl aqueous solution. The precipitate was filtered off, rinsed with H_2O several times and left to evaporate overnight, followed by 24 hours at 60°C and a further 30 minutes at 130°C in vacuum oven.

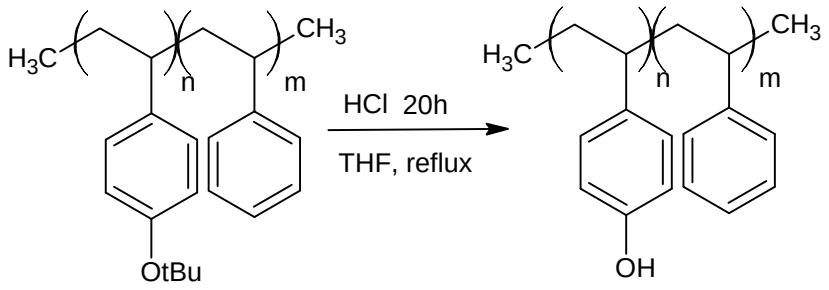

Schematic 2.1

The ^{1}H NMR spectrum of the SHS copolymers showed the presence of impurities (Figure 2.6) such as residual THF (CH_2, δ =1.76 and CH_2O, δ =3.60) and H_2O (δ =3.33). Therefore, to remove the residual solvents, it proved necessary to re-dry the copolymer samples at higher temperature (i.e. 145 ^{o} C) for longer times. Unfortunately, the samples after having been heated to high temperature were no longer soluble in DMSO-d_6 or any other NMR solvent.

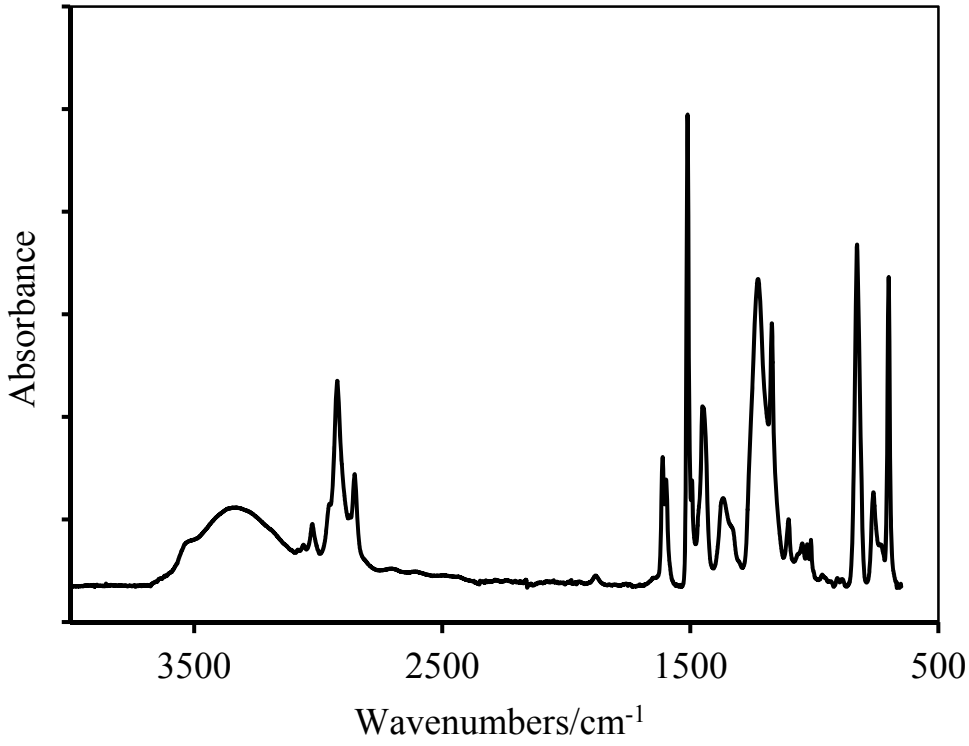

Figure 2.5 FTIR spectrum of a styrene-co-4-hydroxystyrene with 70 mole-% HS in the feed.

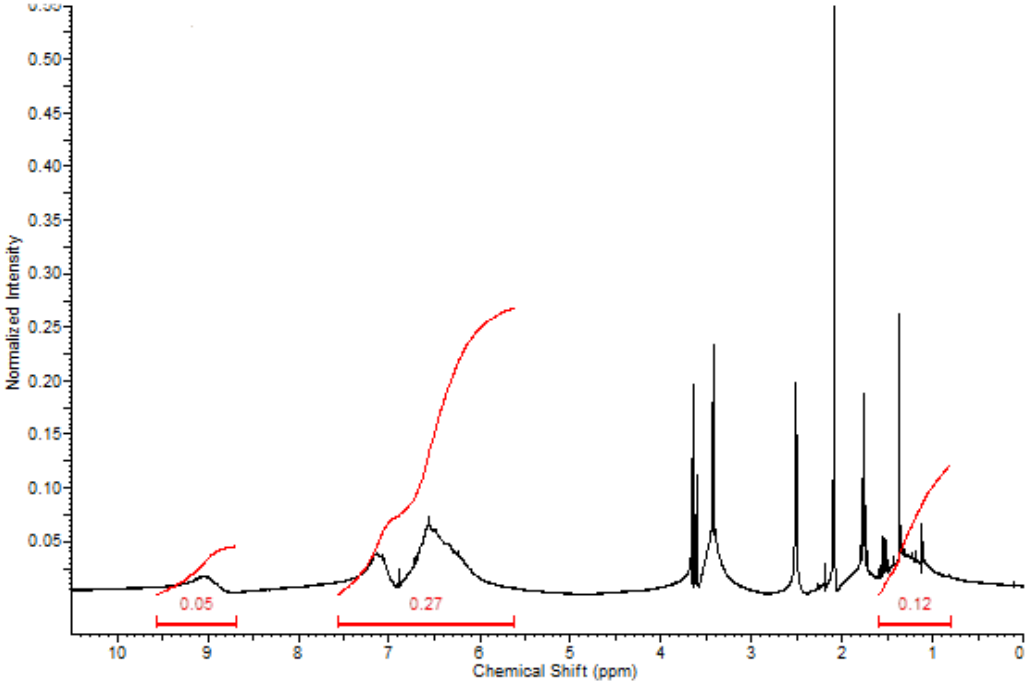

Figure 2.6 ^{1}H NMR spectrum of a styrene-co-4-hydroxystyrene with 70 mole-% HS in the feed.

Procedure 2

The hydrolysis reaction was carried out as in the equation below (Schematic 2.2) by dissolving 1.3g of StBuS copolymer in toluene /methanol (70/30 vol.-%, 7 ml) and then concentrated sulphuric acid (97%, 5 mol-% to tBuS unit) was added as the hydrolytic agent [123]. The mixture was stirred at 60 ^{o}C overnight under N_2 atmosphere, and then for neutralization a 50% -sodium lactate aqueous solution was added. The reaction mixture was poured into pentane and filtered off, rinsed with pentane several times and left to evaporate overnight, followed by 24 hours at 60 °C and a further 30 minutes at 110 °C in vacuum oven.

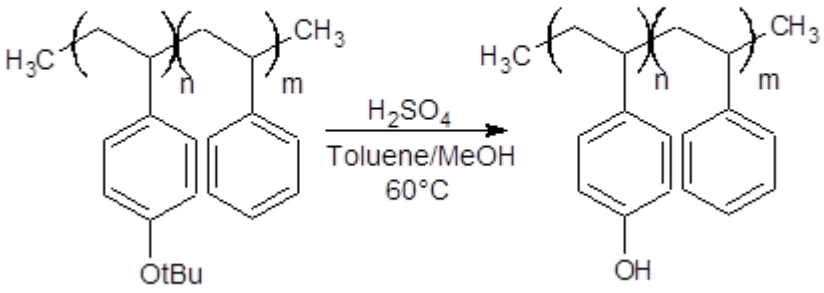

Schematic 2.2

FTIR spectra (Figure 2.7) confirmed that the deprotection had occurred as shown by the disappearance of the peaks corresponding to the tert-butoxy groups at 1365 and 1388 cm^{-1}. NMR spectra were not collected for these samples as they were found insoluble in common ^{1}H NMR solvents.

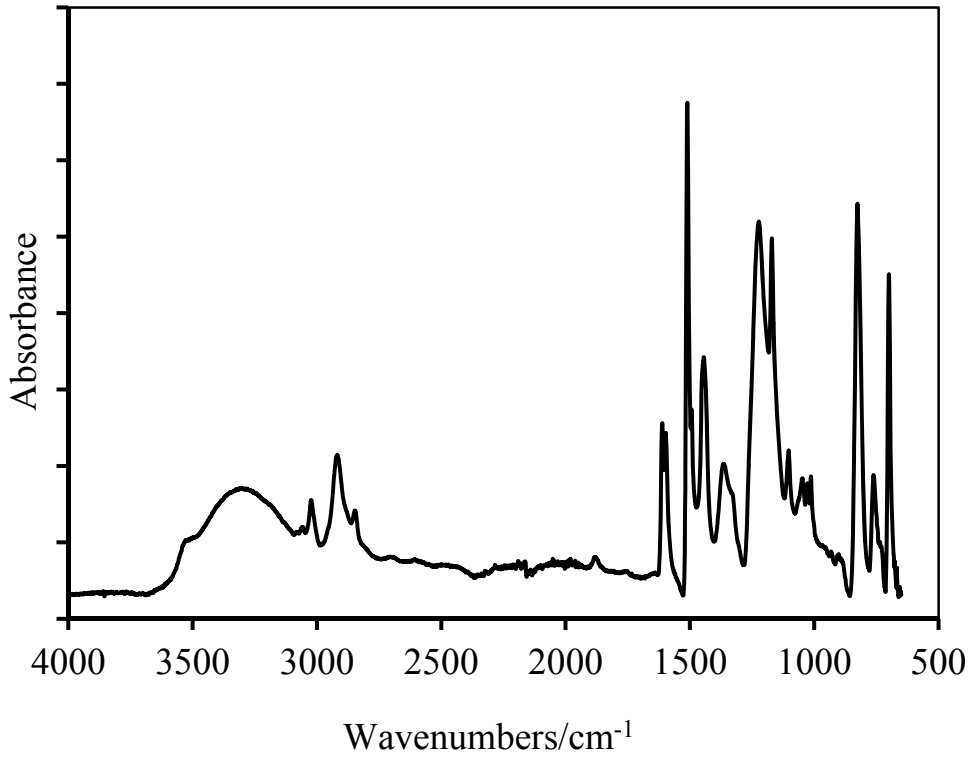

Figure 2.7 FTIR spectrum of styrene-co-4-hydroxystyrene copolymer with 70 mole-% HS in the feed.

Procedure 3

0.5 g StBuS was dissolved in 18 ml acetone (HPLC grade) and then concentrated HCl (3ml) was added. The reaction was heated to reflux at 50^{o}C (Schematic 2.3).

The conversion was allowed to proceed overnight with stirring; followed by slow cooling to room temperature. The solution was poured into excess hexane (20 times) to precipitate the copolymer. The sample was filtered, re-washed in hexane, then filtered and left in the fume-cupboard overnight to evaporate most of the solvent. The residue was dried in a vacuum oven for 4 hours at 85^{o}C. The sample was readily dissolved in DMSO-d_6 and H^1 NMR result indicated that the impurity have all been reduced (Figure 2.8).

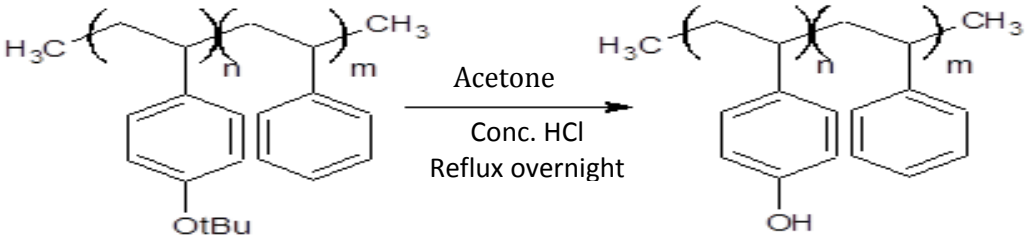

Schematic 2.3

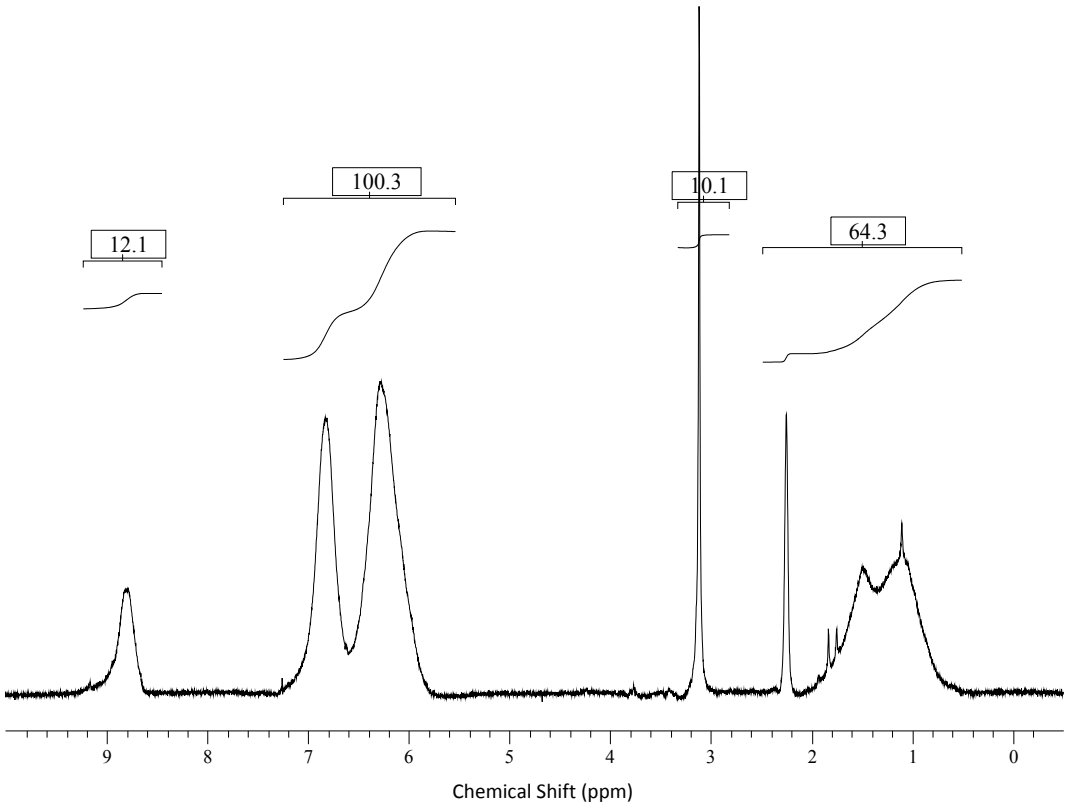

Figure 2.8 H^1NMR spectrum of a styrene-co-4-hydroxystyrene with 70 mole-% HS in the feed.

2.3.3 Synthesis of poly (methyl methacrylate -co- ethyl methacrylate) (PMEMA)

Methyl methacrylate (MMA) and ethyl methacrylate (EMA) monomers were first washed with 1M NaOH solution to remove the inhibitor (i.e. monomethyl ether hydroquinone), followed by washing with 1M HCl and then H_2O.

The final aqueous layer was tested with litmus paper to ensure that no acid or base was left trapped in the monomers. $MgSO_4$ was used to dry the organic layer.

Solutions of MMA and EMA monomers with AIBN (0.5 mole-% relative to total monomer content) as initiator were added in a polymerisation tube.

The polymerisation tube was sealed, purged with N_2 gas for 2-3 minutes and placed in a water bath at 60^{o}C for 30 min. The reaction was then cooled rapidly to stop further polymerisation.

The monomer and initiator contents are given in *Table 2.3*. This produced monomer

feed ratios of 0.80 (PMEMA 1), 0.53 (PMEMA 2), and 0.22 (PMEMA 3) in mole fraction of MMA.

Table 2.3: Quantities of reactants used in the preparation of PMEMA copolymers

	PMEMA 1		PMEMA2		PMEMA3	
	Mass (g)	m moles	Mass (g)	m moles	Mass (g)	m moles
EMA	4	35.05	10	87.61	16	140.18
MMA	16	159.81	10	99.88	4	39.95
AIBN	0.159	0.00097	0.154	0.00094	0.148	0.00090

Copolymer samples were precipitated into methanol, filtered, dissolved in chloroform and then re-precipitated in methanol. Copolymers were dried in a vacuum oven at 80 ^{o}C for 24 hours.

Analytical data are presented for the PMEMA 2 copolymer (Figure 2.9). ^{1}H NMR ($CDCl_3$, 200MHz), δ: 1.35 (broad s, backbone CH_2), δ: 1.85 (broad s, backbone CH), 3.39 (s, -OCH_3), 3.76 (s, -OCH_2). Copolymer compositions were determined using ^{1}H NMR in $CDCl_3$ by comparing the peak area of the -OCH_3 (3 protons) group at 3.39ppm with the peak area of the -OCH_2 (2 protons) groups at 3.76 ppm.

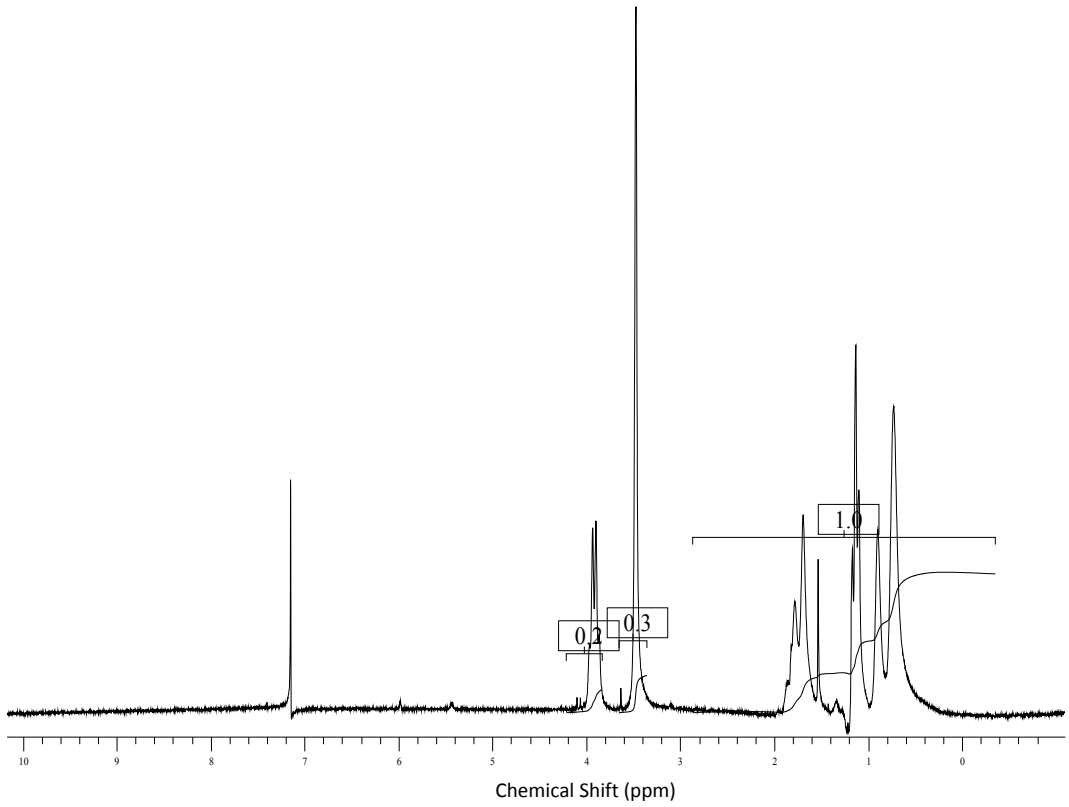

Figure 2.9 ^{1}H NMR spectrum of PMEMA 2

2.4 Poly(4-hydroxystyrene) deuterated

2.4.1. Synthesis of deuterated polystyrene (PS-d_5)

The Willenberg [124] procedure was used to synthesise deuterated polymers, PS. This consisted of the following steps:

1- Dissolve 0.5 g of polystyrene in 4.5 g benzene-d6 to obtain a 10 wt% polymer solution.
2- For 1g from above solution added 0.144 ml from a 1 M ethylaluminum dichloride solution (17.4 wt% = 1 M, for the calculation see appendix).
3- As co-catalyst 20 µl of water were added until the solution was yellow-orange in colour.
4- The solution was left stirring slowly at room temperature for 4 h.

5- To destroy the catalyst excess water was added (≈ 30µl).

6- The polystyrene was precipitated in 20 times methanol while stirring and freed from residuals of catalyst with methanolic HCl (≈ 1 ml).

The procedure gave good results with PS. Figure 2.12 (a, b) shows the ^{1}H NMR spectra of PS and PS-d ($CDCl_3$ as solvent), respectively. As shown in Figure 2.12, the peaks corresponding to protons in the aromatic group which are present in spectrum (a) are no longer evident in Figure 2.12 (b). The integration values indicate that all protons on the benzene ring have been replaced by deuterium.

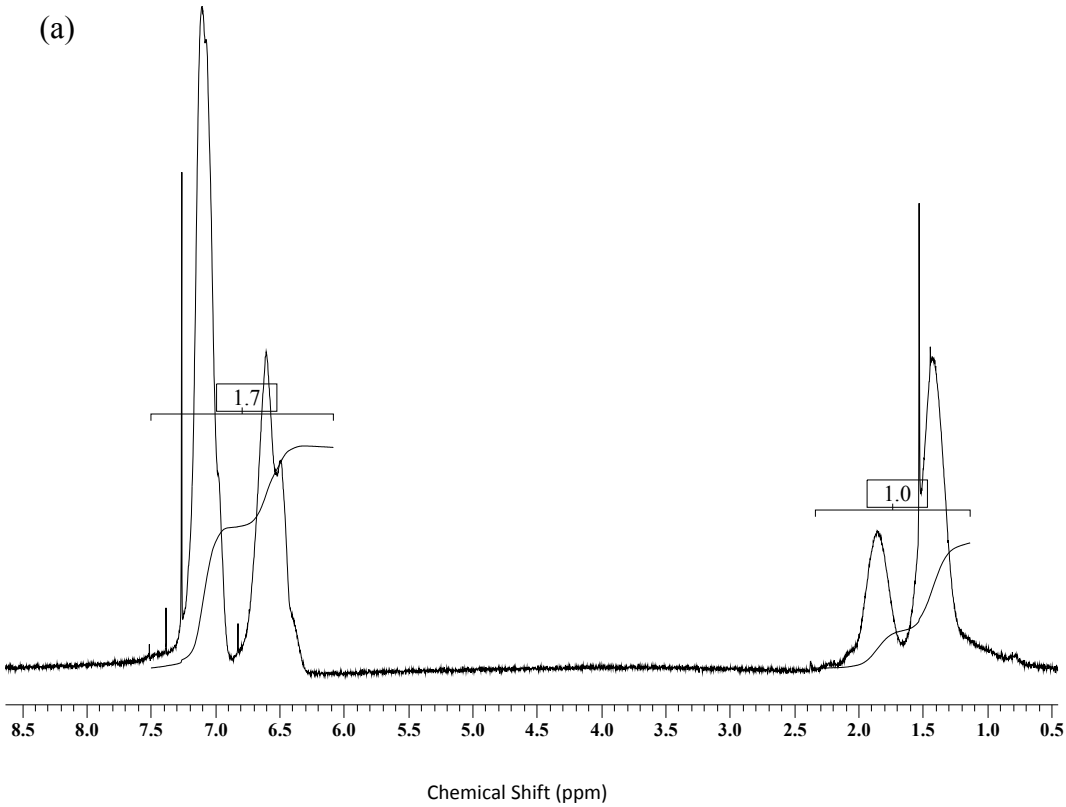

Figure 2.12(a)

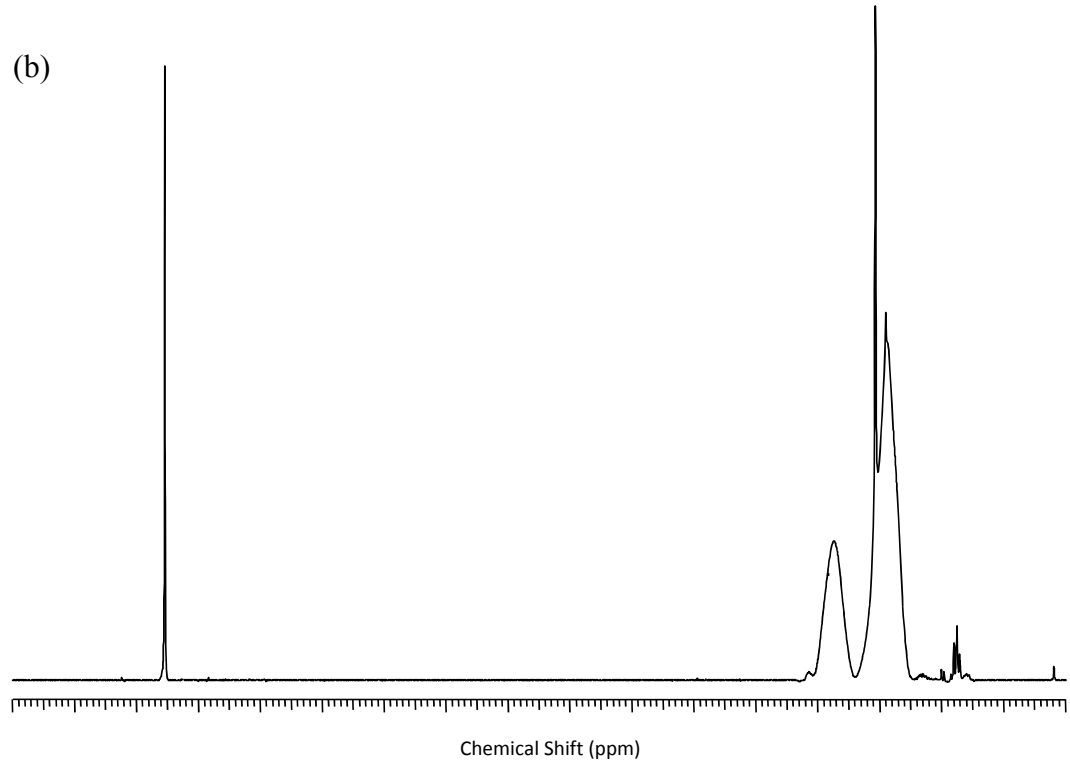

Figure 2.12(b)

Figure 2.12 (a) and (b) ^{1}H NMR spectra of PS before and after deuteration, respectively

2.4.2. Synthesis of deuterated poly(4-acetylstyrene) (ACPS-d_4)

Polystyrene-d5 2.60 g was dissolved in 25 ml cyclohexane. A three-necked round–bottom flask equipped with a condenser, dropping funnel, and magnetic stirrer was placed in a hot bath at 55 °C. $AlCl_3$ (6.7 g) and 25 ml cyclohexane were added and the mixture was stirred vigorously. To this solution (3.5 ml) acetyl chloride (CH_3COCl) was added drop-wise. The reaction mixture turned yellow, with the evolution of hydrogen chloride (HCl) gas during the addition. The reaction was continued for 7 hours until the evolution of hydrogen chloride had ceased. The reaction was stopped, and cyclohexane was removed by rotary evaporation. The residue (light yellow) was air dried overnight and transferred into a beaker containing 100 g crushed ice and 5 ml hydrochloric acid. The precipitate was filtered, dried in vacuum oven at 80 °C for 2h (aluminium chloride decomposed and the polymer was obtained as a yellow precipitate) and then dissolved in 6.5 ml acetone, and precipitated in water.

The Suspension was dissolved in 5.5 ml THF and then precipitated in methanol. Yield: 2.80 g (77.7%). Figure 2.13 shows FTIR spectrum $\nu(cm^{-1})$ of ACPS-d_4: 2923, 2845 alkyl (C-H), 2272 (C-D aromatic), 1677 (C=O) and 1576 (Ar-C=C). ^1H NMR spectrum is shown in Figure 2.14. The ^1H NMR spectrum of ACPS-d_4, when compared to PS-d_5 shows a new signal at 2.5pmm which is attributed to the methyl (CH_3) protons of acetyl moiety and a new signal due to the protons ortho to acetyl group appears around 7.53 ppm; however, in the aromatic region, the broad signal intensity at 7.20 ppm is reduced.

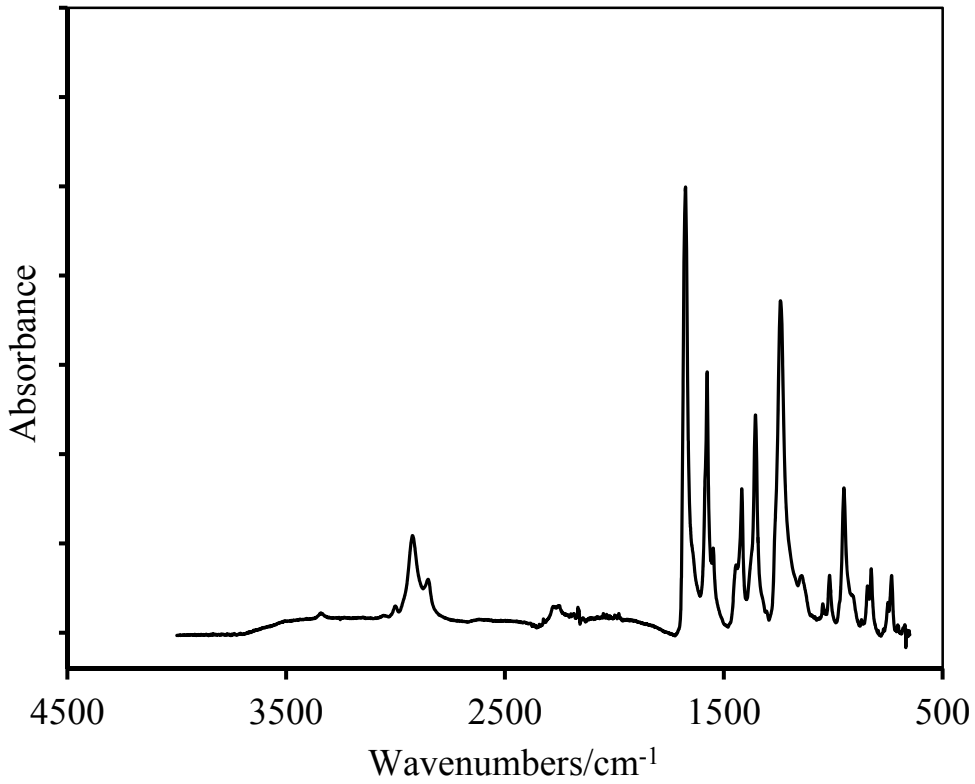

Figure 2.13 FTIR spectrum of ACPS-d_4

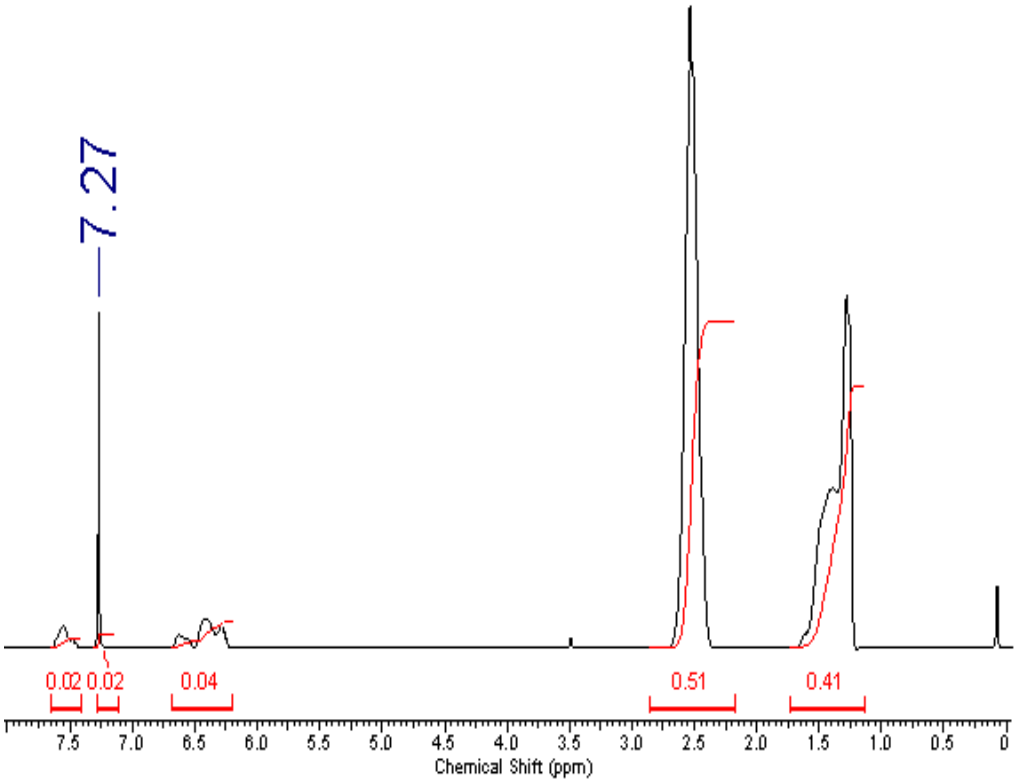

Figure 2.14 ^{1}H NMR spectrum of ACPS-d4

2.4.3. Oxidation of poly(4-acetyl styrene)-d$_4$

Poly4-acetyl styrene-d_4 (ACPS-d_4) (1.0 g, 6.66 mmol) was dissolved in 25 mL $CHCl_3$. This was added to an oxidizing solution consisting of 5 mL of acetic anhydride, 5 mL 30% H_2O_2, and trace amounts of concentrated H_2SO_4 (as the catalyst) and refluxed for 142 h at 85°C. At the end of every 12 h, 2.5 mL of acetic anhydride and 2.5 mL of H_2O_2 were added. After 142 hours the reaction was stopped, the organic layer was separated with a separating funnel and precipitated into 20 times methanol. The precipitate was filtered and dried under vacuum. Yield: 1.3 g (63%). FTIR spectrum *v* (cm^{-1}) of PAS-d_4 are plotted in Figure 2.15: 3024 (Ar- C-H), 2965, 2845 alkyl (C-H), 1720 (O-C=O). The FTIR spectrum showed the appearance of a new peak at 1720 cm^{-1} as a result of new ester C=O stretch (for the acetoxy group), instead of aromatic ketone C=O stretch of acetyl group at 1670 cm^{-1}. The appearance of broad peak at 3430 cm^{-1} indicates that part of PAS-d has converted to P4HS-d, and for this reason was very difficult to measure ^{1}H NMR spectrum.

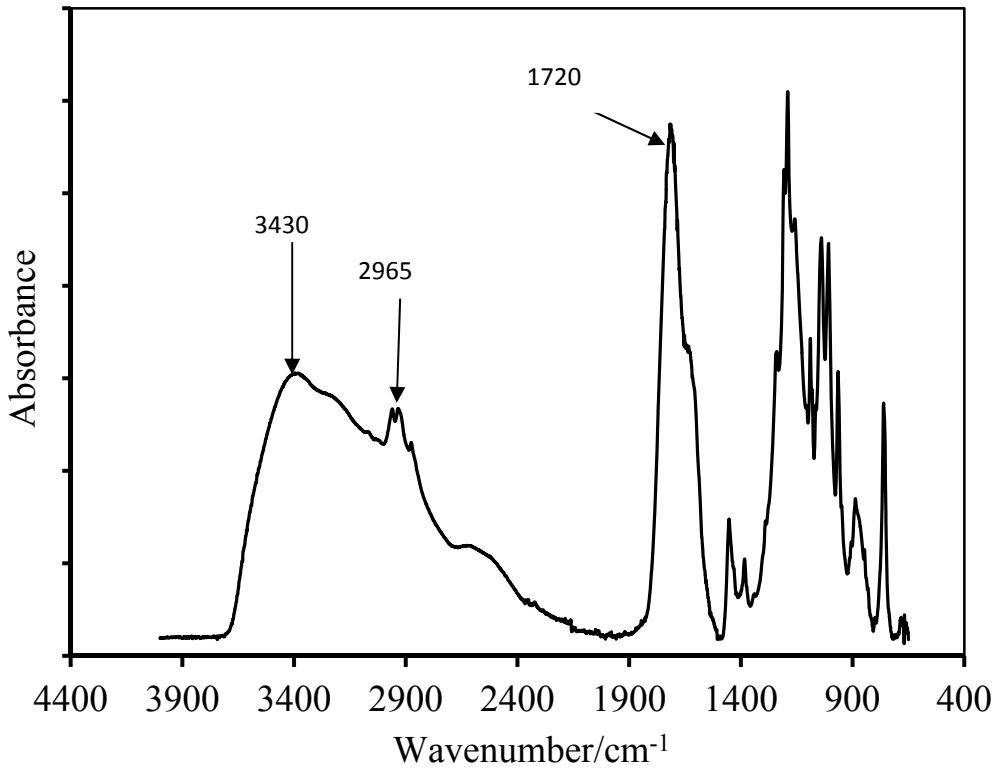

Figure 2.15 FTIR spectrum of PAS-d4

2.4.4 Hydrolysis of deuterated poly(4-Acetoxystyrene) (P4AS-d_4)

Poly(4-acetoxystyrene)-d_4 (50 mg, 0.30 mmol) was dissolved in 2 mL of acetone. To this mixture 0.3 mL of concentrated HCl was added. The mixture was stirred at 50 °C overnight under reflux, followed by cooling to room temperature. The mixture was poured into hexane to precipitate the polymer. The precipitate was filtered, re-dissolved in hexane and then left in the fume-cupboard overnight to evaporate most of the solvent. The solid polymer was dried in a vacuum oven for 4 hours at 85 °C. Yield 25 mg (67%). Figure 2.16 shows FTIR spectrum ν(cm^{-1}) of P4HS-d_4: 3024(Ar-C-H), 2923, 2845 alkyl (C-H), 3300-3500 (OH). The strong carbonyl absorption peak at 1720 cm^{-1} has disappeared. A ^{1}H NMR spectrum (Figure 2.17) also confirms that all PAS-d has converted to P4HS-d, where there is not appearance of strong signal at 2.25 ppm of acetoxy methyl group.

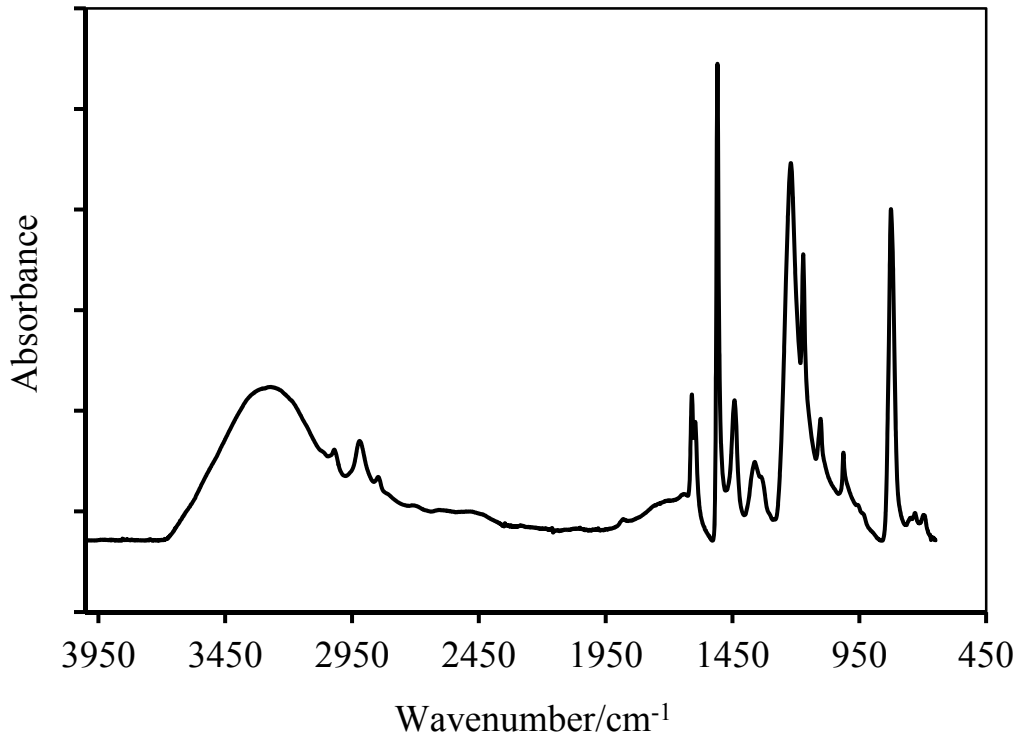

Figure 2.16 FTIR spectrum of P4HS-d4

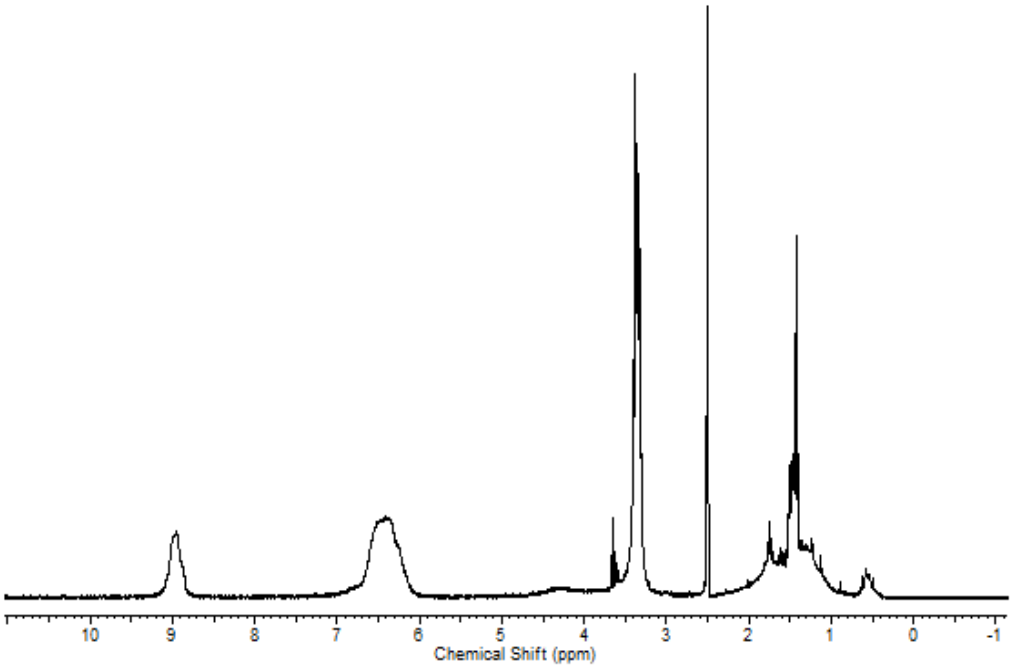

Figure 2.17 ^{1}H NMR spectrum of P4HS-d4

2.5 Blend preparation

2.5.1 Blends of poly (4-hydroxystyrene)/polyethylene oxide (P4HS/PEO)

P4HS/PEO blends were prepared by mixing appropriate amounts of PEO (M_w = 100,000) and P4HS (M_w = 22,000) in 2% (w/v) tetrahydrofuran (THF) solution at 323 K. Special care was taken to remove the solvent from the films. Thus, samples first were left overnight in the fume cupboard and then dried in a vacuum oven at 343 K for two weeks, followed by heating at 423 K for 3 h (under vacuum) and subsequent slow cooling to room temperature. This thermal treatment was found to be effective in removing all residual solvent as indicated by measurements of the the glass transition temperature (T_g) of P4HS (which was found to be significantly depressed when residual THF remains in the sample). The number of moles of each component in the blend and the glass transition temperature, T_g, was determined (Table 2.7) from the amount of polymer and molecular weight of monomers.

Table 2.7 Glass transition temperatures for P4HS/PEO blends

wt% P4HS	mol% P4HS	T_g(mid-point)/K
0	0	216
70	46	350
80	59	370
85	67	405
95	87	415
100	100	427

2.5.2 Blends of poly(4-hydroxystyrene)/poly(ethyl methacrylate) (P4HS/PEMA)

P4HS/PEMA blends of varying composition were prepared by casting solutions containing 2% (w/v) polymer solutions in methyl ethyl ketone (MEK) onto glass plates at room temperature. After drying at room temperature, the samples were transferred to

a vacuum oven at 353 K and dried for 1 day, followed by heating at 423 K for 3 h and then slow cooling to room temperature.

Table 2.8 Glass transition temperatures for P4HS/PEMA blends

wt.% P4HS	mol%P4HS	T_g(mid-point)/K
0	0	347
25	24	376
50	49	397
75	74	414
80	79	420

2.5.3 Blends of styrene-co-4-hydroxystyrene)/polyethylene oxide (SHS/PEO)

SHS/PEO blends were prepared by casting from THF solutions containing 5 wt.-% polymer mixtures, stirred for 6-8 h. The solutions were allowed to evaporate slowly at room temperature for 1 day. The obtained film was dried in a vacuum oven at 50 ^{o}C for 2 days.

Table 2.9 Glass transition temperatures for 59/41 SHS/PEO blends

wt.-% of HS in SHS	mole.-% of HS in SHS	T_g (mid-point)/K
33	30	354
54	50	360
73	70	374

2.5.4 Blends of styrene-co-4-hydroxystyrene/poly(alkyl methacrylate) (SHS/PMMA or PEMA)

The blends were produced by co-dissolution of the relevant components at 59/41 mole ratios in methyl ethyl ketone (MEK) and allowing the solvent to evaporate.

Samples were dried in an oven at 383 K for 24 hours, followed by 48 hours in a vacuum oven at 333 K. Samples were stored in a desiccator prior to use.

Table 2.10 Glass transition temperatures for 59/41 SHS /PMMA blends

Sample	T_g (mid-point) / K
PMMA	385
SHS30/PMMA	401
SHS50/PMMA	409
SHS70/PMMA	419
P4HS PMMA	411

2.5.5 Blends of poly(4-hydroxystyrene)/poly(4-vinylpyridine) (P4HS/P4VP)

Total 0.5g P4HS and P4VP polymers were dissolved in 10 ml N, N-dimethylformamide (DMF). The solution was slowly evaporated at 60 ^{o}C for 3 days; the residual solvent was removed under vacuum at 80 ^{o}C for 1 week.

Table 2.12 Glass transition temperatures for P4HS/P4VP blends

wt.-% P4HS	mole.-% P4HS	T_g (mid)/K
0	0	425
62	59	433
70	67	437
100	100	427

Chapter 3 Enthalpy relaxation of homopolymers and copolymers

3.1 Introduction

In order to investigate the effect of blending on physical aging, it is essential to first collect and analyse in detail the enthalpy relaxation process of the individual blend components. Data can then be obtained for various blend compositions at comparable undercoolings from the glass transition temperature. The C-F equation was employed throughout this work to analyse enthalpy relaxation.

In the following sections, the enthalpic relaxation behaviour of the following homopolymers and copolymers is reported: P4HS, SHS, PEMA, PMEMA, P4VPy and PEO. Since the miscible blends investigated in this work are polymer/polymer or polymer/copolymer mixtures which interact via hydrogen bonding, FTIR measurements were carried out to understand better the effect of interaction between OH groups in P4HS and SHS copolymers.

3.2 Poly(4-hydroxystyrene)and styrene-co-4-hydroxystyrene

3.2.1 Infrared spectroscopy of styrene-co-4-hydroxystyrene

Xu *et al* found that P4HS strongly self-associates through inter and intra-molecular hydrogen bonding of the phenolic hydroxyl groups [46]. Infrared spectroscopy is extremely sensitive to this occurrence. In undiluted P4HS, an absorption peak due to the free hydroxyl stretching vibration is expected to occur at 3530 cm^{-1}. Self-association of phenolic groups in pure P4HS contributes to the vibrational absorption band in the region 3250 cm^{-1} to 3400 cm^{-1}. The P4HS IR spectrum in Figure 3.1 confirms the presence of these bands.

When P4HS is copolymerised with styrene, the interacting OH groups are essentially “diluted”, but infrared spectroscopy is still sensitive to the H-bonding present. Indeed, the SHS copolymers can be looked upon as systems in which H-bonding is diluted by the non-interacting styrene repeat units. This cannot be favourable, since the PHS and PS homopolymers are mutually immiscible [125-127]. However, calculations based on infrared measurements indicate that the free OH fraction changes very little from P4HS to a copolymer with 50 mol% HS composition [113].

As shown in Figure 3.1, the SHS copolymers prepared in this study all displayed very broad -OH stretching bands in the range 3600 to 3100 cm^{-1} as a result of contributions from the stretching modes of free, intra-molecular and intermolecular hydrogen bonding (from high to low wavenumber). There was no distinct "free" -OH stretching band, but a shoulder can be seen tailing towards the high frequency side. This result suggests that the SHS systems are strongly self-associated, which is not surprising, given the acidity of the phenolic –OH groups. Devlin observed a "free" –OH stretching component for SHS copolymers in his study, however, the systems in question had very low levels of HS (typically < 3 mole % HS in the feed) and would be effectively diluted by the styrene co-monomer [128].

Interpretation of the hydroxyl stretching band is more complicated than, say, a carbonyl stretch absorption [129] and consequently the spectra recorded in this study have little more than qualitative value. Also, it should be noted that it is difficult to measure self-association constants for P4HS due to its insolubility in inert solvents, so the extent of H-bonding cannot be quantitavely estimated [130].

However, to separate the various contributions, the second derivative of each spectrum can be calculated using a modified Savitzky-Golay method [131-133] . As can be seen in Figure 3.2, the original band becomes much narrower and the minimum provides its location. Therefore, by using the second derivative, various contributions can be resolved. Data in Figure 3.2 show that the absorption peak due to intermolecular hydrogen bonds is located at about 3280 cm^{-1}. Zhang and co-workers [91] report that the difference in wavenumber ($\Delta\nu$) between the absorption bands of hydrogen-bonded and free hydroxyl groups could be used as a measure of the relative strength of hydrogen bonding. According to this, the large value of $\Delta\nu \cong 250$ cm^{-1} intermolecular interactions measure for the copolymers are indicates that intermolecular interactions stronger than the intra-molecular one are located at 3390 cm^{-1}, with $\Delta\nu \cong 140$ cm^{-1}. For more clarification the important data from Figure 3.2 are listed in Table 3.1. The tabulated results indicate that the positions of all intra- and inter-association peaks are not affected by copolymer composition, as demonstrated in Table 3.1; for example, the position of intra-molecular hydrogen bonds of SHS30 is 3396 cm^{-1} and the position with P4HS is 3393.

Additionally, the peak maximum of the free OH shoulders in all copolymers is similar, which is in good agreement with the results of Zhang et al. results [53]. On the other hand, the peak maximum values of intra and intermolecular interactions in the copolymer increase with the increasing of hydroxyl groups in the composition.

Table 3.1-The position of hydrogen-bonded OH bands of P4HS and SHS copolymers (data from second derivative)

SHS mol% HS	*30*	*50*	*70*	*100*
The position of intra-molecular HB/cm^{-1}	3396	3396	3395	3393
The position of intermolecular HB/cm^{-1}	3285	3284	3283	3283

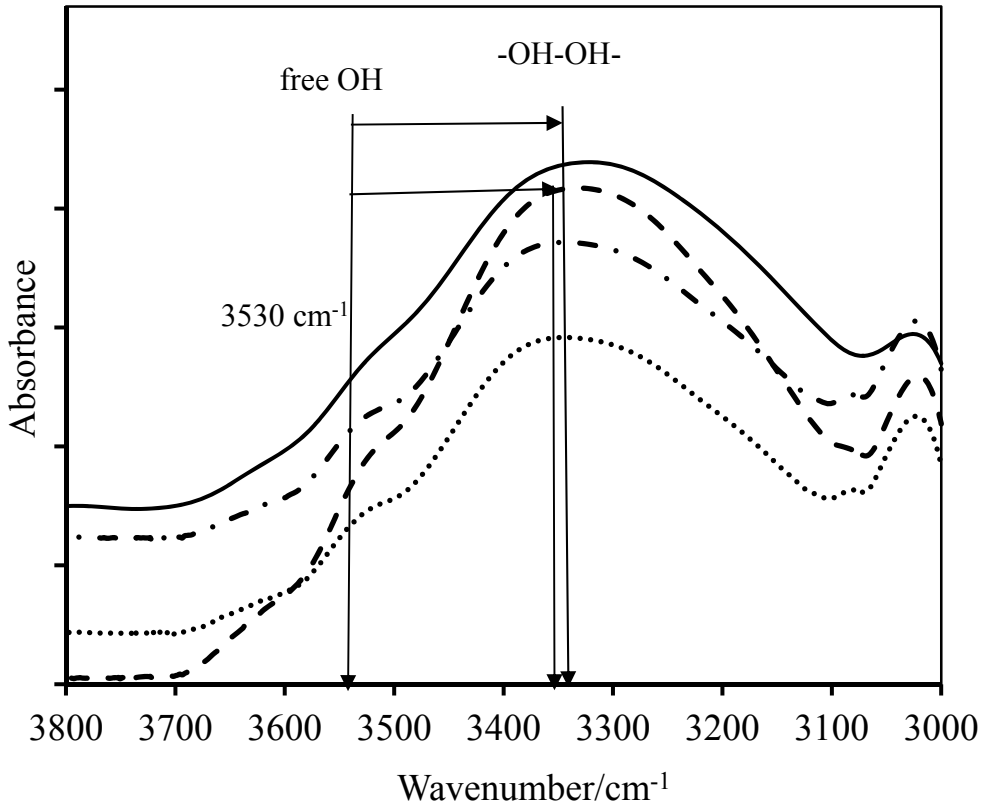

Figure 3.1 FTIR spectra recorded at room temperature in the 3800-3000 cm^{-1} region for P4HS and SHS copolymers: (……) 30, (—•—•—) 50, (— — —) 70, and (———) 100 mole-% HS.

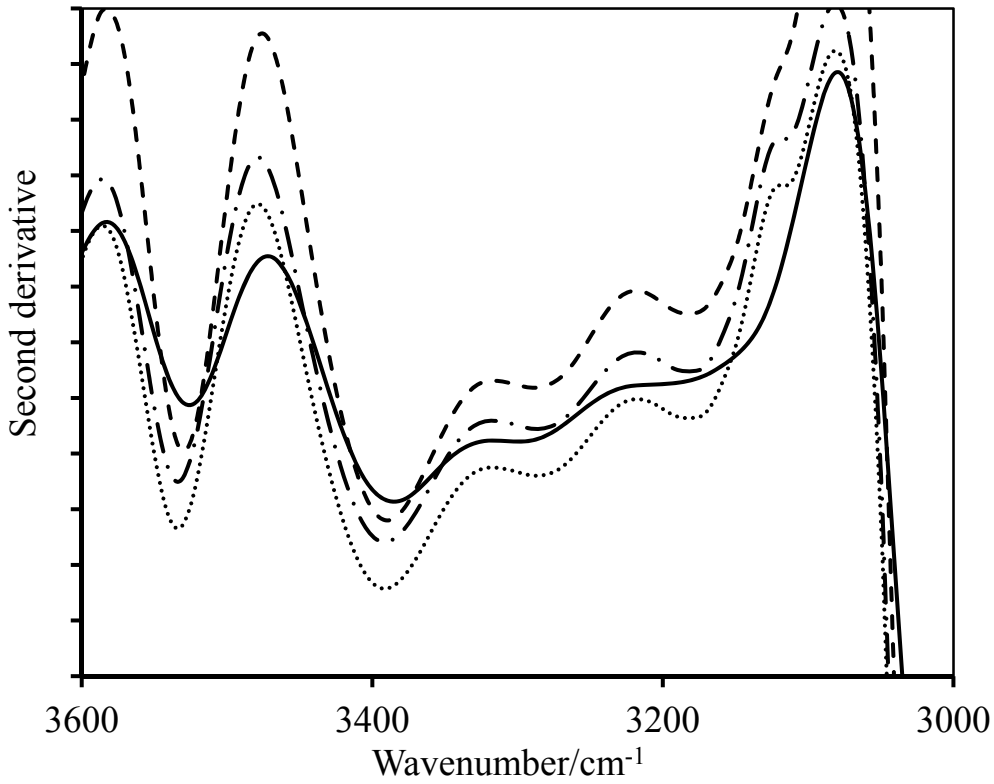

Figure 3.2 Second derivative spectra of P4HS and SHS copolymers: (.....) 30, (—•—•—) 50, (— — —) 70, and (———) 100 mole-% HS.

When trying to interpret subsequent experimental results, it is worth bearing in mind that the less stabilised the system is by H-bonding, the more similar its behaviour will be to that of polystyrene. This, however, will be temperature dependent. As the temperature is decreased, the H-bonds sequences in the chains are expected to lengthen, bringing the copolymer behaviour closer to that of P4HS[134]. The FTIR spectra in this study were collected at ambient temperature, which may explain why the spectra for the SHS copolymers resemble that of P4HS.

3.2.1.2 Effect of temperature on hydrogen bonding

The temperature dependence of the H-bonding interactions was investigated by collecting a series of FTIR spectra, on heating. As shown in Figure 3.3 for P4HS, the intensity of the band at 3530 cm^{-1}(free hydroxyl group) increases as the temperature is increased, whereas the one due to self-association shifts to a higher wavenumber with increasing temperature (Figure 3.3). This indicates that the strength of self-associating

bonds decreases with increasing temperature. However, these bonds still exist even at temperatures as high as 150 ^{o}C.

The broad peaks in the range between 3280 and 3450 cm^{-1} comprise contributions from intra and intermolecular interactions and it is difficult to determine the accurate location of these bands. To resolve this, the second derivative of each spectrum was calculated (Figure 3.4). For further clarification, the spectrum data from Figure 3.4 were tabulated (Table 3.2). At 25^{o}C, the intermolecular OH band (peak maximum located at 3283 cm^{-1}) with $\Delta v \cong 248$ cm^{-1} is much stronger than the intra-molecular one (peak maximum located at 3390) with $\Delta v \cong 140$ cm^{-1}. However, with increasing temperature, the intra-molecular peak shifts towards higher wavenumbers and the intermolecular band disappears when the temperature reaches 100 ^{o}C or higher. In contrast, the intensity of peak maximum of the band of free hydroxyl groups increases as the temperature increases. Consequently, we can report that, at higher temperature, the intra-molecular interactions in P4HS dominate the polymer structure, at the expense of intermolecular bonds.

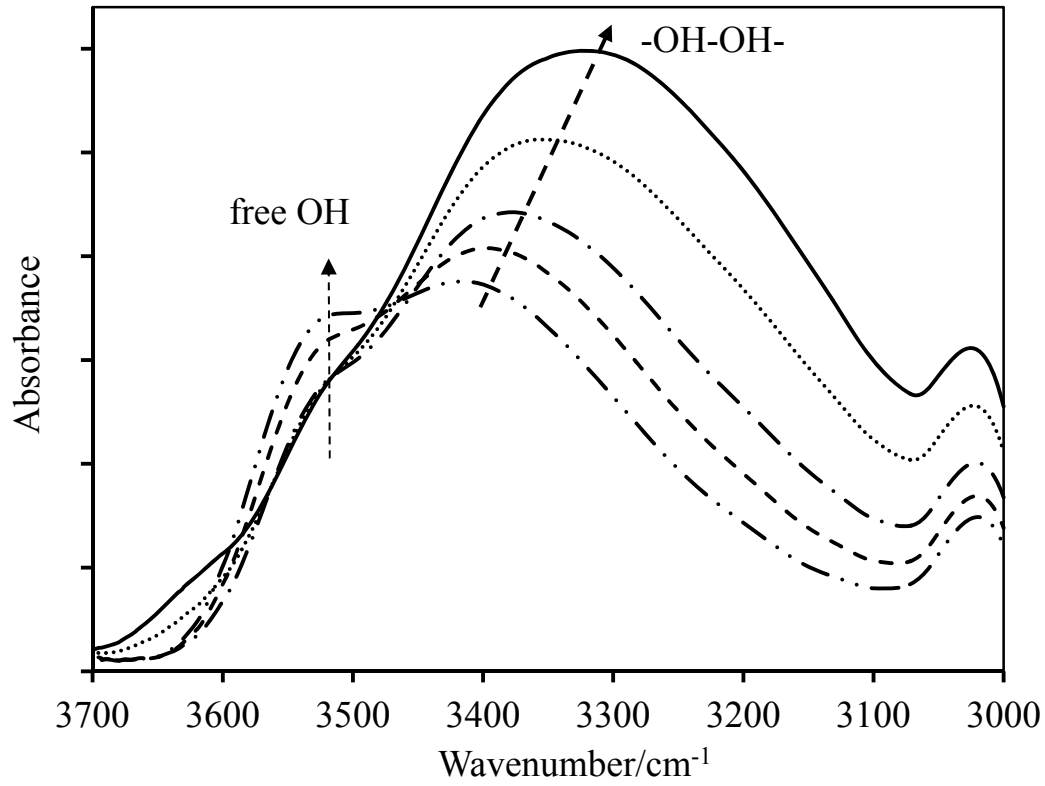

Figure 3.3 FTIR spectra recorded at different temperatures in the3700-3000 cm^{-1} region for pure P4HS: (———) 25 ^{o}C, (……..) 50 ^{o}C, (—•—•—) 100 ^{o}C, (— — —) 125 ^{o}C and (—••—••—) 150 ^{o}C.

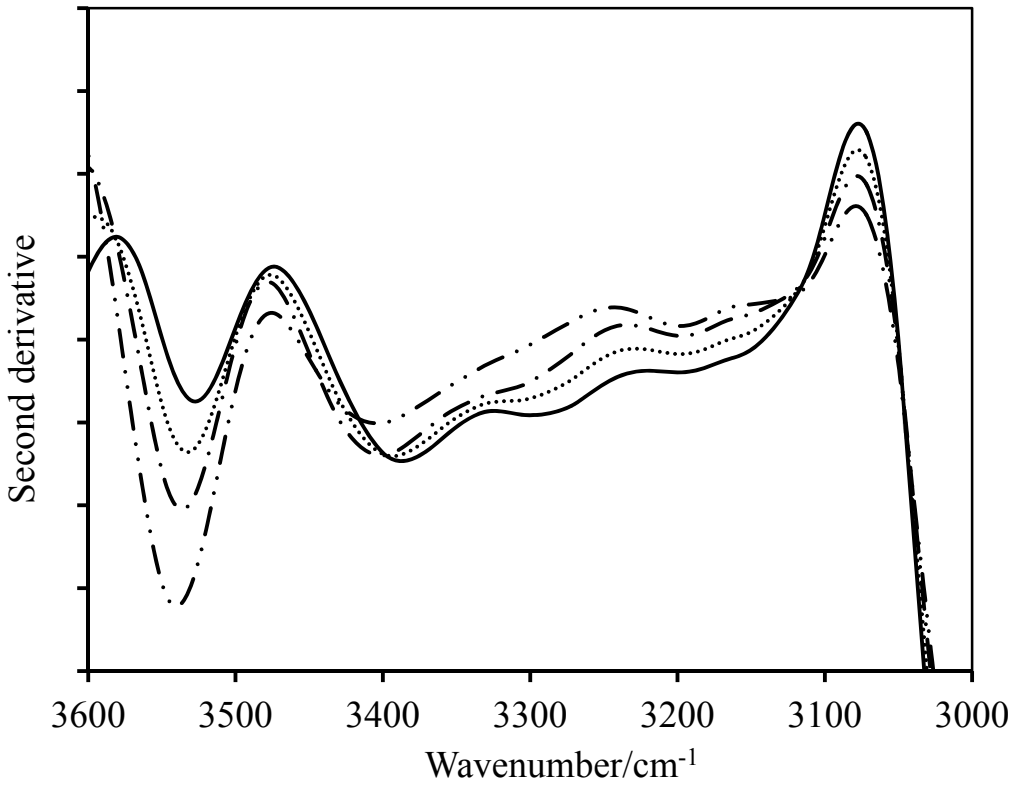

Figure 3.4 Second derivative spectra at different temperatures in the 3700-3000 cm^{-1} region for pure P4HS: (———) 25 ^{o}C, (.....) 50 ^{o}C, (—•—•—) 100 ^{o}C, and (—••—••—) 150 ^{o}C.

Table 3.2- The position of hydrogen-bonded OH bands of P4HS at different temperatures (data collected from Figure 3.4)

Temperature/^{o}C	*25*	*50*	*100*	*150*
The position of intramolecular HB/cm^{-1}	*3390*	*3398*	*3404*	*3410*
The position of intermolecular HB/cm^{-1}	*3283*	*3292*	----------	--------

Figure 3.5 displays the FTIR spectra of SHS copolymers at 150^{o}C. From Figure 3.5, it can be seen that the area under the absorption band at 3390 cm^{-1} decreases and the peak shifts to higher wavenumbers with increasing the temperature. On the other hand, the intensity of the absorption band associated with free hydroxyl groups at 3533 cm^{-1} increases with increasing temperature. The second derivative of each spectrum was calculated (Figure 3.6), and the data from the spectrum shown in Figure 3.6 were tabulated (Table 3.3). The results indicate that as the temperature increases, the band of

intermolecular hydrogen bond interactions does not appear and the band of intra-molecular hydrogen bond interactions shifts to high wav number. Thus, we can conclude that intermolecular hydrogen bonds in SHS copolymers are more affected by temperature than intra-molecular ones. Moreover, the presence of styrene units originates a kind of segregation between SHS chains, which will in tum lead to increase the distance between hydroxyl groups. Consequently, hydroxyl groups of any SHS chain are unable to interact with other hydroxyl groups on other chains, and that will cause an increase of free hydroxyl groups at the expense of intermolecular hydrogen bonds.

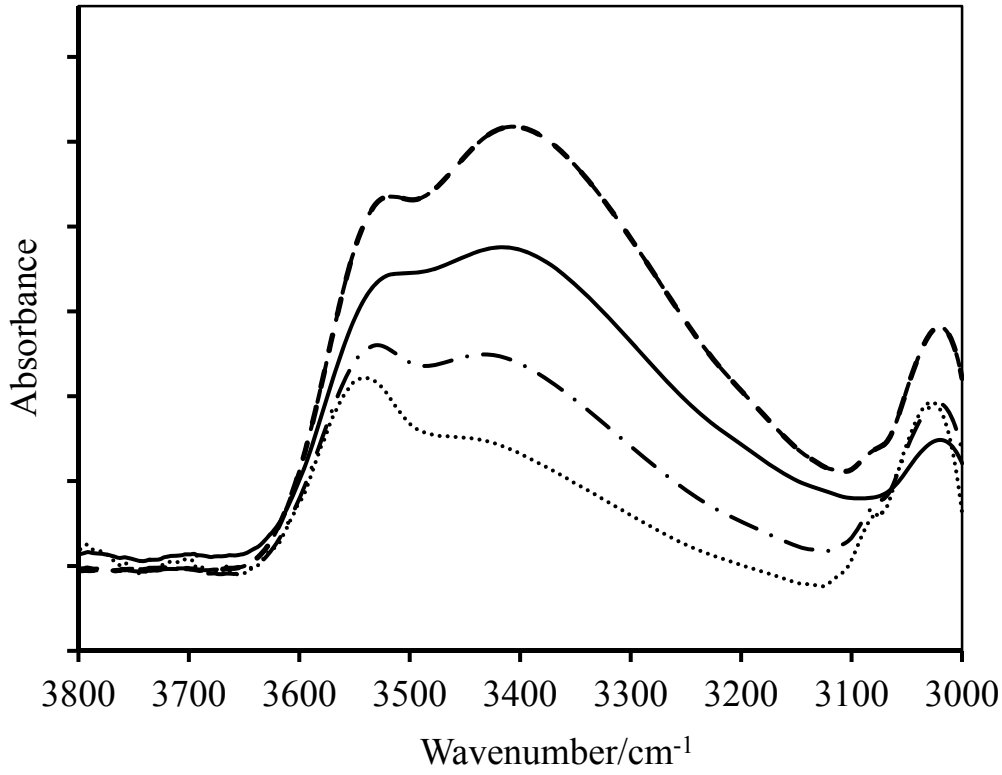

Figure 3.5 FTIR spectra recorded at 150 ^{o}C the 3800-3000 cm^{-1} region for SHS copolymers: (……) 30, (—•—•—) 50, (— — —) 70, and (———) 100 mole-% HS.

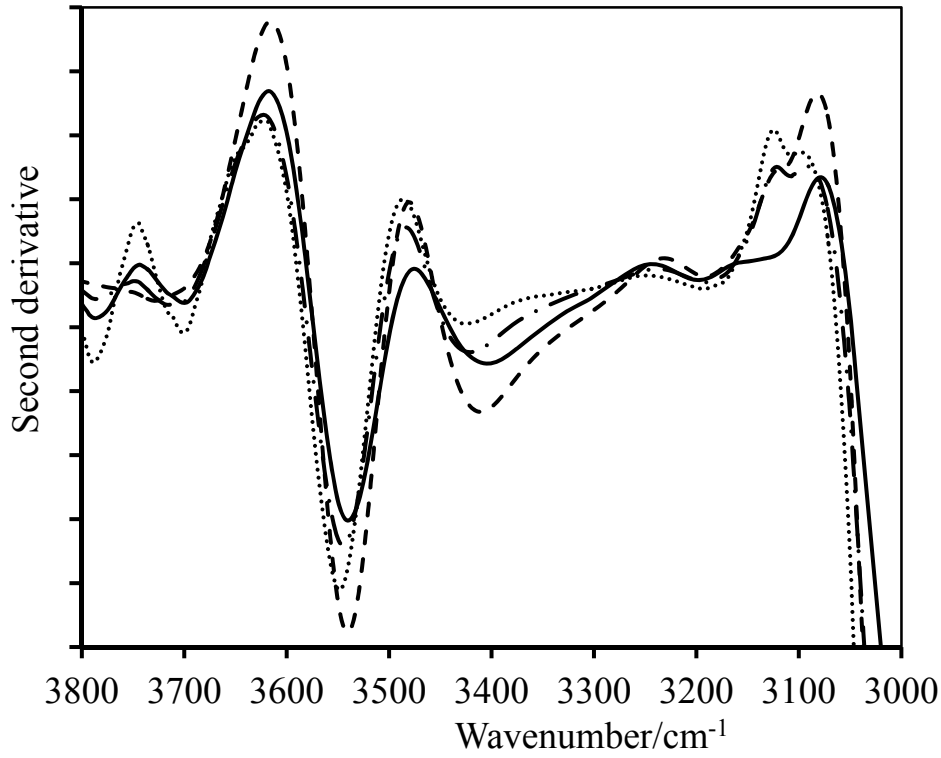

Figure 3.6 Second derivative spectra at 150 °C the 3800-3000 cm^{-1} region for SHS copolymers: (.....) 30, (—•—•—) 50, (— — —) 70, and (———) 100 mole-% HS.

Table 3.3-The position of hydrogen-bonded OH bands of SHS copolymers at150 °C (data from second derivative)

SHS mol% HS	*30*	*50*	*70*	*100*
The position of intra-molecular HB/cm^{-1}	3442	3430	3421	3410
The position of intermolecular HB/cm^{-1}	--------	--------	--------	----------

3.2.2 Enthalpy relaxation of neat P4HS and SHS copolymers

In this thesis, the polymer P4HS plays the role of the reference system, since it is one of the components in all the polymer blends under study. It is therefore necessary to characterize the P4HS behaviour as accurately as possible in order to make an adequate comparison with the blends. Aging data on P4HS are limited in the literature [18, 95]. Thus, it was decided to re-measure the enthalpy relaxation of a 22000 g mol^{-1} sample.

This was due to the fact that enthalpy relaxation appears to change slightly with molecular weight[18, 135].

3.2.2.1 Enthalpy relaxation of P4HS

It is common practice, before carrying out aging experiments, to monitor the thermal stability of the polymer by collecting a series of DSC scans, on heating after cycling through the chosen thermal history several times (without aging). Usually, T_g reaches a constant value after the 7 cycle runs, indicating that structural equilibrium has been reached.

P4HS was dried in a vacuum oven at 120^{o}C for 1 day, annealed at 220^{o}C for 30 min (under vacuum) and then cooled back to ambient temperature in the vacuum oven. T_g value of this sample recorded by heating to 214^{o}C at 20^{o}C/min in DSC; the T_g value was found to be 154^{o}C.

Aging experiments were carried out on P4HS at three temperatures in the range 422 K (T_g-5) to 412 K (T_g-15), in 5 K steps. After each aging step, the DSC trace of an unaged sample is collected. Physical aging is a reversible phenomenon and so one expects T_g to be the same after aging (i.e. when a glassy material is heated above the T_g any previous aging that had occurred will be erased).

The results reported in Figure 3.7 (unaged traces) show that all T_g values are in the range between 153.5^{o}C (426.5K) to 155^{o}C (428K), indicating that T_g is constant within instrumental error.

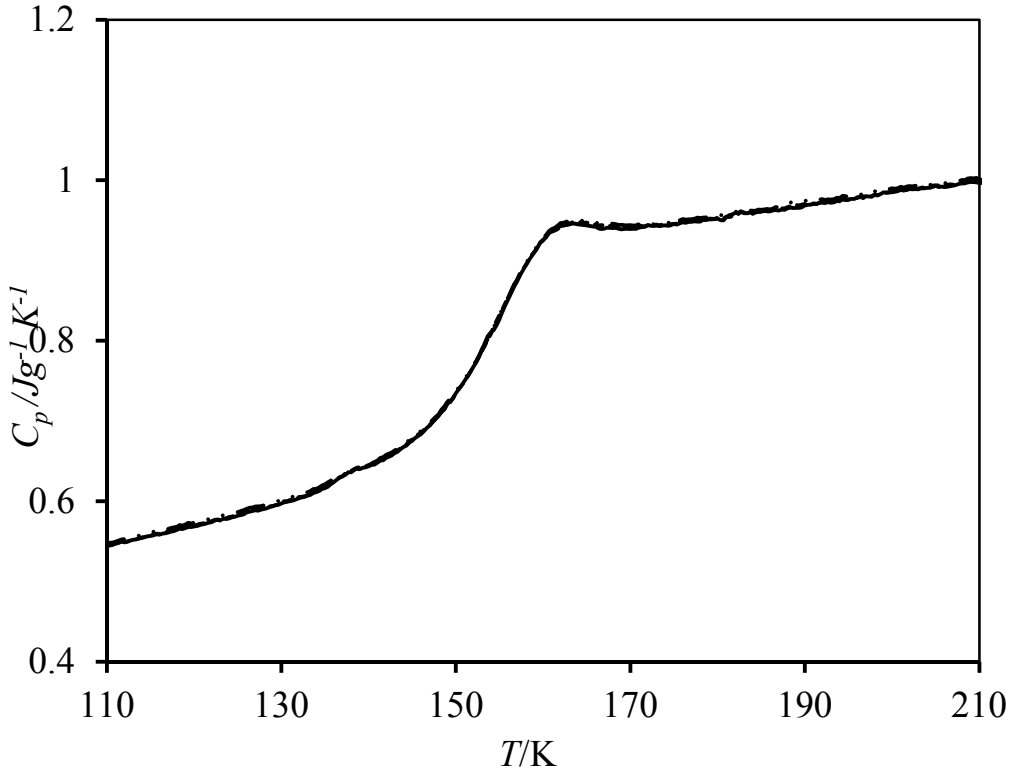

Figure 3.7 Heat capacity versus temperature (unaged traces) for P4HS sample recorded after aging at $T_g - T_a$ = 15 K: 60 (——), 200 (- - - - -), 500 (—••—••—) and 2000 (—•—•—) minutes.

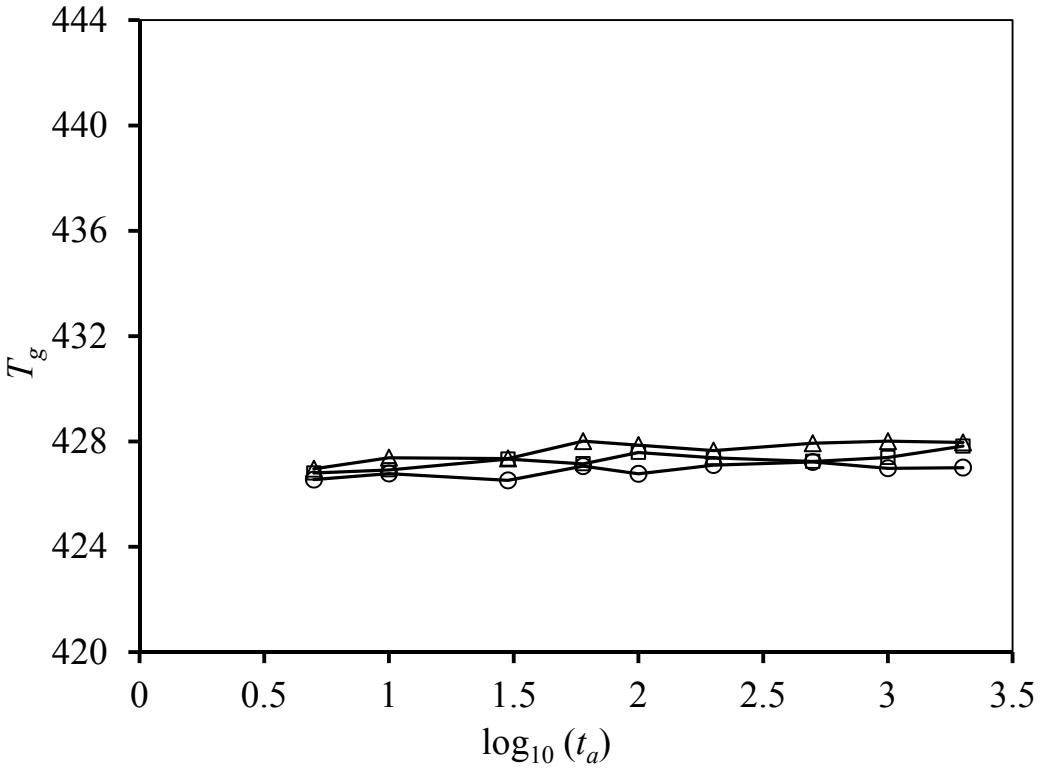

Figure 3.8 Variation of T_g of P4HS sample after different aging times at three annealing temperatures: (O) T_g*-15;* (□) T_g*-10;* (Δ) T_g*-5.*

Figure 3.9 displays typical C_p data for a P4HS sample aged at 15 degrees below T_g. The effect of aging is to increase progressively the size and peak maximum of the endothermic recovery peak. The integration area between any one curve and the unaged reference curve (Figure 3.10) gives the relaxed enthalpy for that particular aging time, $\Delta H(T_a, t_a)$. Plots of enthalpy lost after aging for a time, t_a, at temperature T_a i.e. $\Delta H(T_a, t_a)$ against $\log_{10}(t_a)$, are shown in Figure 3.11. As expected the enthalpy lost after a given aging time increases as T_a decreases, since the distance between the glassy and extrapolated liquid enthalpy lines increases as the system progresses deeper into the glassy region.

The experimental $\Delta H(T_a, t_a)$ data are curve-fitted via a nonlinear least-squares routine, using the CF model (Table 3.4) described in Chapter 1. Figure 3.11 indicates that the time required to reach a plateau decreases with increasing aging temperature, that is moving close to T_g. Ideally, long aging times are required for the data to reach a plateau at $T_a = T_g$-15.

Enthalpy relaxation is believed to depend on the rearrangement of main-chain segments which are trying to reach their configurational energy minimum. This process is increasingly slow at longer aging times because there are fewer segments in a non-equilibrium situation. If the energy barrier to motion is high, as in the case of specific interactions, then more energy should be released. However, the hydrogen bond distribution of P4HS is very sensitive to temperature, as shown by FTIR studies (section 3.2.2). Using the peak shapes in the hydroxyl region, if the $\Delta H(T_a, t_a)$ value originates from a change in hydrogen bond distribution, then the FTIR peaks should change shape with aging time. Therefore, to test whether this is the case, FTIR spectra at $T_a = T_g$-15 (=139 ^{o}C) and two aging times (10 and 1000 minutes) were recorded. The peak shape appeared unchanged with t_a (Appendix B). The FTIR bands also indicate that the hydrogen bond distribution does not depend on the structural state of the sample but depends only on temperature.

A different interpretation for these $\Delta H(T_a, t_a)$ values must be developed, taking into account the experimental result of a hydrogen bond distribution constant with time. If hydrogen bonds acted as rigid cross-links, no segmental motion would be possible and $\Delta H(T_a, t_a)$ would be small. This cannot be the case; in miscibility studies involving the hydrogen bonding properties of P4HS [43, 46, 113, 121, 136] the phenomenon is

considered as a dynamic equilibrium of un-bonded groups reacting to generate hydrogen bonds and vice versa. Nevertheless during aging process the dynamic equilibrium of un-bonded groups is not completely achieved where, during that segmental rearrangement hydrogen bonds are disrupted, but because of high hydroxyl group density part of hydrogen bonds are re-formed in an overall more favourable configuration.

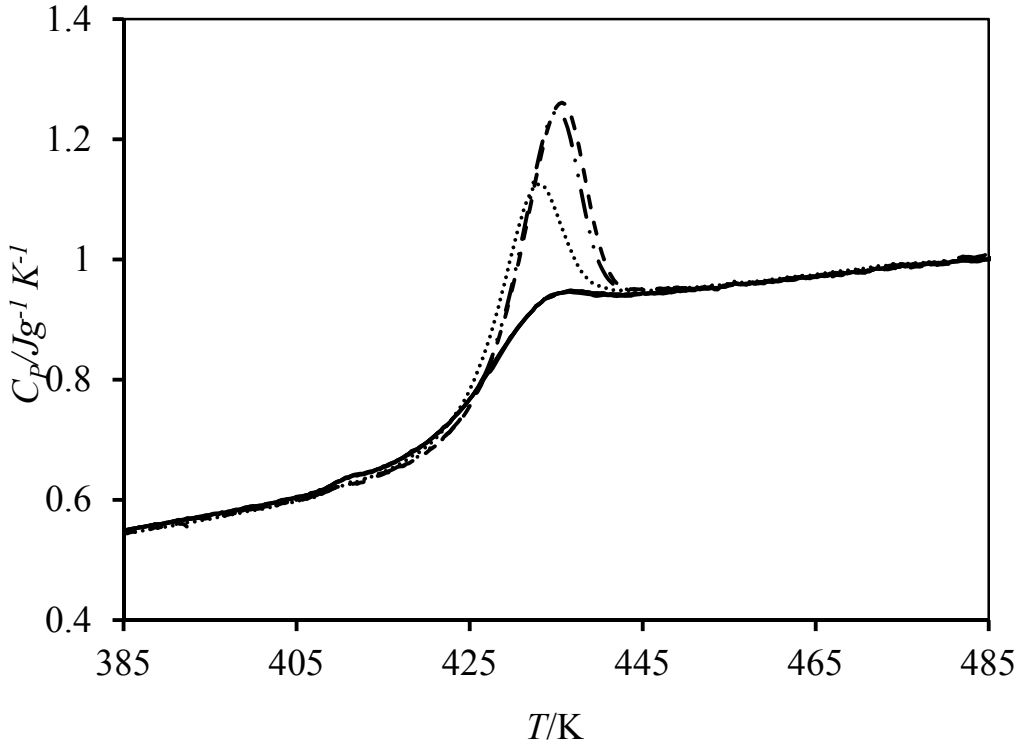

Figure 3.9 Heat capacity curves for P4HS for different aging temperatures at T_g -T_a = 15 K: 200 (……), 500 (—●●—●●—) and 2000 (- - - - -) minutes.

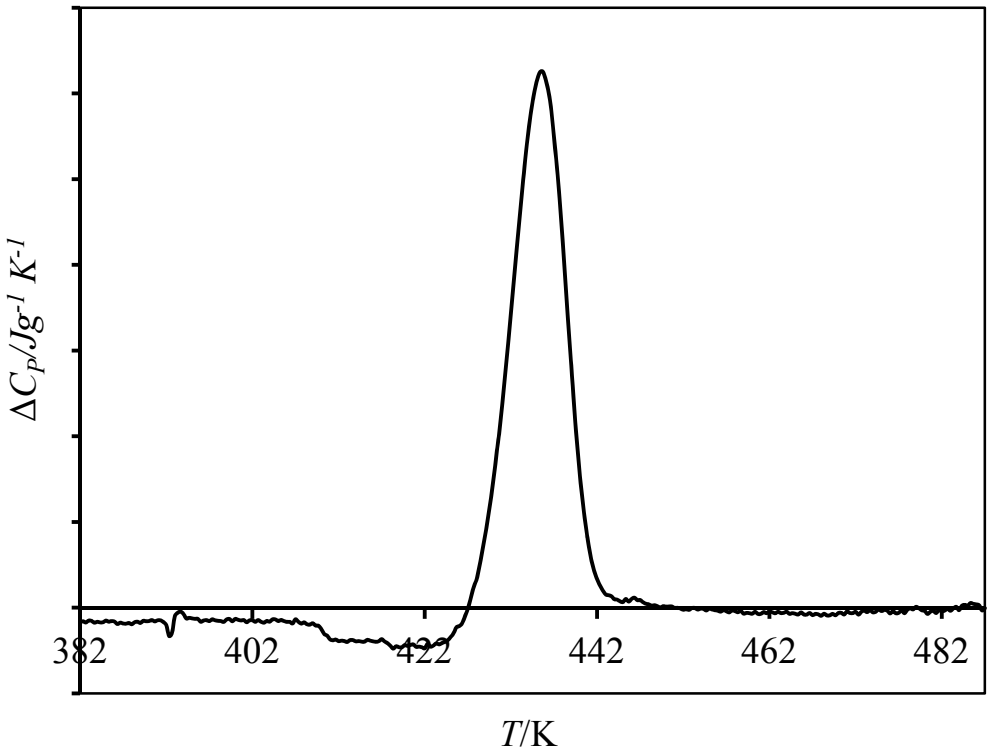

Figure 3.10 Subtraction of C_p unaged data from C_p aging data for P4HS at $T_g - T_a = 15$ K; $t_a = 2000$min.

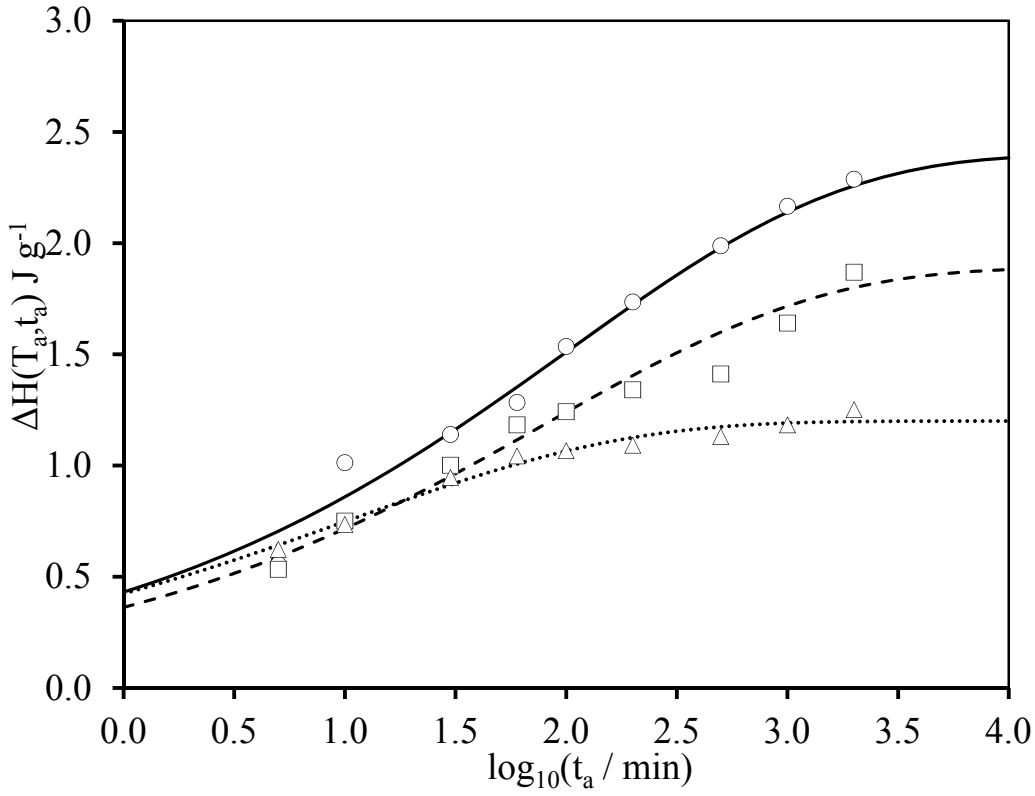

Figure 3.11 Enthalpy relaxation data for P4HS at T_a= (O) (——) 412 K; (□) (- - - - -) 417 K; and (Δ) (……..) 422 K. The CF parameters for the curve are given in Table 3.4.

Table 3.4 - CF parameters obtained from fitting enthalpic relaxation data of P4HS.

T_a / K	$T_g - T_a$ / K	$\Delta H_\infty(T_a)$ / Jg^{-1}	$\log(t_c)$ / min)	β
412	15	2.40	2.01	0.35
417	10	1.89	1.92	0.35
422	5	1.20	1.03	0.35

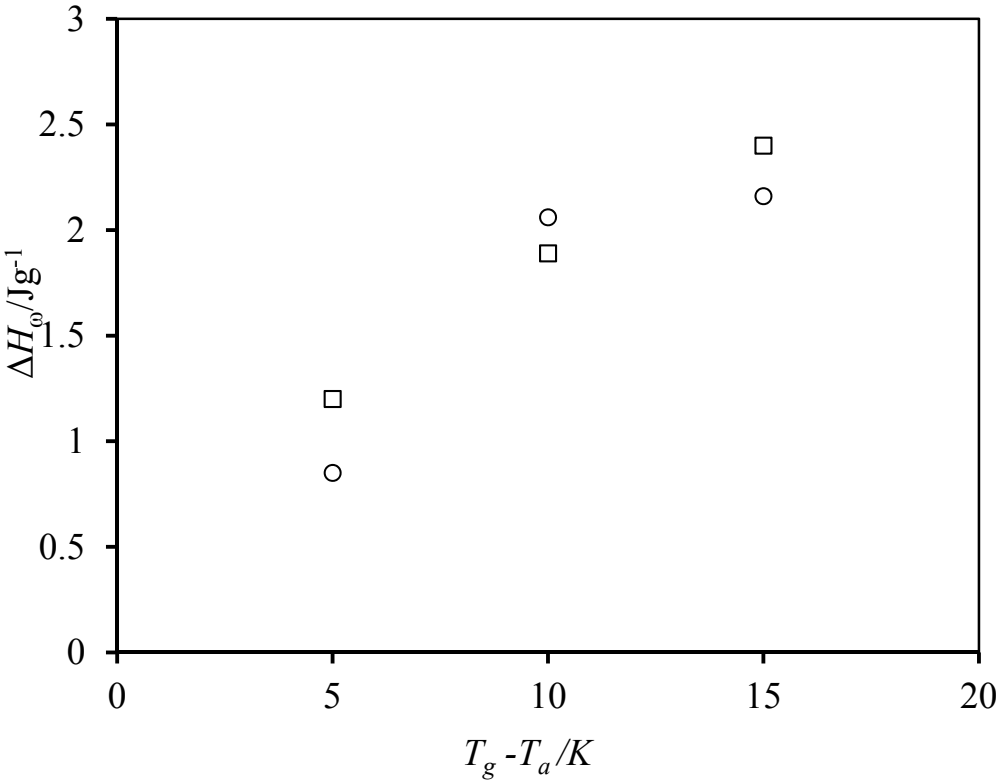

Figure 3.12 ΔH_∞ versus (T_g- T_a) for (□) P4HS and (O) PS (data of PS taken for Brunacci [18]).

To discuss the effect of hydrogen bonding on enthalpy relaxation it is of interest to compare the C_p curves of P4HS and PS. Figure 3.13 includes the DSC scans of the unaged and aged polymers at (T_g-10) for 2000 min. The PS enthalpic peak (data taken from Brunacci [18]) is high and narrow, which indicates a quick release of energy. The P4HS peak, on the other hand, is broad indicating that energy is released over a much wider range of temperature. Such an occurrence is consistent with the hydrogen bonding effect seen on ΔT (Table 3.5); our thermal results of P4HS indicate that ΔT of P4HS (~ 13.35) is larger than that of PS (~4.5).

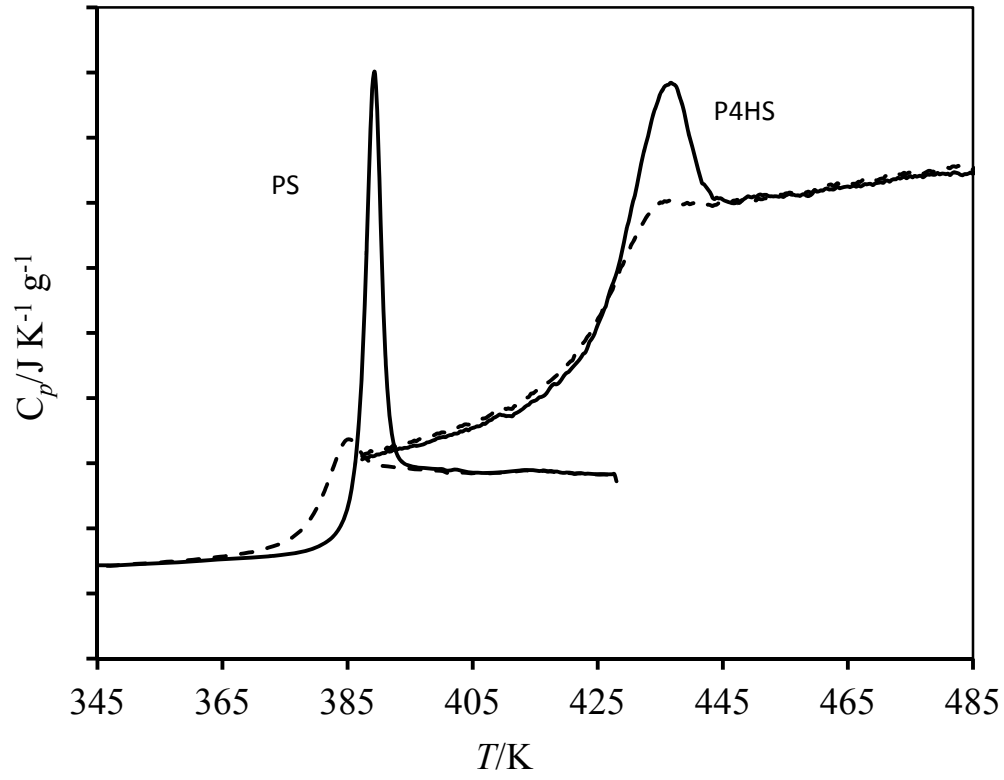

Figure 3.13 C_p curves of unaged (dashed lines) and aged (solid lines) PS and P4HS samples under the same conditions: 1000 minutes at (T_g-10).

Table 3 .5 - T_g data for PS (data of PS taken for Brunacci [18]) *and P4HS*

Sample	T_g *(mid-point)* / *K*	ΔT / *K*	ΔC_p / $JK^{-1}g^{-1}$
PS37k	373	4.5	0.280
P4HS(22k)	427	13.4	0.349

Enthalpy relaxation studies carried out on PS and P4HS by Yoshida et al. [95, 137] suggested that aging is closely linked to the restriction of segmental motion of the main chain [95]. Those authors point out that the difference in enthalpy relaxation between PS and P4HS could be explained as a result of hydrogen bond formation in P4HS. It is therefore expected that restrictions in the main- chain motion due to inter-chain interactions retard the relaxation process [95].

A measure of the kinetics involved in physical aging is also given by the characteristic time t_c of the CF approach, in that large t_c values imply a slow aging process. All t_c values reported in this thesis were obtained from CF approach by curve

fitting plots of $\Delta H(T_a\ ,\ t_a)$ *vs log* t_a; whereas the average relaxation time, $\langle t_c \rangle$, can be calculated from

$$\langle t_c \rangle = t_c\, \Gamma\left(1 + \frac{1}{\beta}\right) \qquad (3.1)$$

where Γ is the gamma function [138].

Figure 3.14 shows log ($\langle t_c \rangle$) as a function of the distance from T_g. It thus appears that P4HS relax faster than PS deep in the glass region (i.e. $T_a = T_g$-15 or less). Supposing that the relaxation rate increases with the increasing of chains rigidity, this is explanation of the faster relaxation rate in the case of a stronger interaction.

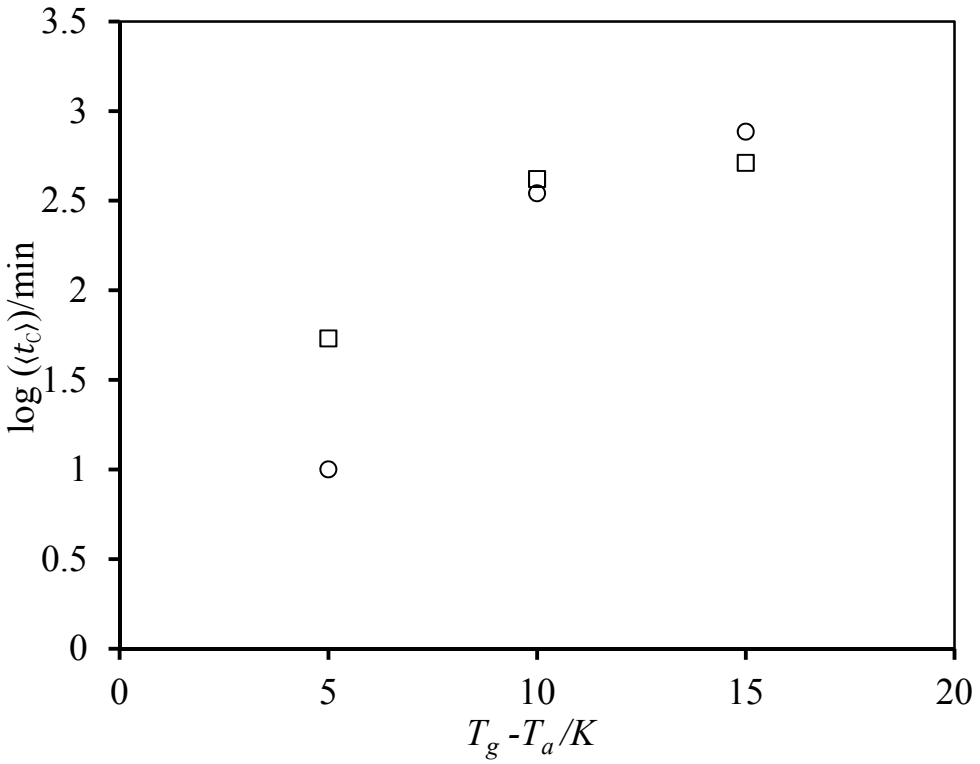

Figure 3.14 log ($\langle t_C \rangle$) versus (T_g- T_a) for (□) P4HS and (O) PS (PS data taken from Brunacci [18]).

3.2.2.2 Enthalpy relaxation of styrene-co-4-hydroxystyrene (SHS) copolymers

The effects of hydrogen bonding upon enthalpy relaxation were monitored by introducing differing amount of hydroxyl groups into the structure (i.e. preparing SHS

copolymers) as described in Chapter 2. Three SHS copolymers were studied with low (30%), intermediate (50%) and high (70%) concentration of HS units. Results in section 3.1 indicated that a further increase in hydroxyl group content would not significantly affect the position of the hydrogen bonding band; the hydroxyl stretching bands of SHS copolymers were found to be almost identical to those of pure P4HS.

The midpoint T_g, T_g temperature range (ΔT) and experimental ΔC_p for the copolymers investigated in this work are reported in Table 3.6. An increase in HS content causes an increase in T_g and broadening of ΔT with respect of PS. This can be ascribed to the existence of H-bonding groups and increase in the chain rigidity in the copolymers. Although the hydroxyl groups in SHS30 are relatively "diluted", there is still evidence of considerable H-bonding interactions as reflected by the high T_g compared to that of PS. The ΔT values for the SHS copolymers are greater than ΔT measured for PS but much lower than the P4HS value. All the samples were dried and stored in desiccators prior to the time of use.

Schroeder et al. [139] found that ΔC_p increased with increasing HS content in a series of SHS copolymers. There was no clear trend between ΔC_p values for the polymers in this study (*Table 3.6*). The lowest value was observed for SHS50; and a large variation was observed for P4HS, with respect to PS.

Table 3 .6 - T_g data for SHS copolymers

Sample	T_g *(mid-point)* / *K*	ΔT / *K*	ΔC_p / $JK^{-1}g^{-1}$
PS37k	373	4.5	0.280
SHS30	409	5.6	0.334
SHS50	419	6.8	0.222
SHS70	441	7.5	0.312
P4HS(22k)	427	13.4	0.349

It is rather difficult to predict what kinetic behaviour will prevail in the SHS copolymers compared to the homopolymers. One could argue that the styrene units have less driving force compared to the strongly interacting HS groups, but more short-range

free volume is available for rearrangements. The resulting t_c might be a compromise between these two factors.

At low hydroxyl group concentration the C_p data for a SHS30 aged at 15K below T_g (Figure 3.15) are similar to those of pure PS. In contrast the IR spectrum of SHS50 resembles closely that of P4HS (see later).

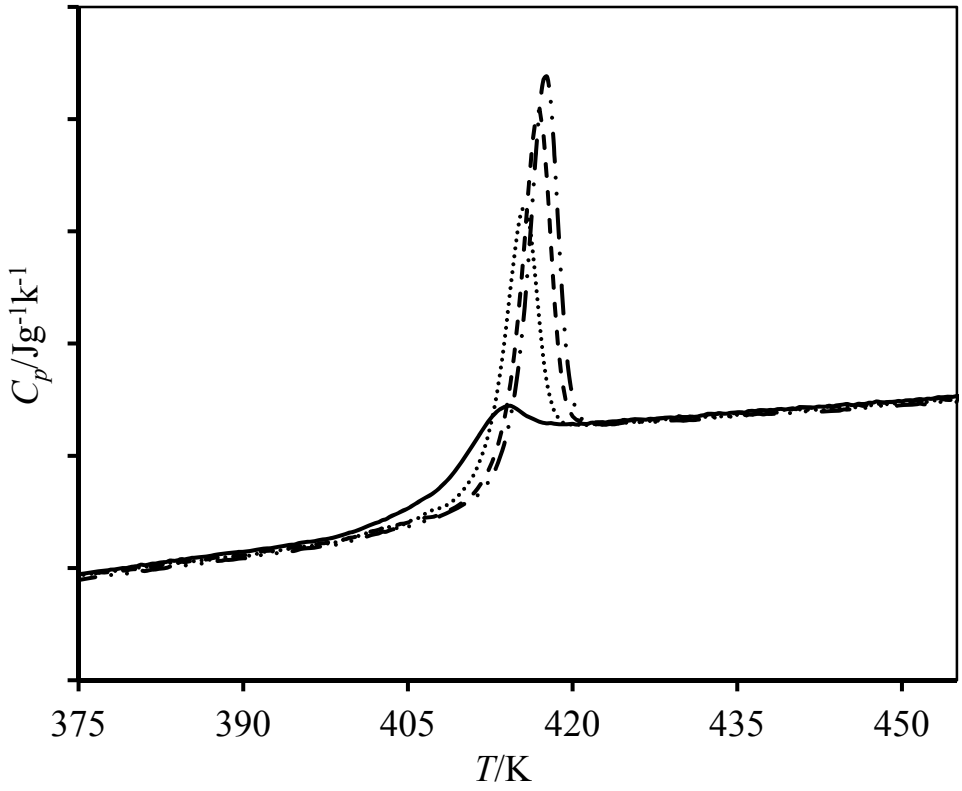

Figure 3.15 Heat capacity curves for SHS30 annealed at T_g -T_a = 15 K: 100 (……..), 500 (- - - - -) and 2000(—••—••—) minutes.

The CF parameters for PS37 (data used from Brunacci [18]) and SHS30 (Tables 3.7 and 3.8) follow similar trends. The enthalpy lost after a given aging time increases as T_a decreases as one would expect, and there appears to be enhancement of enthalpy relaxation close to the T_g. This is perhaps due to favourable positioning of OH groups within the system giving an increase in the relaxation rate (i.e. lower log (t_c)).

Typical heat capacity curves for selected SHS copolymers with identical thermal histories are shown in Figure 3.16 (a, b, c). If we consider first of all the unaged curves, we can see that a 'peak' is observed for PS and SHS30 that diminishes in magnitude in SHS50 and SHS70 and broadens for P4HS.

Visually, the aged peaks for SHS30 appear to be narrow indicating quick release of energy, which increase in magnitude as the distance from T_g increases. This is found by the log(t_c) parameter, calculated using the CF equation (Table 3.8). However, although the interactions in SHS30 are stronger compared with PS, associations are still diluted by styrene units and the system relaxes more slowly near T_g. The hydroxyl groups may have ordered together to create more favourable domains, rendering the styrene units less able move.

Table 3.7 - CF Parameters for PS37k

T_a / K	$T_g - T_a$ / K	$\Delta H_\infty(T_a)$ / Jg^{-1}	log(t_c) / min)	β
358	15	2.16	2.30	0.38
363	10	2.06	2.04	0.40
368	5	0.85	0.48	0.40

Table 3.8 - CF Parameters for SHS30

T_a / K	$T_g - T_a$ / K	$\Delta H_\infty(T_a)$ / Jg^{-1}	log(t_c) / min)	β
398	15	1.84	1.91	0.38
403	10	1.53	1.78	0.38
408	5	1.04	1.45	0.38

Tables 3.9 and 3.10 list the CF parameters for the SHS50 and SHS70 samples, respectively. The aging behaviour is complex. Both copolymers show fast relaxations as indicated by the log(t_c) values, presumably as a result of the increase in H-bonding concentration. The enthalpic relaxation data of these copolymers (Figures 3.17 and 3.18) indicate that the inflection points are not very clear especially at T_a far from T_g; thus it is believed that the CF parameters are not realistic estimations.

Table 3.9 - CF Parameters for SHS50

T_a / K	$T_g - T_a$ / K	$\Delta H_\infty(T_a)$ / Jg^{-1}	$\log(t_c)$ / min)	β
403	15	1.96	1.98	0.39
408	10	1.77	1.89	0.39
413	5	1.11	1.79	0.39

Table 3.10 CF Parameters for SHS70

T_a / K	$T_g - T_a$ / K	$\Delta H_\infty(T_a)$ / Jg^{-1}	$\log(t_c)$ / min)	β
426	15	2.11	1.87	0.37
431	10	1.90	1.81	0.37
436	5	1.19	1.75	0.37

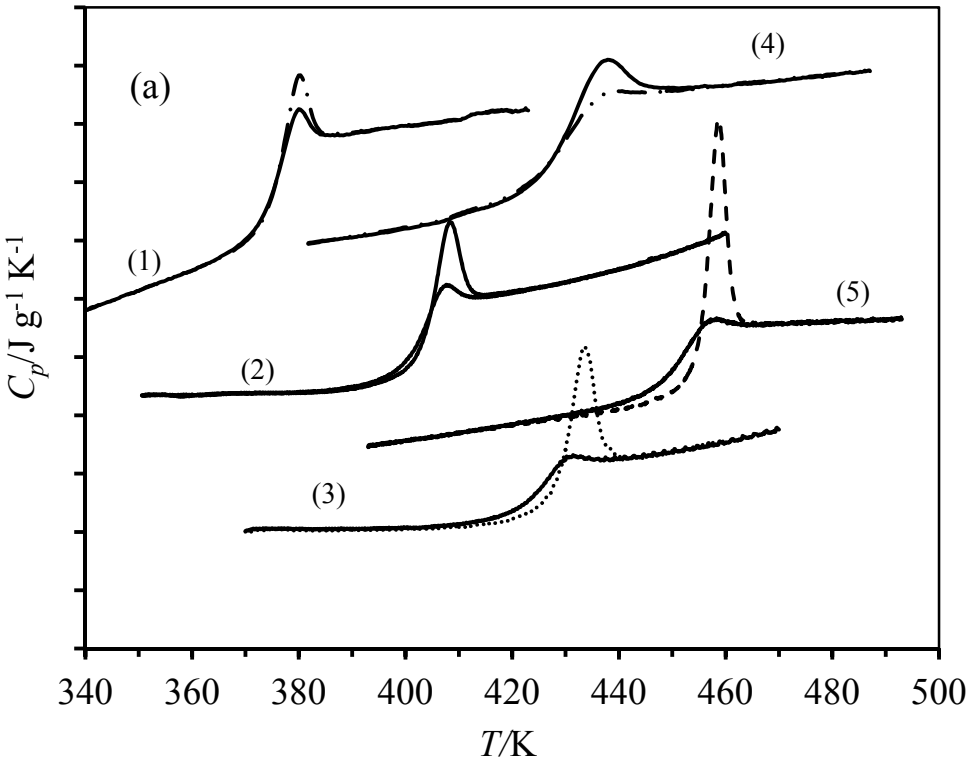

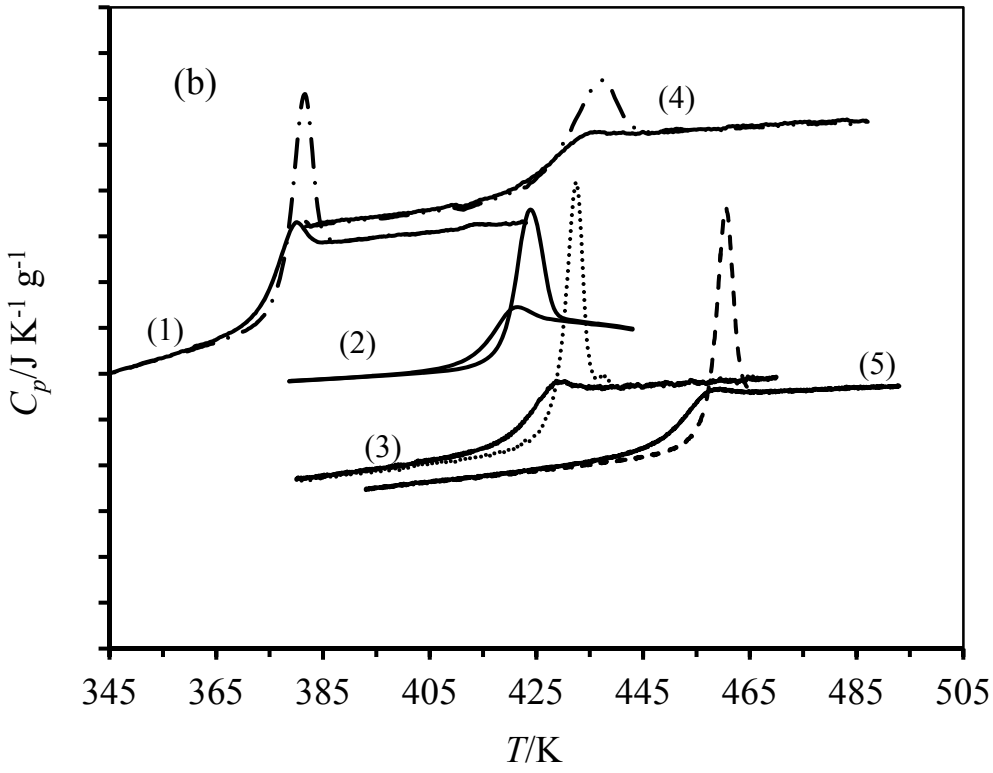

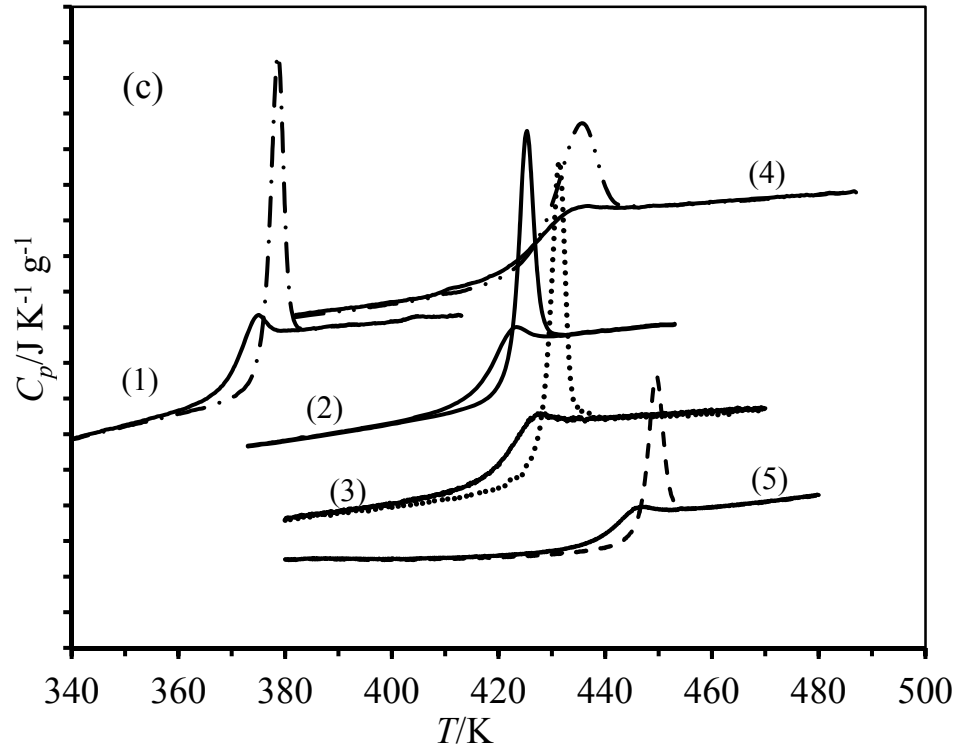

Figure 3.16 Heat capacity curves (aged and unaged) for t_a = 2000 mins. (1) PS, (2) SHS30, (3) SHS50, (4) P4HS and (5) SHS70 (a) T_g – 5, (b) T_g – 10 and (c) T_g - 15.

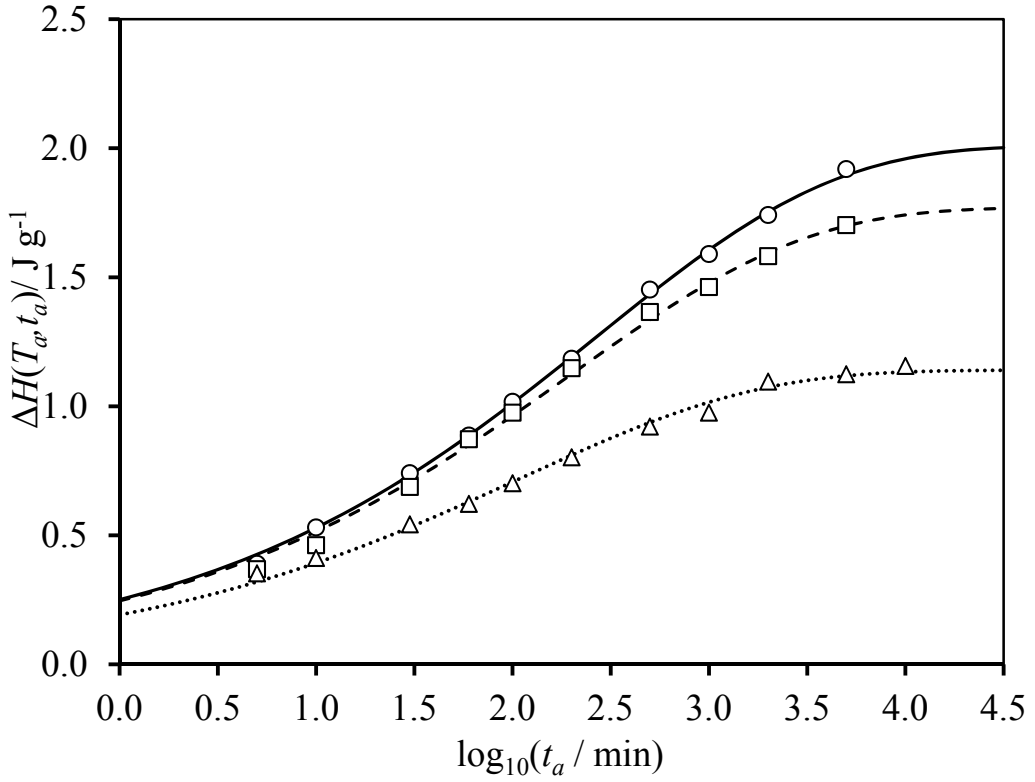

Figure 3.17 Enthalpy relaxation data for SHS50 at different temperatures as follows: (O) (——) 403 K (T_g-15); (□) (- - - - -) 408 K (T_g-10); (Δ) (……..) 413 K (T_g-5).

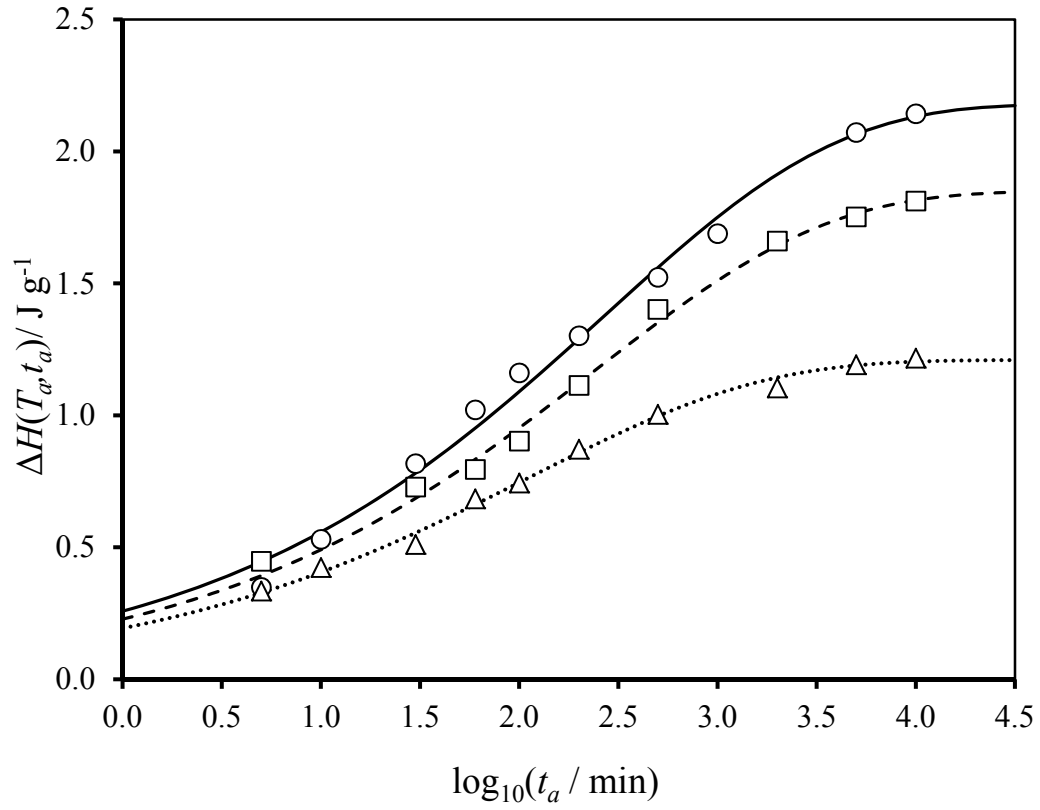

Figure 3.18 Enthalpy relaxation data for SHS70 at different temperatures as follows: (O) (——) 426 K (T_g-15); (□) (- - - - -) 431 K (T_g-10); (Δ) (……..) 436 K (T_g-5).

a) Effect of hydrogen bonding on $\Delta H_\infty (T_a)$

Figure 3.19 displays all the $\Delta H_\infty(T_a)$ data plotted as a function of distance from T_g. As noted above, somewhat unexpected behaviour occurs in the near- T_g region; SHS50 and SHS70 exhibit $\Delta H_\infty(T_a)$ values close to P4HS. However, for SHS30 the $\Delta H_\infty(T_a)$ value is in the middle, between PS and P4HS. This suggests that the aging temperature differences in the SHS system are sufficiently large to affect the hydrogen bond equilibria. Calculation based on infrared measurements [121] indicate that, at room temperature, the free OH group fraction changes little at high HS compositions, compared to P4HS (hence for SHS50 and SHS70). It is the distribution of associated chains that is more affected by dilution. The primary effect must be the shortening of the average chain length, with a consequent diminution in system stabilization. Without this extra term, enthalpy relaxation becomes similar to that of PS. However overall association strength increases when temperature decreases, and the hydrogen bonded sequences in the chains lengthen, bringing the copolymer enthalpy behaviour closer to that of P4HS.

For SHS30 particularly at T_a far from T_g, the dilution effect is too large to be neutralized by any temperature-induced increase in the association strength. In other words, the few hydroxyl groups are not enough to alter the enthalpy relaxation of the system compared to pure PS. However, this does not explain the relatively high values of ΔH_∞ (T_a) close to T_g. Maybe the high unfavourable (non-polar) environment of the hydroxyl groups allows them to release extra energy through a structural rearrangement that makes them able to perform a better level of solvation- even without changing the whole distribution of association chain lengths. On the other hand, the polymer chains are not sufficiently flexible at lower aging temperatures; thus, the favourable structural rearrangements are not allowed. In this case polymer chain is not taken any extra energy, which makes $\Delta H_\infty(T_a)$ closer to pure PS.

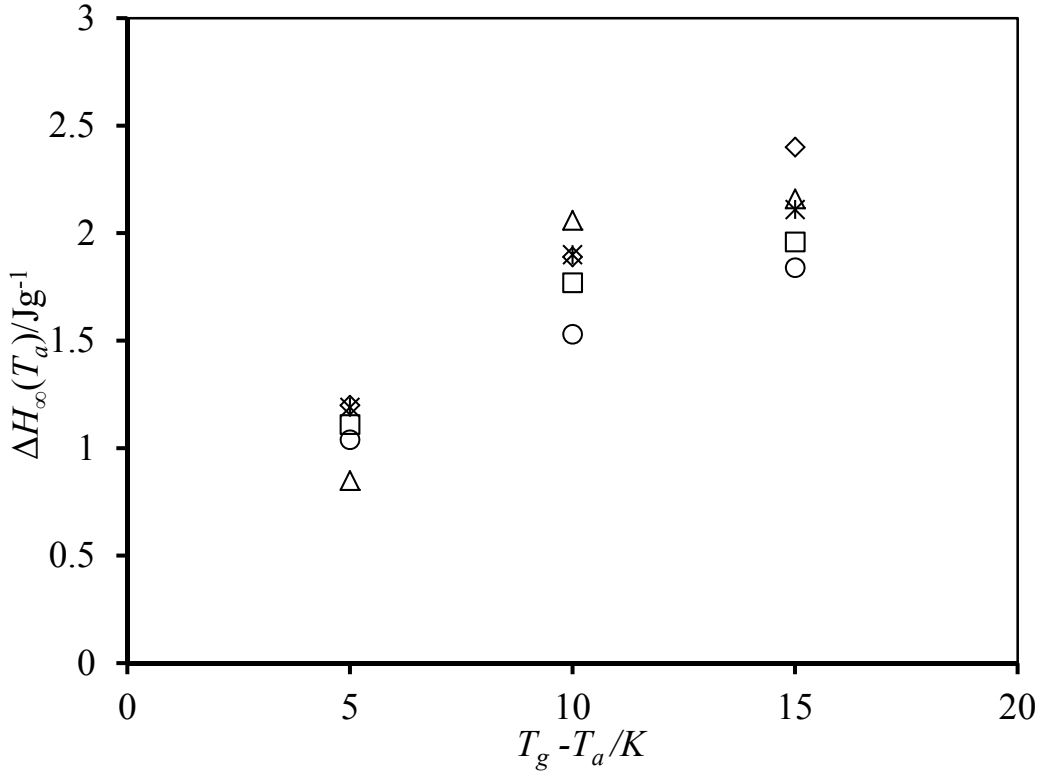

Figure 3.19 $\Delta H_\infty(T_a)$ data for the SHS copolymers, as follows: (◊) P4HS; (ж) SHS70; (□) SHS50; (O) SHS30; (Δ) PS. Data are based on the CF equation calculations.

(b) Hydrogen bonding and the relaxation time function

On the basis of the $\Delta H_\infty(T_a)$ behaviour shown in figure 3.19, the log ($\langle t_c \rangle$) parameter of SHS30 should be comparable to the PS value and slow down with decreasing T_a approaching the P4HS values.

Such expectations are met in the case of SHS30, as Figure 3.20 shows. Above (T_g-10) values converge towards the P4HS average relaxation times. However, below (T_g-10), log ($\langle t_c \rangle$) values tend to approach those of PS. This confirms that, when the interaction is strong, the segmental rearrangements are fast and the enthalpy relaxation is high. In contrast, when the interaction is weakened, the system loses its driving force and the interaction becomes slower.

The trends shown by SHS50 and SHS70 are somewhat similar to those expected for P4HS, with the exception of the value near T_g, where hydroxystyrene units attempt to group together in order to create more favourable domains. However, the overall

results indicate that the presence of styrene units in copolymers has caused dilution of hydrogen bonding interaction that has led to a decrease in the relaxation rate. Therefore, SHS copolymers relax more slowly than P4HS but faster than PS (Figure 3.20).

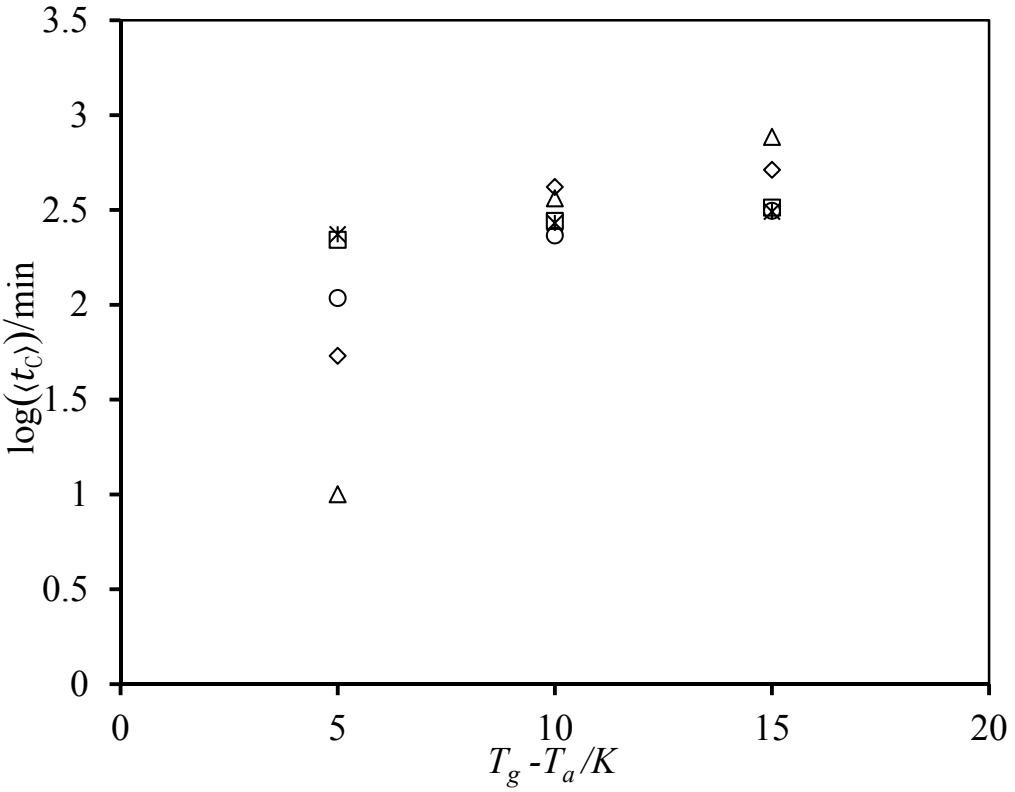

Figure 3.20 Average relaxation time as a function of (T_g-T_a) for the pure polymers and SHS copolymers: (◊) P4HS; (ж) SHS70; (□) SHS50; (O) SHS30; (Δ) PS.

3.3. Poly(ethyl methacrylate) and poly(methyl methacrylate-co-ethyl methacrylate)

3.3.1 Enthalpy relaxation of PEMA

Aging experiments on PEMA were carried out at three temperatures in the range 342 K (T_g-5) to 332 K (T_g-15), in 5 K steps. Figure 3.21 displays typical C_p data for a PEMA sample aged at 15K below T_g. The enthalpic peak of PEMA is high and narrow, as observed for PS. Values of the characteristic time t_c (Table 3.11) indicate that PEMA relaxes slowly compared to P4HS. However, the $\Delta H_\infty(T_a)$ values of PEMA are smaller than those of P4HS, as results of the weak interactions between the PEMA units. Another useful comparison that can be made is between the aging parameters of PEMA

and the behaviour of polymethyl methacrylate (PMMA), since the polymers differ by one CH_2 unit. The CF parameters of PEMA are compared with the PMMA data published by Cowie and Ferguson [22]. One should note that these were obtained using slightly different fitting procedures; the $\Delta H(T_a, t_a)$ data of PMMA were fitted using an adjustable β parameter, whereas, for PEMA, a fixed β value was employed. Interestingly, the PEMA $\Delta H_\infty(T_a)$ values coincide with those of PMMA, which suggests that the interaction strengths in these polymers are similar. log t_c values indicate that PEMA relaxes slower than PMMA at T_a far from T_g and faster than PMMA at T_a close to T_g.

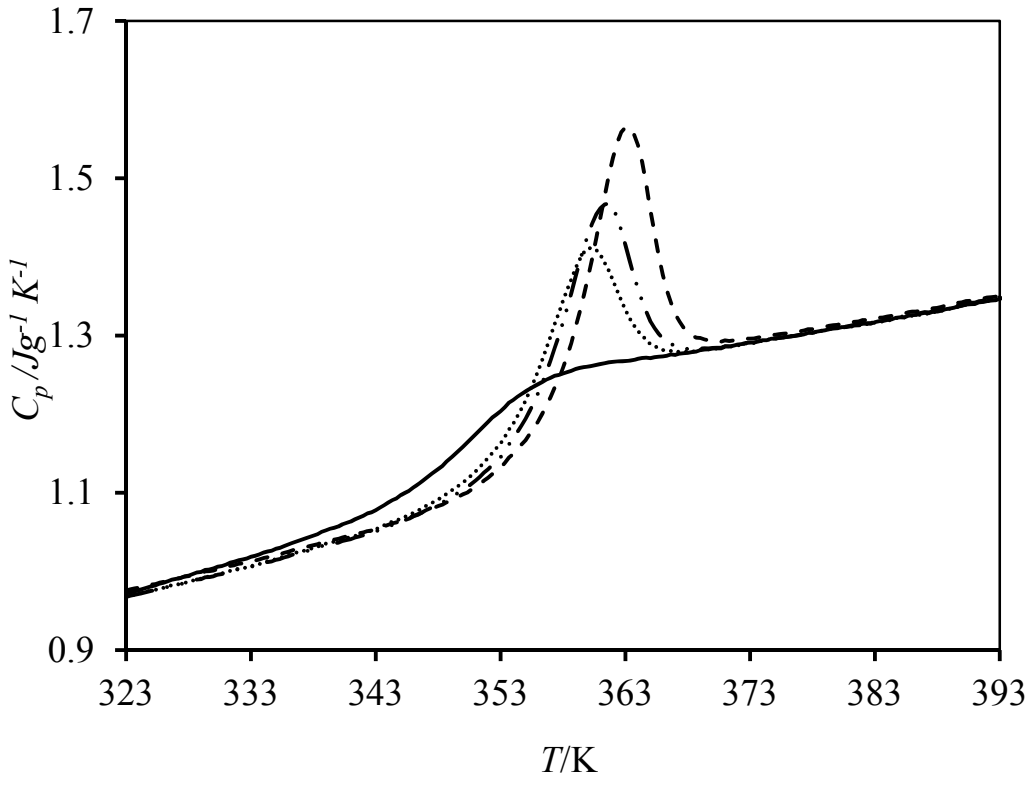

Figure 3.21 Heat capacity curves for PEMA at T_g -T_a = 15 K, for t_a: 200 (…..), 500 (—•••—•••—) and 2000 (— — —) minutes.

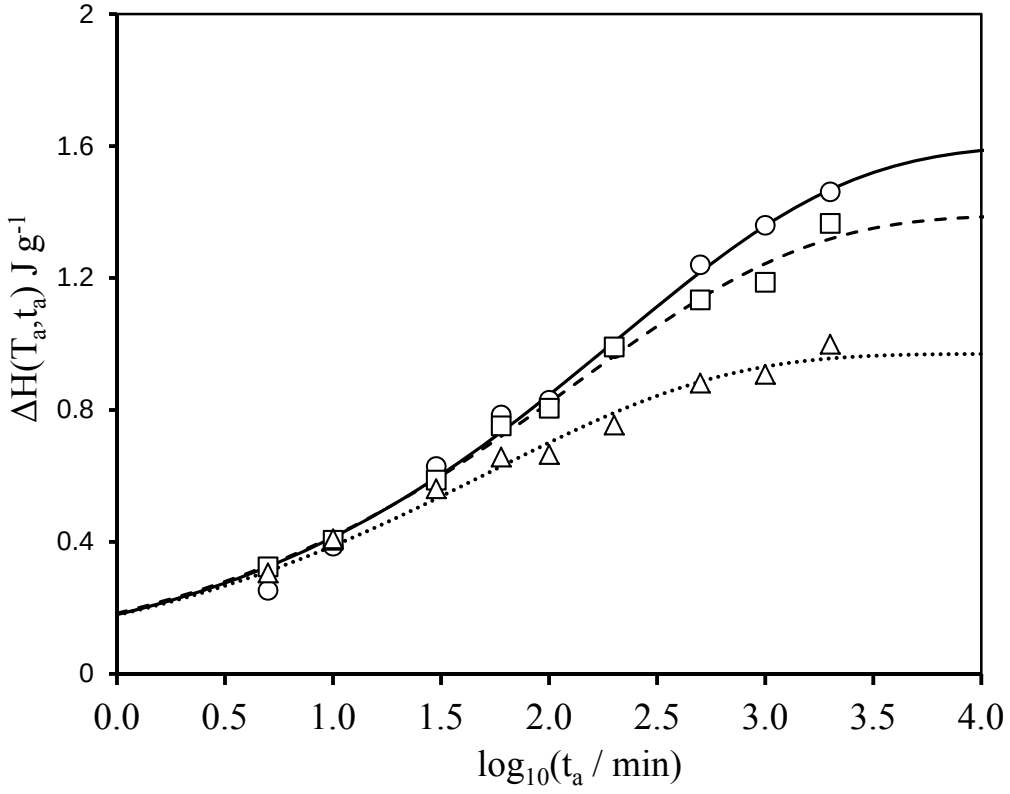

Figure 3.22 Enthalpy relaxation data for PEMA at T_a= (O) (——) 332 K; (□) (- - - - -) 337 K; and (Δ) (……..) 342 K. The CF parameters for the curve are given in Table 3.13

Table 3.11- CF fitting parameters for PEMA at several aging temperatures

T_a (K)	T_g- T_a (K)	$\Delta H_\infty(T_a)$ ($J\,g^{-1}$)	log t_c (min)	β
332	15	1.60	2.31	0.40
337	10	1.39	2.12	0.40
342	5	0.97	1.73	0.40

3.3.2 Enthalpy relaxation of poly(methyl methacrylate-co-ethyl methacrylate)

The mid-point T_g, T_g width (ΔT) and heat capacity difference, ΔC_p, for *poly (methyl methacrylate-co-ethyl methacrylate)* (PMEMA) samples are listed in Table 3.12. These T_g values are intermediate between those of the pure components (i.e. PMMA and PEMA). As the MMA content increases, the glass transition narrows, moves to higher temperatures and the glass state heat capacities become somewhat larger. A study of Figure 3.23 indicates that the shapes of the unaged curves differ

marginally; the enthalpic relaxation peak is evident for PMMA but it reduces with increasing EMA content.

Visually (Figure 3.24a), the aged traces of a PMEMA sample with 82 mol% MMA are similar to those of PMMA, i.e. significant structural changes (e.g. T_g shift) take place only in PEMA rich copolymers.

This, however, provides a limited view of the phenomenon and a further set of C_p curves, collected at the same aging time as in Figure 3.24(a) but for an aging temperature 10K lower (Figure 3.24(b)) the areas of the PMEMA copolymers relaxation peaks have changed, becoming more similar now to PMMA.

Table 3.12 - Glass transition parameters for PMEMA copolymers

wt.-% MMA	mole% MMA	T_g(mid)/ *K*	ΔT/ *K*	ΔC_p/ $J\,K^{-1}g^{-1}$
0	0	347	15.26	0.120
20	18	369	12.87	0.102
50	47	380	14.77	0.201
80	82	386	12.82	0.196
100	100	391	8.3	0.207

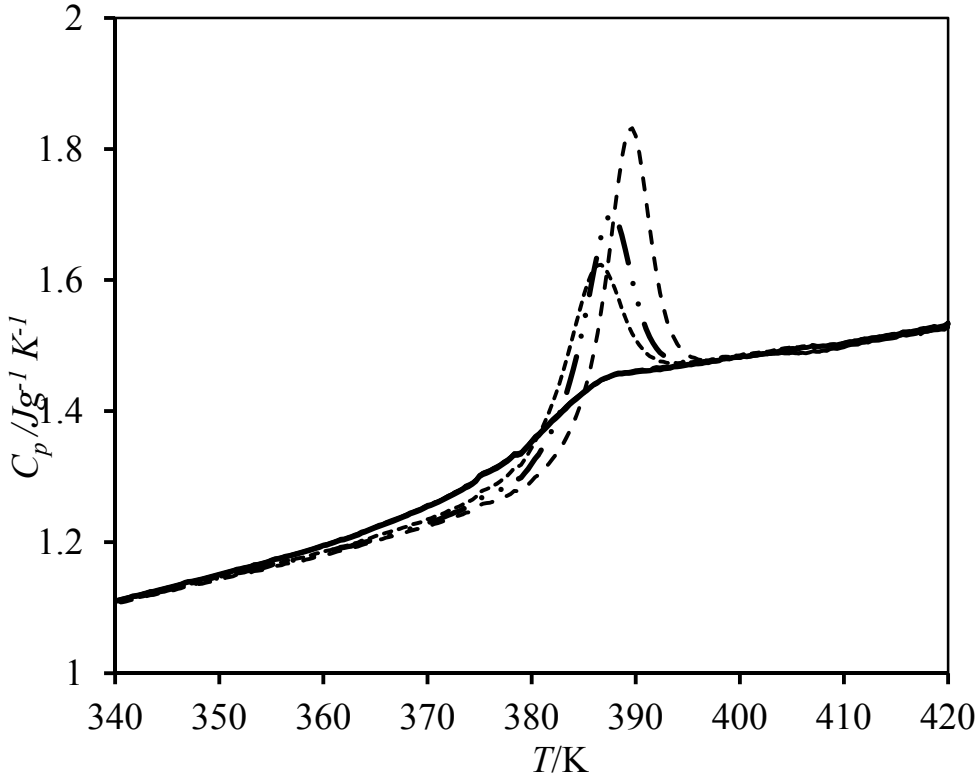

Figure 3.23 Heat capacity curves for PMEMA (47 /53 mole% MMA/EMA) at T_g -T_a = 15 K: 200 (……), 500 (—•••—•••—) and 2000 (- - - - -) minutes.

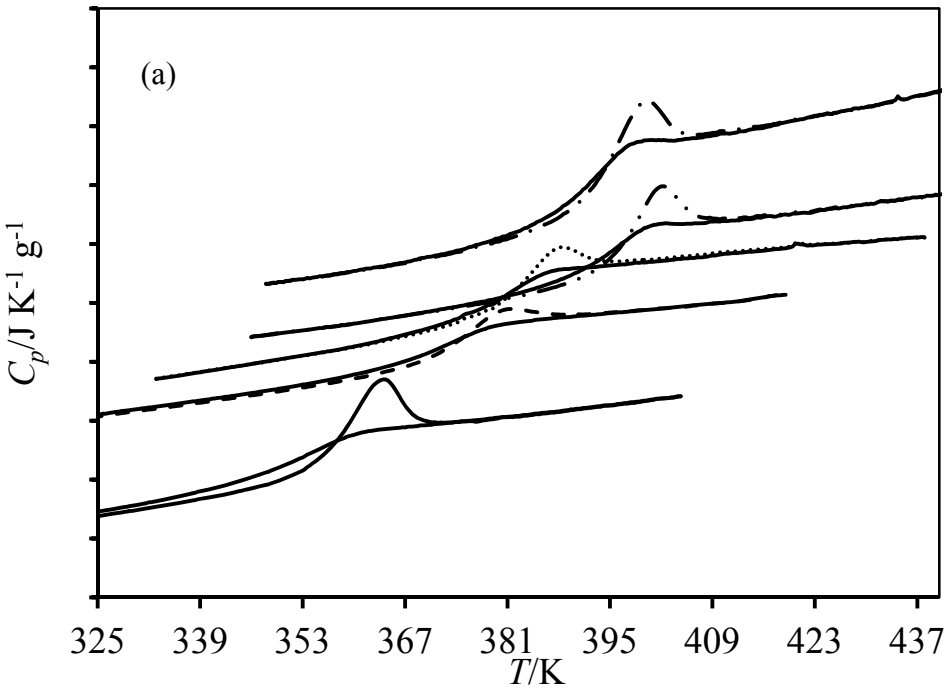

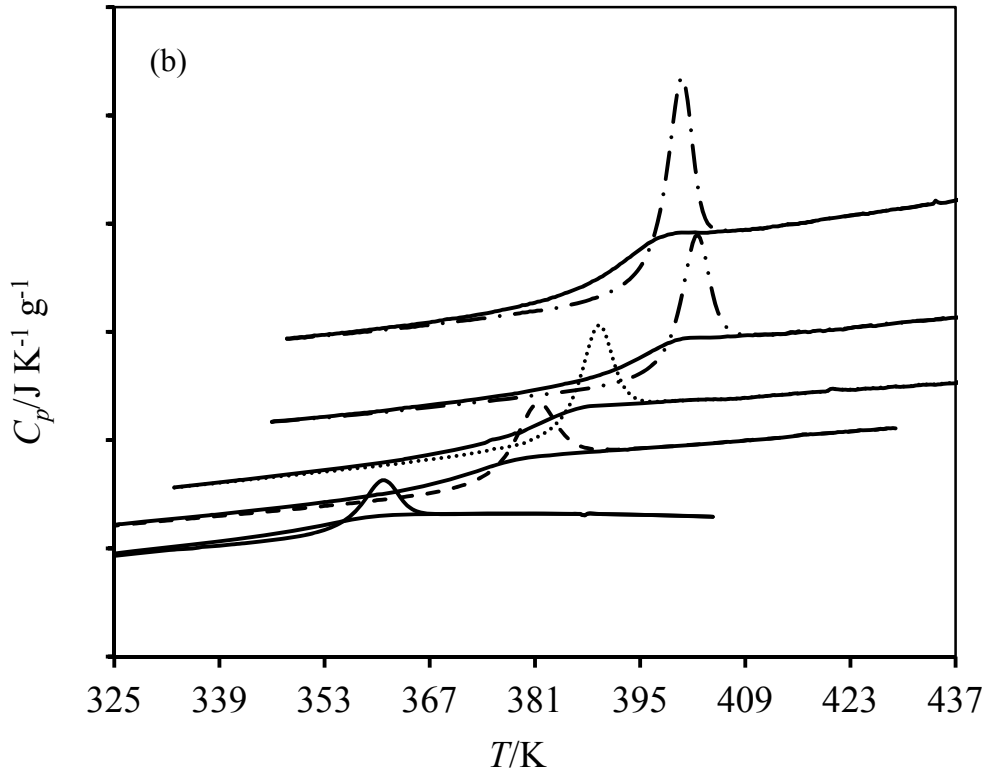

Figure 3.24 Heat capacity curves (aged and unaged) for PMEMA at t_a = 2000 minutes. From top to bottom: PMMA, (78/22), (47/53), (18/82) mole% MMA/EMA and PEMA in the copolymers, (a) T_g – 5, (b) T_g - 15.

Plots of $\Delta H(T_a, t_a)$ versus $\log_{10}(t_a)$ (Figures 3.25(a-c)) indicate that, close to T_g (i.e. T_g- 5) the data pass through an inflection point. On lowering aging temperature, the enthalpy relaxation decreases at short t_a, but at longer t_a there is a crossing point when $\Delta H(T_a, t_a)$ becomes higher than that at higher T_a. In experimental terms, this means that the accessible time-window shortens with decreasing T_a, and only a small portion of the entire $\Delta H(T_a, t_a)$ curve can be measured.

As usual, the CF model was used to fit the experimental $\Delta H(T_a, t_a)$ data and the CF parameters are reported in Table 3.13. Figure 3.26 shows the variation of $\Delta H_\infty(T_a)$ with MMA content. An interesting trend can be seen; equilibrium enthalpy values generally increase with increasing MMA content.

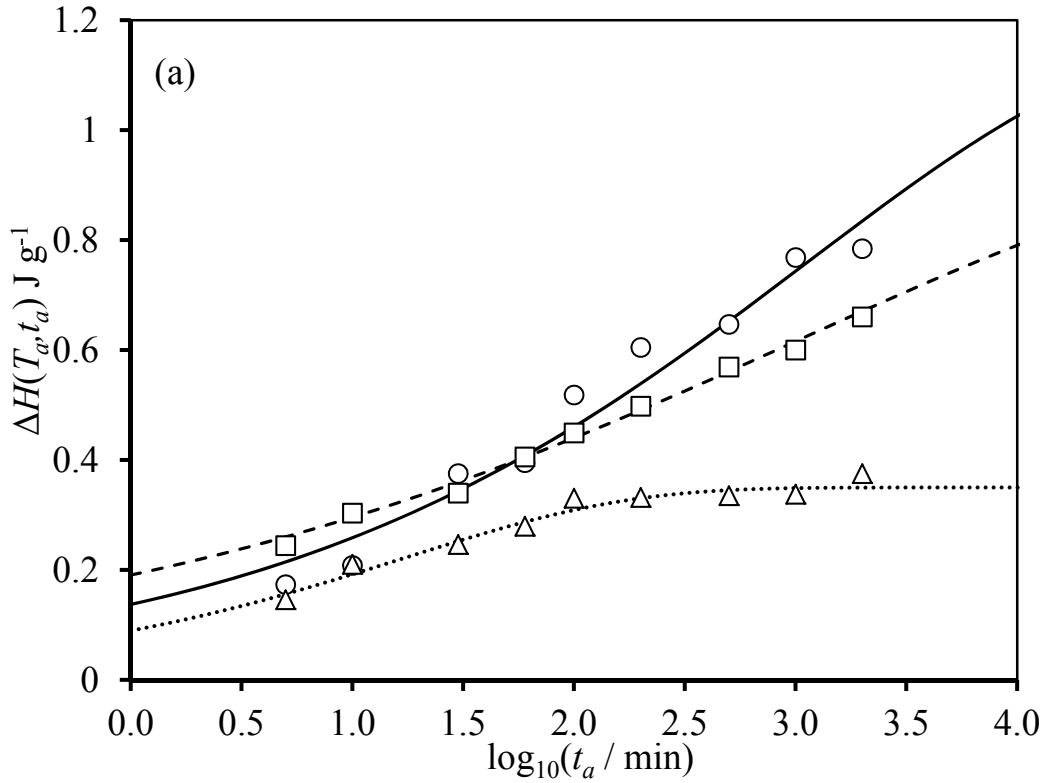
(a)
1.2
1
0.8
0.6
0.4
0.2
0
$\Delta H(T_a,t_a)$ J g^{-1}
0.0
0.5
1.0
1.5
2.0
2.5
3.0
3.5
4.0
$\log_{10}(t_a$ / min)

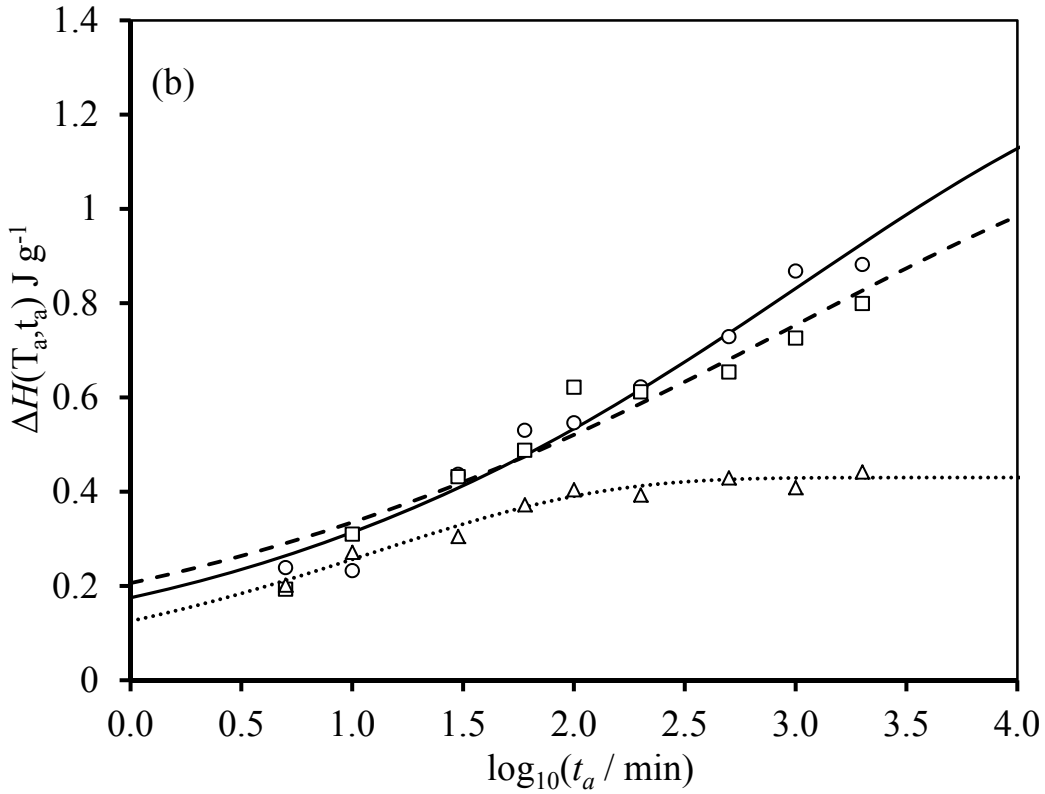
(b)
1.4
1.2
1
0.8
0.6
0.4
0.2
0
$\Delta H(T_a,t_a)$ J g^{-1}
0.0
0.5
1.0
1.5
2.0
2.5
3.0
3.5
4.0
$\log_{10}(t_a$ / min)

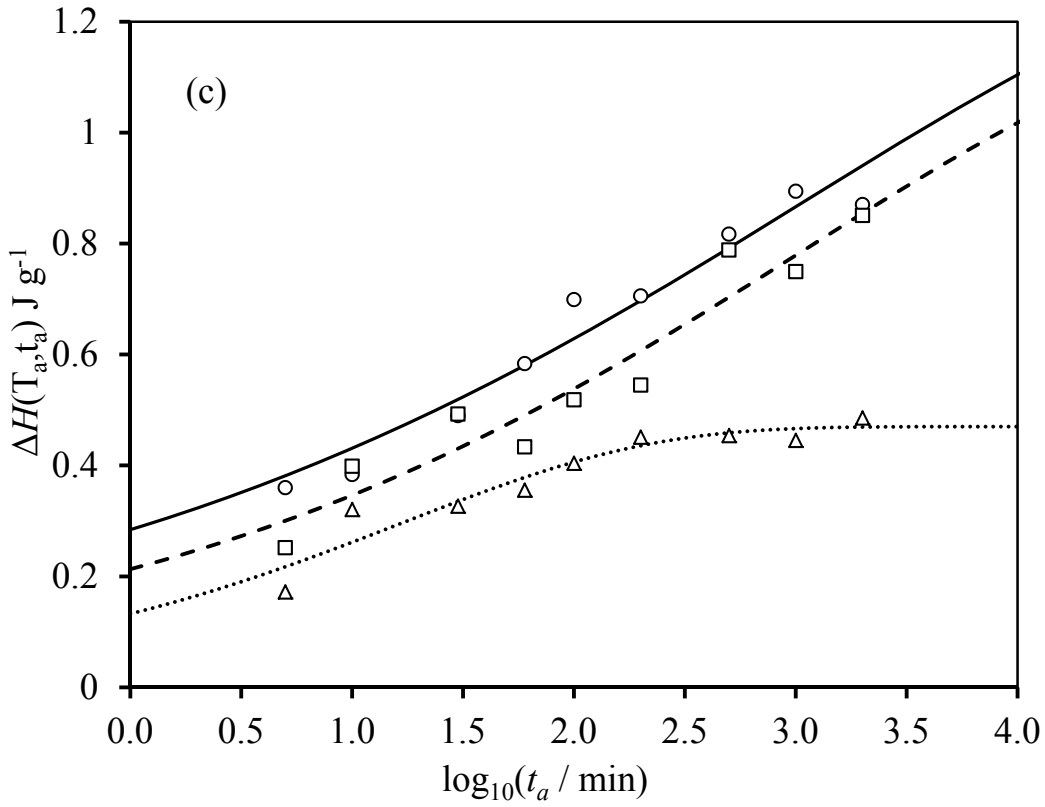

Figure 3.25 Enthalpy relaxation data for the PMEMA: (a) (78/22); (b) (47/53); (c) (18/82) mole% MMA/EMA; (T_g- T_a): (○) 15K; (□) 10K; (Δ) 5K. The continuous lines are fits to the experimental data using the CF equation.

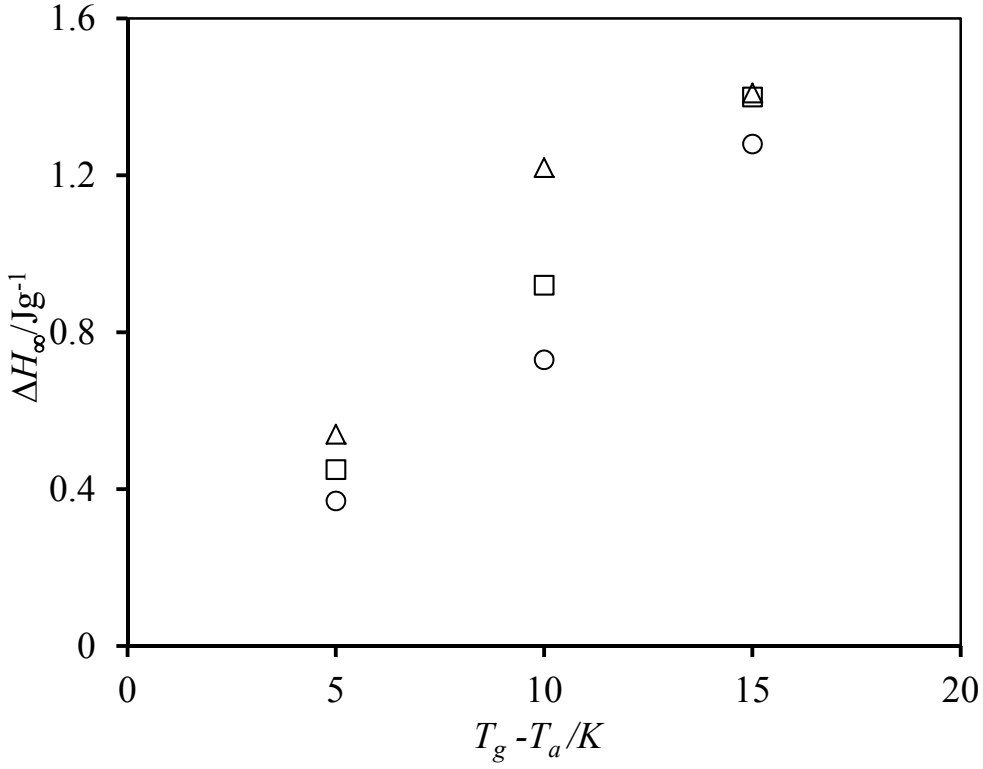

Figure 3.26 Variation of ΔH_∞ (T_a) with ($T_g - T_a$) for PMEMA: (O) (18/82); (□) (47/53); (Δ) (78/22) mole% MMA/EMA.

Table 3.13 CF parameters for PMEMA copolymers.

PMEMA (wt.-% MMA)	PMEMA (mole-%MMA)	T_a *(K)*	T_g- T_a *(K)*	ΔH_∞ (T_a) $(J\,g^{-1})$	log t_c (min)	β
0	0	332	15	1.60	2.31	0.40
		337	10	1.39	2.12	0.40
		342	5	0.97	1.73	0.40
20	22	354	15	1.28	3.20	0.29
		359	10	0.73	2.07	0.29
		364	5	0.37	1.37	0.29
50	53	365	15	1.40	3.14	0.29
		370	10	0.92	2.22	0.29
		375	5	0.45	1.15	0.29
80	82	371	15	1.41	3.05	0.23
		376	10	1.22	3.03	0.23
		381	5	0.54	1.61	0.23
100	100	376	15	1.34	2.43	0.43
		381	10	1.22	2.10	0.35
		384	7	1.06	2.15	0.30

3.4 Poly(4-vinylpyridine)

3.4.1 Infrared spectroscopy

Poly (4-vinylpyridine) (P4VPy) absorbs moisture very easily from the air. This can be detected as a broad absorption band centred at 3400 cm^{-1}. As shown in Figure 3.27, heating at 100°C successfully removes moisture from the P4VPy samples.

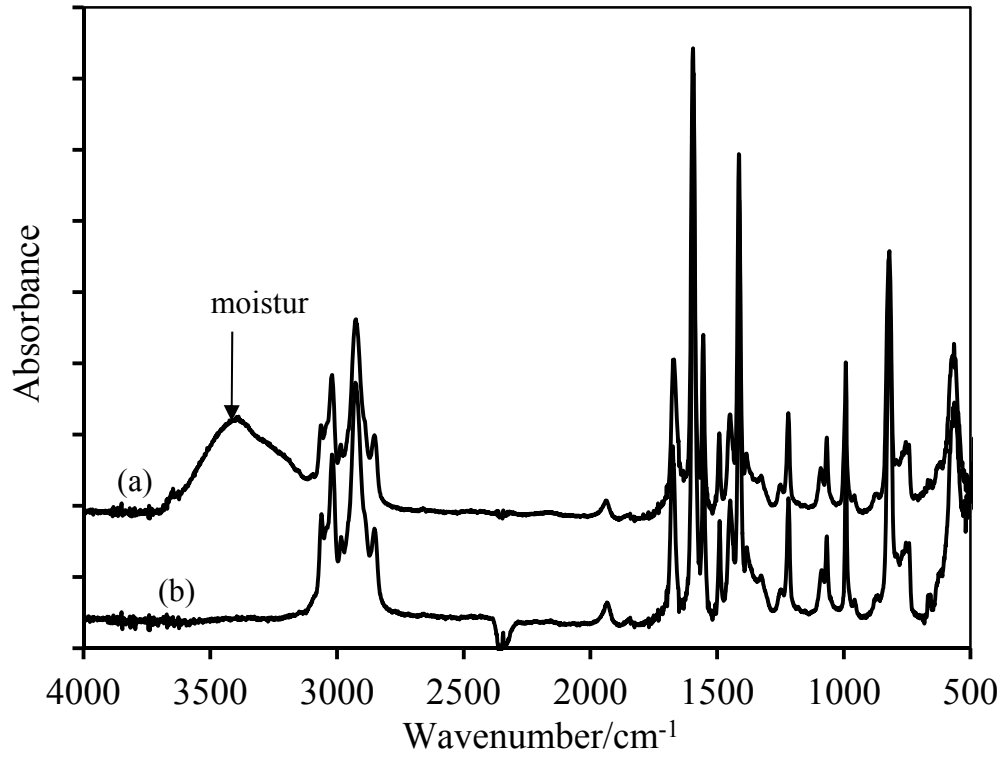

Figure 3.27 FTIR spectra for pure P4VPy at room temperature: (a) before annealing; (b) after heating at 100°C for 20min followed by cooling to room temperature under a nitrogen atmosphere.

3.4.2. Enthalpy relaxation of poly(4-vinylpyridine)

The DSC scans of unaged and aged P4VPy at (T_g-15) are displayed in Figure 3.28, for different aging times. Compared to other polymers investigated in this project, the enthalpic peaks of P4VPy are high and narrow, which points to quick release of energy. Moreover, the aging curves shift to high temperature as the aging time

increases. However, the shifting and the magnitude of the aging curves decrease as T_a increases (Figure 3.29).

Aging data obtained at three different aging temperatures are shown in Figure 3.30 and the corresponding CF parameters listed in Table 3.14. $\Delta H_\infty(T_a)$ values indicate that the distance for P4VPy to reach its thermodynamic equilibrium state is quite short in comparison with P4HS (Figure 3.31). This result is expected due to weaker interactions between the vinyl groups in P4VPy, compared to stronger hydrogen bonding interactions in P4HS.

The $\log(\langle t_C \rangle)$ data in Figure 3.32 demonstrate that P4VPy relaxes more slowly than P4HS and, once again, this can be attributed to the weaker interactions in P4VPy.

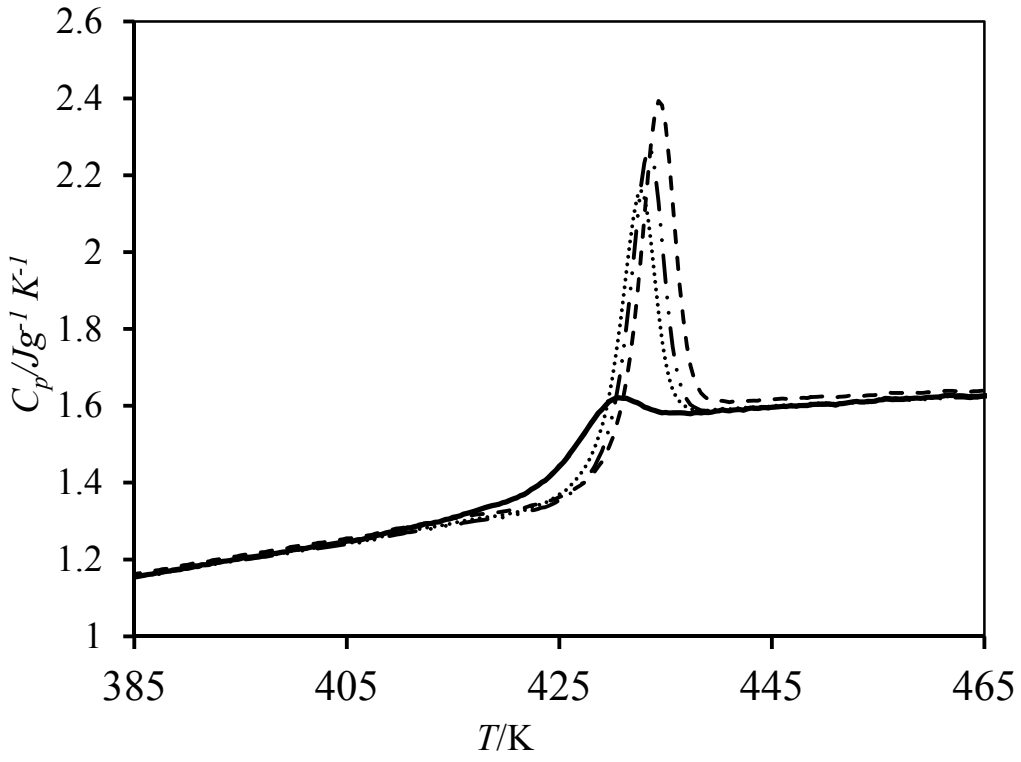

Figure 3.28 Heat capacity curves for P4VPy at T_g -T_a = 15 K: 200 (……), 500 (—••—••—) and 2000 (- - - - -) minutes.

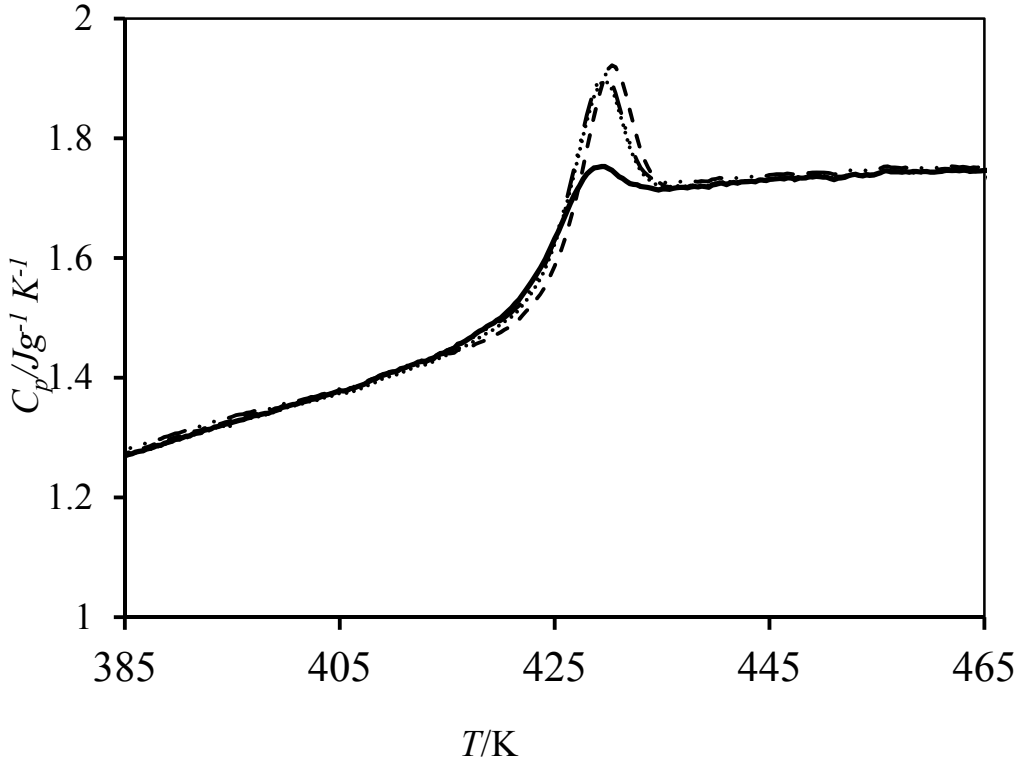

Figure 3.29 Heat capacity curves for P4VPy at T_g -T_a = 10 K: 200 (……), 500 (—••—••—) and 2000 (- - - - -) minutes.

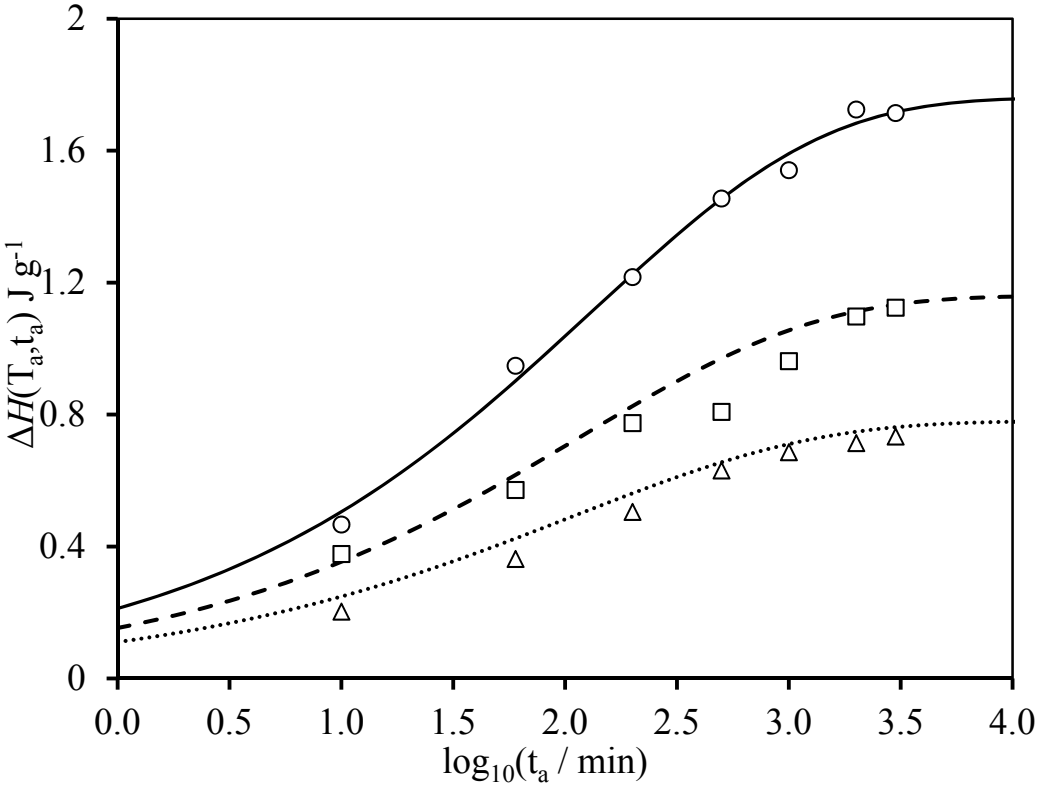

Figure 3.30 Enthalpy relaxation data for pure P4VPy; (T_g- T_a): (○) 15K; (□) 10K; (Δ) 5K. The lines are fits to the experimental data, using the CF equation.

Table 3.14 - CF Parameters for P4VPy

T_a (K)	T_g- T_a (K)	$\Delta H_\infty(T_a)$ ($J\,g^{-1}$)	log t_c (min)	β
410	15	1.80	2.12	0.42
415	10	1.17	2.06	0.42
420	5	0.78	1.81	0.42

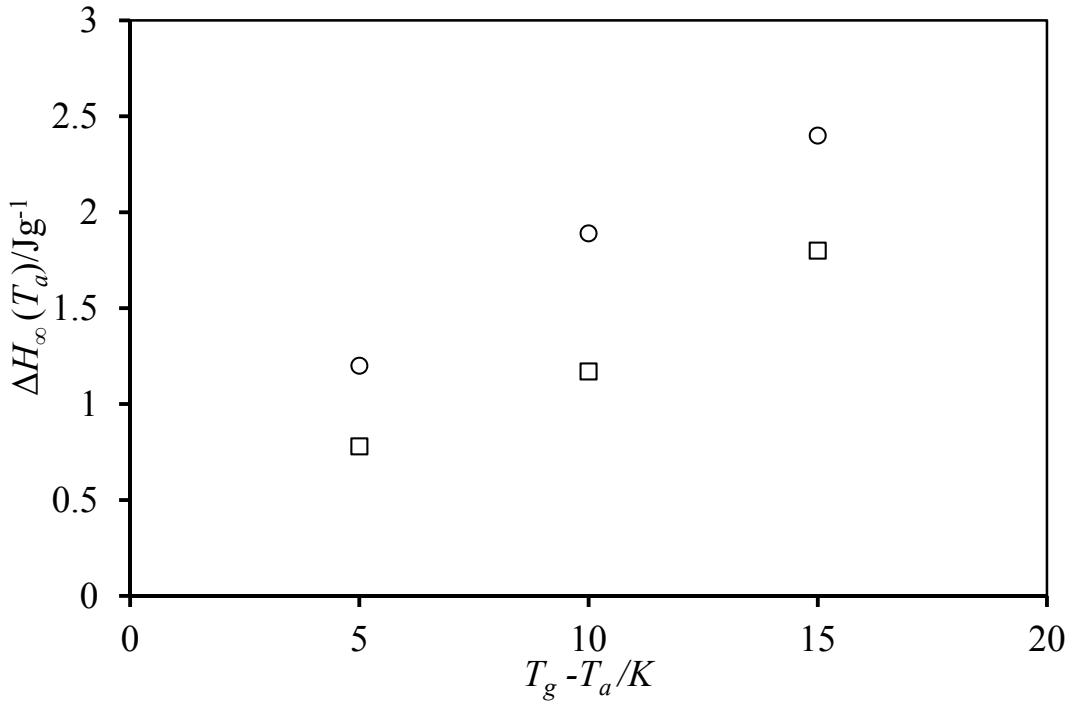

Figure 3.31 $\Delta H_\infty(T_a)$ versus (T_g- T_a) for (O) P4HS and (□) P4VPy.

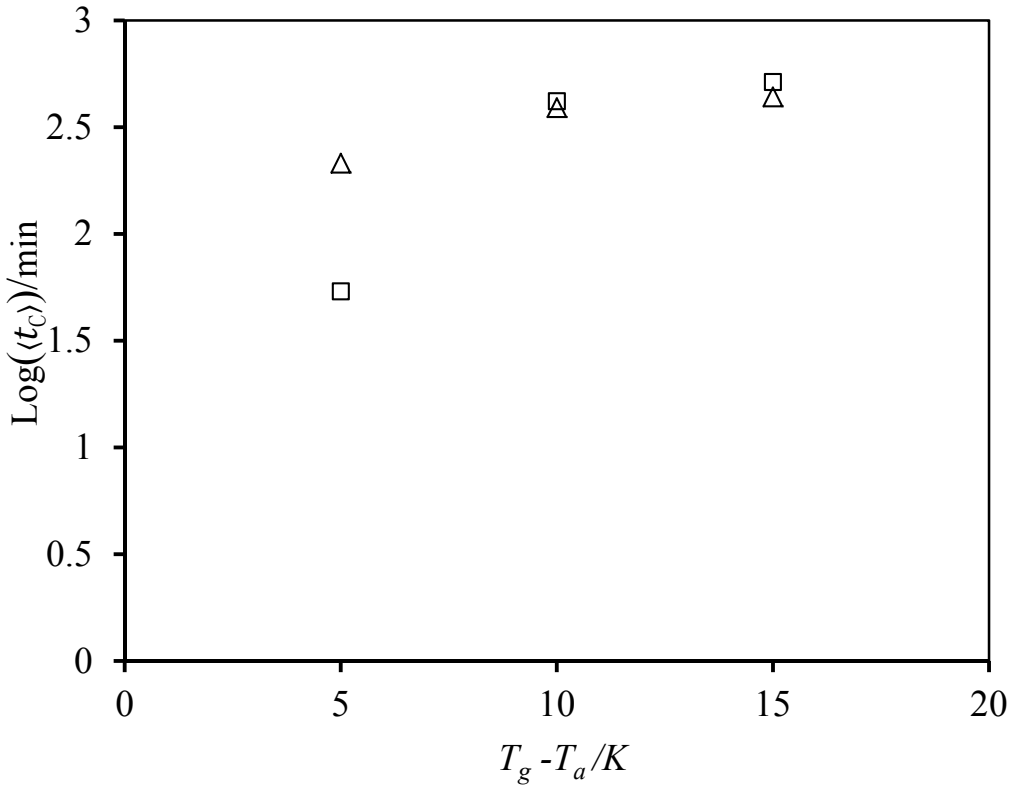

Figure 3.32 log (⟨t_C⟩) versus (T_g- T_a) for (□) P4HS and (Δ) P4VPy

3.5 Aging of polyethylene oxide

Despite numerous papers on polyethylene oxide (PEO) and its blends, to date, only two papers have been published on the physical aging of PEO [102, 103]. Those papers dealt with studies of the volume and dielectric relaxation in PEO and so no enthalpy relaxation measurements have been reported. In this project, attempts were made to measure the enthalpy relaxation of PEO, despite difficulties due to conducting experiments at low temperature and dealing with a sample of high crystallinity.

Aging measurements on PEO were carried out at Strathclyde University as our DSC instrument was not equipped to access low temperatures.

The DSC scans of unaged and aged PEO at (T_g-5) were measured by heating the sample from -80^{o}C to -5^{o}C (heating rate 10^{o}C/min). Figure 3.33 displays heat capacity curves of PEO at T_g-5, for different aging times. Several attempts were made to collect enthalpy relaxation data at aging temperature lower than 5 degrees under T_g but these were unsuccessful. This was attributed to the small amorphous content in highly

crystalline polymer and the inability of the DSC instrument to detect a small change in heat capacity at the glass transition. Hence, a series of experiments was conducted by changing the heating rate with which the DSC traces were recorded. As shown in Figure 3.34, no T_g can be seen in the DSC trace of a PEO sample heated at a rate of 10^oC/min. However, the reduction of the heating rate to 5^oC/min leads to a clear glass transition for the unaged sample (Figure 3.35). Unfortunately, after aging, none of the DSC traces of the unaged and aged samples showed evidence of a glass transition (Figures 3.36 (a) and (b)). Measurements at lower heating rate e.g. 2 or 1^oC/min could not be carried out as the time allowed on the instrument was very limited.

The aging data collected at T_g*-5* were fitted to the C-F model and the parameters are given in Table 3.15. The plot of $\Delta H(T_a, t_a)$ versus $\text{Log}(t_a)$ is shown in Figure 3.37.

The enthalpy relaxation value at T_g*-5* for PEO is very low in comparison to values reported in the previous sections for homopolymers and copolymers. This is certainly to be attributed to the low fraction of amorphous chains in the semi-crystalline sample. The low $\Delta H_\infty (T_a)$ value supports this conclusion. The enthalpy relaxation study of other semi-crystalline Polymer (i.e. poly(arylene ether ether ketone)) (PEEK) has also reported that the increase in the fraction of amorphous chains in semi-crystalline polymer would be result in the shift of the relaxation spectrum to longer times [140].

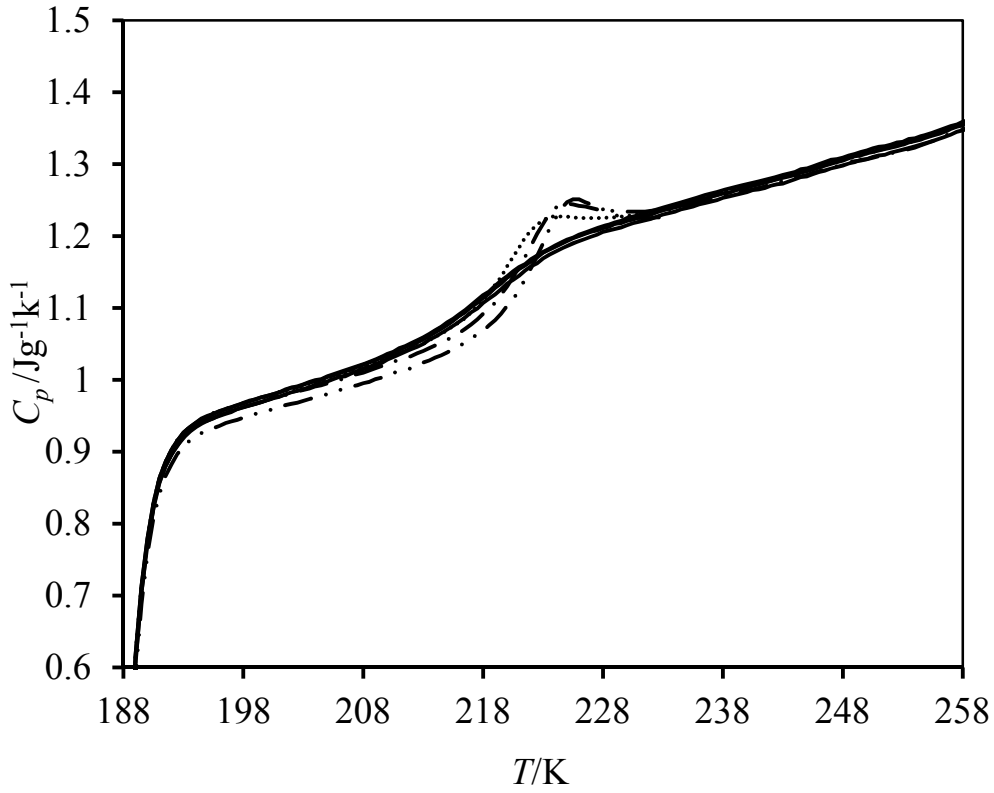

Figure 3.33 Heat capacity curves for PEO at T_g -T_a = 5 K: 60 (……), 200 (- - - - -) and 500 (—••—••—) minutes.

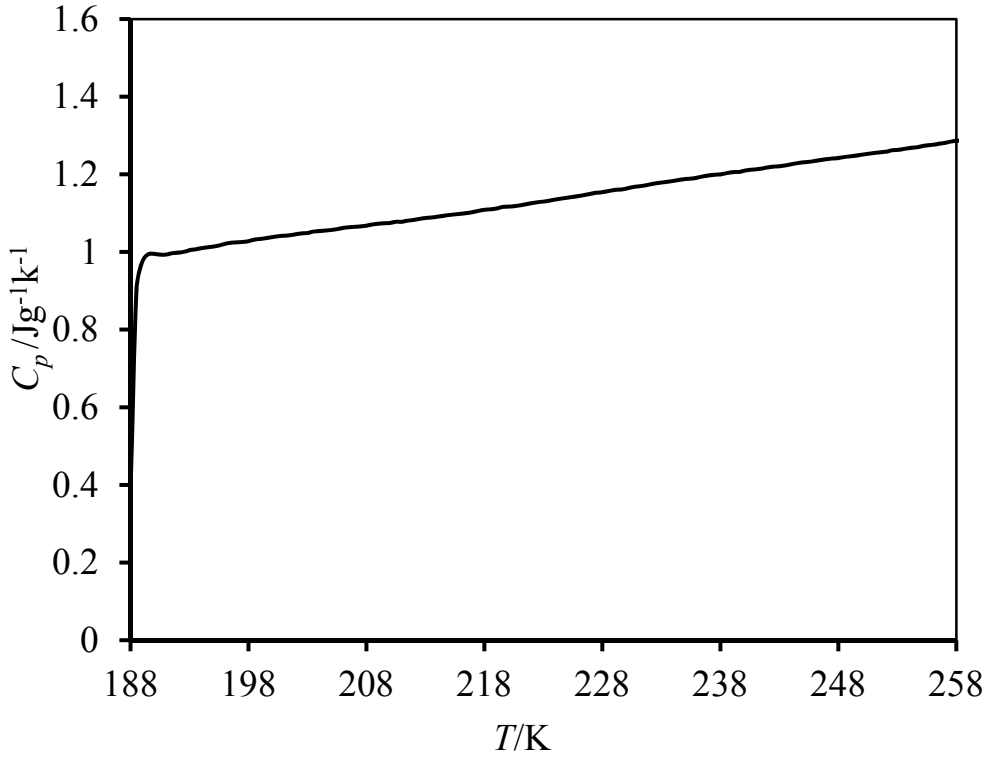

Figure 3.34 Heat capacity curves for unaged PEO recorded at a heating rate of 10^{o}C/min.

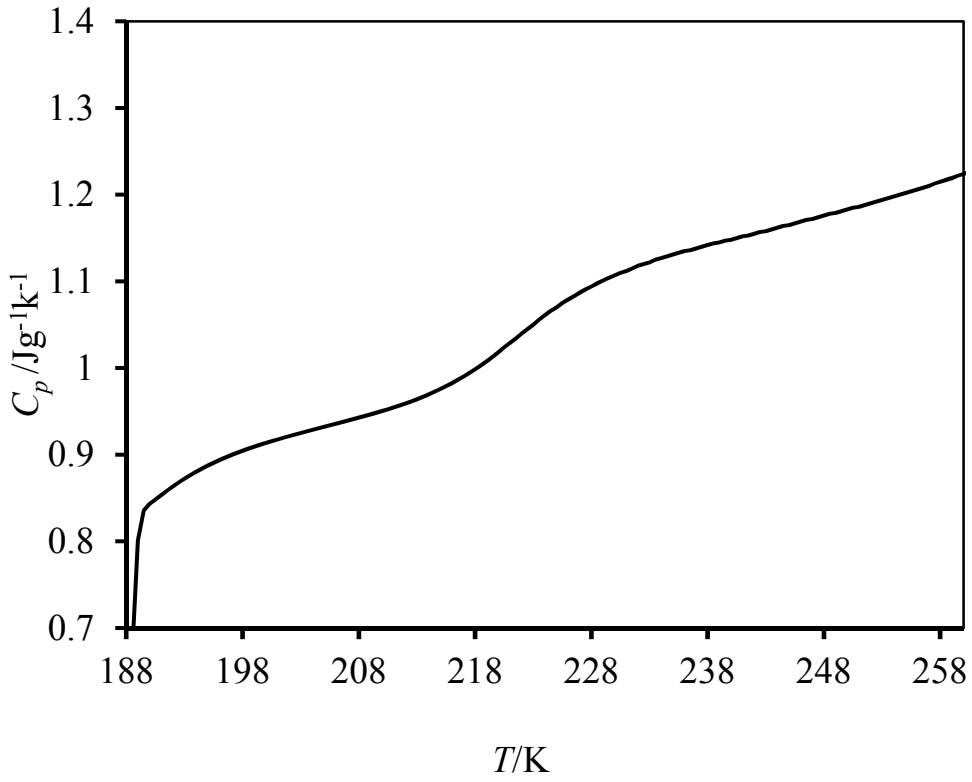

Figure 3.35 Heat capacity curves for unaged PEO recorded at a heating rate of 5^{o}C/min.

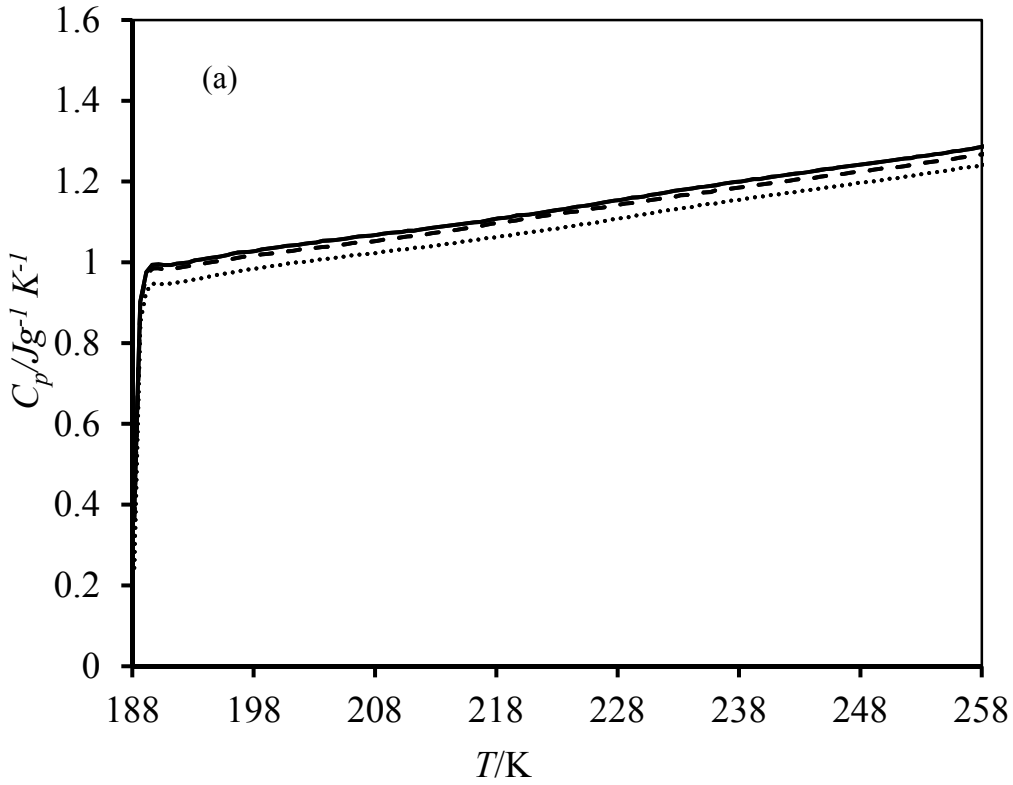

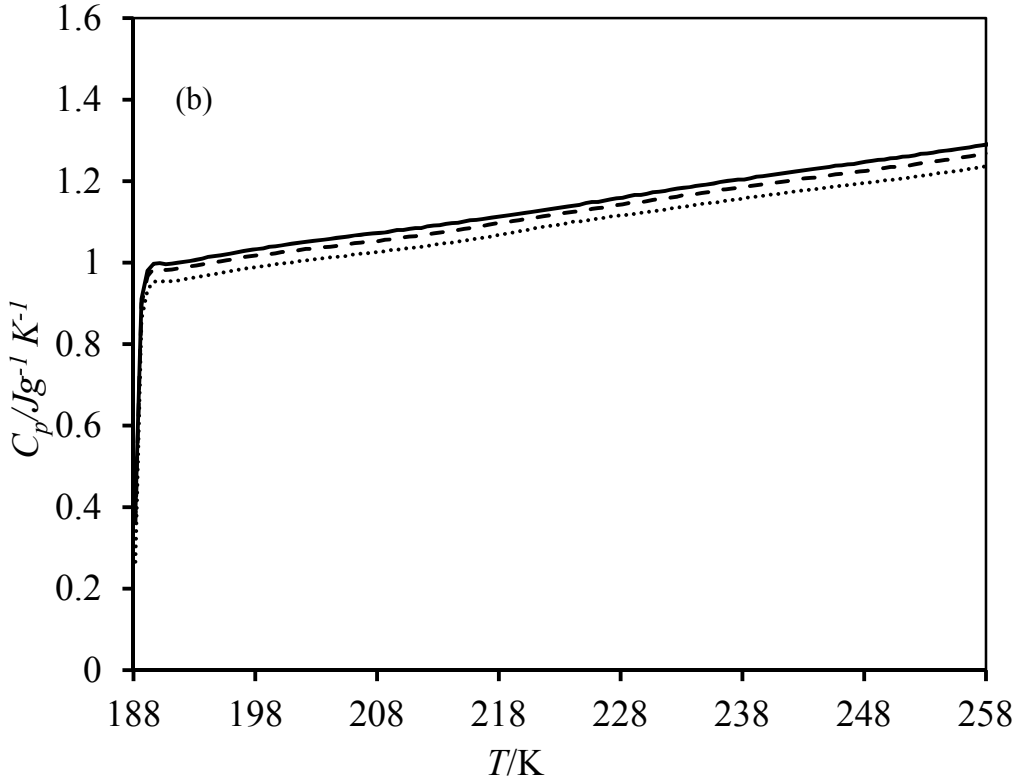

Figure 3.36 Heat capacity data for PEO at T_g -T_a = 10 K: 60 (……), 200 (- - - - -) and 500 (—••—••—) minutes; (a) unaging (b) aging; heating rate of 5°C/min.

Table 3.15 CF Parameters for PEO

T_a *(K)*	T_g- T_a *(K)*	$\Delta H_\infty(T_a)$ *(J g^{-1})*	log t_c (min)	β
214	5	0.29	1.54	0.65

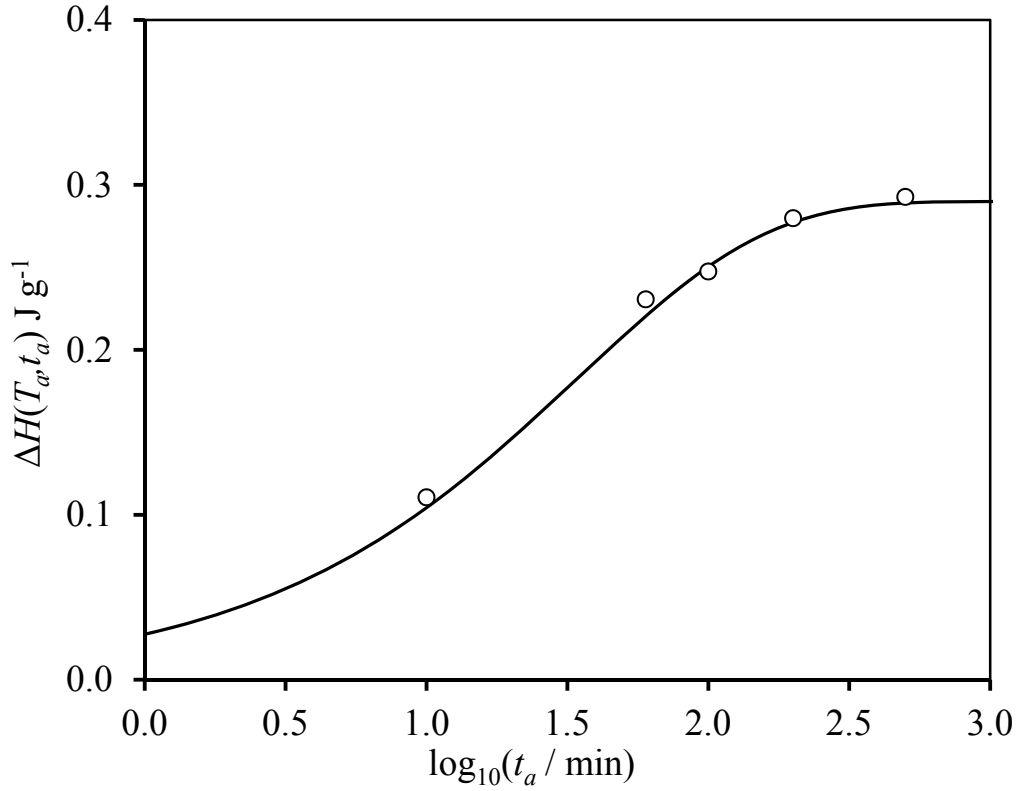

Figure 3.37 Enthalpy relaxation data for pure PEO; (T_g- T_a): (○) 5K. The continuous line is a fit to the experimental data using the CF equation.

Chapter 4 Hydrogen bonding and enthalpy relaxation of poly(4-Hydroxystyrene) blends

4.1 Introduction

The phenolic hydroxyl group in poly(4-hydroxystyrene) (P4HS) can form intermolecular hydrogen bonds with several kinds of hydrogen-bond acceptors. For example, poly(alkyl acrylates) such as PMMA and PEMA have been reported by Coleman et al. [43] to form miscible blends with P4HS. Polypyridines (for example: P4VPy) and ether polymers (PVME and PEO) also form one-phase mixtures with P4HS [141]. The results indicate that P4HS is miscible with PVME and PEO at all compositions. Physical aging studies of PEO and PVME blends with P4HS are reported in this chapter. Comparisons are made between the aging behaviour of ether/P4HS blends and that of the P4HS/PEMA system. It was hoped that analysis of the carbonyl stretching absorption in PEMA blends could provide additional information on the effect of intra- and inter-molecular H-bonding [34, 41, 42]. The third system reported in this chapter is the P4HS/P4VPy blend. Previous studies have indicated that the interaction between P4HS and P4VPy is very strong [142, 143]. To date, no aging data have been reported for these blends.

The first part of this chapter aims to discuss the effect of composition and temperature on hydrogen bonding strength in P4HS/PEMA, P4HS/PEO and P4HS/P4VPy blends. The results of the enthalpy relaxation measurements are then discussed with reference to pure P4HS.

4.2 Infrared spectroscopy

Infrared spectroscopy has been widely utilized to investigate hydrogen-bonding interactions in polymer blends, particularly in the hydroxyl stretching region from 3000 to 3700 cm^{-1}, by following the shift in frequency of the absorption peak [142, 144-146]. Although, there are several infrared studies on P4HS-based blends [54, 147-150], in order to link interactions and aging, it was necessary to use FTIR to qualitatively and quantitatively evaluate changes in the carbonyl and hydroxyl vibration regions in our blend samples. The changes in hydrogen bond distributions will assist with interpreting the aging data.

4.2.1 P4HS/ PEO blends: Qualitative analysis

As discussed in section 3.2, the peak of the free hydroxyl stretching vibration in undiluted P4HS (Figure 4.1) occurs at 3530 cm^{-1}. This non-hydrogen bonded OH absorption gradually disappears as the PEO content increases [113]. The self-association of phenolic groups in P4HS is responsible for the vibrational absorption peak at ~3360 cm^{-1}. This peak shifts progressively to lower wavenumbers with increasing PEO content, as shown in Figure 4.1. Coleman and co-workers [113] suggest that the difference in wavenumber ($\Delta\nu$) between the free hydroxyl band and the band attributed to hydrogen bonded OH groups can be used as a measure of the relative strength of hydrogen bonding. Accordingly, the large value of $\Delta\nu \approx 205$ cm^{-1} in P4HS/PEO blends demonstrates that hydrogen bonding between PEO and P4HS is stronger than the self-association $\Delta\nu \approx 170$ cm^{-1} between P4HS repeat units. To determine the exact location of the bands, the second derivative of each spectrum was calculated (Figure 4.2) and values are reported in Table 4.1.

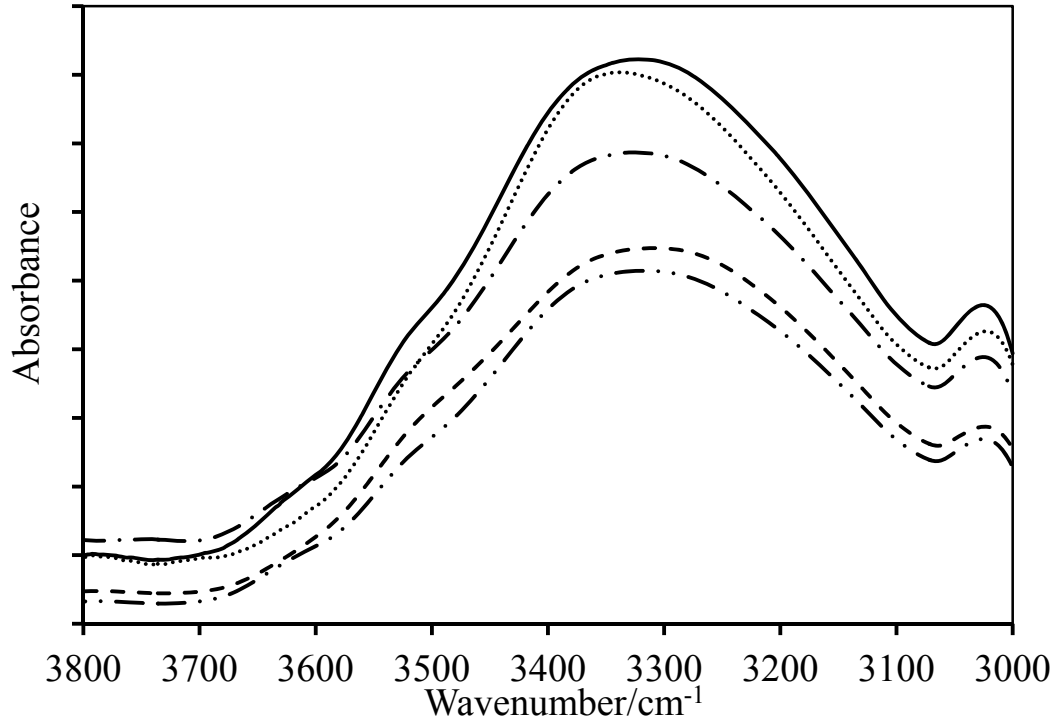

Figure 4.1 FTIR spectra recorded at room temperature in the 3700-3000 cm^{-1} region for P4HS/PEO blends containing: : (—••—••—) 46, (— — —) 59, (—•—•—) 67, (……..) 87 and (———) 100 mole-% P4HS.

Table 4.1- the position of intra-molecular hydrogen- bonded OH bands of P4HS/PEO blends (data from second derivative)

mole-% of P4HS in blends	ν_{HB} /cm^{-1}
59	3384
67	3390
87	3393
100	3398

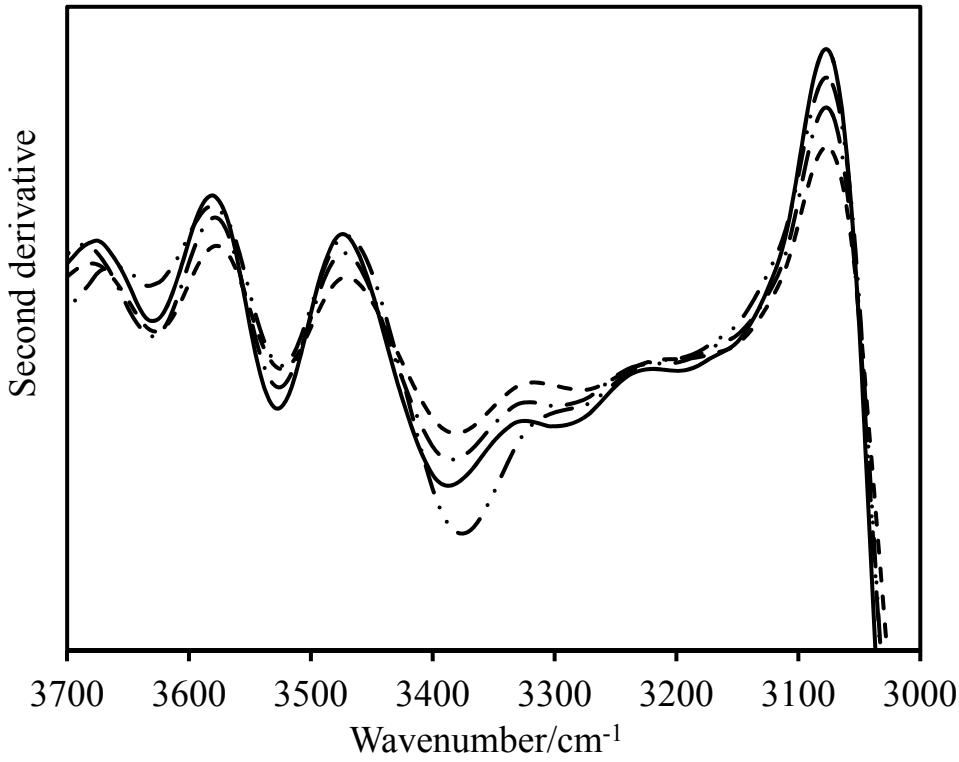

Figure 4.2 Second derivative spectra of P4HS/PEO blends containing: (—••—••—) 59, (— — —) 67, (—•—•—) 87 and (———) 100 mole% P4HS.

4.2.2 P4HS/ PEMA blends

The FTIR spectra of P4HS/PEMA blends in Figure 4.3 show features that are similar to those discussed for the PEO blends: the free OH band at 3530 cm^{-1}decreases as the PEMA content in the blend increases, and the main peak at 3360 cm^{-1} shift to higher wavenumbers. This peak shift is attributed to the appearance of another contribution, namely inter-molecular interactions between the carbonyl groups of PEMA and the P4HS hydroxyl groups. Figure 4.3 shows qualitatively that the number of free and self-associated hydroxyls decreases to the benefit of inter-associated hydrogen bonds, at higher PEMA contents. For a 74/24 P4HS/PEMA sample, a nearly Gaussian-shaped band centred at 3447 cm^{-1} is observed, which is due almost entirely to inter-associated hydroxyl groups. As noted by Li and Brisson[15], at low P4HS contents, the hydroxyls of P4HS will be randomly distributed among a large number of carbonyl groups since the PEMA network will dominate. However, increasing the amount of P4HS increases the probability of self-association occurring and this accounts for the

increased distribution of the hydroxyl band, which now contains contributions from free, self-associated and inter-molecular hydroxyl vibrations.

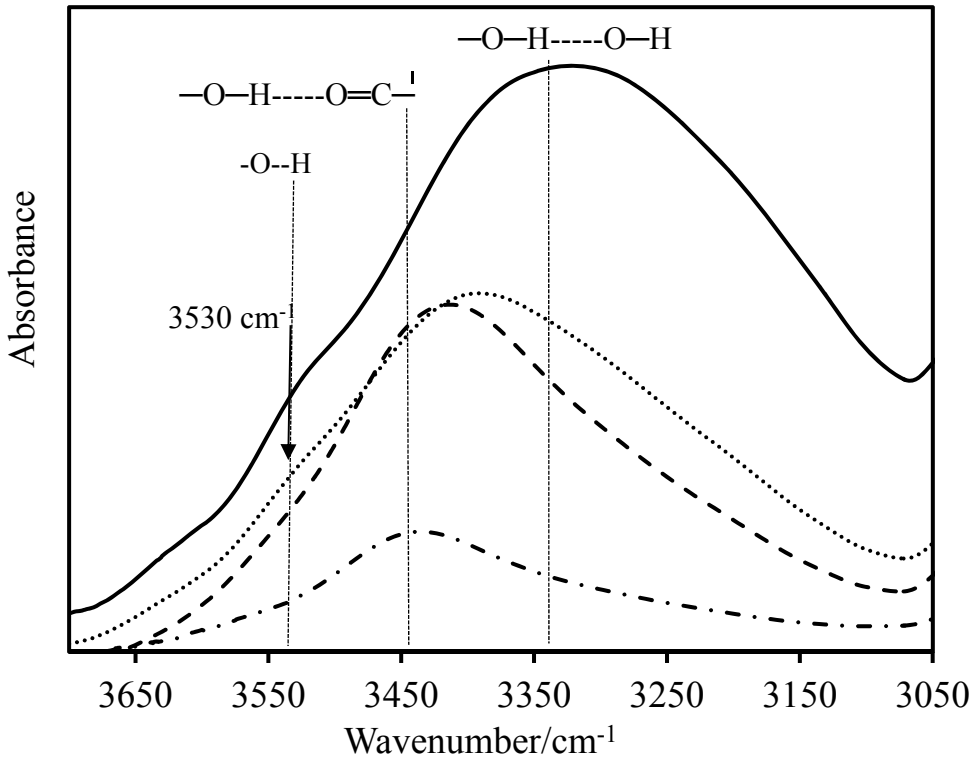

Figure 4.3 FTIR spectra recorded at room temperature in the 3700-3000 cm^{-1} region for P4HS/ PEMA blends containing: (—•—•—) 24, (— — —) 51, (……..) 74 and (———) 100 mole-% P4HS.

4.2.3 P4HS/ P4VPy blends

Figure 4.4 gives FTIR spectra of the hydroxyl stretching vibration region for pure P4HS, and two P4HS/P4VPy blend (67/33, and 59/41 mole%) . The absorption band due to hydrogen bonds between the phenolic-OH group in P4HS and the pyridine groups in P4VPy is centred at about 3150cm^{-1}. The Δv value (380 cm^{-1}) measured for the P4HS/P4VPy blends is larger than those reported for other P4HS blends (see previous sections) and much greater than the self-association ($\Delta v \approx 170$ cm^{-1}) among P4HS units. It is therefore indicative of very strong interactions between the polymer units.

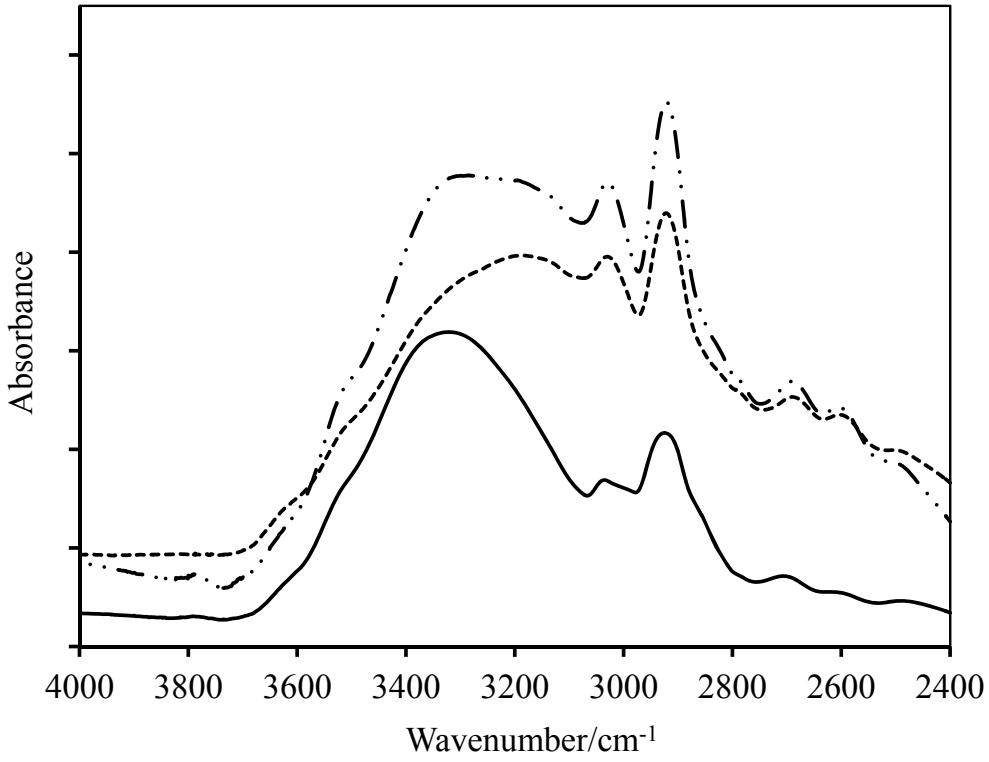

Figure 4.4 FTIR spectra recorded at room temperature in the hydroxyl region for (———) pure P4HS, (—••—••—) 67/33 and (---------) 59/41 P4HS/P4VPy blends.

4.2.4 Effect of temperature on hydrogen bonding

Figures 4.5 and 4.6 display the FTIR spectra of P4HS/PEO 87/13 at various temperatures and the second derivative, respectively. The results are tabulated in Table 4.2.

The FTIR spectra show that the area under the absorption band at 3324 cm^{-1} (i.e. hydrogen bonds between P4HS and PEO) decreases steadily and the peak shifts to higher wavenumbers with increasing temperature. On the other hand, the intensity of the band of free hydroxyl groups at 3533 cm^{-1} increases with increasing temperature. Although the number of hydrogen bonds decreases with increasing temperature, these still exist even at temperatures as high as 150^{o}C. Similar conclusions can be drawn for other compositions.

The shift of the intra-molecular H-bonding absorption band with temperature is composition dependent: in 59/41 P4HS/PEO (Figure 4.7) $\Delta\nu$ changes from 198 cm^{-1} at

25 ^{o}C to 143 cm^{-1} at 150 ^{o}C, which is less than the shift observed for 87/13 P4HS/PEO (Figure 4.6) ($\Delta\nu \approx$192 cm^{-1} at 25 ^{o}C, 100 cm^{-1} at 150 ^{o}C). These results indicate that hydrogen bond interactions in 59/41 P4HS/PEO are stronger than in the 13/87 blend, as the temperature increases. Second derivative spectra (Figure 4.8) indicate the presence of two peaks in the region between 3200-3450 cm^{-1}, one attributed to inter-associations and located at 3270-3290 cm^{-1} and the second one due to intra-associations, at 3380-3410 cm^{-1}. At 59/41 P4HS/PEO blend composition the increase in the intensity of the free hydroxyl band with temperature is less than that of 87/13 P4HS/PEO. Furthermore, the shift in the position of the intra-molecular band with increasing temperature is less pronounced than for 87/13 P4HS/PEO. Finally, the band due to intermolecular interactions is located at low wavenumber in the 59/41 blend compared to the 87/13 sample (Table 4.3). Thus, we can conclude that the strength of the inter- and intra-molecular interactions increases with increasing PEO content. Moreover, the shift of inter- and intra-association bands is also linked to the PEO content.

Table 4.2- The position of hydrogen- bonded OH bands of 87/13 P4HS/PEO blend (data from second derivative)

Temperature/ ^{o}C	*25*	*100*	*150*
The position of intra-molecular HB/cm^{-1}	*3391*	*3404*	*3420*
The position of intermolecular HB/cm^{-1}	*3287*	*--------*	*-------*

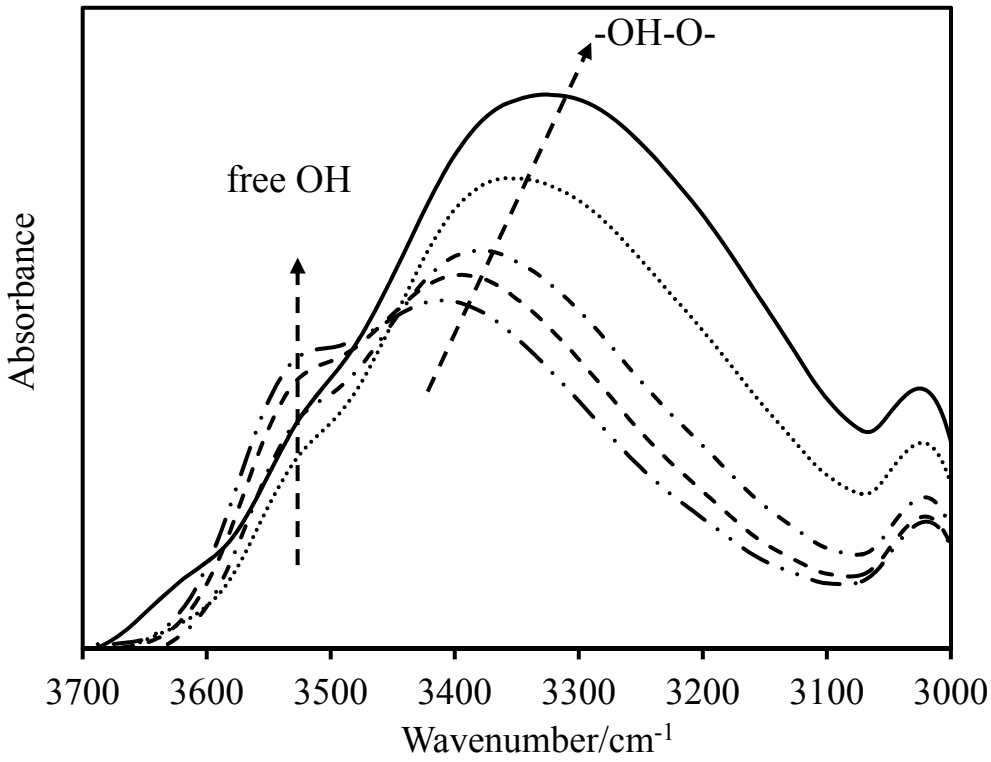

Figure 4.5 FTIR spectra recorded at different temperatures in the 3700-3000 cm^{-1} region for 87/13 P4HS/PEO blends: (———) 25 °C, (……) 50 °C, (—•—•—) 100 °C, (— — —) 125 °C and (—••—••—) 150 °C.

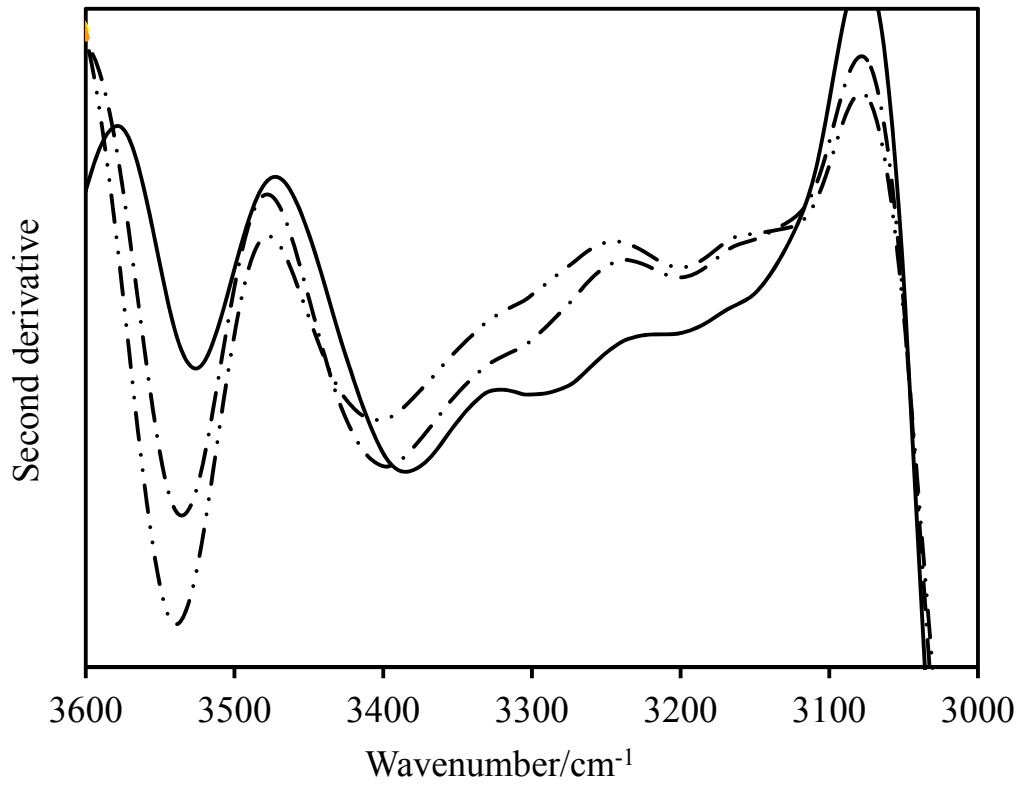

Figure 4.6 Second derivative spectra at different temperatures in the 3700-3000 cm^{-1} region for 87/13 P4HS/PEO: (———) 25 °C, (—•—•—) 100 °C, and (—••—••—) 150 °C.

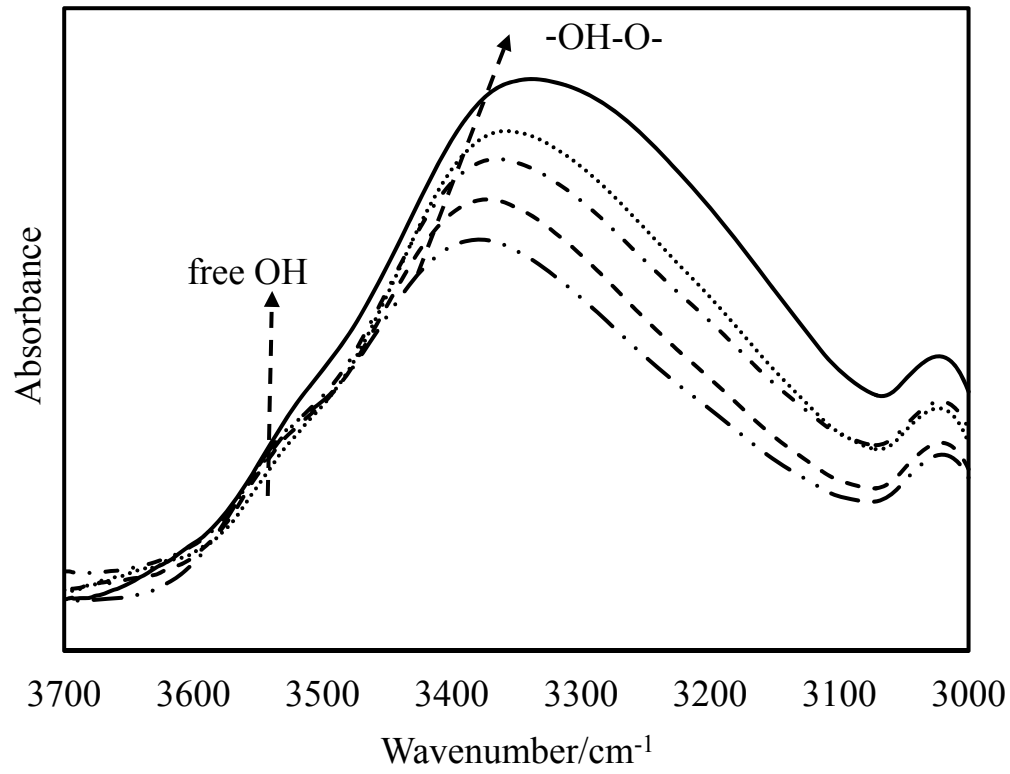

Figure 4.7 FTIR spectra recorded at different temperatures in the 3700-3000 cm^{-1} region for 59/41 P4HS/PEO blends: (———) 25 ^{o}C, (……..) 50 ^{o}C, (—•—•—) 100 ^{o}C, (— — —) 125 ^{o}C and (—••—••—) 150 ^{o}C.

Table 4.3- The position of hydrogen- bonded OH bands of 59/41 P4HS/PEO blend (data from second derivative)

Temperature	*25*	*100*	*150*
The position of intra-molecular HB/cm^{-1}	*3380*	*3393*	*3405*
The position of intermolecular HB/cm^{-1}	*3272*	--------	-------

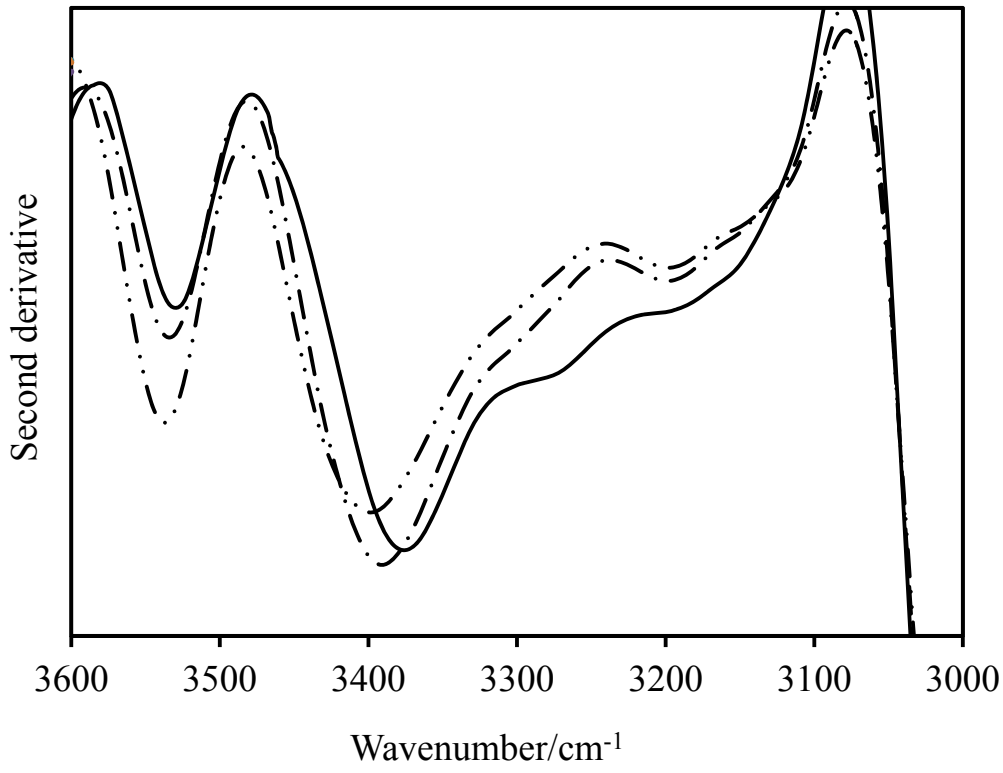

Figure 4.8 Second derivative spectra at different temperatures in the 3700-3000 cm^{-1} region for 59/41 P4HS/PEO: (——) 25 ^{o}C, (—•—•—) 100 ^{o}C, and (—••—••—) 150 ^{o}C.

For comparison with a well-studied system, FTIR spectra of a 59/41 P4HS/PVME blend were also recorded (Figure 4.9), as a function of temperature. It is evident that the temperature dependence of the FTIR spectra of the PVME blend (Figure 4.9) is similar to that of the PEO system, at a similar composition (Figure 4.7). The decrease in the wavenumber due to inter-association in the P4HS/PVME blend is $\Delta\nu \approx 190$ cm^{-1} (corresponding to a shift from 3530 to 3340 cm^{-1}) at 25 ^{o}C, which is bigger than the shift in wavenumber ($\Delta\nu \approx 170 cm^{-1}$) due to the self-association in P4HS. However, the decrease in the wavenumber due to hydrogen bonding interactions in P4HS/PVME, $\Delta\nu \approx 190$ cm^{-1}, is slightly less than observed in P4HS/PEO, $\Delta\nu \approx 198$ cm^{-1}. Therefore, the hydrogen bonding interactions in P4HS/PVME blends are stronger than that in pure P4HS but slightly weaker than that in P4HS/PEO blends.

The FTIR spectra of 59/41 P4HS/PVME also present a similar trend to the one observed for P4HS/PEO: $\Delta\nu \approx 143$ cm^{-1} at 150 ^{o}C in 59/41 P4HS/PEO compared to a value of $\Delta\nu \approx 132$ cm^{-1} for P4HS/PVME at the same temperature. This leads to the conclusion that hydrogen bonds in P4HS/PVME are weaker than in P4HS/PEO blends.

In fact, Le Menestrel et al. [151] have also noted that the P4HS/PEO specific interaction is stronger than that of P4HS/poly(vinyl alkyl ethers). The results from this work also support that claim.

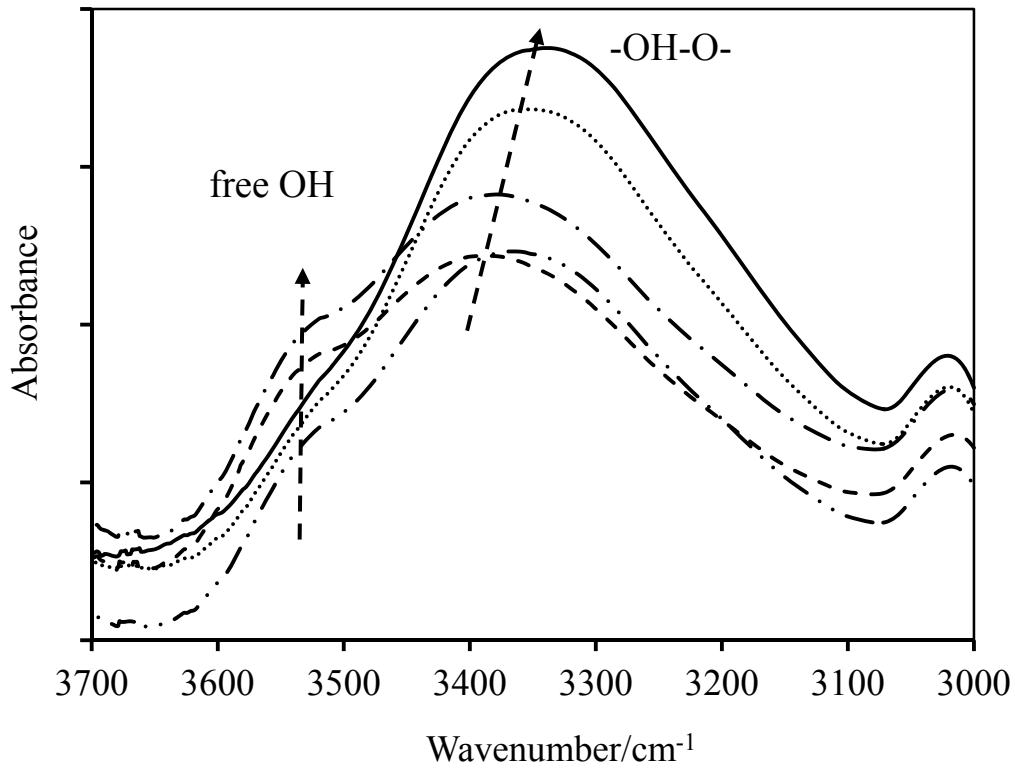

FTIR 4.9 Spectra recorded at different temperatures in the 3700-3000 cm^{-1} region for 59/41 P4HS/PVME blends: (———) 25 ^{o}C, (……..) 50 ^{o}C, (—••—••—) 100 ^{o}C, (—•—•—) 125 ^{o}C and (— — —) 150 ^{o}C.

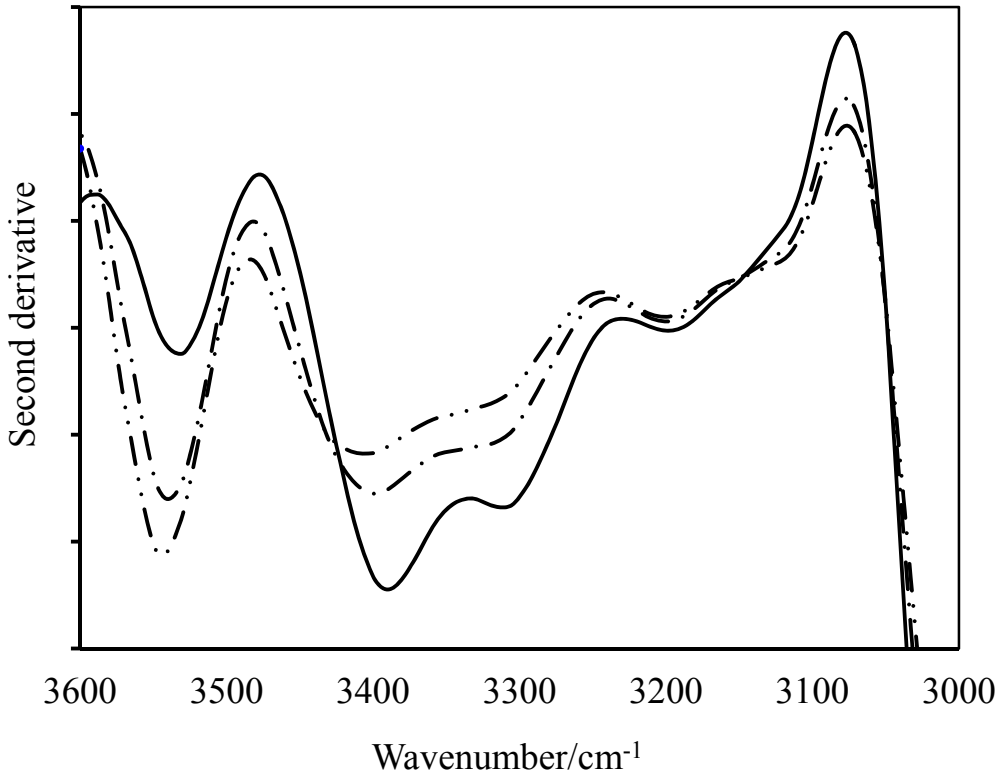

Figure 4.10 Second derivative spectra at different temperatures in the 3700-3000 cm^{-1} region for PVME/P4HS 41/59 mole.-%: (———) 25 ^{o}C, (—•—•—) 100 ^{o}C, and (—••—••—) 150 ^{o}C.

Figure 4.11 gives FTIR spectra of the 59/41 P4HS/P4VPy blend at different temperatures. Interestingly, the absorption band at 3150cm^{-1} does not shift as the temperature is increased. On the other hand, the absorption band at 3368 cm^{-1} due to self-association in P4HS increases as the temperature increases (Figure 4.12). All of these results indicate that the hydrogen bonds in P4HS/P4VPy blends are much more stable than those of other P4HS-based blends, like P4HS/PEO and P4HS/PVME.

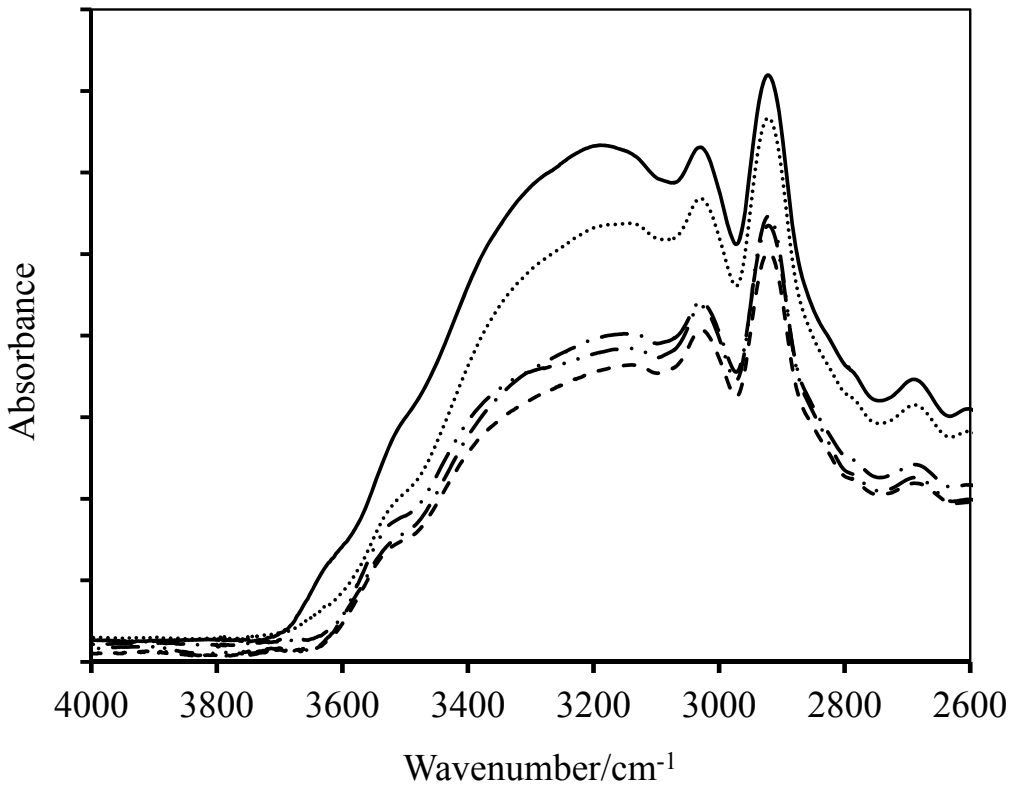

Figure 4.11 FTIR spectra recorded at different temperatures in the 3700-3000 cm^{-1} region for P4HS/P4VPy 59/41 mole% blends: (——) 25°C , (……..) 50 °C, (—•—•—)100 °C, (— — —) 125 °C and (—••—••—)150 °C.

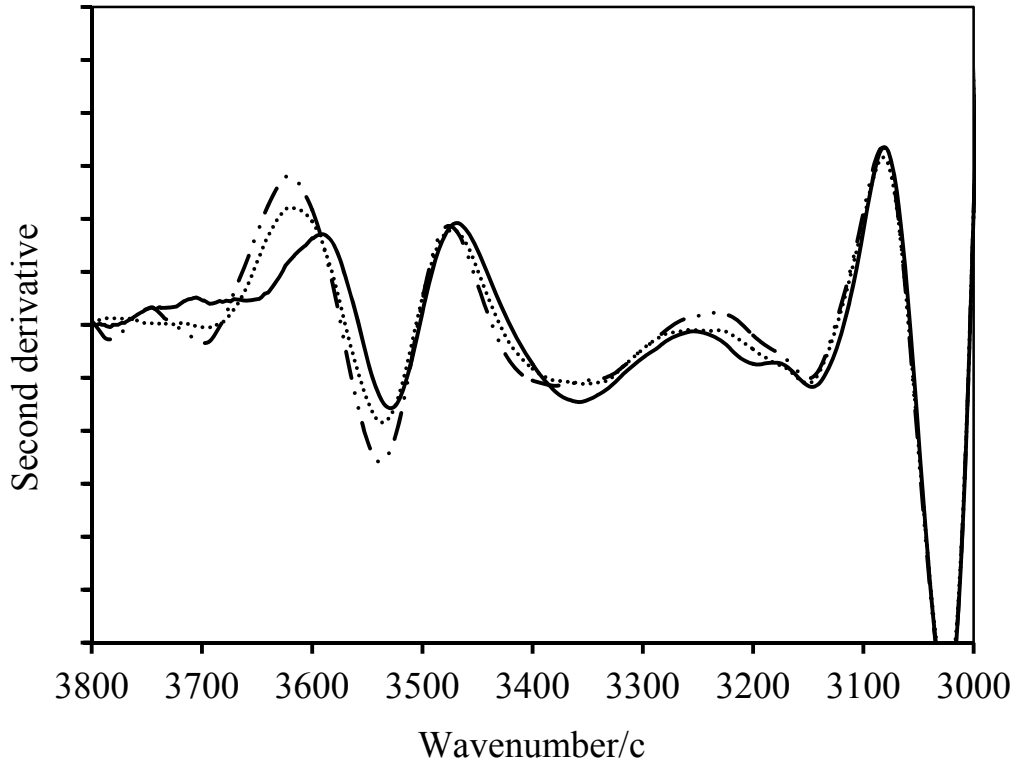

Figure 4.12 Second derivative spectra of 59/41 P4HS/P4VPy at: (——) 25 °C, (.....) 100 °C, and (—••—••—) 150 °C.

4.3 Enthalpy relaxation

4.3.1 Enthalpy relaxation of P4HS/PEMA blends

The mid-point T_g, T_g temperature range (ΔT) and experimental ΔC_p are displayed in Table 4.4. Glass transition temperatures for the blends are intermediate between the T_gs of P4HS and PEMA and increase with increasing P4HS content, as expected. Figure 4.13 shows the composition dependence of T_g. To a first approximation, the variation of T_g with blend composition can be predicted from ideal mixing (additivity of free volume) according to the Flory-Fox equation, as follows:

$$\frac{1}{T_{\mathrm{g}}} = \frac{w_1}{T_{\mathrm{g1}}} + \frac{w_2}{T_{\mathrm{g2}}} \qquad (4.1)$$

where T_g, T_{g1} and T_{g2} are the glass transitions of the blend and the two homopolymers, respectively, and w_1 and w_2 the weight fractions of component 1 and 2. As shown in Figure 4.13, the experimental data exhibit positive deviations from the Flory- Fox equation. To account for these, the experimental T_g versus composition data were fitted to the Kwei equation [152]:

$$T_{\mathrm{g}} = \frac{w_1 T_{\mathrm{g1}} + k w_2 T_{\mathrm{g2}}}{w_1 + k w_2} + q w_1 w_2 \qquad (4.2)$$

where k is treated as a random fitting parameter and the term qw_1w_2 accounts for the presence of strong interactions in the mixture. Painter and co-workers [153] have reported that the k parameter is

$$k = \frac{\Delta C_{p2}}{\Delta C_{p1}} \qquad (4.3)$$

where ΔC_{p2} and ΔC_{p1} are the discontinuities in the specific heat at the respective T_gs, and the subscripts 1 and 2 denote the PEMA and P4HS, respectively. In the limiting case, when $k = 1$, equation 4.2 reduces to a simple expression [152]:

$$T_{\mathrm{g}} = \left(w_1 T_{\mathrm{g1}} + w_2 T_{\mathrm{g2}}\right) + q w_1 w_2 \qquad (4.4)$$

The fit of the T_g, data to equation 4.4 gave a q value of 46. This is a first estimate of a q value for the P4HS/PEMA system, which is close to the q value of 49 reported by Hsu [154] for P4HS/PMMA.

The micro-heterogeneity level in the polymer blends can be evaluated by the magnitude of ΔT. Large ΔT values usually give evidence of increased micro-heterogeneity. All P4HS/PEMA blends have ΔT values larger than those of the pure polymers. Moreover, both blends rich in P4HS or PEMA give relatively high ΔT values, indicating that these are less homogeneous than those close to 1:1 ratios.

The change in heat capacity at T_g, $\Delta C_{p,}$ can be linked to the change in the degrees of freedom at the glass transition resulting from free volume changes [3]. In general, the value of ΔC_p decreases as the content of PEMA increases.

Table 4.4- T_g data for PEMA/P4HS blends.

P4HS/PEMA (wt-%)	P4HS/PEMA (mole-%)	T_g *(K)*	ΔT *(K)*	ΔC_p J K^{-1} g^{-1}
0/100	0/100	347	12.29	0.119
25/75	24/76	371	25.77	0.150
50/50	49/51	397	18.04	0.245
75/25	74/26	420	16.18	0.296
80/20	79/21	423	25.01	0.245
100/0	100/0	427	13.35	0.349

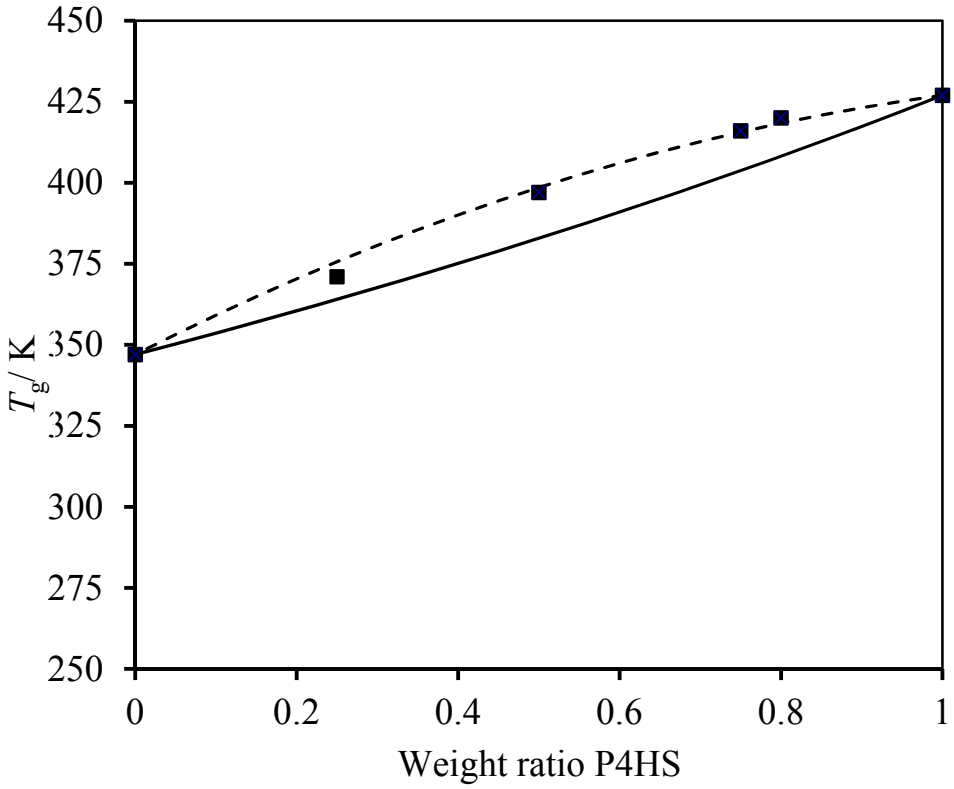

Figure 4.13 Composition dependence of T_g for PEMA/P4HS blends: experimental data (■), and fits to the Fox (solid line), and Kwei (long dashed line) equations.

Figure 4.14 shows typical C_p data for a 49/51 P4HS/PEMA sample aged at 10 K below T_g. Similar trends were observed for all of the blends.

The C_p curves of all P4HS/PEMA blends aged at 10 K below T_g are shown in Figure 4.15, for annealing times of 100 and 2000 min. These provide a qualitative measure of the difference in enthalpic recovery behaviour between the blends. The blends of P4HS/PEMA with high PEMA and P4HS content present relatively broad enthalpy relaxation peaks. It should be noted that aging 79/21 P4HS/PEMA for 2000 min at 10K below the T_g seemed to give two close enthalpic peaks at 433 K. The presence of double enthalpic relaxation peaks has been noted in immiscible blends [105, 107]. It is worth noting that the 79/21 P4HS/PEMA sample had the biggest value of ΔT (Table 4.4), which is evidence of a wide range of hydrogen bonding distributions within the blend network and/or greater microheterogeneity. At this polymer composition, the blend network will be controlled by the stiffer P4HS chains and there will be free, self-associated and inter-molecular hydrogen bonding interactions. For this blend, at these aging temperatures and times, there appears to be some sort of phase separation, as

reflected by the two enthalpic recovery peaks. No other blend composition displayed this behaviour at the aging times and temperatures investigated. Consequently, enthalpy relaxation appears to be sensitive to phase behaviour in these blends, whereas a conventional DSC temperature scan is not.

The 49/51 P4HS/PEMA exhibits a relatively narrow enthalpy recovery peak. It is interesting to note that this blend had a low ΔT value, which seems consistent with the observation made earlier from the IR spectrum (Figure 4.3) that all hydroxyls form hydrogen bonds with the PEMA carbonyl groups.

Figures 4.16 (a-c) shows plots of $\Delta H(T_a, t_a)$ versus $\log(t_a)$ with fits from the CF model. The variation of $\Delta H_\infty(T_a)$ with $(T_g - T_a)$ for P4HS/PEMA blends is displayed in Figure 4.17. The figure also includes P4HS and PEMA data for comparison. $\Delta H_\infty(T_a)$ values increase with increasing distance from T_g, as would be expected.

There is an important point to note: the blends have higher values of $\Delta H_\infty(T_a)$ than PEMA, except for the blend with the highest PEMA content (76 mole.-%). This is probably a result of the inability of the CF model to precisely predict $\Delta H_\infty(T_a)$ when there is no clear inflection point in the data.

$\log(\langle t_c \rangle)$ against $(T_g - T_a)$ for each blend are given in Figure 4.18. The relaxation rate of neat PEMA at all undercoolings is faster than that of the PEMA/P4HS blends. In contrast, PEMA/P4HS blends relax more slowly than pure P4HS (Table 4.5 and Figure 4.18). It is interesting to note that the $\log(t_c)$ values for the 49/51 and 24/76 P4HS/PEMA samples are higher than values for other blend compositions, reflecting the presence of more/stronger interactions in these blends.

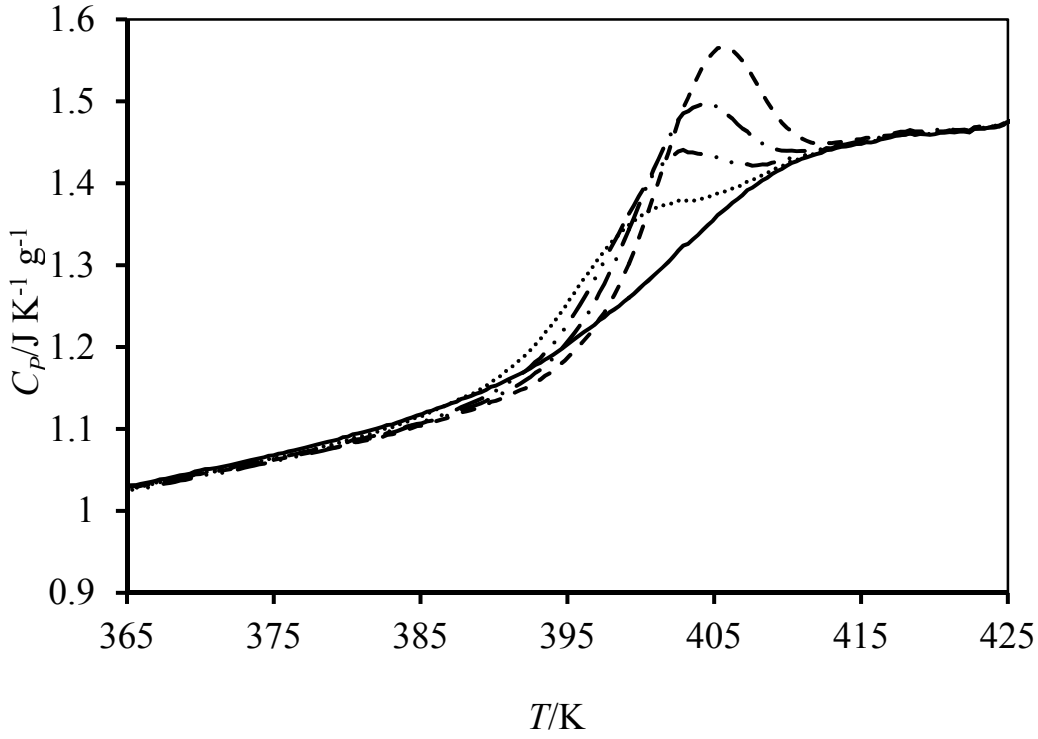

Figure 4.14 Heat capacity curves for 49/51 P4HS/PEMA aged at T_g -T_a = 15 K for 200(……..), 500(—••—••—), 1000(—•—•—) and 2000 (— — —) minutes.

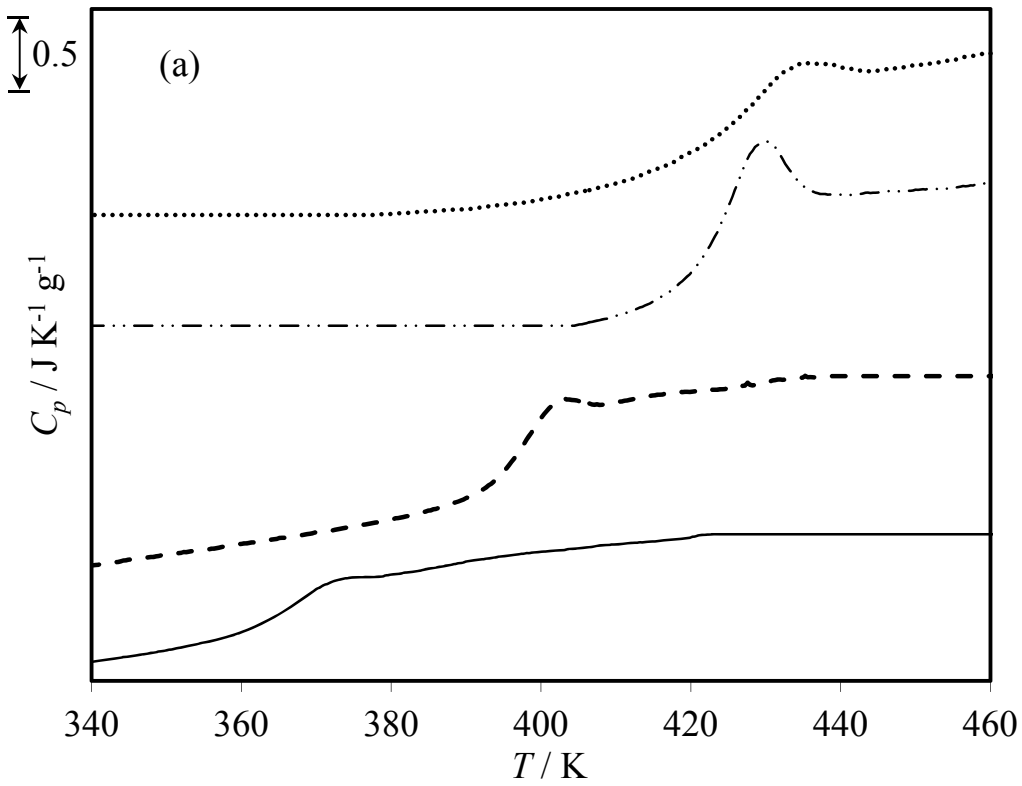

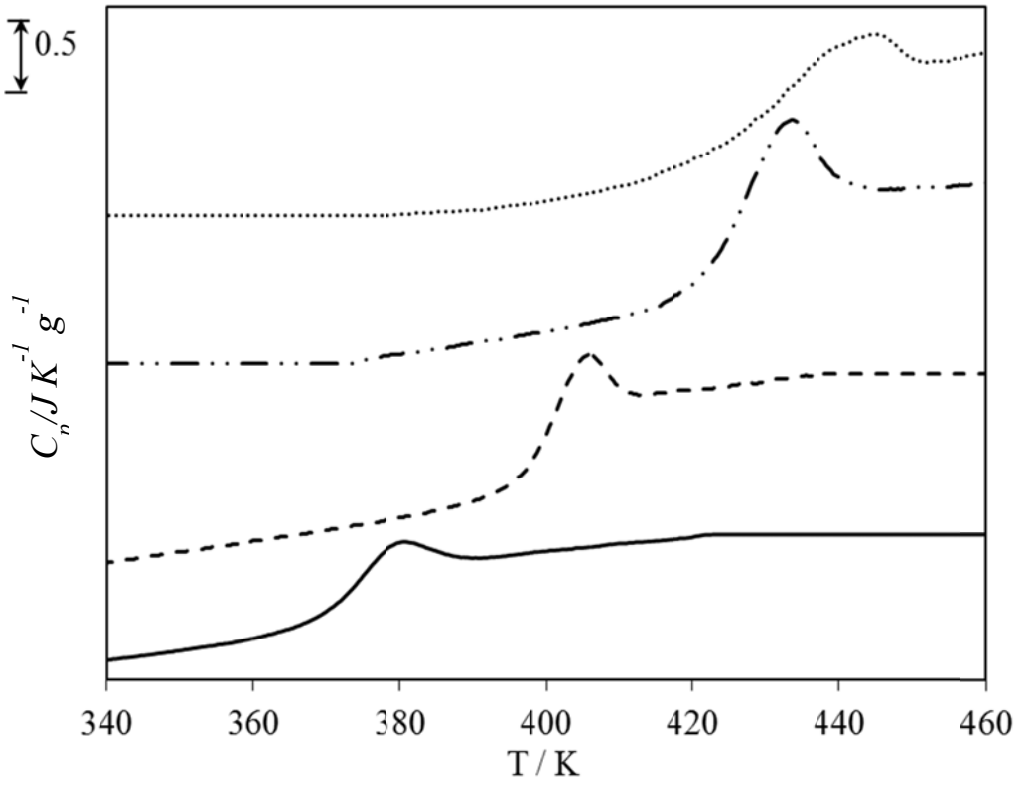

Figure 4.15 C_p curves for the P4HS/PEMA blends aged 15 K below T_g for (a) 100 min and (b) 2000 min: (..……..) 79/21, (—••—••—) 74/26, (— — —) 49/51, and (———) 24/76 mole %. Curves have been displaced vertically for clarity.

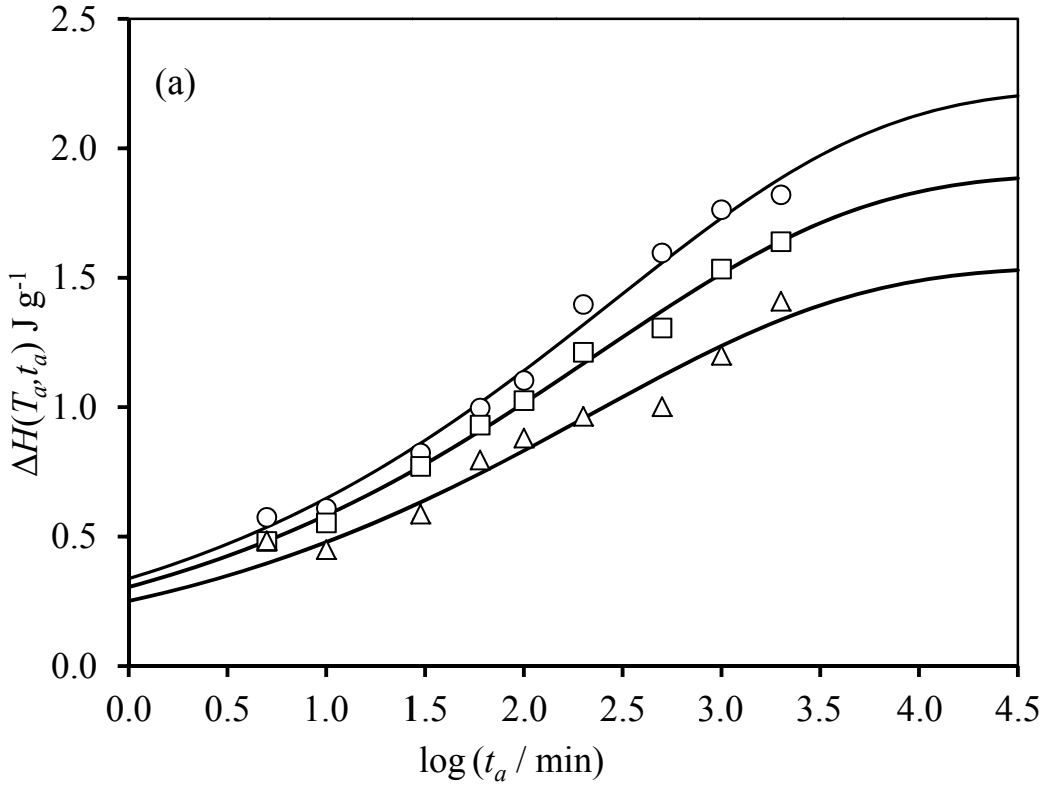

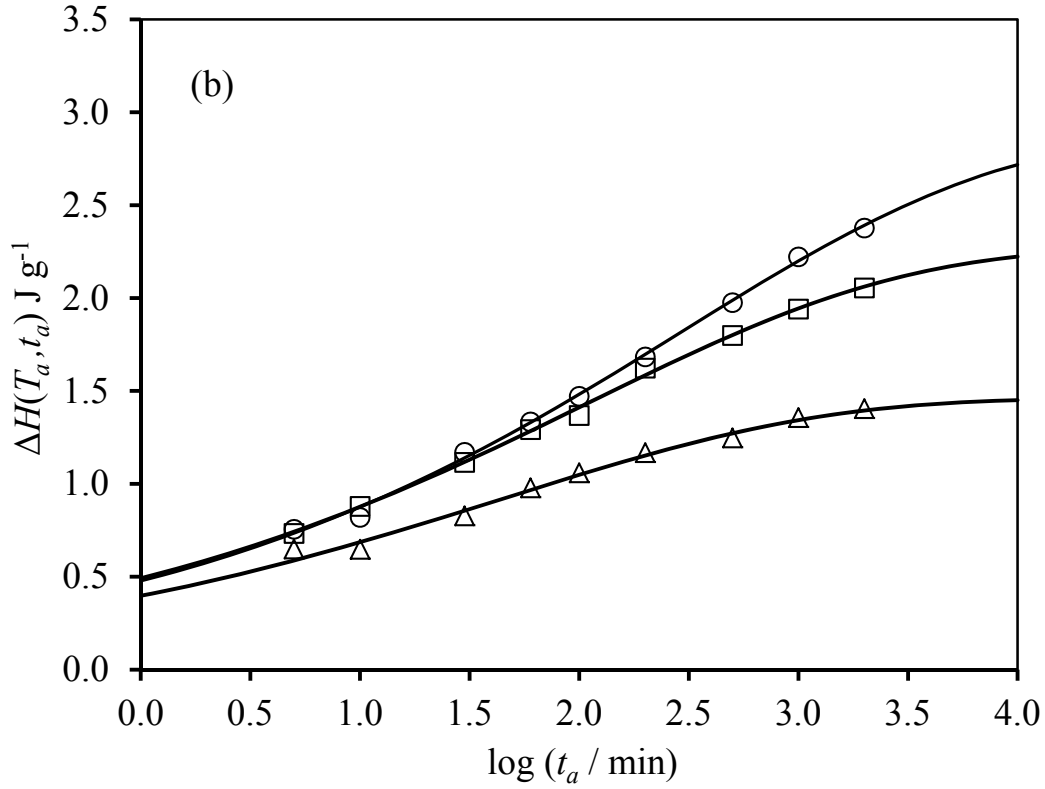
(b)
3.5
3.0
2.5
2.0
1.5
1.0
0.5
0.0
0.0
0.5
1.0
1.5
2.0
2.5
3.0
3.5
4.0
$\Delta H(T_a,t_a)$ J g^{-1}
log (t_a / min)

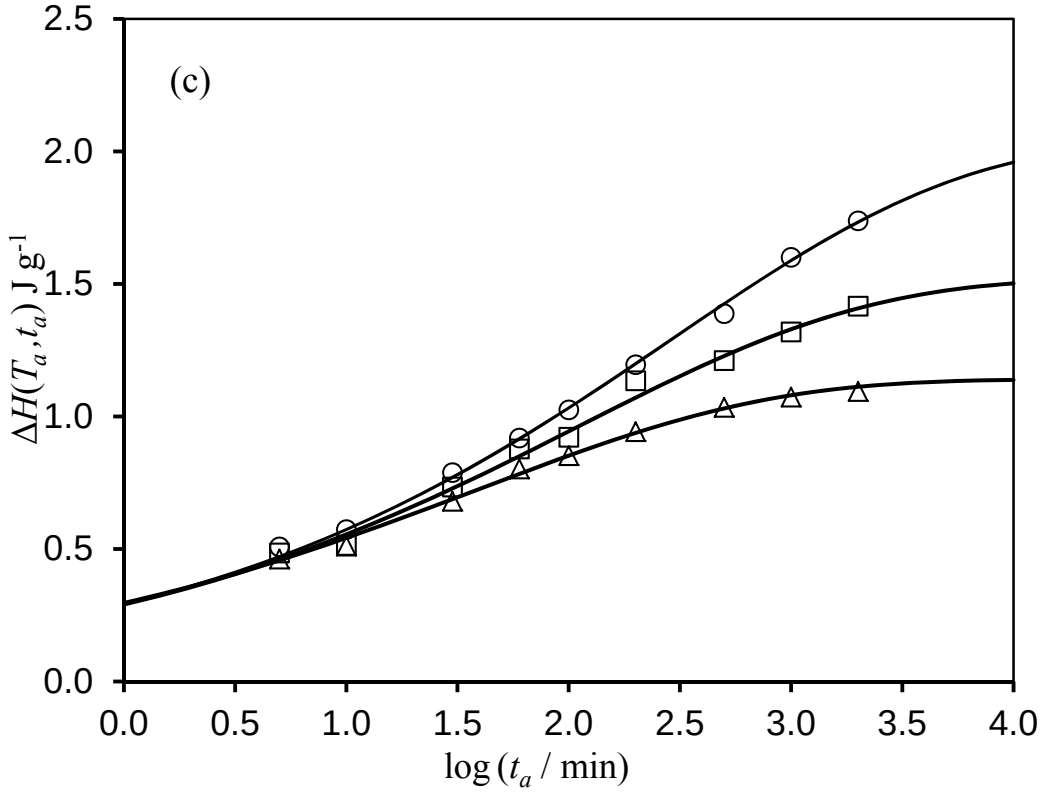
(c)
2.5
2.0
1.5
1.0
0.5
0.0
0.0
0.5
1.0
1.5
2.0
2.5
3.0
3.5
4.0
$\Delta H(T_a,t_a)$ J g^{-1}
log (t_a / min)

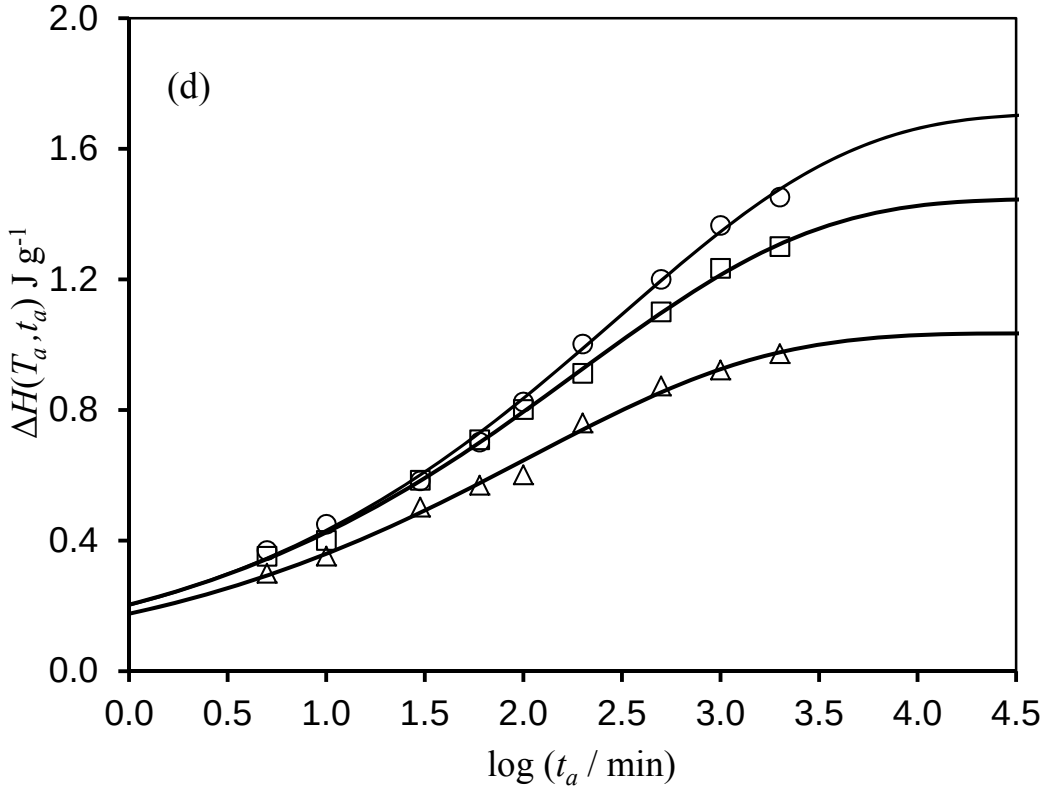

Figure 4.16 Enthalpy relaxation data for the P4HS/PEMA blends: (a) (79/21); (b) (74/26); (c) (49/51); (d) (24/76); (T_g- T_a): (○) 15K; (□) 10 K; (Δ) 5 K. The continuous lines are fits to the experimental data, using the CF equation.

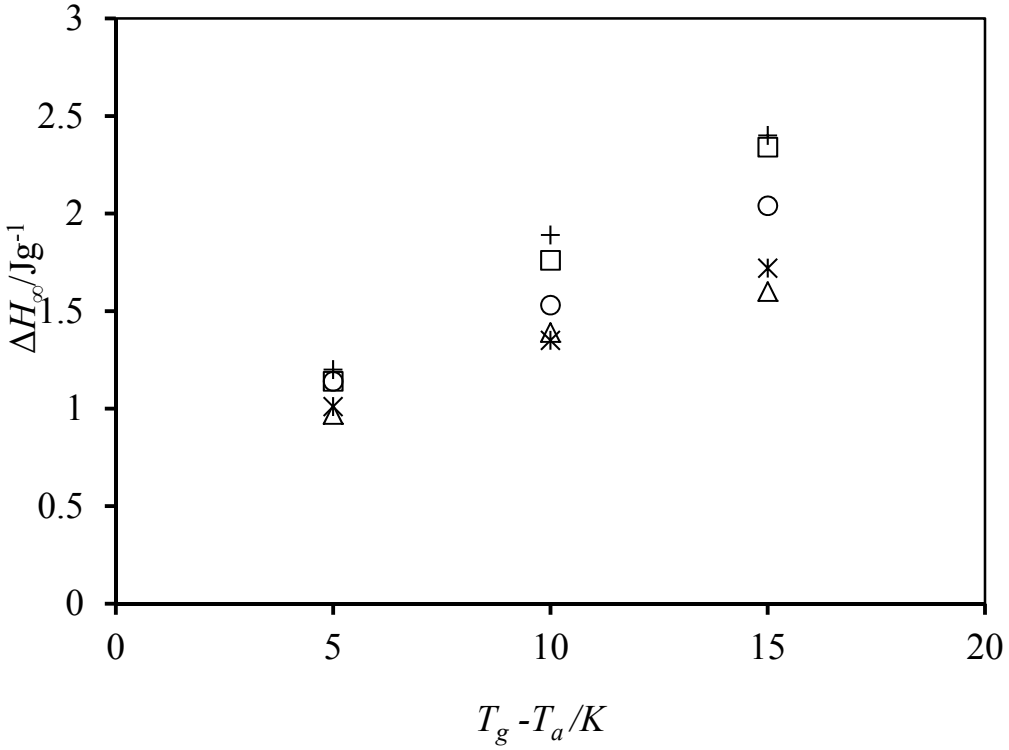

Figure 4.17 $\Delta H_\infty(T_a)$ versus (T_g- T_a) for P4HS (+), PEMA (Δ), and P4HS/PEMA: (74/26) (□), (49/51) (O), and (24/76 mole-%) (Ж).

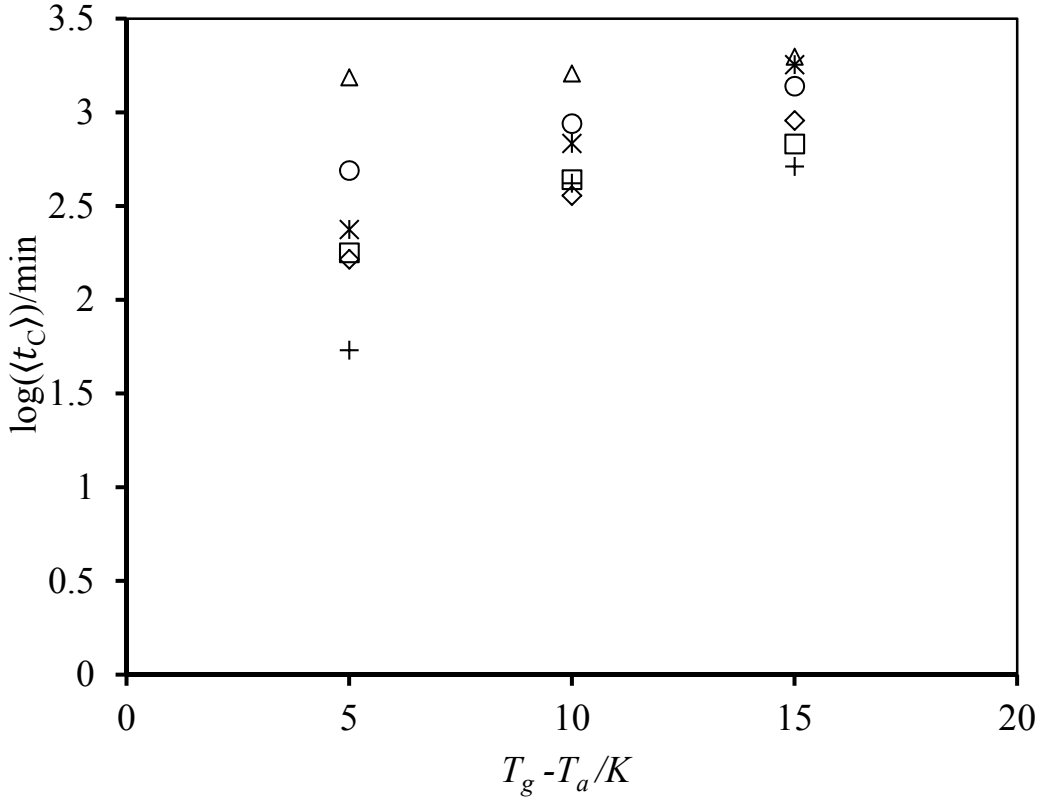

Figure 4.18 Variation of log (⟨t_C⟩) with (T_g-T_a) for P4HS (+), PEMA (□), P4HS/PEMA: (79/21) (Δ), (74/26) (O), (49/51) (ж), and (24/76 mole-%) (◊).

Table 4.5- CF fitting parameters for P4HS/PEMA blends at several aging temperatures

P4HS/PEMA (mole-%)	T_a (K)	T_g- T_a (K)	$\Delta H_\infty(T_a)$ ($J\ g^{-1}$)	log t_c (min)	β
100/0	412	15	2.40	2.01	0.35
	417	10	1.89	1.92	0.35
	422	5	1.20	1.03	0.35
79/21	408	15	2.23	2.45	0.32
	413	10	1.89	2.36	0.32
	418	5	1.54	2.34	0.32
74/26	405	15	2.34	2.21	0.34
	410	10	1.76	1.81	0.34
	415	5	1.14	1.47	0.34
49/51	382	15	2.04	2.46	0.33
	387	10	1.53	2.04	0.33
	392	5	1.14	1.58	0.33
24/76	356	15	1.71	2.48	0.36
	361	10	1.45	2.28	0.36
	366	5	1.04	2.03	0.36
0/100	332	15	1.60	2.31	0.40
	337	10	1.39	2.12	0.40
	342	5	0.97	1.73	0.40

4.3.2 Enthalpy relaxation of P4HS/PEO

The P4HS/PEO blends were found to be miscible over the whole composition range and exhibited a single glass transition temperature. The T_g values increase with increasing P4HS content, as shown in Table 4.6, where the mid-point T_g, temperature range (ΔT) and experimental ΔC_p are listed. Figure 4.19 shows the composition dependence of T_g. The experimental T_g versus composition data are fitted well by the Kwei equation (Eq. 4.2): the k parameter was calculated from the experimental ΔC_p data (Table *4.6*) and fitting led to q= 103. This is consistent with literature studies linking high strength of interactions with high absolute values of q, for example, q=160 in P4HS/P2VPy blends [143] and q = 140 in P4HS/PVP blends [155]. Thus, the large q value for P4HS/PEO blends implies strong interactions between PEO and P4HS.

Enthalpy relaxation measurements were carried out and Figures 4.20, 4.21 and 4.22 display typical C_p data for P4HS/PEO with 87/13, 59/41 and 46/54 mole % aged at 15K below T_g.

To qualitatively discuss differences in enthalpic behaviour, a comparison is made, in Figure 4.23, between C_p curves for all of the P4HS/PEO samples aged at 10 K below T_g, for t_a equal to (a) 100 and (b) 2000 min. All of the blends show relatively broad enthalpic peaks. The position of the peak maximum generally increases with increasing P4HS content.

The comparison at $T_g - T_a$ = 15 K between 87/13 P4HS/PEO (Figure 4.20) and 59/41 P4HS/PEO (Figure 4.21) indicates that the former blend has narrower enthalpic peaks This is consistent with the hydrogen bonding effect seen on ΔT (Table *4.6*).

The appearance of the enthalpic peaks near the middle of the T_g transition for 59/41 and 46/54 P4HS/PEO (Figures 4.21 and 4.22) suggests that not all of the segments undergo aging. It follows that there is a fraction of polymer segments that does not contribute to the overall $\Delta H(T_a, t_a)$.

Table 4.6- T_g Data for P4HS/PEO blends.

P4HS/PEO (wt-%)	P4HS/PEO (mole-%)	T_g *(K)*	ΔT *(K)*	ΔC_p $J.K^{-1}.g^{-1}$
0/100	0/100	219		0.181
70/30	46/54	357	21.24	0.185
80/20	59/41	374	25.70	0.404
85/15	67/33	408	31.35	0.329
95/05	87/13	424	19.32	0.179
100/0	100/0	427	13.35	0.296

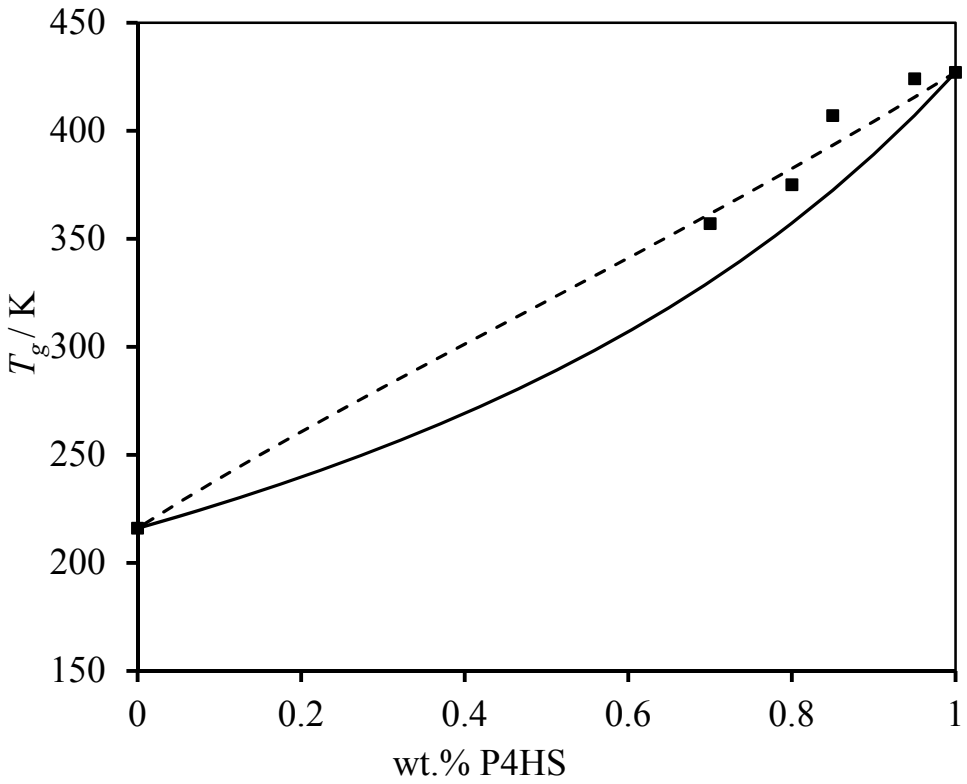

Figure 4.19 Composition dependence of T_g for P4HS/PEO blends: experimental data (■), and fits to the Flory-Fox (solid line), and Gordon-Taylor (long dashed line) equations.

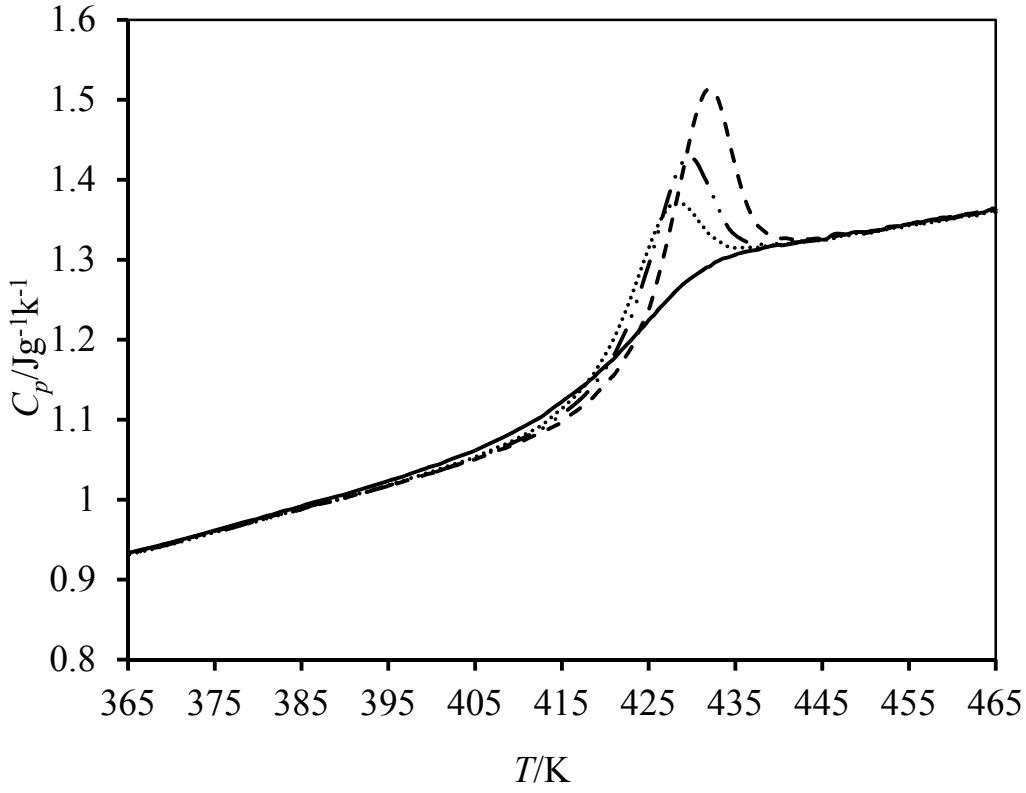

Figure 4.20 Heat capacity curves for 87/13 P4HS/PEO at T_g -T_a = 15 K for (…....), 500 (—••—••—), and 2000 (— — —) minutes

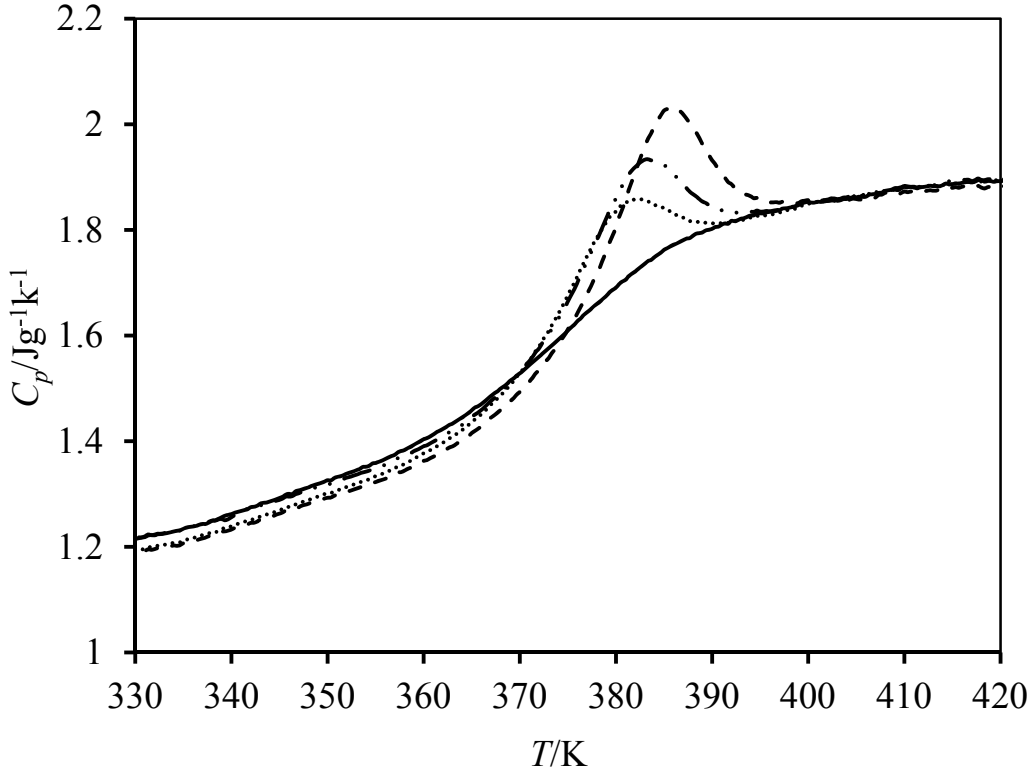

Figure 4.21 Heat capacity curves for 59/41 P4HS/PEO at T_g -T_a = 15 K for 200 (……), 500(—••—••—) and 2000 (— — —) minutes.

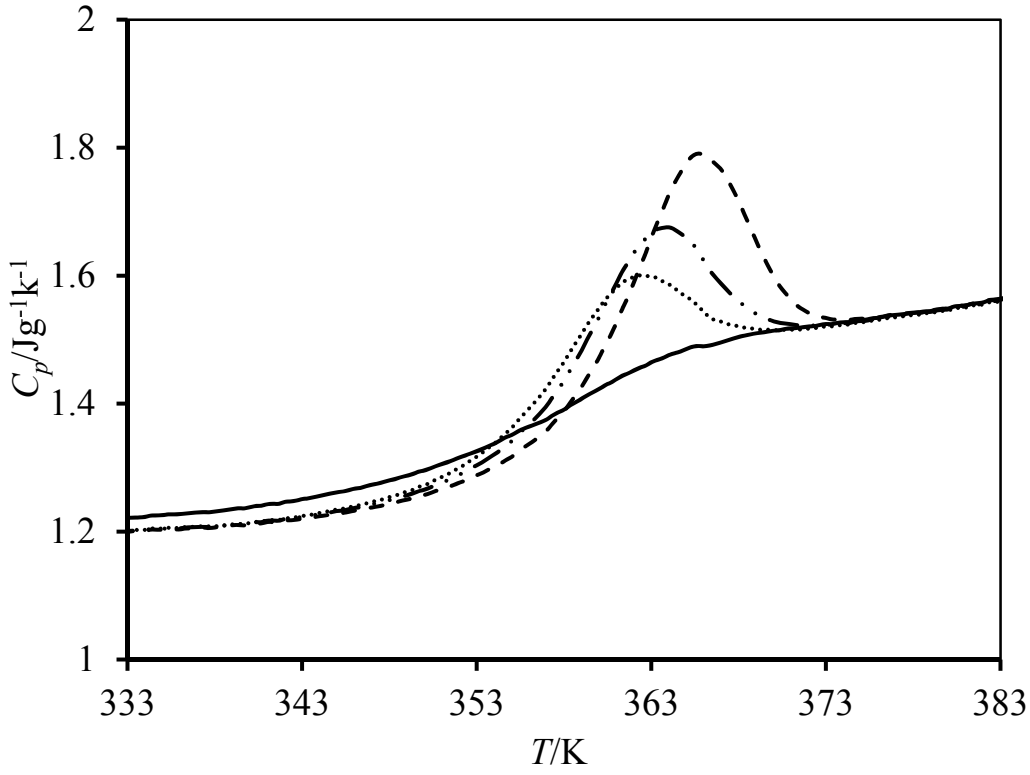

Figure 4.22 Heat capacity curves for 54/46 P4HS/PEO at T_g -T_a = 15 K for 200 (……), 500(—••—••—) and 2000 (— — —) minutes.

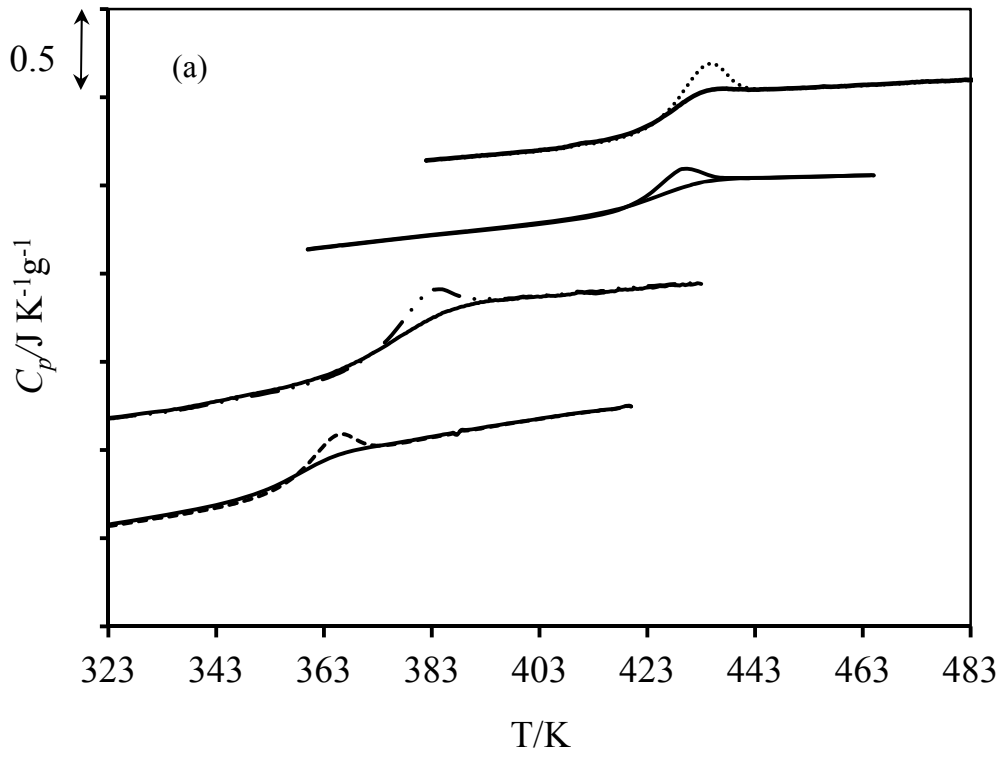

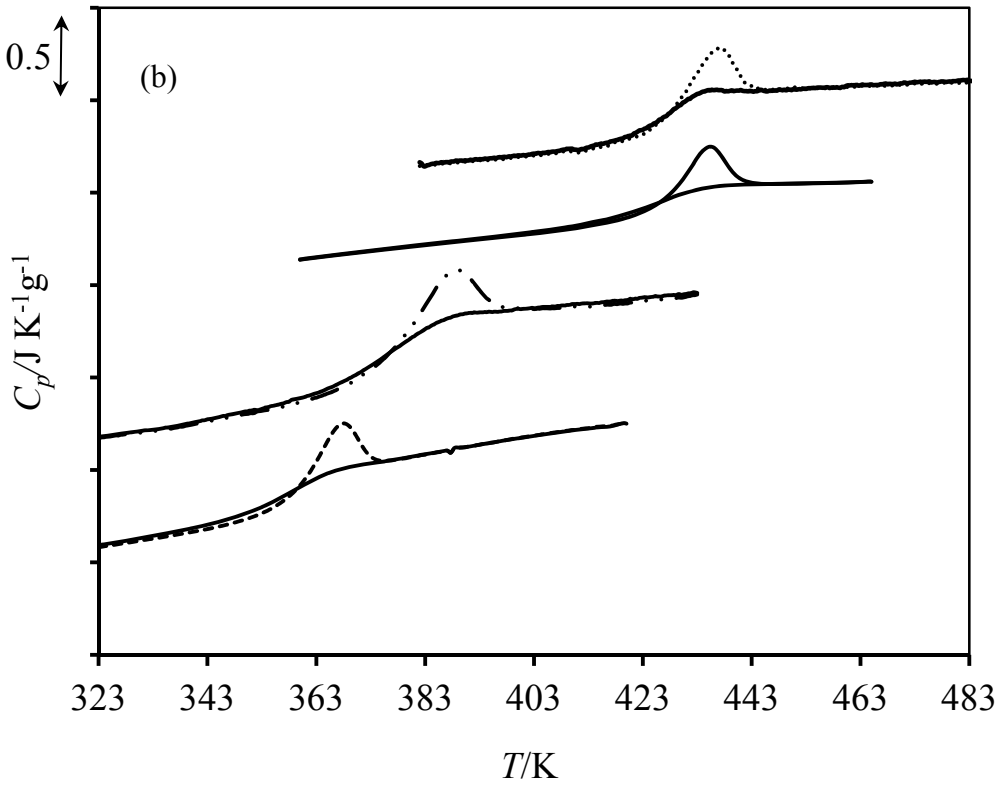

Figure 4.23 C_p curves for the P4HS/PEO blends aged at 10 K below T_g for (a) 100 min and (b) 2000 min: (……..) P4HS; (——) 87/13; (—••—••—) 59/41 and (— — —) 46/54 mole-%.

Plots of enthalpy lost after aging for a time, t_a, at temperature T_a ($\Delta H(T_a, t_a)$) against log(t_a) are shown in Figure 4.24 (a) – (d), with fits using CF model. The CF parameters obtained at each aging temperature are reported in figure 4.25 and Table 4.7. Furthermore, in order to facilitate comparison between the blends and P4HS, the CF parameters for P4HS are repeated.

Values of log $\langle t_c \rangle$ are plotted against ($T_g - T_a$) for each blend (Figure 4.25). It is interesting to note that with increasing PEO content in the blends, the relaxation slows down, as a result of the increasing number of interactions. As observed for PEMA, pure P4HS relaxes faster than the blend. This suggests that the presence of intermolecular interactions leads to a decrease in the relaxation rate, as a result of a reduction in the population of motional active-side groups (i.e. hydroxyl groups in P4HS) in the glassy state. Similar results have been reported for P4HS/PVME [91]. Dielectric studies of

P4HS/PVME blends indicate that blending leads to considerable reduction of the side-group β-relaxations of both polymers.

Table 4.7- CF fitting parameters for P4HS/PEO blends at several aging temperatures

P4HS/PEO (wt-%)	P4HS/PEO (mole-%)	T_a (K)	T_g- T_a (K)	ΔH_∞ (T_a) ($J\,g^{-1}$)	log t_c (min)	β
100/0	100/0	412	15	2.40	2.01	0.35
		417	10	1.89	1.92	0.35
		422	5	1.20	1.03	0.35
95/05	87/13	409	15	1.93	2.44	0.41
		414	10	1.48	2.25	0.41
		419	5	1.21	2.13	0.41
85/15	67/33	393	15	2.29	2.64	0.35
		398	10	1.80	2.34	0.35
		403	5	1.48	2.14	0.35
80/20	59/41	359	15	3.31	2.62	0.32
		364	10	3.02	2.54	0.32
		369	5	2.14	2.20	0.32
70/30	46/54	342	15	2.45	2.80	0.39
		347	10	1.95	2.55	0.39
		352	5	1.54	2.24	0.39

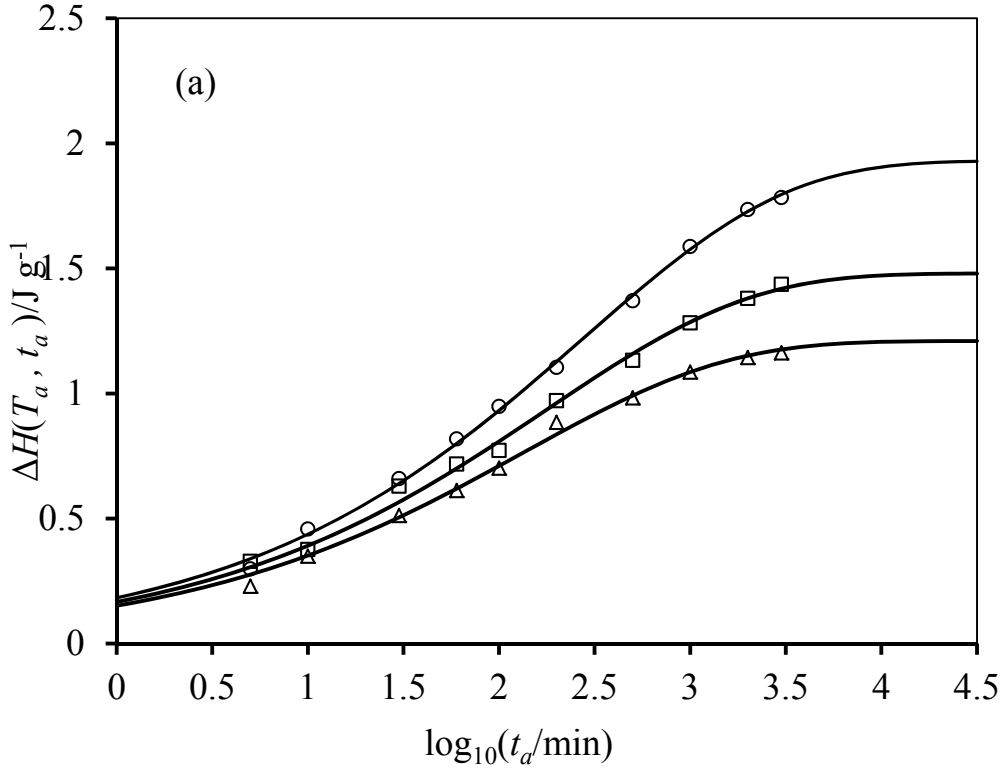
(a)
$\Delta H(T_a, t_a)$/J g^{-1}
$\log_{10}(t_a$/min)

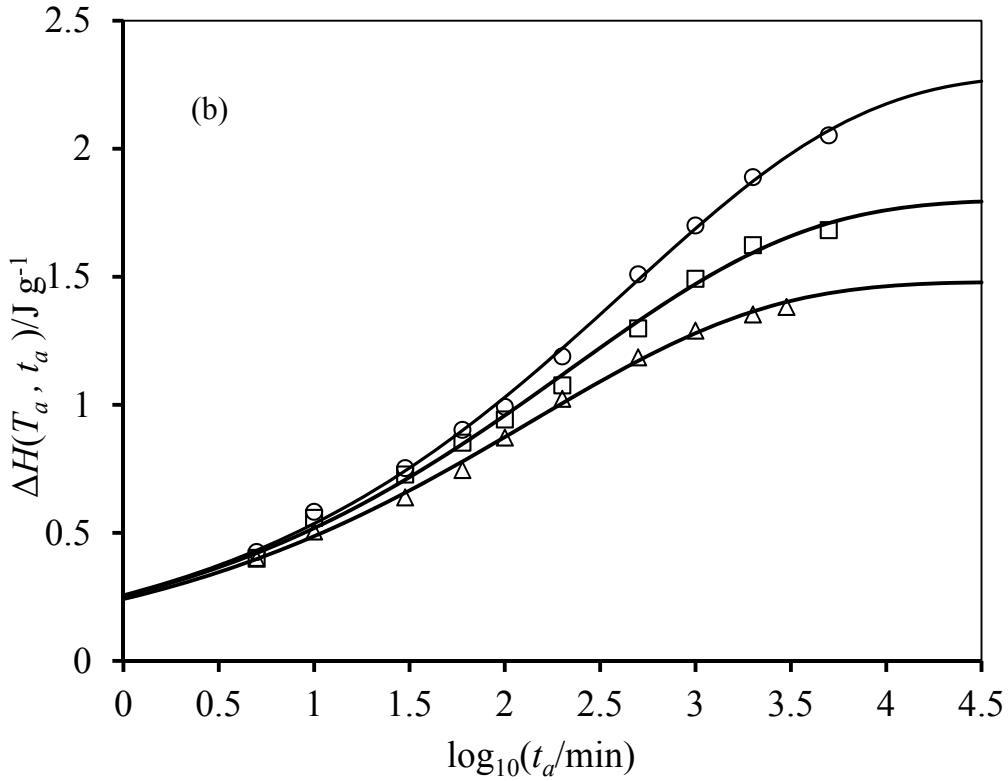
(b)
$\Delta H(T_a, t_a)$/J g^{-1}
$\log_{10}(t_a$/min)

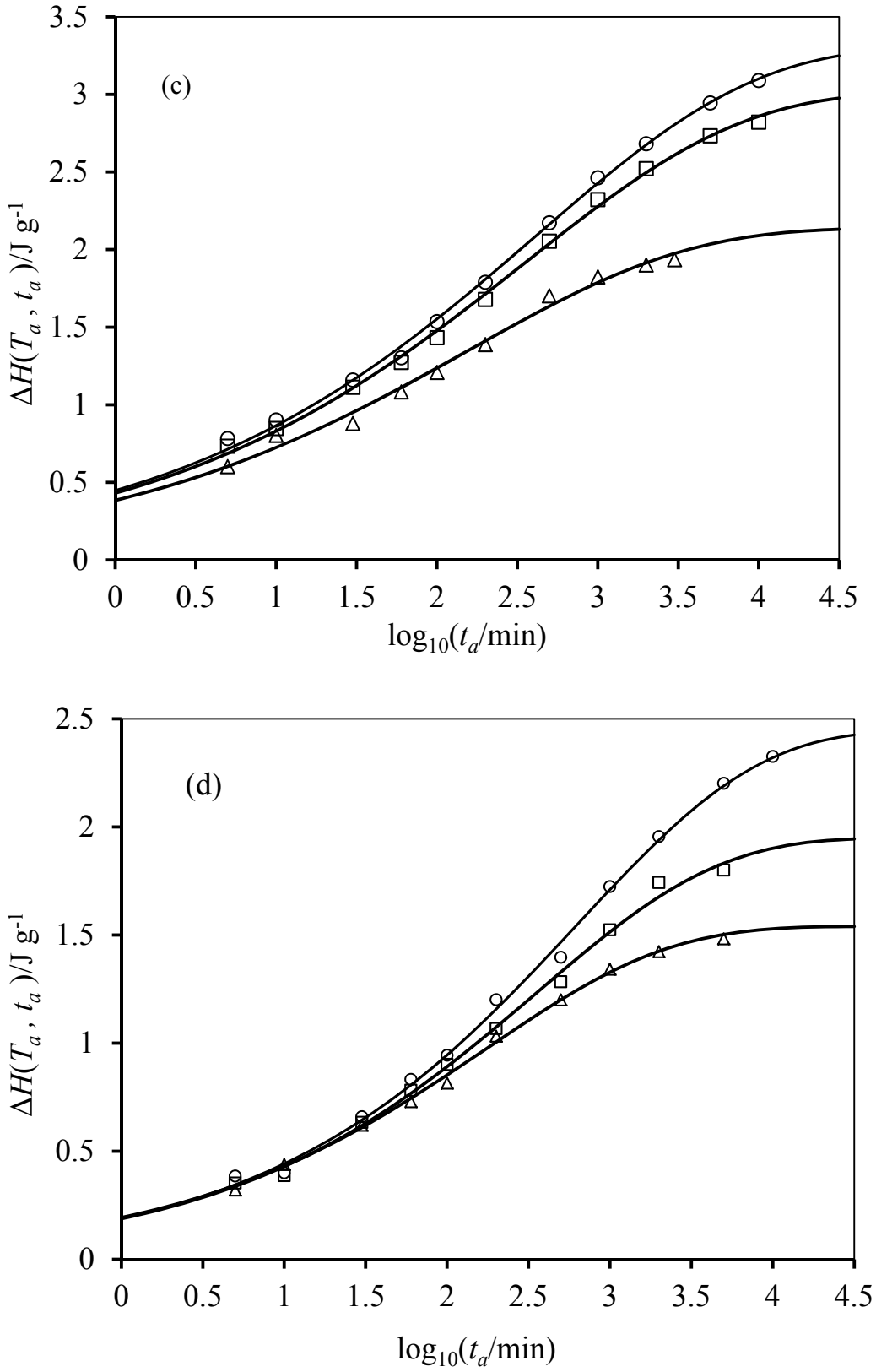

Figure 4.24 Enthalpy relaxation data for the P4HS/PEO blends by mole-%: (a) (87/13) at T_a= 409 K (O), 414 K (□) and 419 K (Δ); (b) (67/33) at T_a= 393 K (O), 398 K (□) and 403 K (Δ); (c) (51/41)at T_a= 359 K (O), 364 K (□) and 369 K (Δ); (d) (46/54) at T_a= 342 K (O), 347 K (□) and 352 K (Δ).

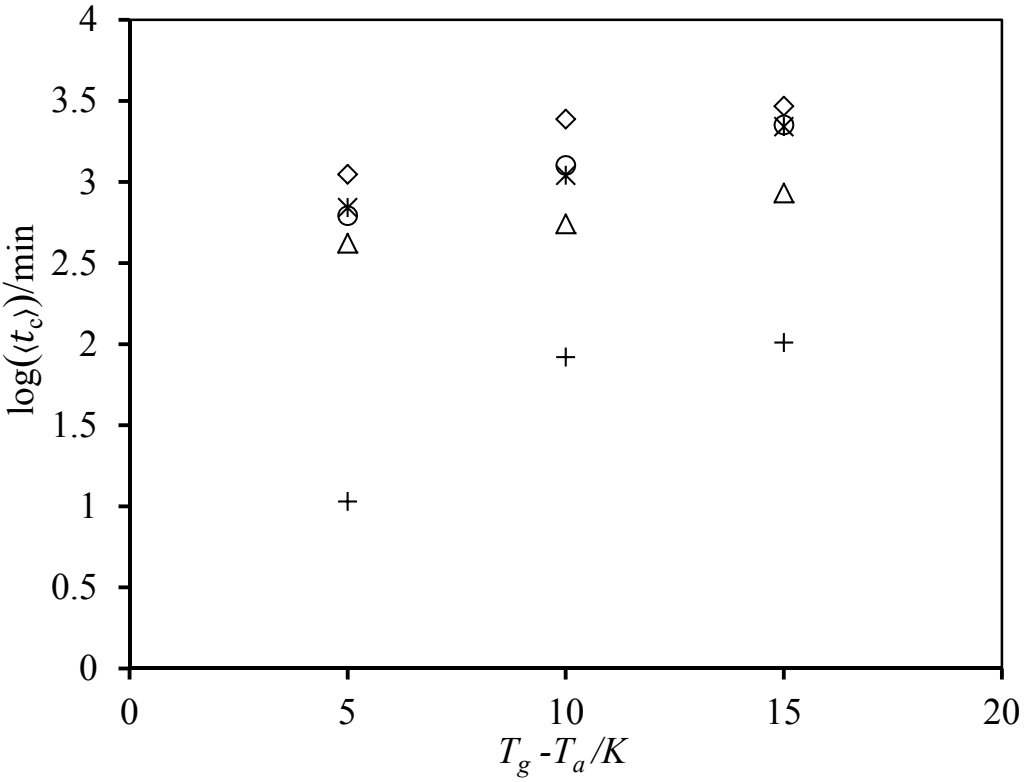

Figure 4.25 Variation of log (⟨t_c⟩) with (T_g -T_a) for P4HS (+), P4HS/PEO: (87/13) (Δ), (67/33) (Ж), (59/41) (◊), and (46/54) (○) mole-%.

The average relaxation times ⟨t_c⟩ obtained for 59/41 P4HS/PEO are compared with the ⟨t_c⟩ values of P4HS, PEMA, PVME [3], 36/64 PS/PVME [106], a 59/41P4HS/PVME blend[110] and a 49/51 P4HS/PEMA blend, in Figure 4.26, as a function of undercooling below T_g. Although PEMA relaxes more slowly than PVME (which is chemically similar to PEO), the relaxation process in P4HS/PVME and P4HS/PEO blends is obviously slower than in the P4HS/PEMA system, at the same composition (Figure 4.26). This is related to the higher strength of inter-molecular bonds in P4HS/PEO, and less rigidity chains compared to P4HS/PEMA, and are in agreement with the FTIR measurements reported earlier.

Figure 4.27 displays the ΔH_∞ data of P4HS/PEO blends and P4HS versus distance from T_g. The lowest equilibrium enthalpy values were found at all aging temperatures for the 13/87 PEO/P4HS blend and the highest values measured for the 59/41 sample. It is interesting to recall that 59/41 P4HS/PEO also has slow relaxation kinetics. At this mole fraction most of the hydroxyl groups are bonded to ether groups. This means that the 59/41 4HS/PEO blend has more flexible segments which can relax,

and stronger interactions, which leads to a greater ΔH_∞ value. Moreover, PALS results of similar blends (i.e. P4HS/PVME blends) indicate that the fractional free volume decreases with increasing P4HS content, which is due to increased hydrogen bonding and reduced chain mobility as the T_g of the blend increases [110]. Those results also show that only blend has fractional free volume less than pure P4HS is 59/41. This provided evidence of a more compact packing. For the other compositions, the volume increase mean increasing in dissociation of self-associated hydroxyls, which must lead to relative poorer packing where the formation of hydroxyl–ether linkages are unable to overcome that volume increase.

Although this project did not focus on PALS measurements, nonetheless, the enthalpy relaxation data of P4HS/PEO blends in this study are quite similar to data for P4HS/PVME blends. Thus, it can be suppose that the reason for high ΔH_∞ values for the 59/41 P4HS/PEO blend relate to the effect of packing as well. So, it is suggested that the 59/41 P4HS/PEO blend has more compact packing than P4HS, whereas for the other compositions, packing is poorer.

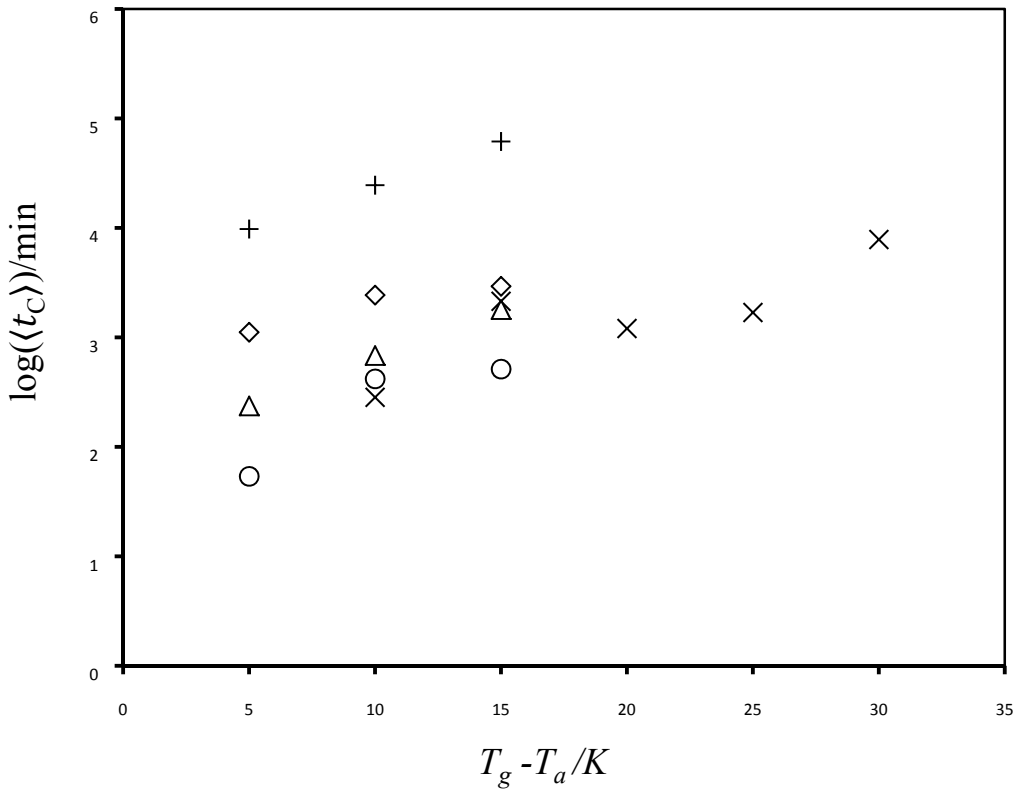

Figure 4.26- Average relaxation time as a function of $(T_g - T_a)$ for: (◊) (59/41) P4HS/PEO; (+) (59/41) P4HS/PVME(derived from ref [110]); (O) P4HS; (Δ) (49/51) P4HS/PEMA; (×) (36/64) PS/PVME(derived from ref [106]).

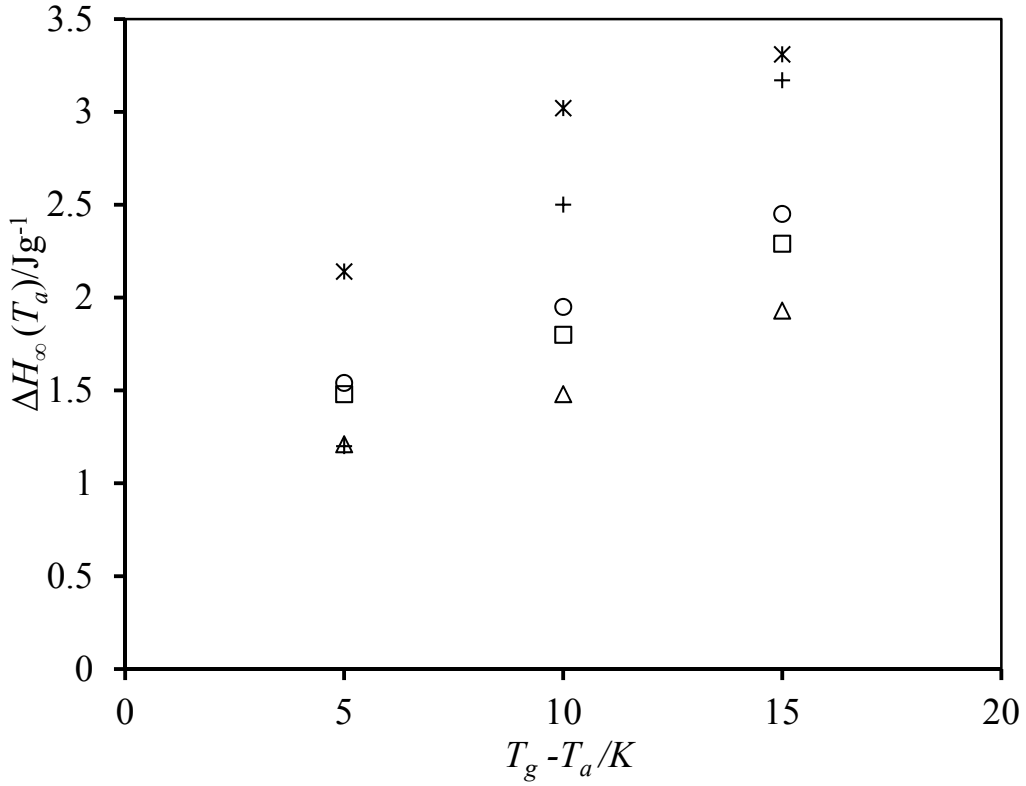

Figure 4.27 $\Delta H_\infty(T_a)$ versus (T_g- T_a) for P4HS (+), P4HS/PEO: (87/13) (Δ), (67/33) (□), (59/41) (ж), and (46/54) (○) mole%.

4.3.2 Enthalpy relaxation of P4HS/P4VPy

The enthalpic peaks of the P4HS/P4VPy blend are short and broad (Figure 4.28), indicating that energies are released over a wide temperature range. This is consistent with the hydrogen bonding effect seen on ΔT (Table 4.8).

Table 4.8 Glass transition temperatures for P4HS/P4VPy blends

wt.-% P4HS	mole-% P4HS	T_g(mid)/K	ΔT	ΔC_p
0	0	425	7.48	0.276
62	59	448	14.48	0.313
70	67	441	15.51	0.363

$\Delta H_\infty(T_a)$ data for 59/41 P4HS/P4VPy are shown in Table 4.9. At all aging temperatures, the equilibrium enthalpies of the P4HS/P4VPy blend are close to that of P4VPy. Thus, the presence of very strong hydrogen bonds in the 59/41 P4HS/P4VPy blend will have effects on the segmental motion of the main chain, and any attempt at movement of the segments under temperature will lead to breaking the hydrogen bonds, which will evidently cause an increase in the relaxation speed. Consequently, the relaxation rate of P4HS/P4VPy blends should be faster than those relaxations of other strong hydrogen bonding blends of P4HS (i.e. P4HS/PEO and P4HS/PVME blends). Similar results have been reported on P2VPy blends with the poly(p-(hexafluoro-2-hydroxyl-2-propyl)styrene) (HFS) which has similar hydrogen bonding interactions. Masser and Runt [156] have found that very strong hydrogen bonds in HSF/P2VPy blends lead to increasing the fragility of blend segments to the maximum; consequently any movement will cause breaking of hydrogen boning. A dielectric spectroscopy relaxation study by Zhang et al. [157] of quite similar blends (i.e. P4HS/P2VPy blends) also indicated that the relaxation time distributions of P4HS/P2VPy blends are close to that of neat P2VPy, as a result of the very strong intermolecular interactions and the relatively small T_g difference. Moreover, the absence of any flexibility of P4VPy, that is, domain the relaxation of P4VPy/P4HS blends, is also another reason for faster relaxation of 59/41 P4HS/P4VPy blend, where the hydrogen bonding interactions of the blend will be more rigid than in other blends of P4HS with semi-crystalline polymers like PEO or viscous PVME, that produce more flexible hydrogen bonding interactions between the segments.

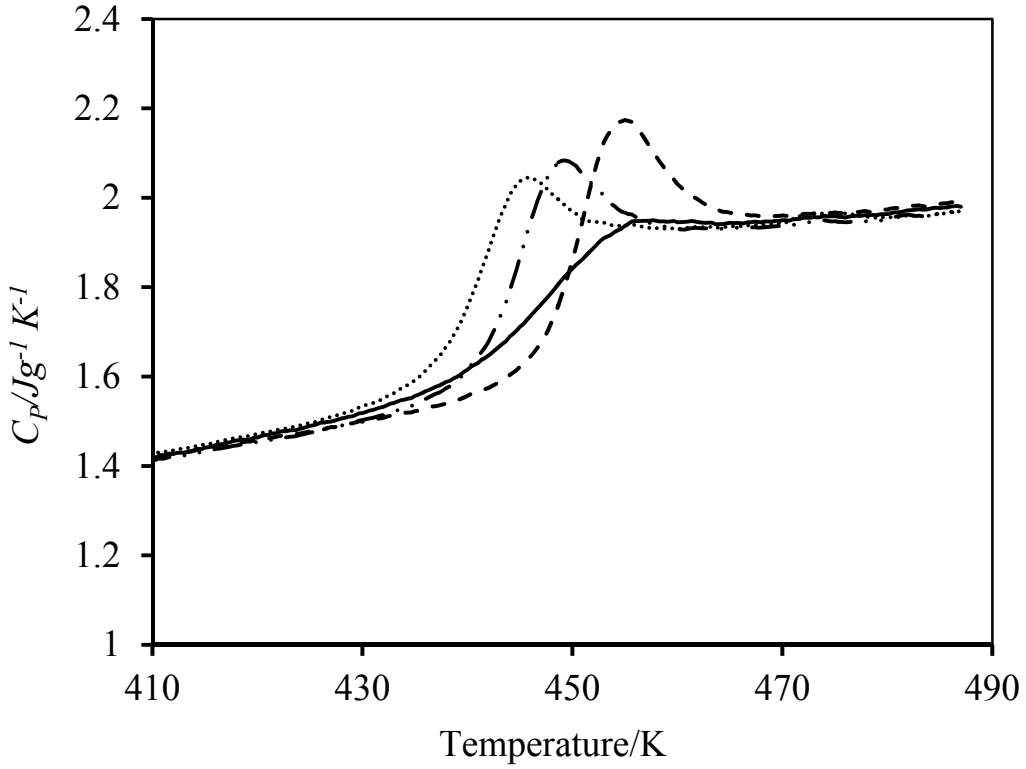

Figure 4.28 Heat capacity curves for a 59/41 P4HS/P4VPy at T_g -T_a = 15 K: 200 (……), 500 (—••—••—) and 2000 (— — —) minutes

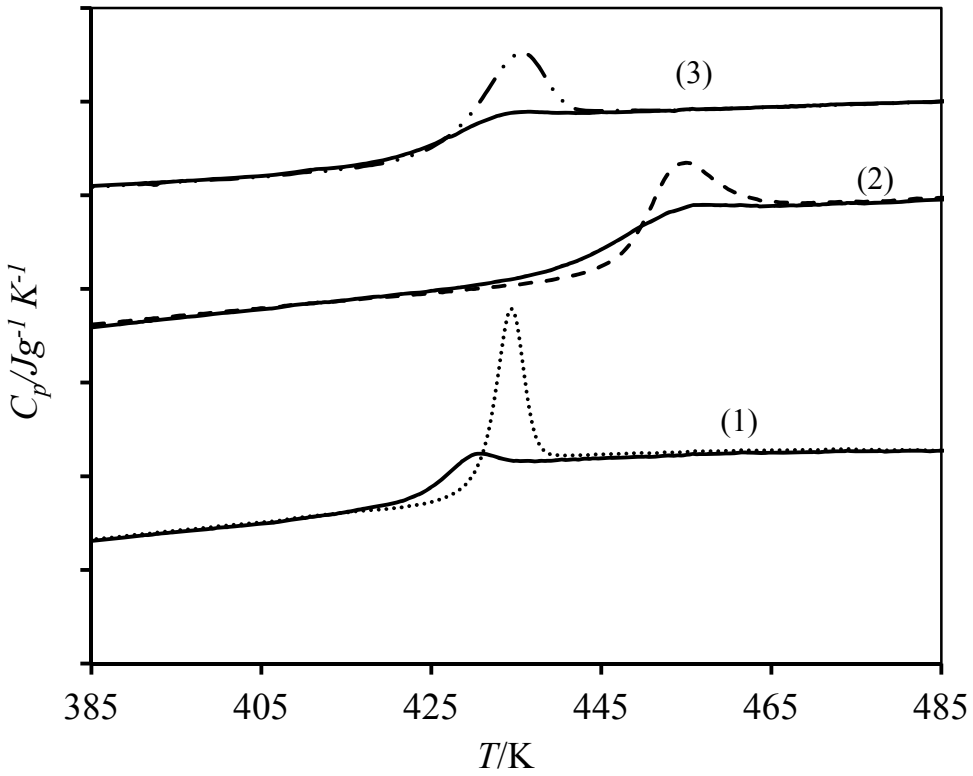

Figure 4.29 Heat capacity curves (aged and unaged) for t_a = 2000 mins. (1) P4VPy, (2) 59/41 P4HS/P4VPy and (3) P4HS at $T_g - T_a$ =15K. Data for P4VPy are shifted down by 0.5J $g^{-1}K^{-1}$, while the data for P4HS/P4VPy and P4HS are shifted upwards by 0.5 and 2.0 $Jg^{-1}K^{-1}$, respectively, for clarity.

Table 4.9- CF parameters for P4HS/P4VPy blends

(wt.-% P4HS)	(mole.%P4HS)	T_a (K)	T_g- T_a (K)	$\Delta H_\infty(T_a)$ ($J\,g^{-1}$)	log t_c /min	β
0 (i.e. P4VPy)	0	410	15	1.80	2.12	0.42
		415	10	1.17	2.06	0.42
		420	5	0.78	1.81	0.42
62	59	433	15	1.80	2.19	0.43
		438	10	1.20	2.04	0.43
		443	5	1.16	1.99	0.43
100 (i.e. P4HS)	100	412	15	2.40	2.01	0.35
		417	10	1.89	1.92	0.35
		422	5	1.20	1.03	0.35

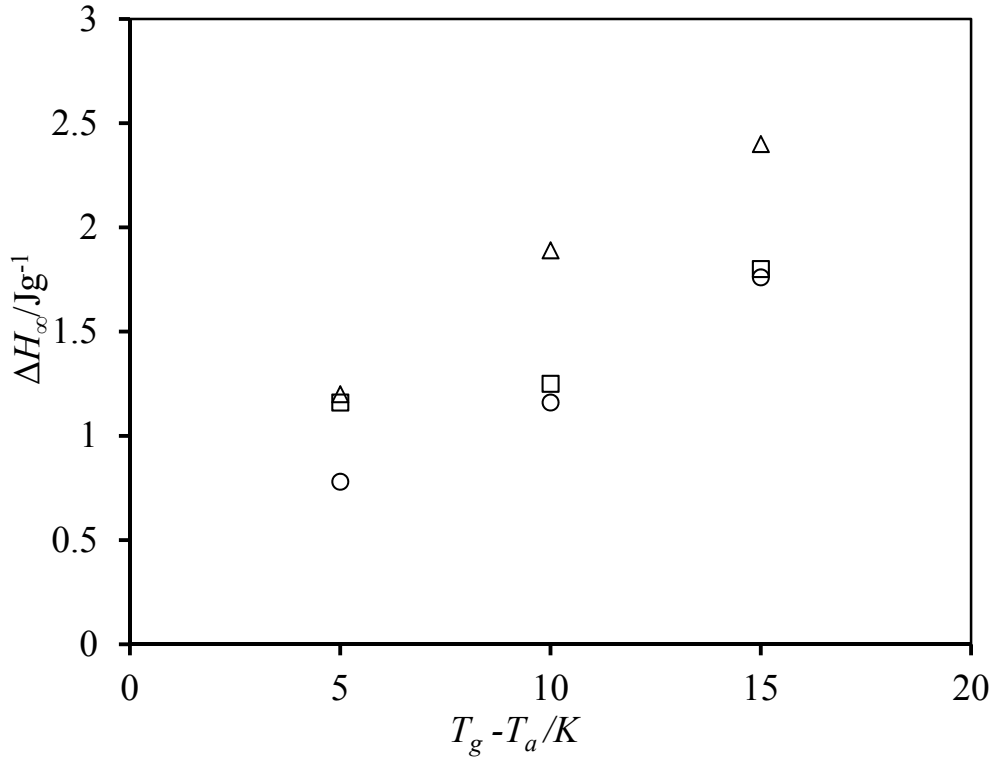

Figure 4.30 ΔH_∞ versus (T_g- T_a) for (□) 59/41 P4HS/P4VPy; (Δ) P4HS; (O) P4VPy.

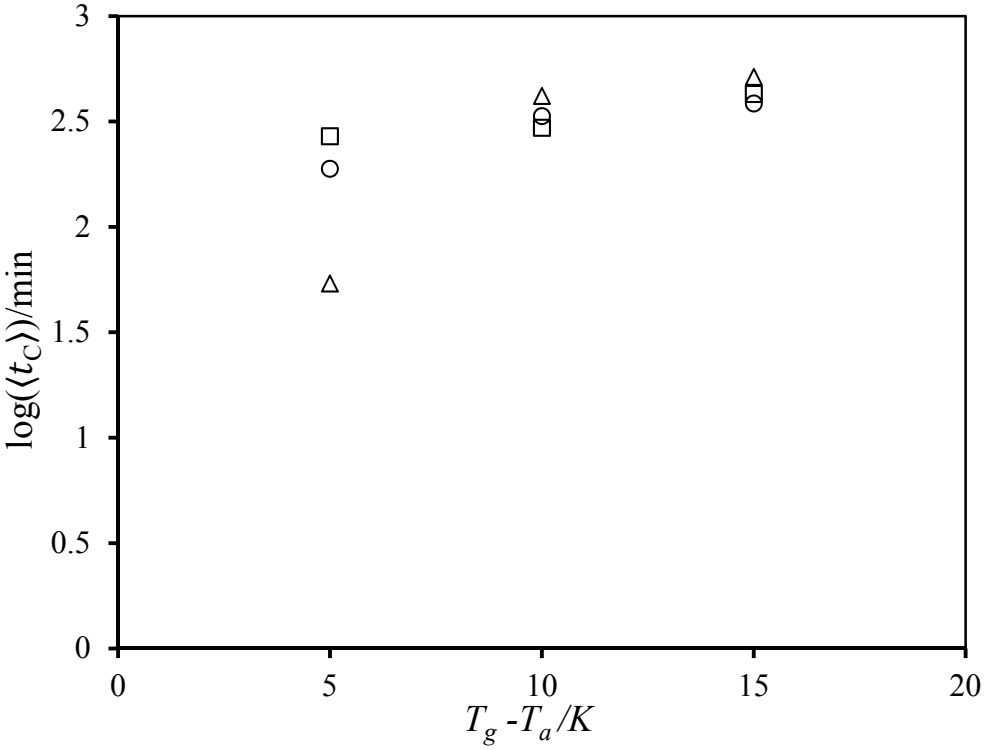

Figure 4.31 Average relaxation time as a function of (T_g – T_a) for (□) 59/41 P4HS/P4VPy; (Δ) P4HS; (O) P4VPy.

4.4- Average segmental activation energies for P4HS blends

Using t_c and β values derived from the CF analysis of enthalpic aging, it is possible to calculate average segmental activation energies $\langle E_a \rangle$ at different aging temperatures from the following equation [135]

$$\langle E_a \rangle = RT_a[\langle ln\tau \rangle - lnt_0] \qquad (4.6)$$

where the constant $t_0 = 10^{-8}$ sec is related to the vibrational frequency of the lattice, and $\langle \ln \tau \rangle$ is related to the relaxation time distribution. A review of the mathematical expressions that describe the determination of $\langle \ln \tau \rangle$ from the CF model parameters t_c and β is given in reference [2].

Values of activation energy provide a qualitative guide to the energies expended in the localised molecular rearrangements responsible for the physical aging.

As shown in Table 4.10, for P4HS/PEMA $\langle E_a \rangle$ values are higher for the blends, compared to PEMA (see also Figure 4.32). The increased $\langle E_a \rangle$ values can be attributed to chain stiffness effects, which increase with increasing P4HS content, as confirmed by the composition dependence of the T_g. Dielectric relaxation studies of these blends carried out by Zhang and co-workers [112] also indicate that the activation energy of P4HS/PEMA blends increase with increasing P4HS composite in the blend. Although the activation energy of those studies came from a different technique than that used here, nonetheless, it is interesting to noted that the $\langle E_a \rangle$ value recorded for neat PEMA (~73 kJ/mol) at T_g-15 approaches the values obtained by Zhang et al. [112] (68 kJ/mol) at the same temperature.

$\langle E_a \rangle$ values for P4HS/PEO blends at 5, 10 and15 K below T_g are shown in Table 4.11. The trend is similar to that observed for PEMA blends. Moreover, $\langle E_a \rangle$ values are much closer to those of P4HS than that of PEO, suggesting that P4HS dominates the glass transitions. The high values of $\langle E_a \rangle$ suggest that the interactions between the polymer chains conduce to a network, which greatly hinders PEO relaxation. This meaningfully hinders the rate of aging when measured enthalpically.

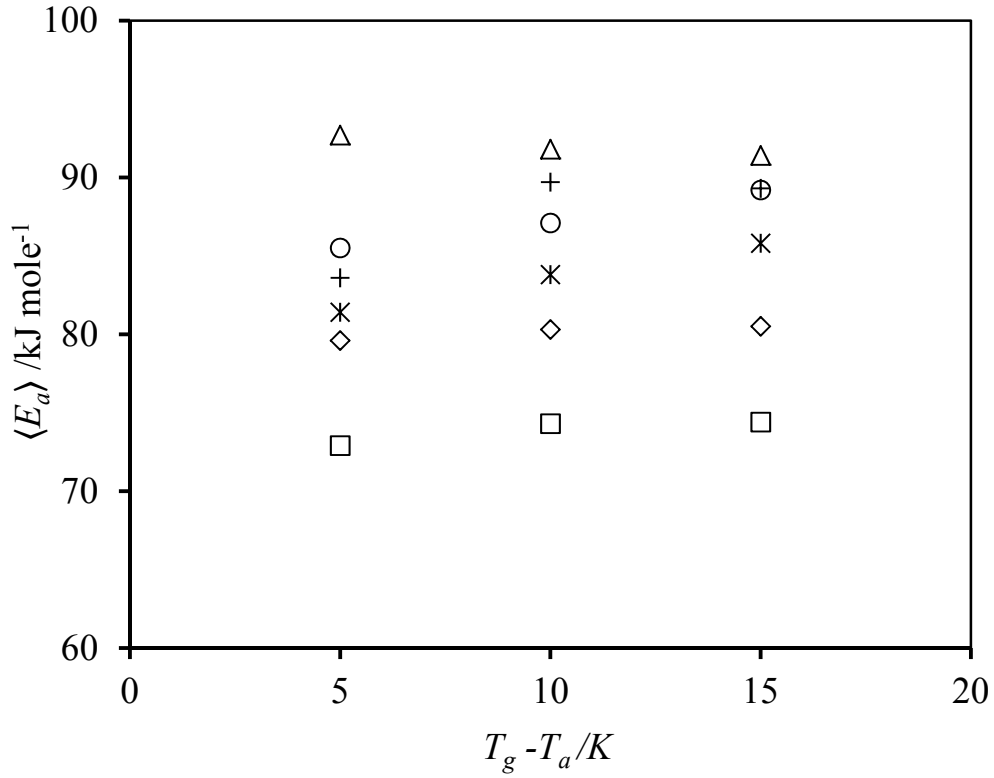

Figure 4.32 ⟨E_a⟩ versus (T_g- T_a) for P4HS (+), PEMA (□), P4HS/PEMA: (79/21) (Δ), (74/26) (O), (49/51) (ж), and (24/76 mole-%) (◊).

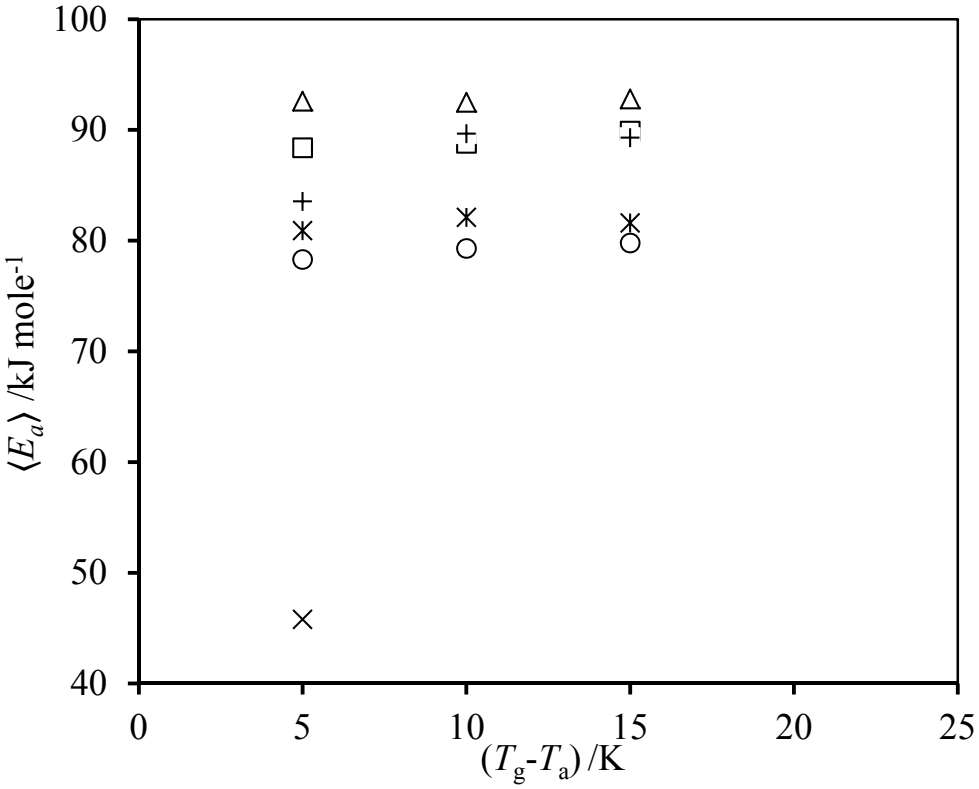

Figure 4.33 ⟨E_a⟩ versus (T_g- T_a) for P4HS (+), PEO (x), P4HS/PEO: (87/13) (Δ), (67/33) (□), (59/41) (Ж), and (46/54) (○) mole%.

Table 4.10- Average activation energies for P4HS/PEMA blends at several aging temperatures

P4HS/PEMA (mole-%)	T_a *(K)*	log t_c (min)	β	$\langle E_a \rangle$ (kJ mole^{-1})	$\langle E_a \rangle^{(a)}$ (kJ mole^{-1})
100/0	412	2.01	0.35	89.3	87.5
	417	1.92	0.35	89.7	
	422	1.03	0.35	83.6	
79/21	408	2.45	0.32	91.4	92.0
	413	2.36	0.32	91.8	
	418	2.34	0.32	92.7	
74/26	405	2.21	0.34	89.2	83.7
	410	1.81	0.34	87.1	
	415	1.47	0.34	85.5	
49/51	382	2.46	0.33	85.8	83.7
	387	2.04	0.33	83.8	
	392	1.58	0.33	81.4	
24/76	356	2.48	0.36	80.5	80.1
	361	2.28	0.36	80.3	
	366	2.03	0.36	79.6	
0/100	332	2.31	0.40	74.4	73.9
	337	2.12	0.40	74.3	
	342	1.73	0.40	72.9	

(a) average value of $\langle E_a \rangle$

Table 4.11- Average activation energies for P4HS/PEO blends at several aging temperatures

P4HS/PEO (mole-%)	T_a *(K)*	log t_c (*min*)	β	$\langle E_a \rangle$ (kJ mol^{-1})	$\langle E_a \rangle^{(a)}$ (kJ mol^{-1})
100/0	412	2.01	0.35	89.3	87.5
	417	1.92	0.35	89.7	
	422	1.03	0.35	83.6	
87/13	409	2.44	0.41	92.8	92.6
	414	2.25	0.41	92.5	
	419	2.13	0.41	92.6	
67/33	393	2.64	0.35	89.9	89.0
	398	2.34	0.35	88.8	
	403	2.14	0.35	88.4	
59/41	359	2.62	0.32	81.6	81.5
	364	2.54	0.32	82.1	
	369	2.20	0.32	80.9	
46/54	342	2.80	0.39	79.8	79.1
	347	2.55	0.39	79.3	
	352	2.24	0.39	78.3	
0/100	---	----	----	----	45.8
	---	----	----	----	
	214	1.54	0.65	45.8	

Values of activation energy are expected to depend on the interaction strength between the blend components. For instance, the interaction between PVME and PS in PS/PVME is reported to be quite weak [39, 158], this being due to the formation of a complex between the lone pairs of electrons of the ether oxygen and the benzene ring

[39]. Thus, $\langle E_a \rangle$ values for this system (Table 4.12) are only slightly higher than those for PVME, and much smaller compared to PS values [2], which seems to support the suggestion that PVME dominates the aging behaviour in the blends [106].

The $\langle E_a \rangle$ values of PS/PVME provide an interesting contrast to those of P4HS based blends (Table 4.12). Strong interactions in P4HS/PEMA, P4HS/PEO and P4HS/PVME blends and the formation of a transient network structure considerably retard the segmental relaxation processes that occur during the aging and significantly increase the activation energy. The results in Table 4.12 also show that the activation energies of P4HS/P4VPy blends are higher than those of P4HS/polyether and P4HS/PEMA. This seems consistent with the infrared measurements carried out on these systems.

Table 4.12- Average activation energies for P4HS based blends at several aging temperatures.

Polymer or blend	T_a *(K)*	β	log t_c (*min*)	$\langle E_a \rangle$ (kJ mole^{-1})
P4HS	412	0.35	2.01	89.3
	417	0.35	1.92	89.7
	422	0.35	1.03	83.6
P4HS/PEO 59/41	359	0.32	2.62	81.6
	364	0.32	2.54	82.1
	369	0.32	2.20	80.9
P4HS/PEMA 49/51	382	0.33	2.46	85.8
	387	0.33	2.04	83.8
	392	0.33	1.58	81.4
PEMA	332	0.40	2.31	74.4
	337	0.40	2.12	74.3
	342	0.40	1.73	72.9
P4HS/PVME 59/41(from ref [110])	381	0.24	3.32	89.6
	386	0.24	2.92	87.8
	391	0.24	2.54	86.0
PVME/PS (Data from ref [106])	250	0.36	3.25	60.3
	255	0.41	2.74	59.4
	260	0.37	2.47	58.9
	265	0.32	2.46	59.3
	270	0.49	2.15	60.4
PVME	240	0.50	2.44	55.0
	245	0.66	1.82	53.8

(Data from ref [3])	250	0.91	1.23	52.6
	360	0.30	2.30	82.9
PS	364	0.41	2.02	80.3
(Data from ref [18])	367	0.39	0.48	79.2
	433	0.43	2.19	96.4
P4HS/P4VPy	438	0.43	2.04	96.3
59/41	443	0.43	1.99	97.0

Chapter 5 Physical aging of styrene-co-4-hydroxystyrene blends

5.1 Introduction

It has been pointed out by Zhang et al.[53] that the dilution of hydroxyl groups in P4HS by styrene units does not affect the strength of the hydrogen bonds with polyethers, since P4HS and SHS have the same proton donating group and similar structure. However, the existence of styrene units between the hydroxystyrene groups in systems such as SHS/(poly(vinyl ethyl ether) (PVEE) has been found to increase the dynamic heterogeneity compared with P4HS/PVEE[53]. Similar results have been reported for SHS/PEO using dielectric relaxation spectroscopy (DRS)[68]. Moreover, the SHS/PEO dielectric measurements have indicated that the fragility in SHS/PEO blends increased significantly with increasing SHS content in the blend[68]. Consequently, we concentrate our attention in this chapter first of all on the reinvestigation of the effect of dilution on the hydrogen bonding strength SHS blends with PMMA, PEMA, PEO, and PVME using FTIR. Moreover FTIR measurements will be done here to determine hydrogen bonding fraction where they are possible (i.e. SHS/poly(alkyl methacrylate) blends. Second is discussed of the dilution on the the physical aging behaviour of the systems.

5.2 Infrared spectroscopy

5.2.1 SHS/Poly(alkyl methacrylate) blends

5.2.1.1 SHS/PMMA blends

Figure 5.1 shows the FTIR spectra of 59/41 mole% SHS/PMMA blend in the carbonyl region (1650 - 1850 cm^{-1}). The shoulder at 1708 cm^{-1}, which is not present in the PMMA spectrum increases in height relative to the 1730 cm^{-1} peak with increasing hydroxyl content in the SHS/PMMA blends. This is therefore assigned to hydrogen-bonded carbonyl groups[136]. As we progress down the series, i.e. with increasing hydroxyl concentration, the peak centred at 1730 cm^{-1} due to the free carbonyl group vibration decreases in intensity.

It is interesting to note that a broader carbonyl peak is observed for the 59/41 SHS30/PMMA sample, possibly reflecting a more disorganised blend network.

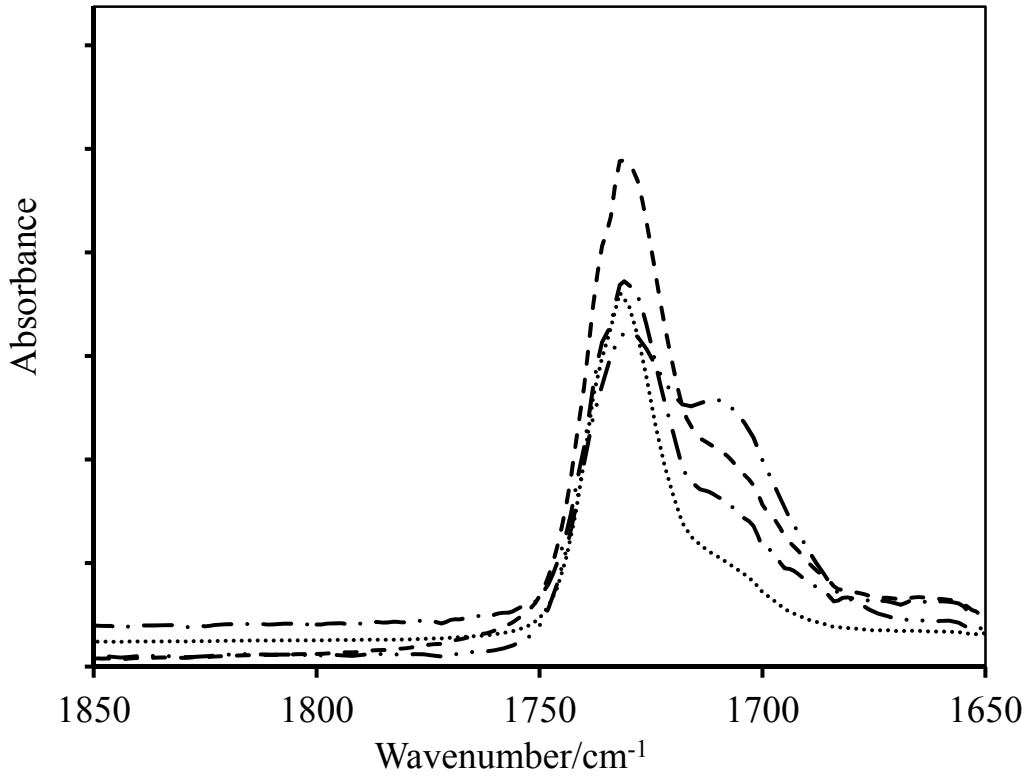

Figure 5.1 FTIR spectra in the carbonyl vibration region from 1800 to 1650 cm^{-1} for 59/41 SHS/PMMA blends containing: (……) 30, (—•—•—) 50, (— — —) 70, and (—••—••—) 100 mole% HS.

The spectral changes in the hydroxyl region due to blending with PMMA are illustrated in Figure 5.2 for a copolymer with 30 mole % HS. It is evident that the free hydroxyl band (~3530 cm^{-1}) present in the copolymer is not seen in the blend. Therefore, new hydrogen bonds are formed in the blend between the phenolic hydroxyls of SHS and the carbonyl groups in PMMA. The fact that the new hydrogen bonded hydroxyls absorb at a higher wavenumber (3430 cm^{-1}) than the self-associated hydroxyls (~3350 cm^{-1}), suggests that the inter-molecular hydrogen bonds in the blends are weaker.

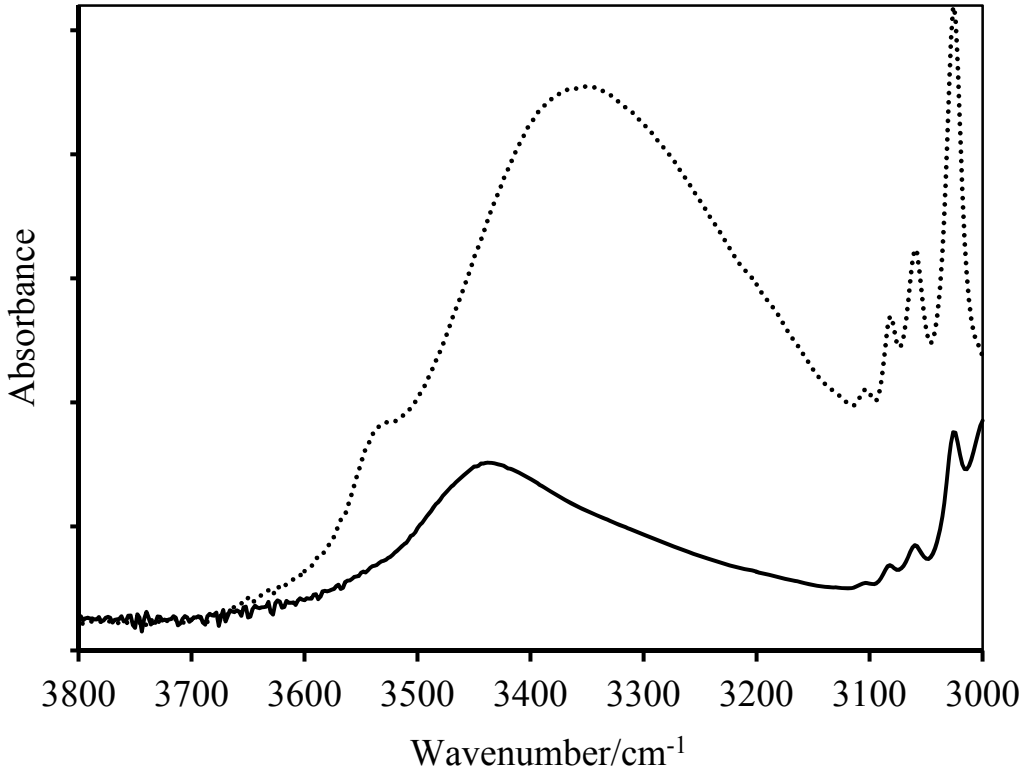

Figure 5.2 FTIR spectra in the hydroxyl vibration region from 3800 - 3000 cm^{-1} for **(.....)** SHS30 and **(——)** 59/41 SHS30/PMMA.

The hydroxyl spectra for all of the SHS/PMMA blends are plotted in Figure 5.3. All of the blends exhibited broad hydroxyl absorptions which include contributions from both hydroxyl-hydroxyl and hydroxyl-carbonyl interactions. As the HS content of the copolymer component increases, the hydroxyl band broadens suggesting an increase in the distribution of hydrogen bonding sites, presumably due to increased opportunities for self-association.

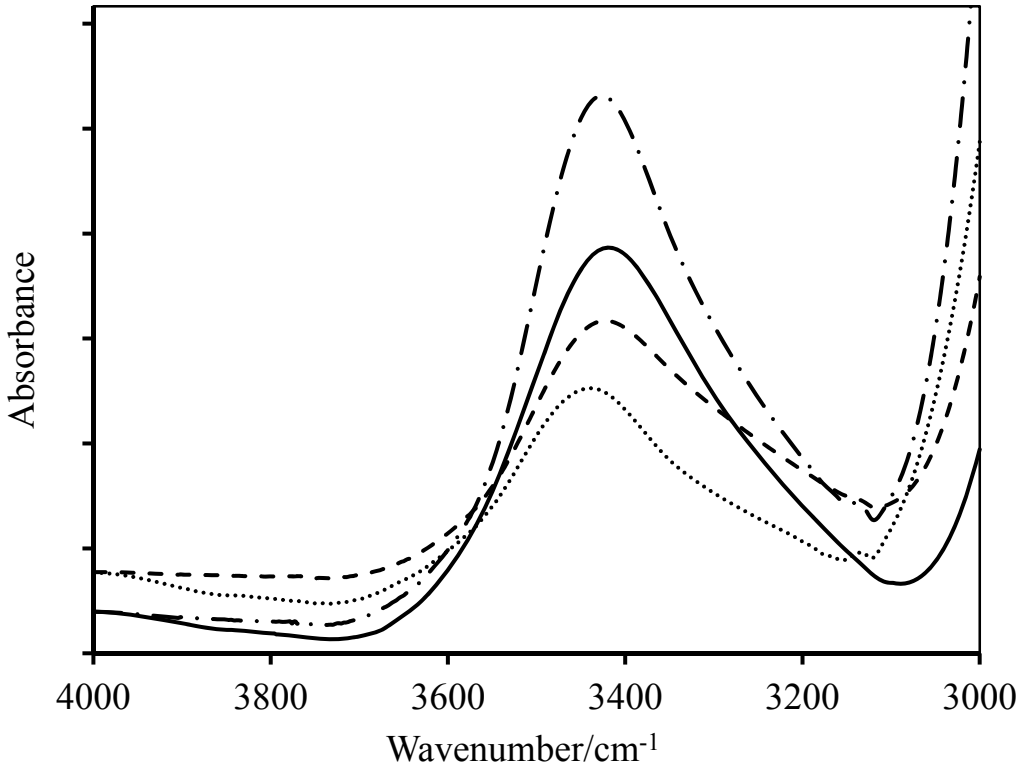

Figure 5.3 FTIR spectra in the hydroxyl vibration region of 59/41 SHS/PMMA blends containing: (…….) 30, (—•—•—) 50, (— — —) 70, and (———) 100 mole% HS.

Table 5.1-The position of hydrogen- bonded OH bands of 59/41 SHS/PMMA blends

mole-% HS in the copolymer	ν/cm^{-1}
30	3460
50	3446
70	3437
100	3428

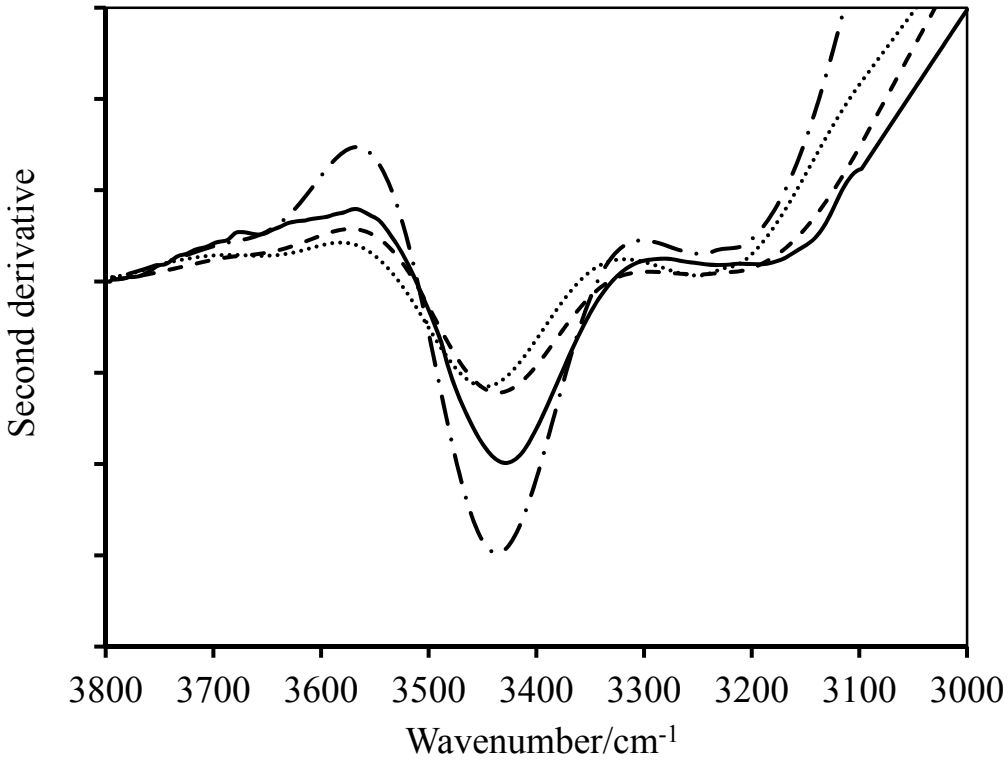

Figure 5.4 Second derivative spectra of 59/41 SHS/PMMA blends containing: (…….) 30, (—•—•—) 50, (— — —) 70, and (———) 100 mole% HS.

5.2.1.2 SHS/PEMA blends

Only one blend of PEMA with a SHS copolymer (i.e. SHS 50 mole-%) was prepared and its behaviour compared to that of PEMA/P4HS (*section 4.2.2*). Figure 5.5 compares the FTIR spectra of the blends and pure PEMA in the carbonyl region (1680 - 1850 cm^{-1}). As for the PMMA blends, the shoulder at 1708 cm^{-1} increases with increasing hydroxyl content; when PEMA is blended with pure P4HS the intensity of the two carbonyl peaks becomes approximately equal,. This investigation confirms the results by Xiang et al. who demonstrated that increasing HS content in the blends leads to increasing of hydrogen bonding interaction between carbonyl groups in PEMA and hydroxyl groups on copolymers [159].

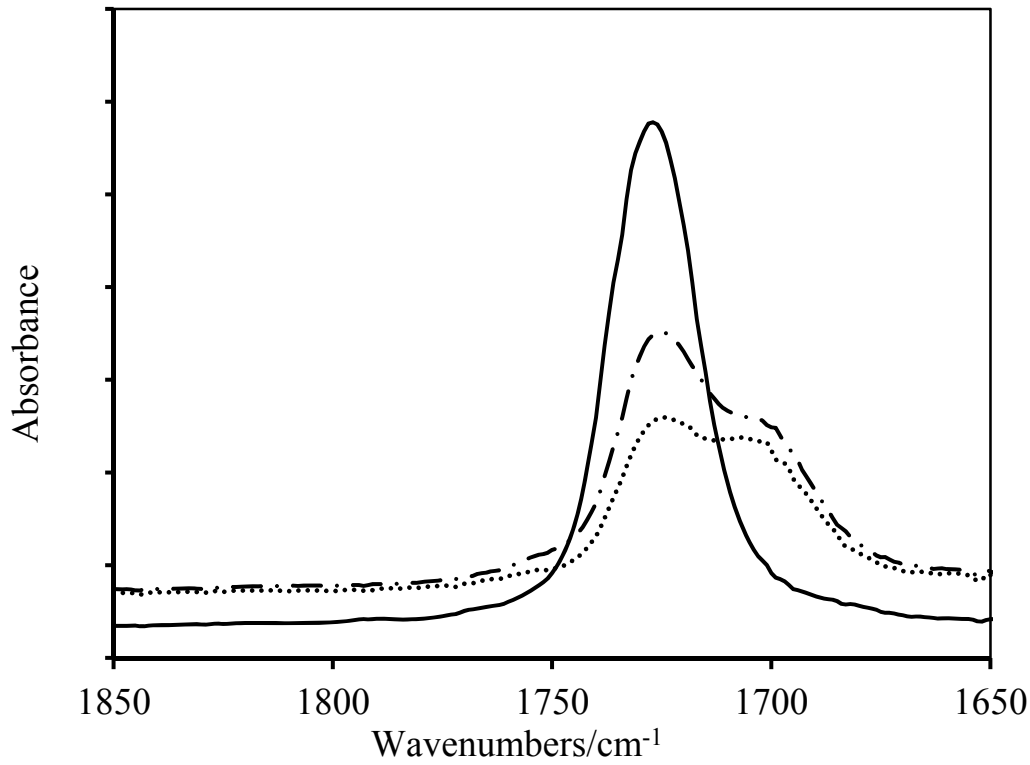

Figure 5.5 FTIR spectra in the carbonyl vibration region from 1850 to 1650 cm^{-1} for of (……..) 49/51 P4HS/PEMA, (—•—•—) 59/41 SHS50/PEMA, and **(———)** PMMA.

As discussed for the PMMA system, the free hydroxyl band (~3530 cm^{-1}) present in the copolymer is no longer observed in the blend (Figure 5.6). The fact that the new hydrogen bonded hydroxyls absorb at a higher frequency (3420 cm^{-1}) compared with the self-associated hydroxyls (~3355 cm^{-1}), suggests that the inter-molecular hydrogen bonds in the blends are weaker.

An additional point to note by comparison of the FTIR spectra in the hydroxyl vibration region for SHS/PMMA and SHS/PEMA blends (Figures 5.3 and 5.6) is that the strength of inter-molecular hydrogen bonds in these systems is quite similar. This is consistent with results reported for pure P4HS blended with PMMA and PEMA [43]. Thus, we can conclude that the addition of methylene units does not affect the hydrogen bonding strength between hydroxyl groups of SHS copolymers and carbonyls of PMMA or PEMA. Regarding the strength of hydrogen bonded carbonyl groups the results in Figure 5.5 indicate that the increases of the intensity of the hydrogen bonding band at 1704 cm^{-1} with increasing of hydroxyl content in the blend is at the expense of the intenisity of free carbonyl band centered at 1728 cm^{-1}.

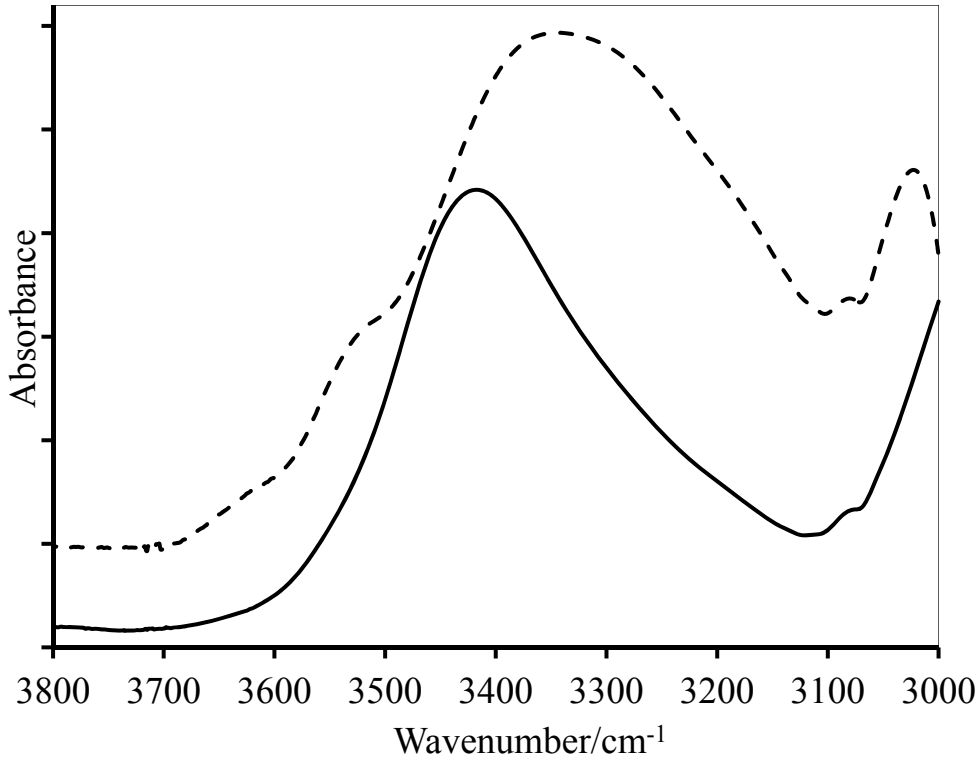

Figure 5.6 FTIR spectra in the hydroxyl vibration region from 3800 - 3000 cm^{-1} for **(……)** SHS50 and **(——)** SHS50/PEMA.

5.2.2 SHS/ polyether blends: Qualitative analysis

Three SHS/PEO blends were studied in the attempt to explore the effect of dilution on the strength of the hydrogen bonding interaction and to assess the effect of copolymer composition on the strength of the intra- and inter-association.

5.2.2.1 SHS/PEO blends

The FTIR spectra of the SHS /PEO blends at a fixed blend composition equal to 59/41 mole% are displayed in Figure 5.7.

The FTIR results (Figures 5.7 and 5.8) show that the strength of hydrogen bonds in SHS/PEO blends are quite similar to those in P4HS/PEO blends since the distance between the free hydroxyl band at 3530 cm^{-1} and the hydrogen bonding bands of P4HS/PEO or any of SHS copolymers with PEO are $\Delta\nu \cong 150$ cm^{-1}. However, the

broad of hydrogen bonding bands of SHS/PEO is much less than those of copolymers one (Figure 5.9) which reflects fact that all hydroxyl groups on each chain in the copolymer seek to interact with oxygen atoms of PEO or with hydroxyl groups on other chain.

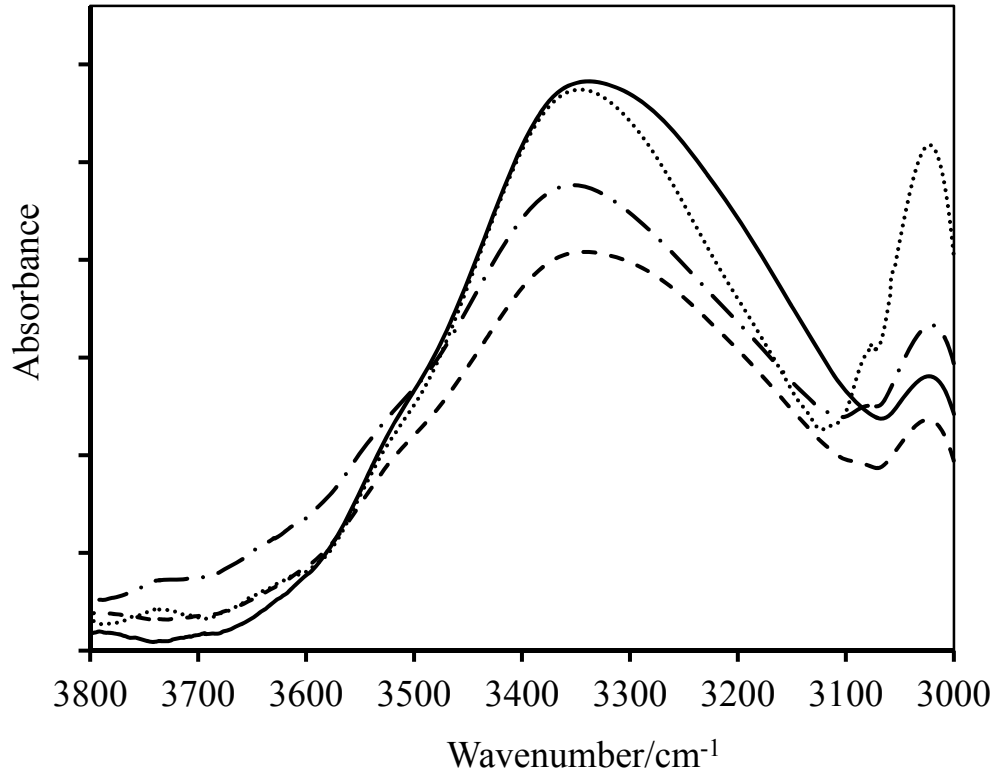

Figure 5.7 FTIR spectra recorded at room temperature in the 3800-3000 cm^{-1} region for SHS/PEO 59/41 mole% containing: : (……) 30, (—•—•—) 50, (— — —) 70, and (———) 100 mole-% HS.

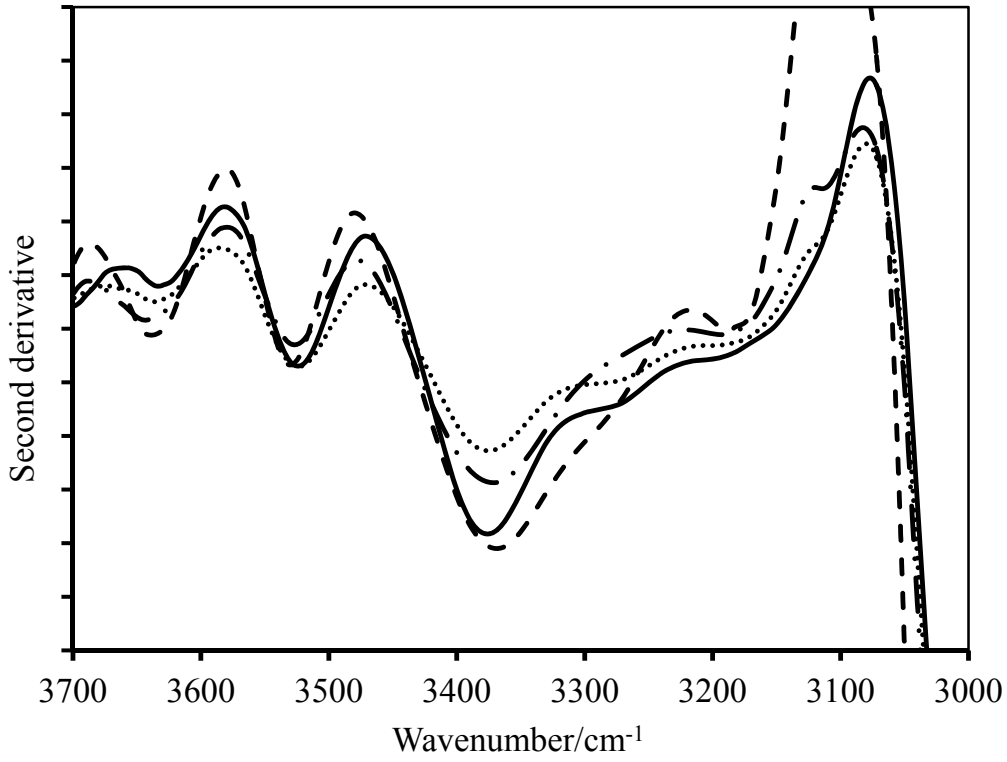

Figure 5.8 Second derivative spectra of SHS/PEO 59/41 mole% containing: (— — —) 30, (—•—•—) 50, (.....) 70, and (———) 100 mole-% HS.

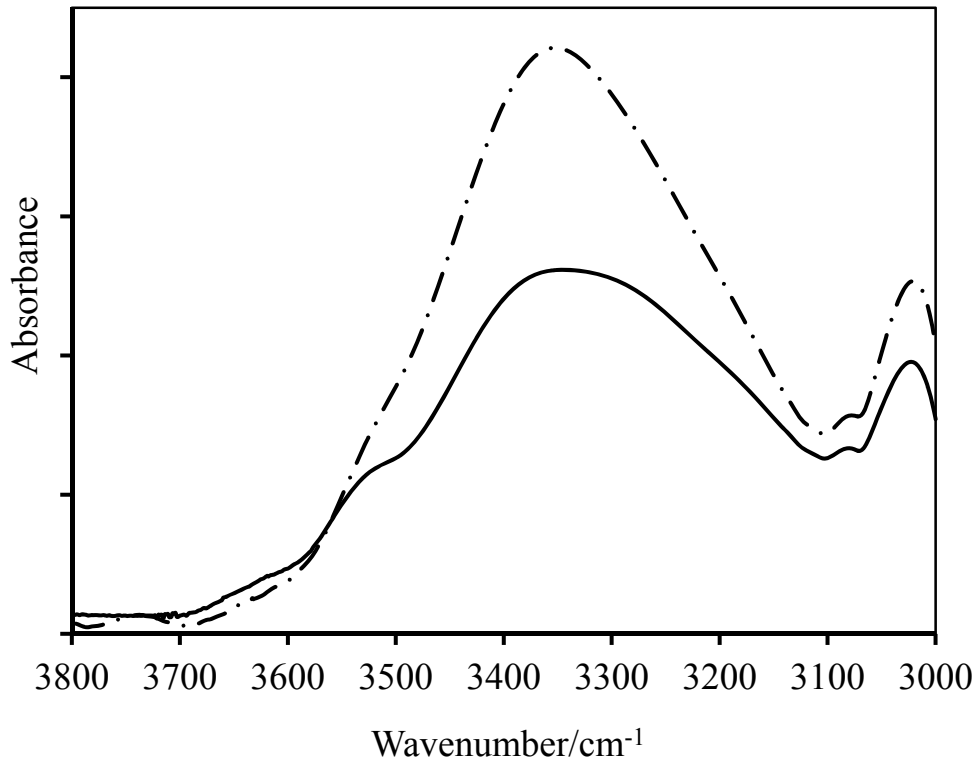

Figure 5.9 FTIR spectra in the hydroxyl vibration region from 3800 - 3000 cm^{-1} for **(—•—•—)** 59/41 SHS50/PEO and **(———)** SHS50.

Return to the comparison between P4HS/PEO and SHS/PEO blends (i.e. when the number of hydroxyl groups in the copolymer is reduced to half by styrene units) in the hydroxyl region Figure 5.7 show that the band of P4HS/PEO is broad than those of SHS/PEO blends. The broad peak between 3050 and 3500 cm^{-1} in Figure 5.7 includes contributions from the stretching modes of intra-molecular hydrogen bonding and intermolecular hydrogen bonding, from high to low wavenumbers.

Second derivative calculations (Figure 5.8) clearly show that a band appears for 59/41 P4HS/PEO blend at 3280 cm^{-1} and this attributed to intermolecular hydrogen bonds with a $\Delta v \cong 250$ cm^{-1}. The intra-molecular band is located at 3383 cm^{-1}, with $\Delta v \cong 136$ cm^{-1}, whereas for SHS50/PEO blend the presence of intermolecular interactions cannot be confirmed even with second derivative calculation. Similar results have been indicated of SHS/PVEE blends [53]. Therefore, we can say that increasing the percentage of HS units in SHS copolymers leads to increasing the presence of intermolecular interactions in SHS/PEO blend and vice versa.

5.2.2.2 SHS/PVME blends

FTIR spectra of PVME blends with SHS copolymers were recorded for comparing the behaviour of this blend with that of the PEO system. Almost all of the hydroxyls are expected to form inter-molecular hydrogen bonds as can be seen in Figure 5.10 due to the absence of a free hydroxyl vibration at ~ 3530 cm^{-1}. Moreover, we would anticipate the intensity of intermolecular hydrogen bonding band to increase with increasing HS content [160]. Second derivative spectra (Figure 5.11) show that the intensity of SHS30/PVME blend is higher than those of SH50/PVME and PHS/PVME blends.

FTIR spectra in hydroxyl region of 59/41 SHS50/PVME and 33/67 SHS50/PVME blends are measured. Figure 5.12 shows that the peaks of SHS50/PVME blends shifted to lower wavenumbers (~3308 cm^{-1}) compared with the peak of SHS copolymer (~ 3375cm^{-1}), and as we have mentioned before that the difference in wavenumbers ($\Delta\upsilon$) between the free hydroxyl band (~3530 cm^{-1}) and the band attributed to hydrogen bonded -OH groups could be used as a measure of the relative strength of hydrogen bonding. Correspondingly, the large value of $\Delta\upsilon \cong 222$ cm^{-1} in SHS50/PVME

blends demonstrates that the hydrogen bonding between PVME and SHS is stronger than the self-association $\Delta\upsilon \cong 165$ cm^{-1} between SHS repeat units. Moreover, the increasing of hydroxyl groups in the blends results in increasing the width of the peaks as a result of overlapping between intra- and inter-actions as shown in Figure 5.12. Thus, for the clarification of this point second derivative spectra of those blends were calculated (Figure 5.13). As PVME content increases in the blend the opportunity to configure intermolecular interactions between hydroxyl groups and oxygen atoms of PVME grows at the expense of forming self-association interaction, so, the amount of intermolecular interactions in the SHS50/PVME blend containing 67 mole% of PVME is bigger than those containing 41 mole% PVME.

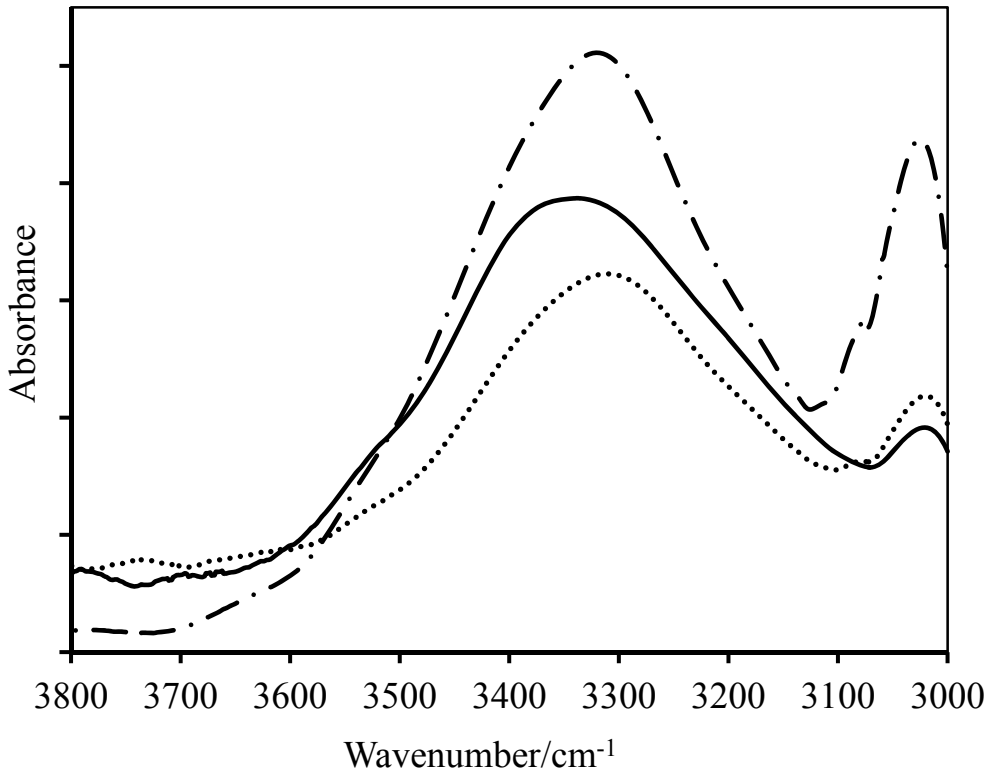

Figure 5.10 FTIR spectra recorded at room temperature in the 3800-3000 cm^{-1} region for 59/41 SHS/PVME containing: (—•—•—) 30, **(……)** 50, and (———) 100 mole-% HS.

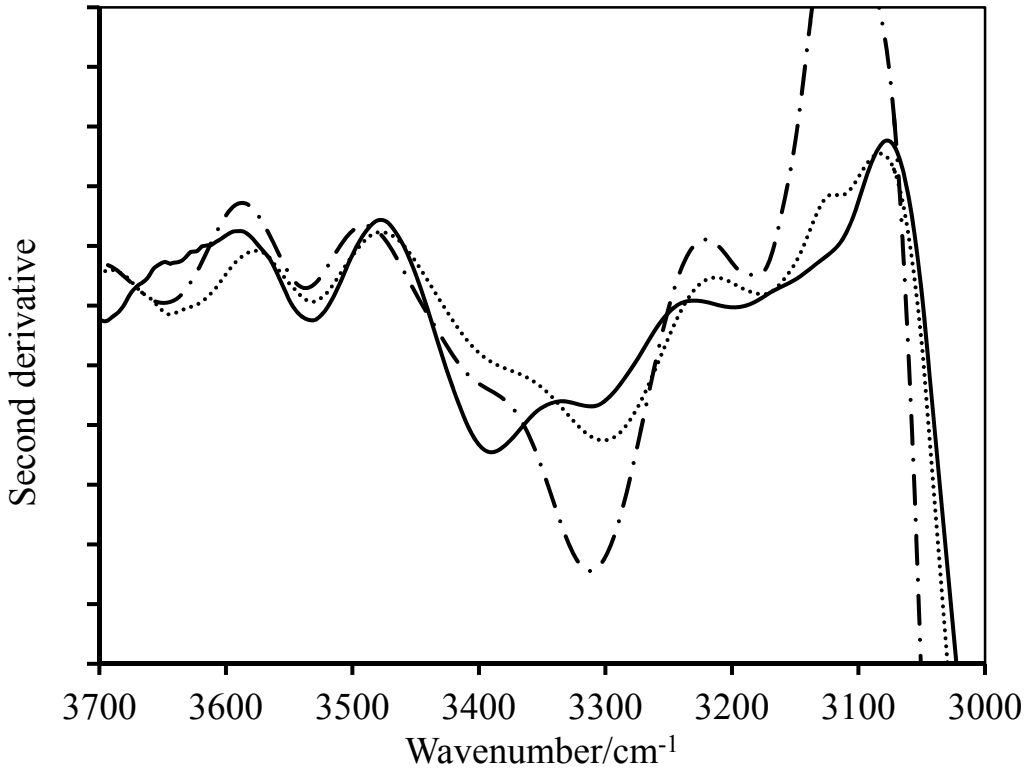

Figure 5.11 Second derivative spectra of 59/41 SHS/PVME containing: (—•—•—) 30, **(……)** 50, and (———) 100 mole-% HS.

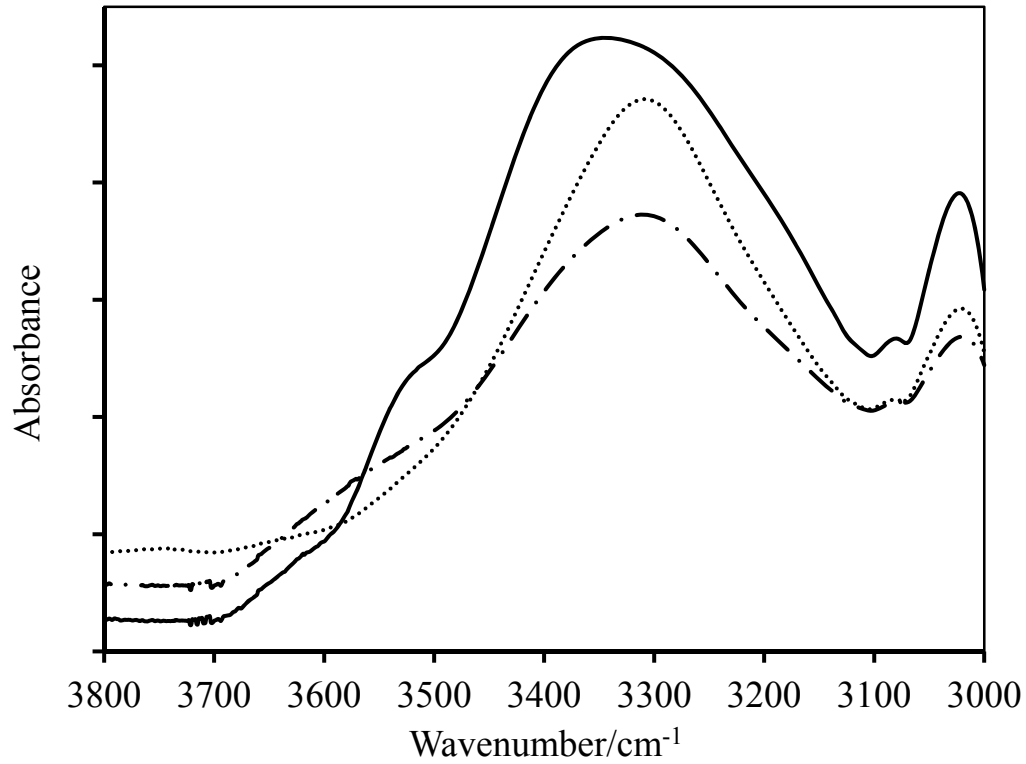

Figure 5.12 FTIR spectra recorded at room temperature in the 3800-3000 cm^{-1} region for SHS50/PVME containing: **(……)** 33, (—•—•—) 59, and (———) 100 mole-% SHS copolymer in the blends.

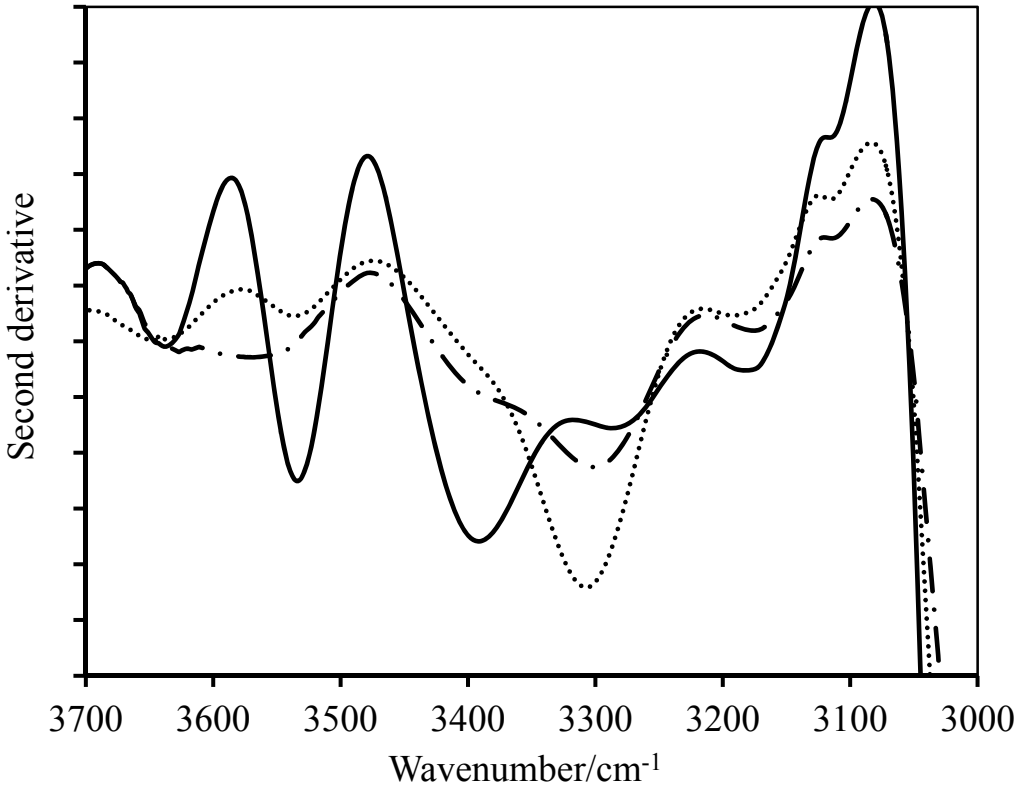

Figure 5.13 Second derivative spectra of SHS50/PVME containing: **(……)** 33, (—•—•—) 59, and (——) 100 mole-% SHS copolymer in the blends.

5.2.3. The effect of hydroxyl groups dilution on intermolecular hydrogen bonding in SHS/polyether blends

To form intermolecular hydrogen bonds the proton donating groups needs to be easily accessible. For example, in the case of SHS/polyether blends, a particular hydroxyl groups in the SHS copolymer may be close to an ether group, but because adjacent OH groups on the same chain are already hydrogen bonded to other hydroxyl groups that may cause inability of the hydroxyl group to orient itself fittingly to form an intermolecular hydrogen bond. Thus, we have examined the effect of spacing (dilution) between hydroxyl groups on the formation of intermolecular hydrogen bonds using blends of SHS (30, 50 and 100 mole-% HS) and two polyethers (i.e. PEO and PVME).

To compare the FTIR data of these blends, the difference in the stretching frequency of hydrogen bonded hydroxyl band in the pure copolymer and the stretching frequency of the hydrogen bonded hydroxyl in the 59/41 SHS/PVME blend is used and

defined as Δv. Physically, the total amount of hydroxyl groups that are included in intermolecular hydrogen bonding is related to the magnitude of Δv.

The –OH band in the IR spectra should contain three contributions: from free hydroxyl groups (1), from hydroxyl groups that are hydrogen bonded to other hydroxyl groups (2), and from hydroxyl groups that are hydrogen bonded to ether groups (3)[161]. However, only (1) and (2) contribute to the IR spectra in the pure copolymer, whereas in the blends (1), (2), and (3) contribute. Consequently, a measure of the amount of intermolecular hydrogen bonding between two components in a blend is the difference between the stretching frequency of the hydrogen bonded hydroxyl band in the blend and the stretching frequency of hydroxyls bonded in the pure copolymer. Therefore, the probability of hydroxyl groups within pure copolymer to be able to form intermolecular hydrogen bonds can be proportional to Δv [161].

The values of Δv for PEO and PVME blends with SHS copolymers, as calculated from the spectra reported in Figures 5.8 and 5.11 are tabulated in Table 5.2and plotted in Figure 5.14 as a function of the amount of HS in the copolymer.

Table 5.2- Difference in frequency of hydrogen- bonded OH bands (Δv) between pure SHS and SHS/polyethers blends (59/41 mole-%)

mole-% HS in SHS copolymer	Δv PEO/(cm^{-1})	Δv PVME/(cm^{-1})
30	55	66
50	34	45
100	22	15

An evaluation of the plot shows that as the HS content in SHS copolymer decreases the value of Δv increases for each of polyethers. This can be considered as evidence that the extent of intermolecular hydrogen bonding between SHS and polyether increases as the amount of HS decreases in the copolymer down to 30 mole%. The results by Radmard and Dadmun of SHS with other polyethers also indicated that increasing HS content in SHS copolymers leads to a decrease in the presence of intermolecular hydrogen bonding between hydroxyl groups and ethers oxygen [161]. Further of this, as the distance between hydroxyl groups in SHS copolymers increases the tendency for the hydroxyl groups to form intermolecular hydrogen bonds with the

polyethers improves. This may be attributed to an increase in the amount of rotational freedom of various hydroxyl groups with respect of each other as they are further separated along the copolymer chain. The increasing distance between hydroxyl groups of SHS affect their accessibility to form intermolecular hydrogen bonds, and decreases the presence of intra-molecular hydrogen bonding. This results in an increase in the number of hydroxyl groups from SHS that can participate in intermolecular hydrogen bonding.

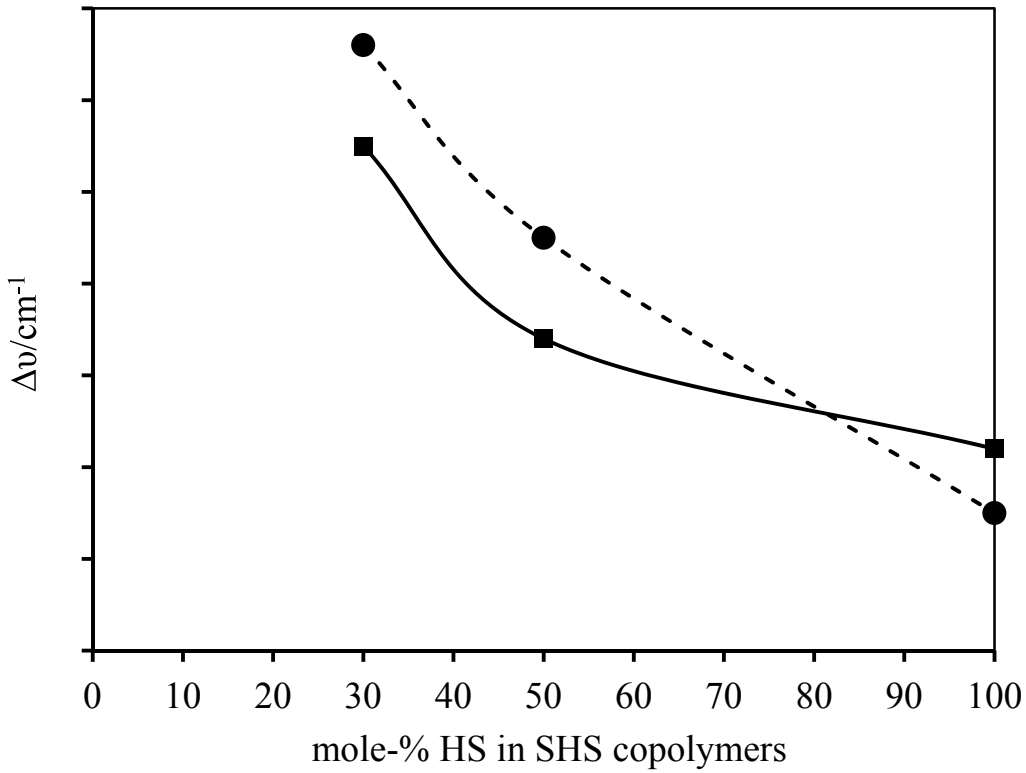

Figure 5.14 Effect of spacing of the hydroxyl groups along the copolymer chain on the intermolecular hydrogen bonding strength, Δ*v*, of (●) PVME, and (■) PEO blends. Lines are guide to the eye only.

5.2.4 Effect of temperature on hydrogen bonding

The temperature effect on the hydrogen bonding was studied for three blend systems using FTIR as detailed below.

a) SHS/PEMA

As discussed in the literature for similar blends (i.e. P4HS or SHS with poly (n-alkyl methacrylate)) [42, 43] the effect of temperature should be evident in three

spectral regions: (a) the 1000-1600 cm^{-1} region, which is mostly composed of aromatic ring vibrations, (b) the carbonyl stretching region (1650-1800 cm^{-1}) and (c) the hydroxyl vibration region (3000-3800 cm^{-1}) [41]. However, the discussion presented below focuses on the two main regions of importance to the blends, neglecting the first region (i.e. 1000-1650 cm^{-1}).

A typical sequence of spectra collected at different temperatures in the carbonyl vibration region is displayed in Figure 5.15. The contributions from free (1730 cm^{-1}) and hydrogen bonded C=O groups (1705 cm^{-1}) are easily separated. It can be seen that increasing temperature leads to a decrease in the number of H-bonded C=O groups. To investigate the effect of temperature quantitatively, we have separated the free and hydrogen-bonded contributions by fitting the IR spectra in the region 1600 to 1800 cm^{-1} using two Gaussian functions. The parameters resulting from the curve fitting procedure (vibration position,ν, and absorption intensities, A) are listed in Table 5.3. Taking the curve fitting results, the concentration of free and hydrogen bonded carbonyl groups can be calculated, keeping into account of the different absorption coefficients of bonded and free carbonyl groups. It was found that the absorptivity ratio of carbonyl vibrations varies from 1.2 to 1.75 depending on the systems [42]: for inter-association in PHS blends the a_{HB}/a_F ratio is equal to 1.5 according to previous infrared studies of hydroxyl-carbonyl inter association [34]. The fractions of hydrogen bonded or free groups, f_{HB} and f_F respectively, are given by [34],

$$f_{HB} = (1 - f_F) = \frac{A_{HB}}{\left[A_{HB} + A_F\left(\frac{a_{HB}}{a_F}\right)\right]} \qquad (5.1)$$

where A_{HB} and A_F are the absorbance of hydrogen bonded and free carbonyls respectively; a_{HB} and a_F are the corresponding absorption coefficients. Typical curve fits are shown in Figure 5.15 (b) and (c) for spectra collected at 25 and 150^oC, respectively. Hydrogen bonding fractions results (Table 5.3) indicate that the number of hydrogen bonds in SHS50/PEMA is bigger than the Hydrogen bonding fraction of P4HS/PEMA as published by Serman and co-workers [43]. The dilution of hydroxyl groups in SHS50/PEMA by styrene leads to increased distance between hydroxyl groups, so, they are unable to form self-association bonds but free to form intermolecular interaction with carbonyl groups. However, with increasing temperature there is a decrease in

hydrogen bond strength, but not enough to break the hydrogen bonds between hydroxyl and carbonyl groups. Nevertheless, the position of the hydrogen bonded C=O band would be shifts to higher wavenumbers.

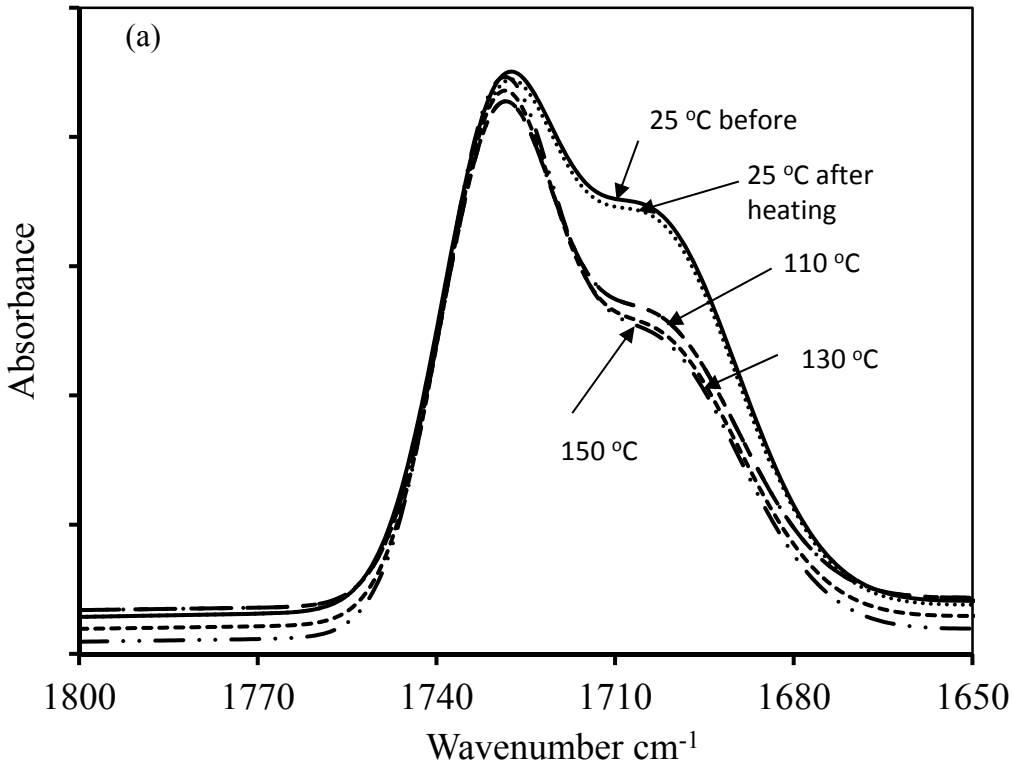

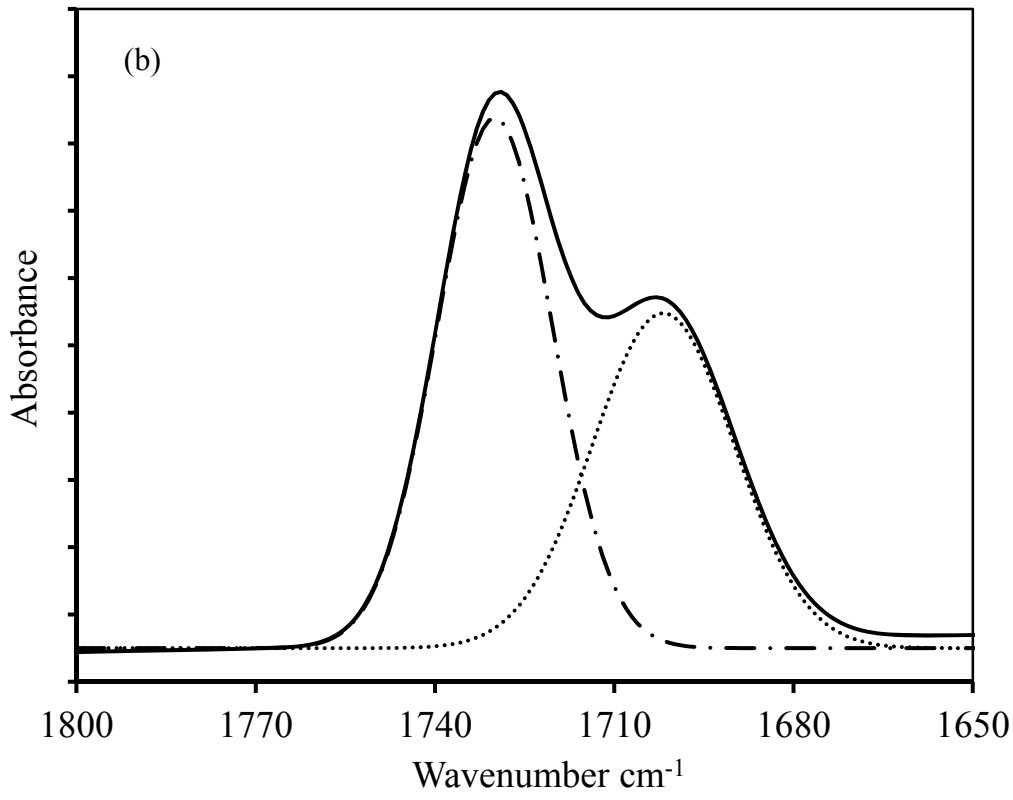

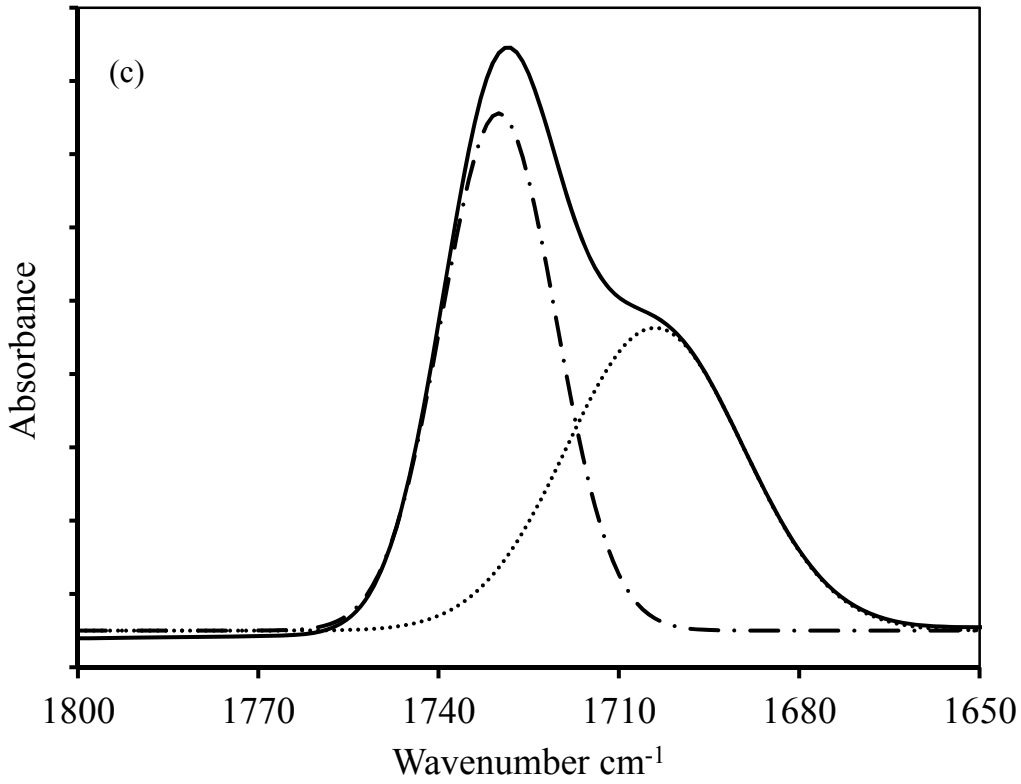

Figure 5.15 FTIR spectra in the carbonyl region of 59/41 SHS50/PEMA blend recorded as function of increasing temperature (a), and a curve fitting for 25 ^{o}C (b) and 150 ^{o}C (c).

Table 5.3- Curve fitting results for carbonyl region of SHS50/PEMA 59/41 mole-%.

Temperature/ ^{o}C	A_F	A_{HB}	ν/cm^{-1} F C=O	ν/cm^{-1} H-B C=O	fFC=O	fHB C=O
25	6.43	30.06	1728	1712	0.243	0.757
110	8.31	24.55	1728	1713	0.337	0.663
120	8.44	24.29	1728	1713	0.343	0.657
130	8.93	24.06	1728	1713	0.358	0.642
140	8.87	23.30	1728	1713	0.363	0.637
150	8.79	23.14	1728	1713	0.363	0.637
25	6.80	28.45	1728	1713	0.264	0.736

Figure 5.16 illustrates the effect of the changes in the temperature in hydroxyl region for SHS50/PEMA: the intensity of the free hydroxyl band (~3530 cm^{-1}) at 25 ^oC increases as the temperature rises to 110 ^oC or more. The quantitative separation in hydroxyl region (i.e. 3000 to 3550 cm^{-1}) of the free and hydrogen-bonded contributions of SH50/PEMA using two Gaussian functions is quite difficult. The second derivative is more appropriate to clarify the positions of bands at different temperature. As shown in Figure 5.17at room temperature only one band is observed centred at 3442 cm^{-1}. The complete disappearance of the free OH band demonstrates that all hydroxyl groups in SHS50/PEMA are connected with C=O groups. Furthermore, the disappearance of bands in the region between 3200 and 3380 cm^{-1} reflects fact that OH groups are unable to self-associate. However, a temperature increase above 100 ^oC frees some of the hydroxyl groups from interacting with C=O groups, so, they appear as a free OH band at about 3540 cm^{-1}(Figure 5.17).

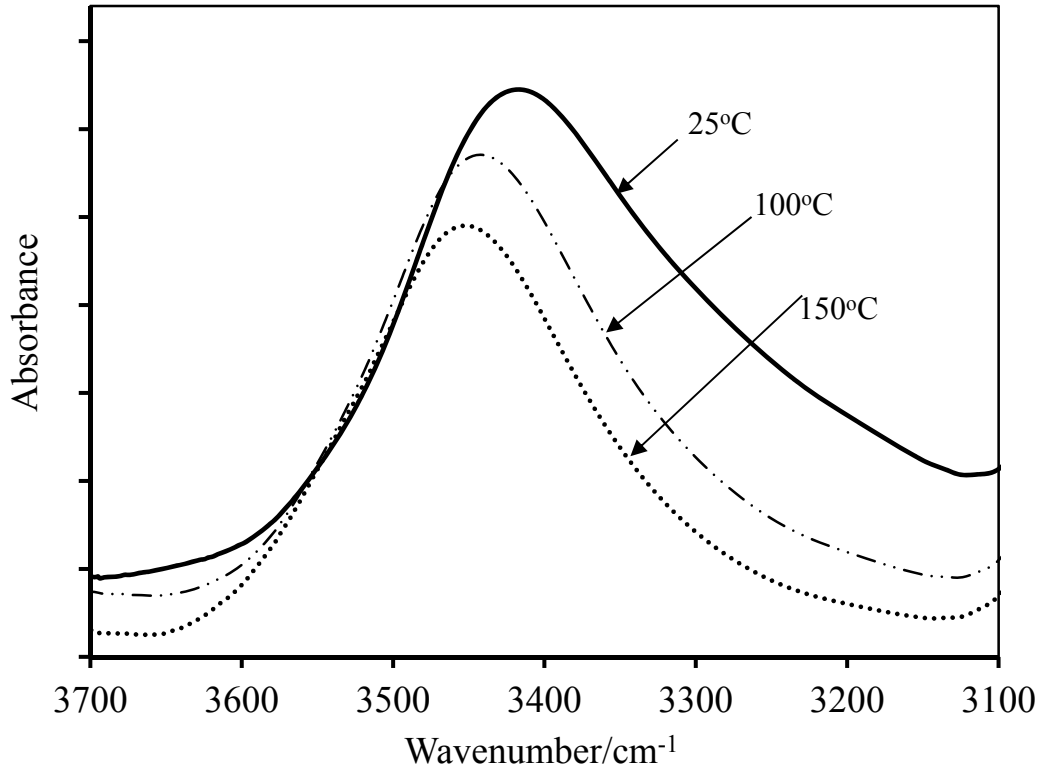

Figure 5.16 FTIR spectra recorded at different temperatures in the 3800-3000 cm^{-1} region for 59/41 SHS50/PEMA blend

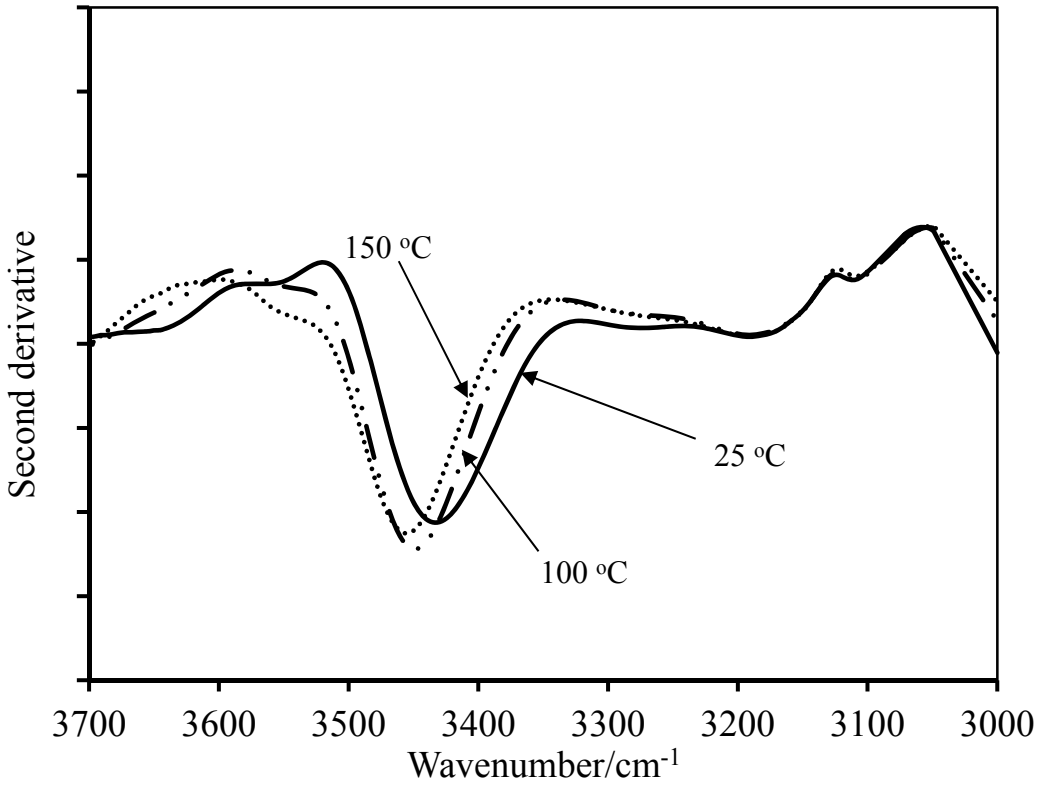

Figure 5.17 Second derivative spectra recorded at different temperatures in the 3800-3000 cm^{-1} region for 59/41 SHS50/PEMA blend.

a) SHS50/PVME blends

FTIR spectra of 59/41 a SHS50/PVME blend at various temperatures are displayed in Figure 5.18. It can be seen from Figure 5.18 that the area under the absorption band at 3320cm^{-1} (i.e. hydrogen bonds between SHS and PVME) decreases steadily and the peaks shift to higher wavenumbers with increasing temperature. On the other hand, the absorption band at 3530 cm^{-1} (i.e. free hydroxyl group) increases as the temperature is increased. Therefore, we can conclude that the number of the hydrogen bonds decreases with increasing temperature. However, hydrogen bonds still exist even at temperatures as high as 150 ^{o}C. The same tendency can be observed for other compositions. As a result, SHS/PVME blends are miscible over a wide range of temperatures. To resolve the broad band at 3320 cm^{-1} and also in the attempt to show the effect of temperature on intra- and intermolecular bands, the second derivative of each spectrum was calculated (Figure 5.19). It is clearly seen that at ambient temperature there are two bands at 3305 and 3395 cm^{-1}, respectively. The first band is attributed to intermolecular hydrogen bonds, and other one reflects the existence of intra-molecular hydrogen bonds.

Furthermore, the intermolecular OH band with $\Delta\nu \cong 225$ cm^{-1} is much stronger than the intra-molecular one ($\Delta\upsilon \cong 140$ cm^{-1}). Increasing temperature close to the glass transition has caused considerable changes in the strength and intensity of inter- and intra-association bands. From Figure 5.19 it can be seen that when temperature rises to 100 ^{o}C the intermolecular hydrogen bonding becomes weak and the band shifts to high wavenumbers (~ 3340 cm^{-1}), also the intensity becomes low resulting in a decrease in the number of intermolecular interactions. On the other hand the intensity of the intra-molecular band increases, which reflects an increase in the number of intra-molecular bonds. However, the strength of the intra-molecular bonds decreases with increasing temperature, whereas the band has shifted to high wavenumber (~ 3415 cm^{-1}). As temperature increases to 150 ^{o}C or more the intermolecular hydrogen band shifts overlaps with the intra-molecular band, causing a broad band centred at ~ 3425 cm^{-1}. Thus, it can be said that when the temperature rises to 150 ^{o}C or over the separation of the overlapping bands becomes difficult, even with second derivative calculations. As for the effect of temperature on the free OH band, Figure 5.19 clearly illustrates that the increasing of temperature lead to an increase in the intensity of the OH band, which means an increase in free hydroxyl group numbers.

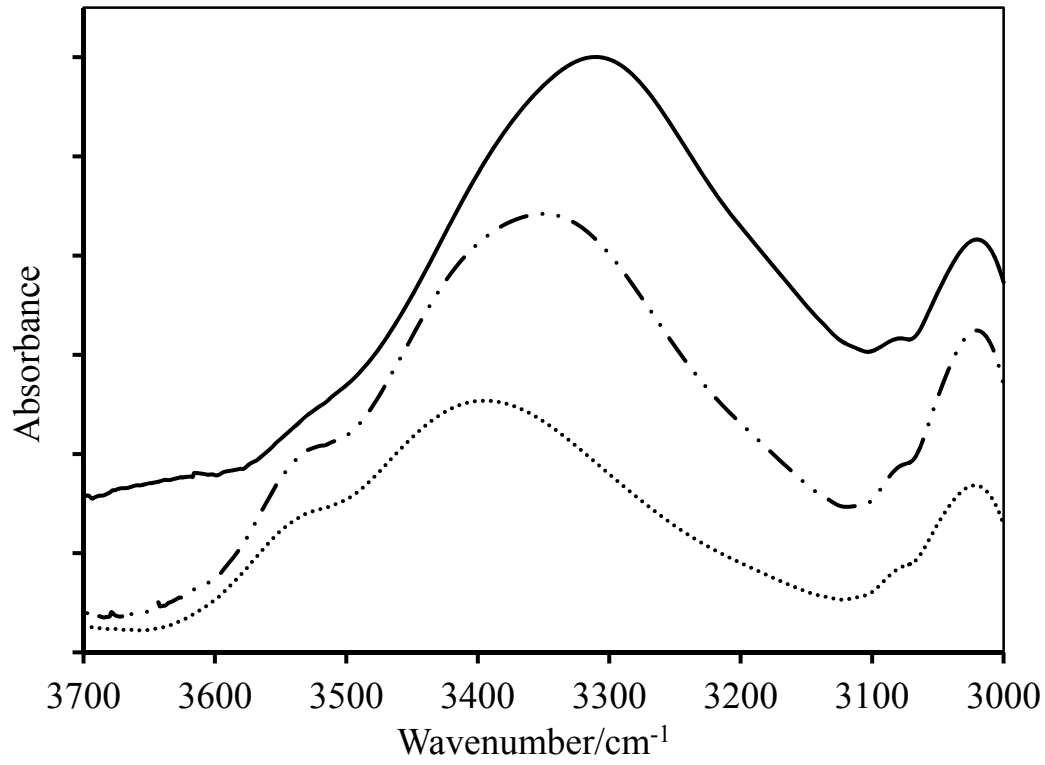

Figure 5.18 FTIR spectra at different temperatures in the 3700-3000 cm^{-1} region for 59/41 SHS50/PVME blends: (——) 25 °C, (—••—••—) 100 °C, and (.....) 150 °C.

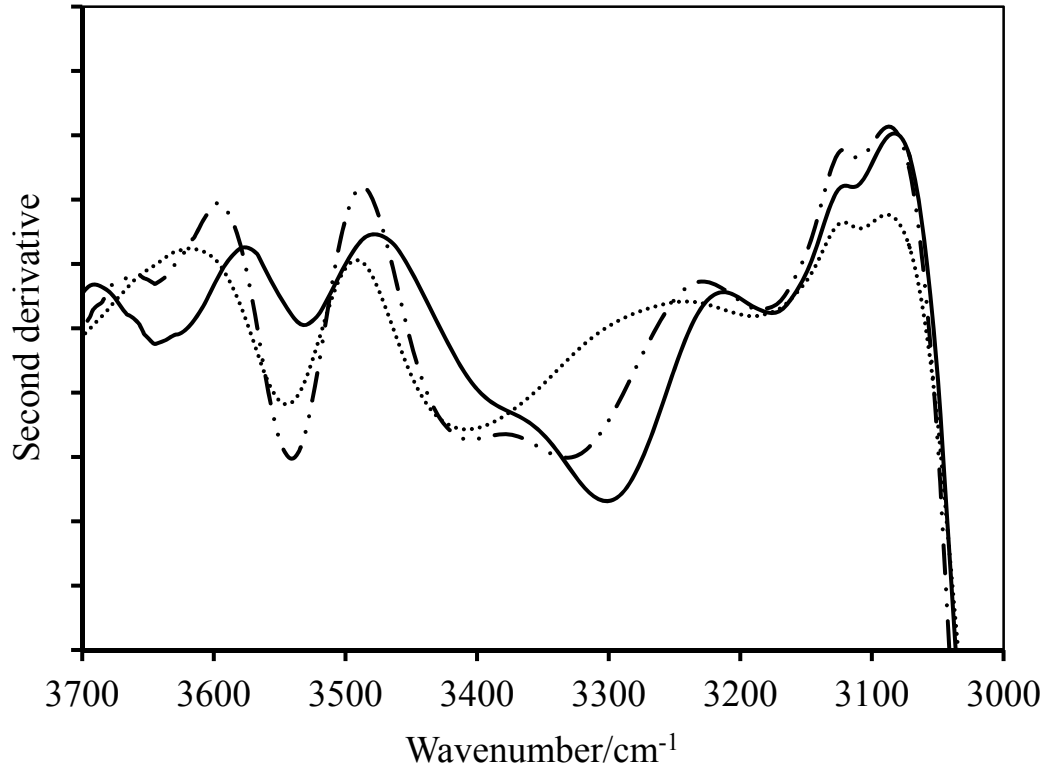

Figure 5.19 Second derivative of FTIR spectra of 59/41 SHS50/PVME blend at: (——) 25 °C, (—••—••—) 100 °C, and (.....) 150 °C.

b) SHS50/PEO blends

Our results in chapter 4 indicated that the increasing of the temperature affects hydrogen bonding of P4HS/PEO blends: the hydrogen bonding bands shifts to high wavenumbers and the intensity decreases. However, with increasing the composition of PEO in the blend the effect of temperature decreases. Figure 5.20 presents IR spectra of a 59/41 SHS50/ PEO blend at different temperatures. As temperature increases the hydrogen bonding interactions in strength and the hydrogen bonding band shifts from ~ 3360 cm^{-1} at 25 °C to ~ 3403 cm^{-1} at 150 °C.The spectra have been compared to a P4HS/PEO blend with same blend composition, and the comparison indicates that even when the temperature is as high as 150 °C there is no effect on the strength and number of hydrogen bonds.

In an attempt to separate the peaks, we have calculated the second derivative at different temperature (Figure 5.21). However, it seems that the second derivative is unable to separate the overlapping peaks and the reason might be attributed to the magnitude in the number of bonds between oxygen ether and hydroxyl groups in comparison to the number of intra or inter interactions between hydroxyl groups themselves.

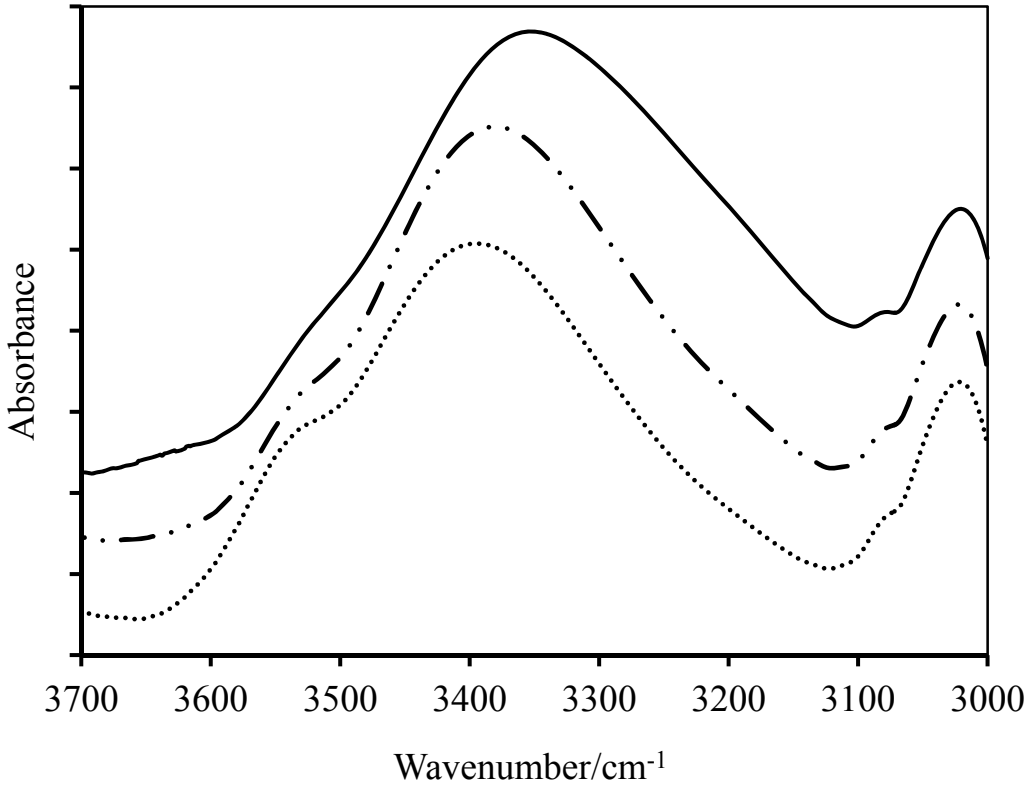

Figure 5.20 FTIR spectra at different temperatures in the 3700-3000 cm^{-1} region for 59/41 SHS50/PEO blend: (———) 25 °C, (—••—••—) 100 °C, and **(……)** 150 °C.

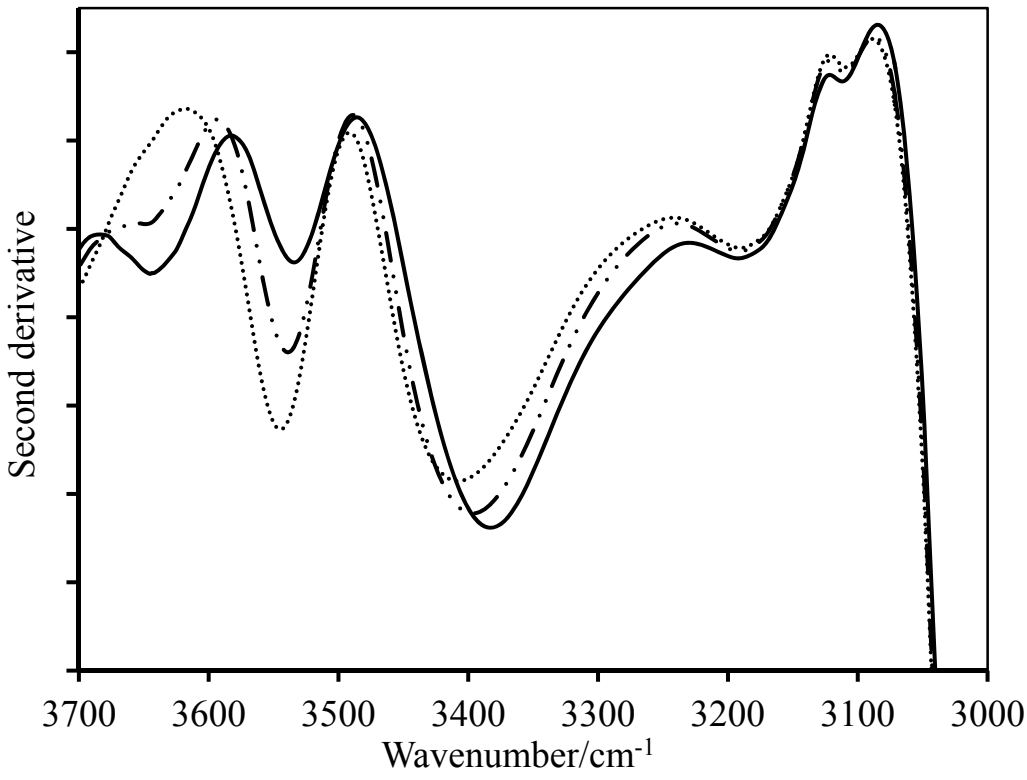

Figure 5.21 Second derivative spectra of 59/41 SHS50/PEO blend at: (———) 25 °C, (—••—••—) 100 °C, and **(……)** 150 °C.

5.3 Enthalpy relaxation

5.3.1 Enthalpy relaxation of SHS/poly(alkyl methacrylate) blends

5.3.1.1 SHS/PMMA blends

The midpoint T_g, T_g temperature range (ΔT) and experimental ΔC_p values for SHS/PMMA blends are shown in Table 5.4. Shown in Figure 5.22 is the HS content composition dependence of T_g(mid) for the PMMA blends. In general, increasing the HS content in either the copolymers or blends results in an increase in T_g(mid). In comparison with SHS copolymers (Chapter 3, Table 3.8), the data in Table 5.4 clearly shows that SHS/PMMA blends have lower T_g than the corresponding SHS copolymers suggesting that the blends are less constrained than the corresponding copolymers, and perhaps not as strongly hydrogen bonded.

Table 5.4 T_g data for 59/41PMMA/SHS blends

Sample	T_g (mid) / K	ΔT / K	ΔC_p / $JK^{-1}g^{-1}$
PMMA	385	8.3	0.207
SHS30/PMMA	401	8.6	0.276
SHS50/PMMA	409	6.6	0.271
SHS70/PMMA	419	10.3	0.283
P4HS/PMMA	411	8.8	0.304

The level of microheteroegeneity in the blends can be judged by the magnitude of ΔT. Large values of ΔT usually indicate increased microheterogeneity. In general, ΔT values were higher for the blends than the copolymers, which is not unexpected given the inherent heterogeneity of polymer blends and increased hydrogen bonding distributions. The change in heat capacity (ΔC_p) at T_g can be related to the change of degrees of freedom at the glass transition resulting from free volume changes [162]. Moreover, the ΔC_p value of SHS30/PMMA blend is lower than the value for the copolymer. However, copolymers with 50 and 70 mole % HS, have lower values of ΔC_p than those of the blends.

Based on the T_g and ΔC_p values we can initially say that the interactions in SHS/PMMA blends increase with increasing the amount of HS groups in the copolymer.

In the present work we display the effect of styrene dilution of hydroxyl groups in the SHS copolymers on the enthalpy relaxation of SHS/PMMA blends as function of physical aging.

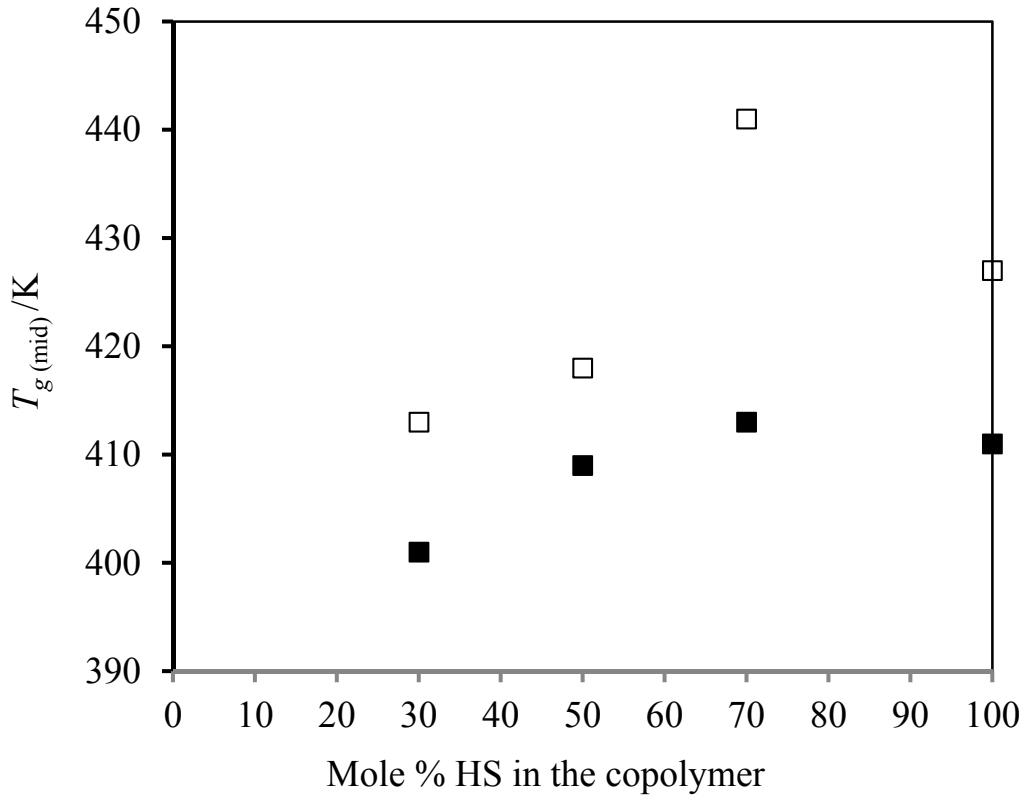

Figure 5.22 Composition dependence of midpoint T_g for 59/41 *SHS/PMMA blend (■) and* SHS copolymers (□).

More specifically we have measured the enthalpy relaxation of 59/41 SHS/PMMA blends for three SHS compositions (30, 50, and 70 mole-% HS). Figure 5.23 shows typical C_p data for 59/41 SHS50/PMMA aged at 15 K below T_g. The size and the maximum of the endothermic recovery peak increase with increase in aging time. This behaviour is similar for all of the blends. The comparative C_p curves for all of SHS/PMMA blends aged at three temperatures below T_g are shown in Figure 5.24 for 2000 min. These authorize us to evaluate qualitatively the difference in enthalpic recovery behaviour between the blends. The blends with high styrene content in the

copolymer presented relatively high and narrow enthalpy relaxation peaks, which point to a quick release of energy. However, the peaks of the blends with high hydroxyl group content in the copolymers, on the other hand, are broad and short indicating that energy is released over a much wider range of temperature. Such an occurrence is consistent with the hydrogen bonding effect seen on ΔT.

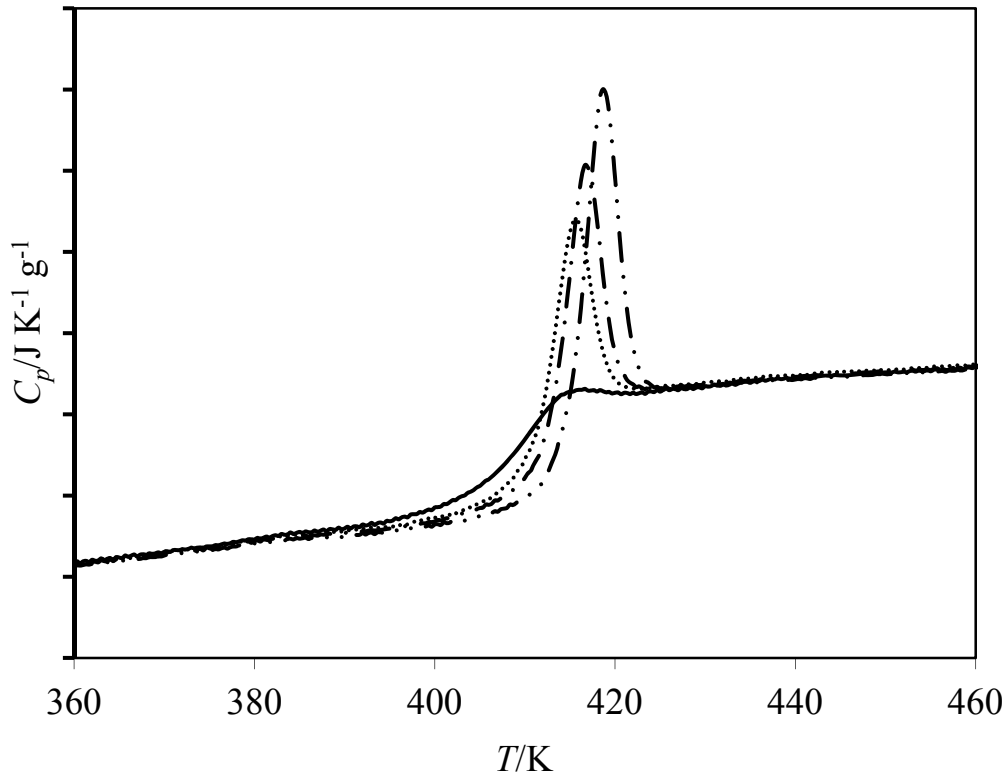

Figure 5.23 Heat capacity curves for 59/41 SHS50/PMMA blend at T_g -T_a = 15 K: 200 (……..), 500 (- - - - -) and 2000 (—●●—●●—) minutes.

The SHS/PMMA blend data were fitted to the CF model and the parameters are given in Table 5.5. Plots of t ΔH (T_a, t_a) versus log (t_a), including the theoretical curves obtained from the CF model are shown in Figure 5.25. The main point to note is that generally the enthalpy lost after a given aging time increases as T_a decreases. This is what we would expect since the distance between the glassy and extrapolated liquid enthalpy lines increase as the system progresses deeper into the glassy region.

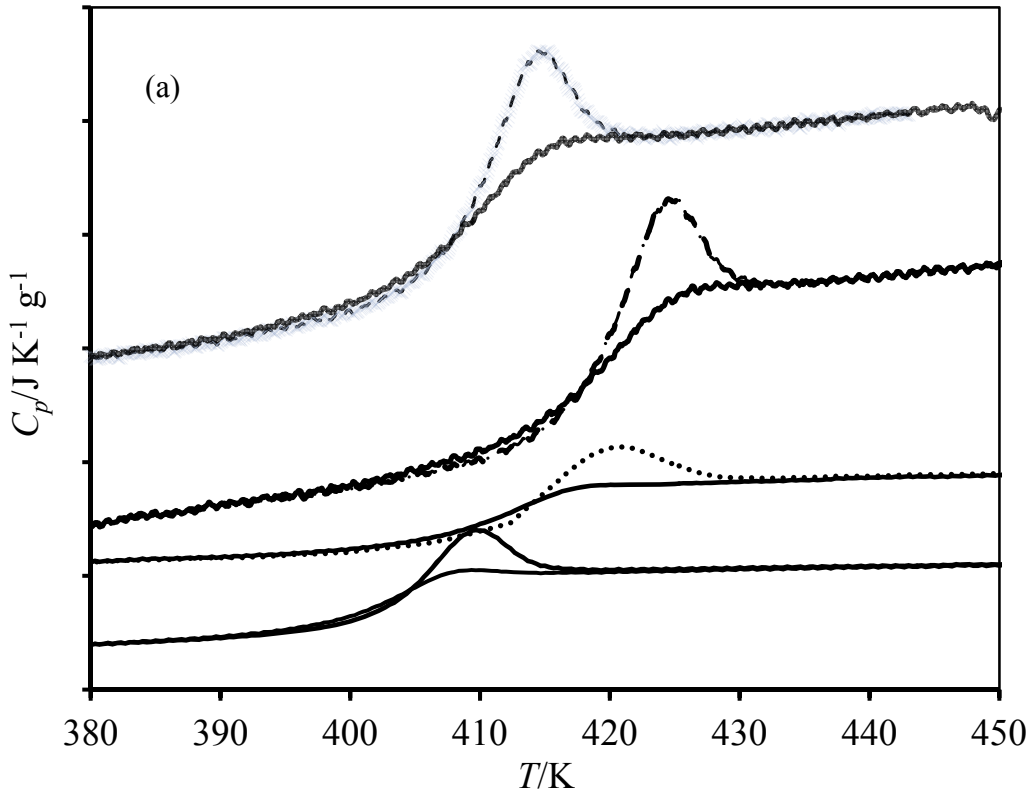
(a)
C_p/J K^{-1} g^{-1}
380
390
400
410
420
430
440
450
T/K

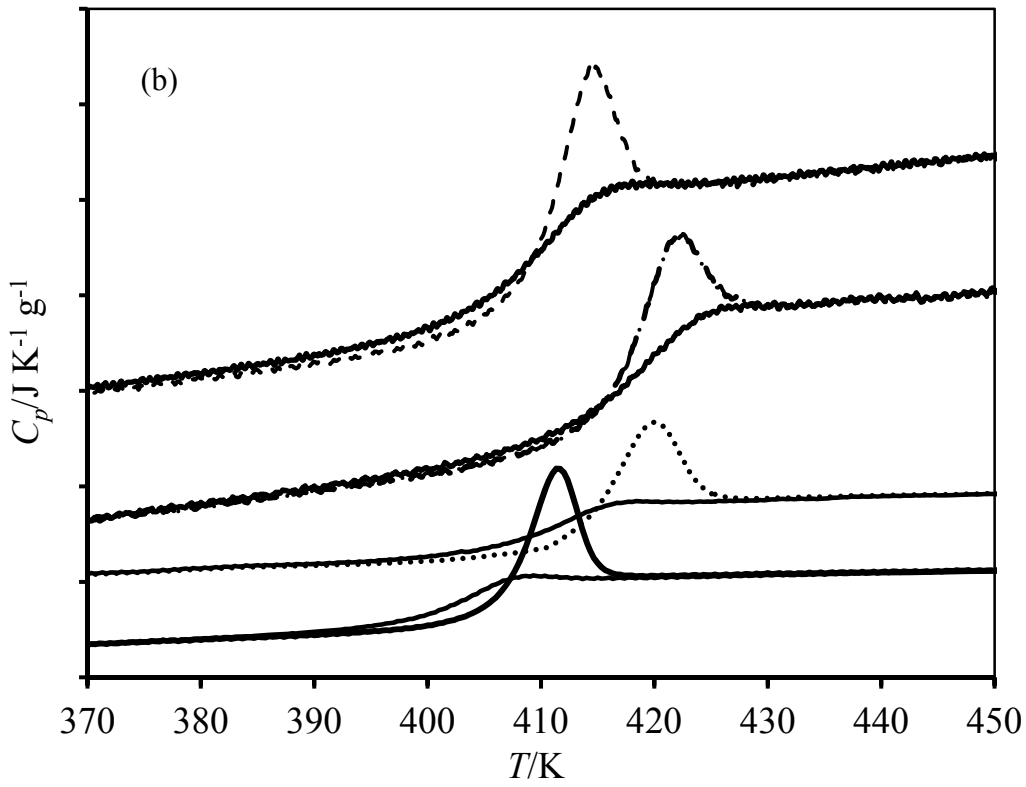
(b)
C_p/J K^{-1} g^{-1}
370
380
390
400
410
420
430
440
450
T/K

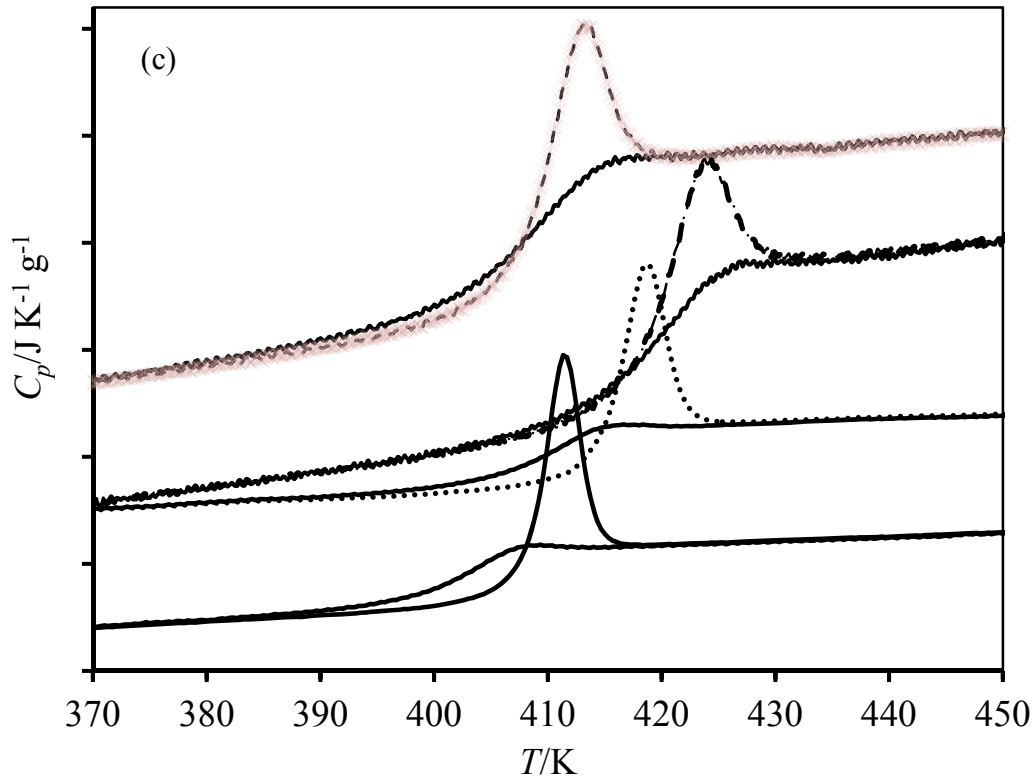

Figure 5.24 Heat capacity curves (aged and unaged) for t_a = 2000 minutes. From bottom to top SHS30/PMMA, SHS50/PMMA, SHS70/PMMA and PHS/PMMA: (a) T_g – 5, (b) T_g – 10 and (c) T_g - 15.

Table 5.5 CF parameters for 59/41 SHS/PMMA blends.

blends	T_a *(K)*	T_g- T_a *(K)*	$\Delta H_\infty(T_a)$ *(J g^{-1})*	log t_c (min)	β
SHS30/PMMA	386	15	1.77	2.46	0.32
	391	10	1.65	2.33	0.32
	396	5	0.78	1.23	0.32
SHS50/PMMA	394	15	1.89	2.59	0.24
	399	10	1.76	2.51	0.24
	404	5	0.94	1.48	0.24
SHS70/PMMA	404	15	1.96	2.25	0.47
	409	10	1.78	2.06	0.47
	414	5	1.42	2.12	0.47
P4HS/PMMA	396	15	2.93	2.58	0.39
	401	10	3.08	2.53	0.39
	406	5	2.35	2.03	0.39

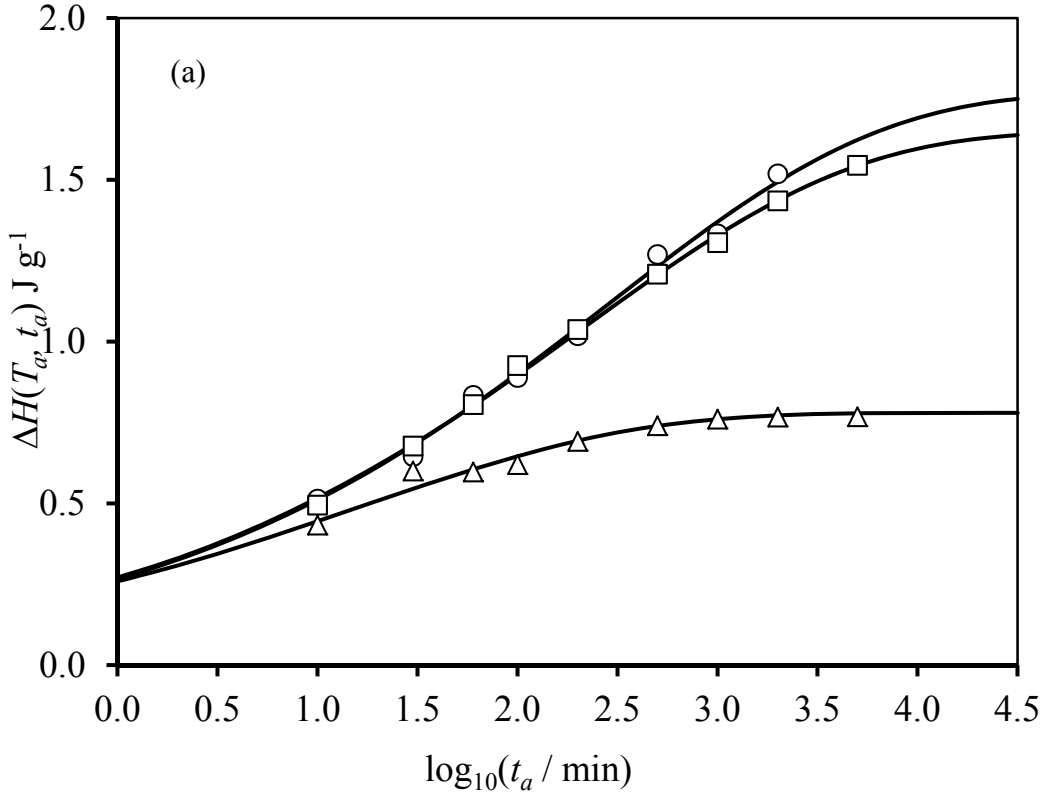
(a)
2.0
1.5
1.0
0.5
0.0
$\Delta H(T_a, t_a)$ J g^{-1}
0.0 0.5 1.0 1.5 2.0 2.5 3.0 3.5 4.0 4.5
$\log_{10}(t_a$ / min)

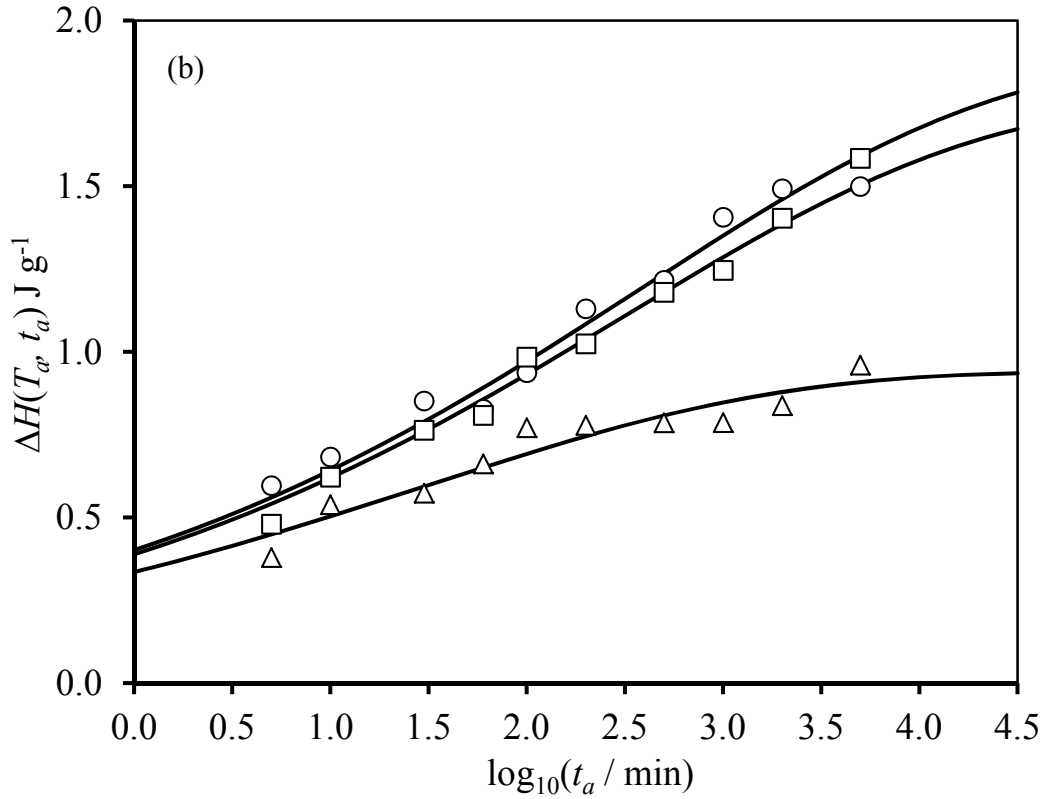
(b)
2.0
1.5
1.0
0.5
0.0
$\Delta H(T_a, t_a)$ J g^{-1}
0.0 0.5 1.0 1.5 2.0 2.5 3.0 3.5 4.0 4.5
$\log_{10}(t_a$ / min)

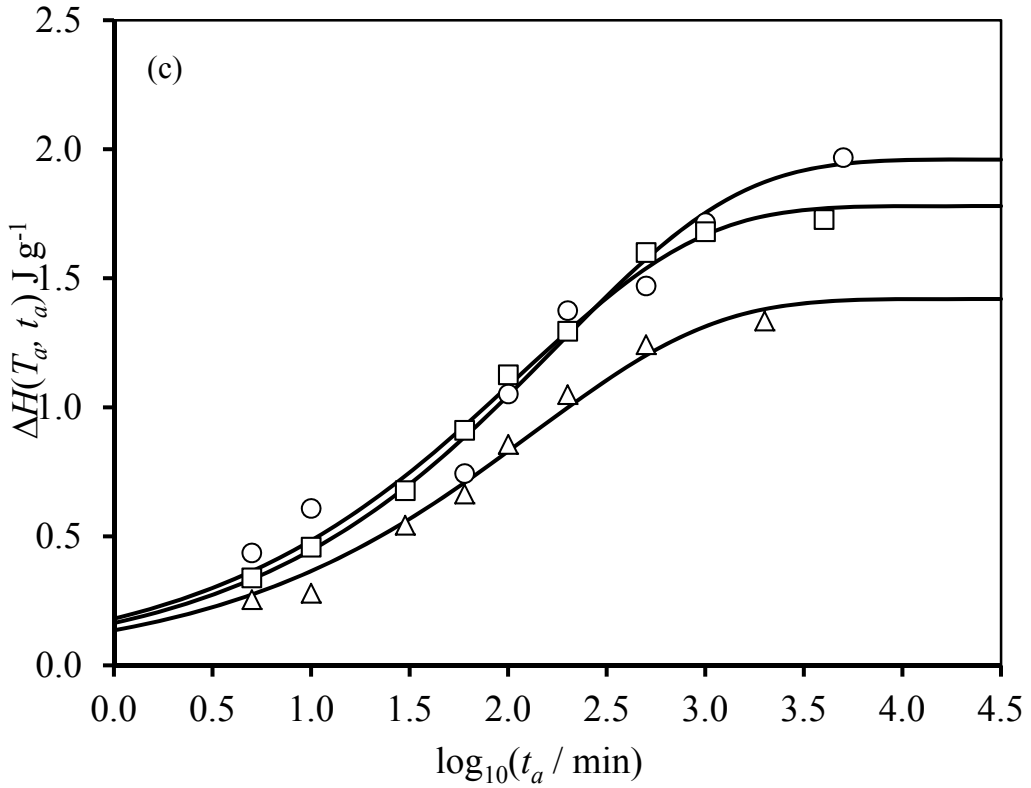

Figure 5.25 Enthalpy relaxation data for the blends: (a) SHS30/PMMA at T_a = 386 K (○), 391 K (□) and 396 K (Δ); (b) SHS50/PMMA at T_a = 394 K (○), 399 K (□) and 404 K (Δ), (c) SHS70/PMMA at T_a = 398 K (○), 403 K (□) and 408 K (Δ). Solid lines are fits to the experimental data using the CF equation.

Figure 5.26 displays all the $\Delta H_\infty(T_a)$ data plotted as a function of distance from T_g. In the cases of SHS/PMMA blends $\Delta H_\infty(T_a)$ values increase with increasing the percentage of HS in the copolymers.

The kinetics of aging could be measured by monitoring log ($\langle t_C \rangle$) against (T_g – T_a). A small value implies a fast relaxation process. The fastest relaxation rate is observed for PHS/PMMA (Figure 5.27). The rate of relaxation increases with increasing HS groups in the copolymers. Thus, both SHS50/PMMA and SHS70/PMMA aged slower than PHS/PMMA. Moreover, aging at 5 K below T_g caused an increase in the relaxation rate as reflected by a lower value of the log($\langle t_C \rangle$) parameter. This suggests a less cooperative relaxation process at this T_a. Furthermore, all PMMA blends relaxed slower than the corresponding SHS copolymers at similar undercooling. This is illustrated for all systems in Figure 5.28 (a) – (c). Data in Figure 5.28 demonstrate that

there is good agreement between the increase in relaxation rate with increasing HS content in the copolymers and FTIR results.

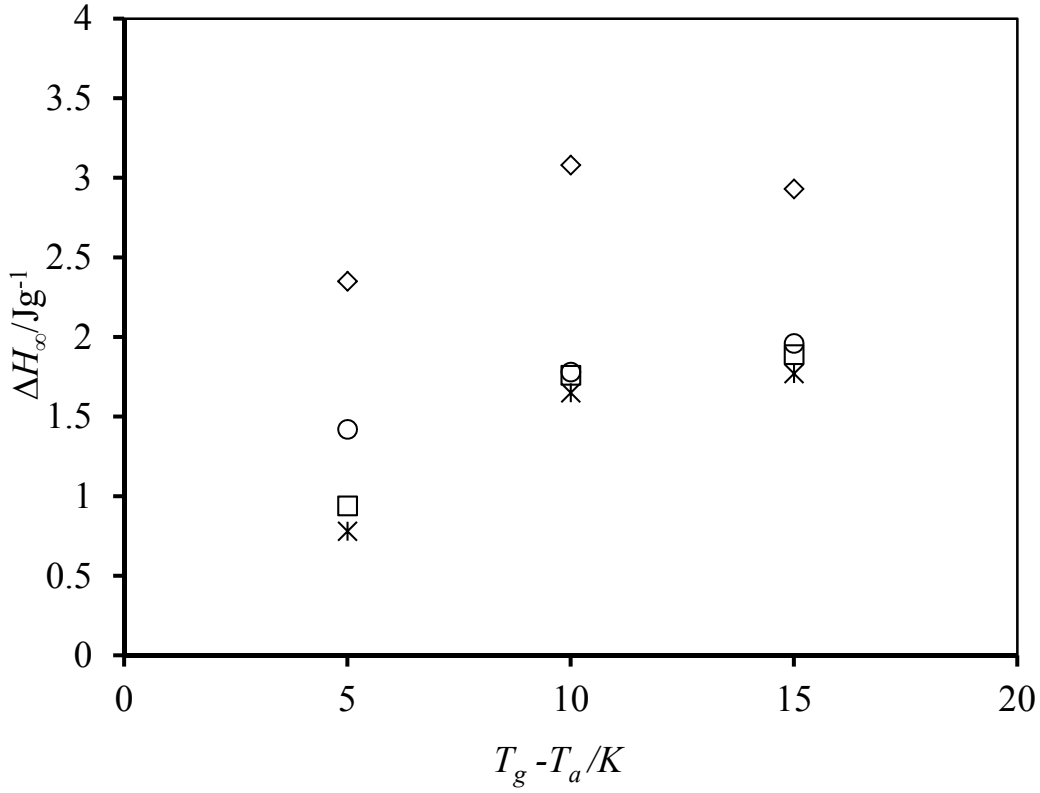

Figure 5.26 Enthalpy relaxation for the 59/41 SHS/PMMA blends contents percentages of 4-hydroxystyrene in the copolymers as follows: (ж) 30; (□) 50; (O) 70 mole-%; and (◊) P4HS/PMMA blends. Data are based on the CF equation calculations.

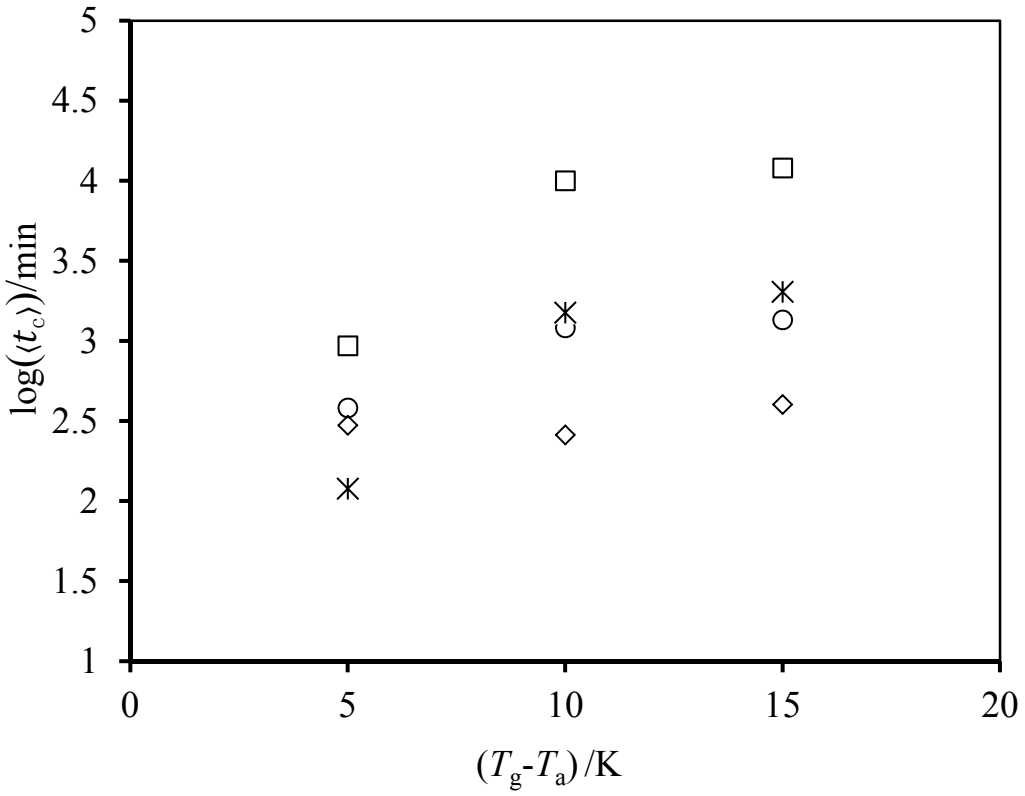

Figure 5.27 Average relaxation time as a function of (T_g-T_a) for the 59/41 SHS/PMMA blends content HS in the copolymers as follows: (ж) 30; (□) 50; (O) 70 mole-% HS; and (◊) P4HS/PMMA blends. Data are based on the CF equation calculations.

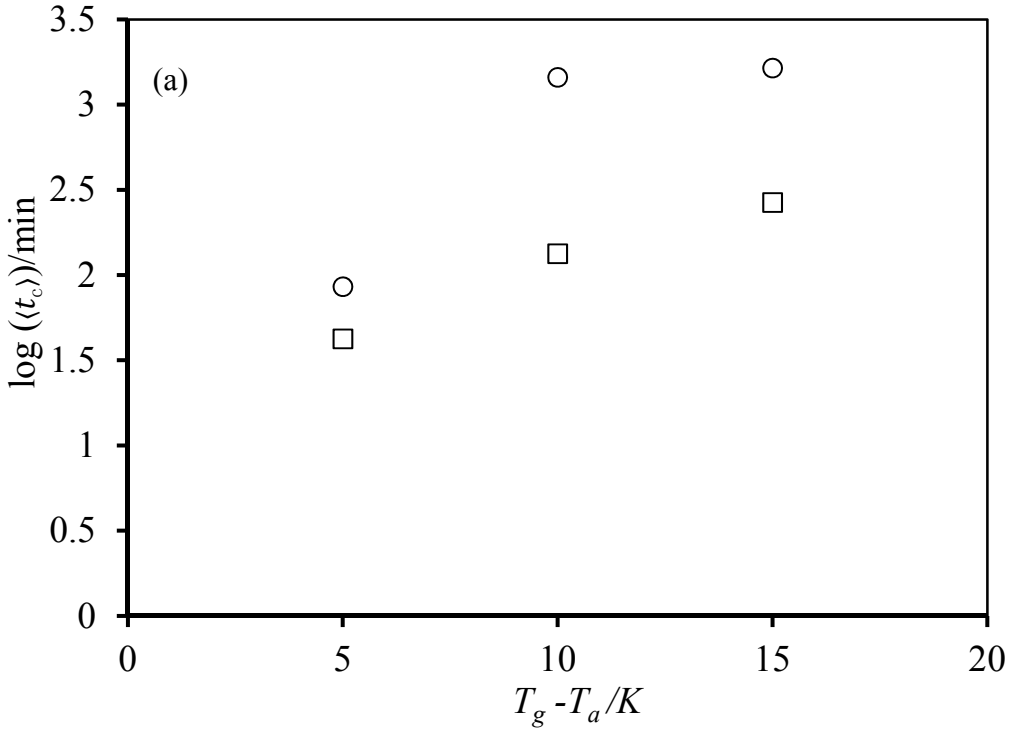

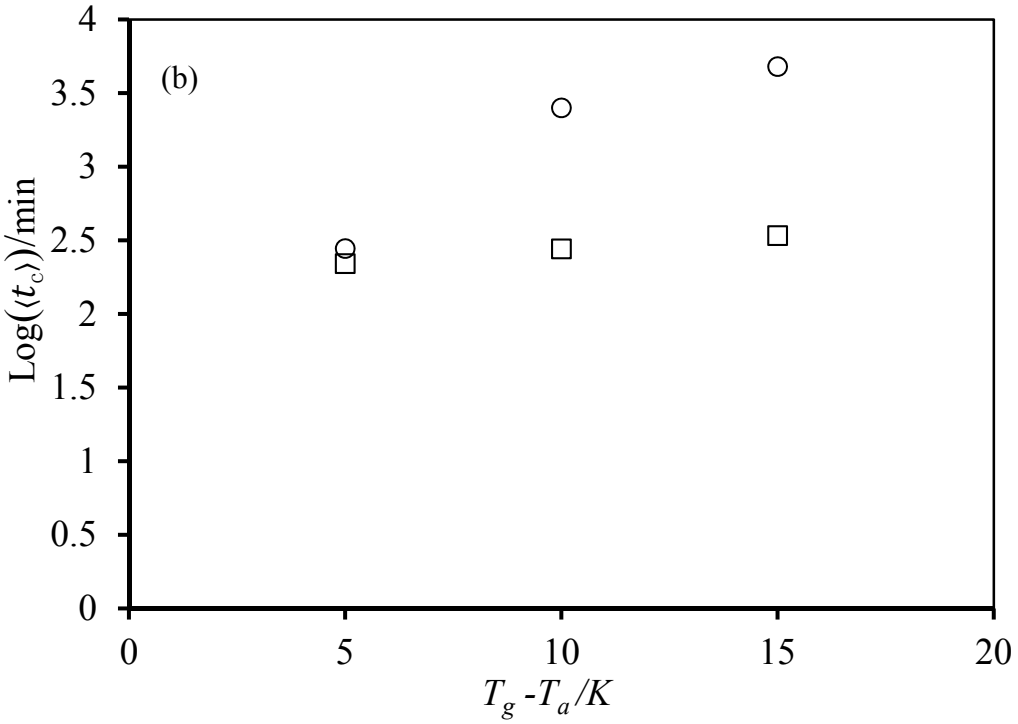

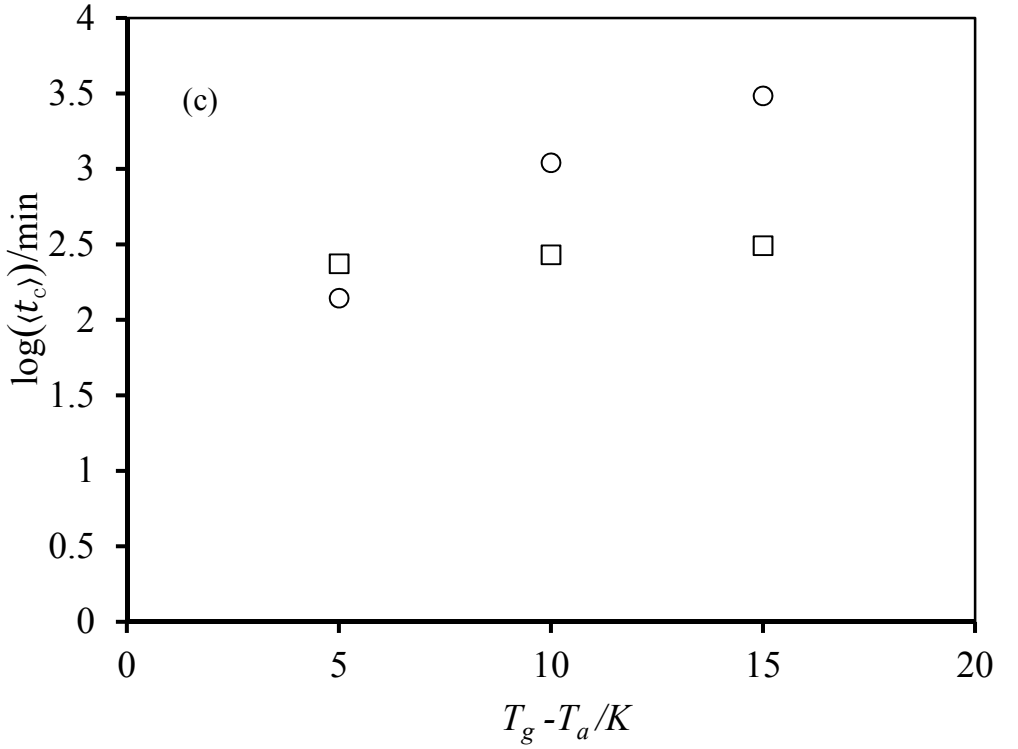

Figure 5.28 Variation of log(⟨t_C⟩) with (T_g – T_a) for (a) SHS30/PMMA (O), SHS30 (□); (b) SHS50/PMMA (O), SHS50 (□); and (c) SHS70/PMMA (O), SHS70 (□).

5.3.1.2 SHS/PEMA blends

The FTIR results have clearly confirmed that hydrogen bonding strength between hydroxyl groups of SHS copolymers and carbonyls of PMMA are quite similar to that between SHS and PEMA, which indicates that addition of methylene units have little effect on the interactions. Thus, only one SHS/PEMA blend (i.e. SHS50/PEMA) was studies in the attempt to investigate the effect of dilution and methylene addition in these systems.

As for SHS/PMMA, the C_p data of SHS50/PMMA aged for 2000 min at three temperatures below T_g were collected and then are compared with P4HS/PEMA in Figure 5.29. These make it possible to qualitatively the difference in enthalpic recovery behaviour between the blends. The blends with high styrene content in the copolymer presented relatively high and narrow enthalpy relaxation peaks. The enthalpy relaxation peaks in P4HS/PEMA, on the other hand, are broad and short. Moreover, for SHS50/PEMA the relaxation peak becomes broader at temperatures close to T_g as a result of hydroxyl groups that may have ordered together to create more favourable domains hindering the movement of styrene units. This phenomenon is absent in P4HS/PEMA. Thus, the shape of the relaxation peak does not change with temperature.

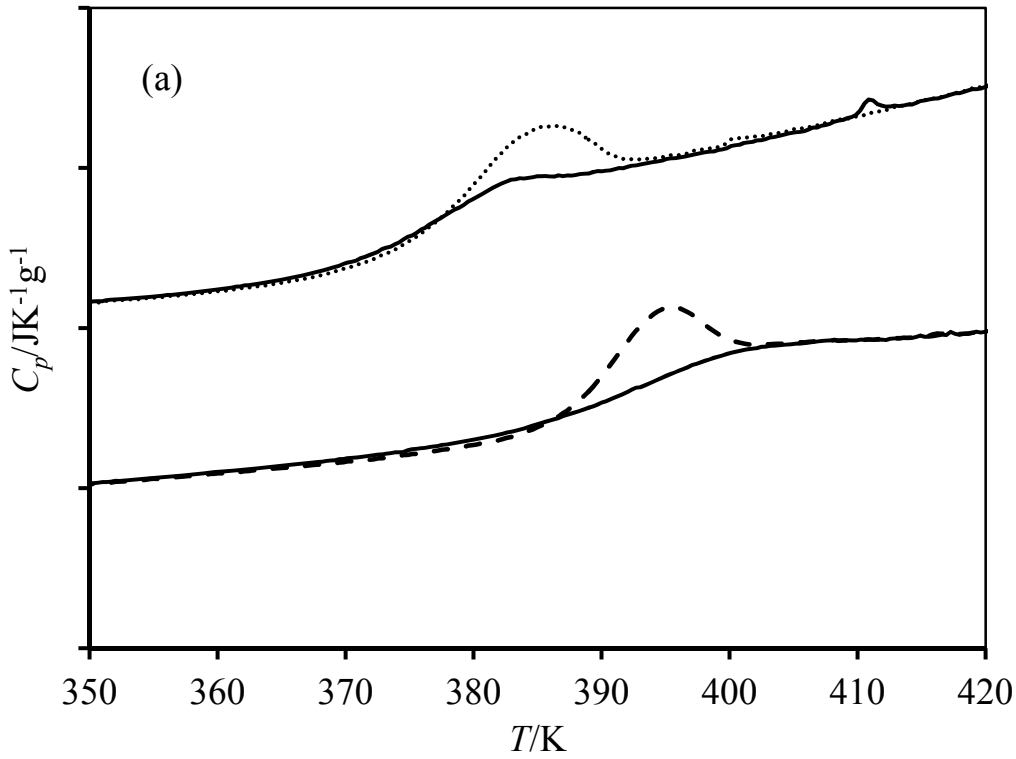
(a)
C_p/JK^{-1}g^{-1}
350
360
370
380
390
400
410
420
T/K

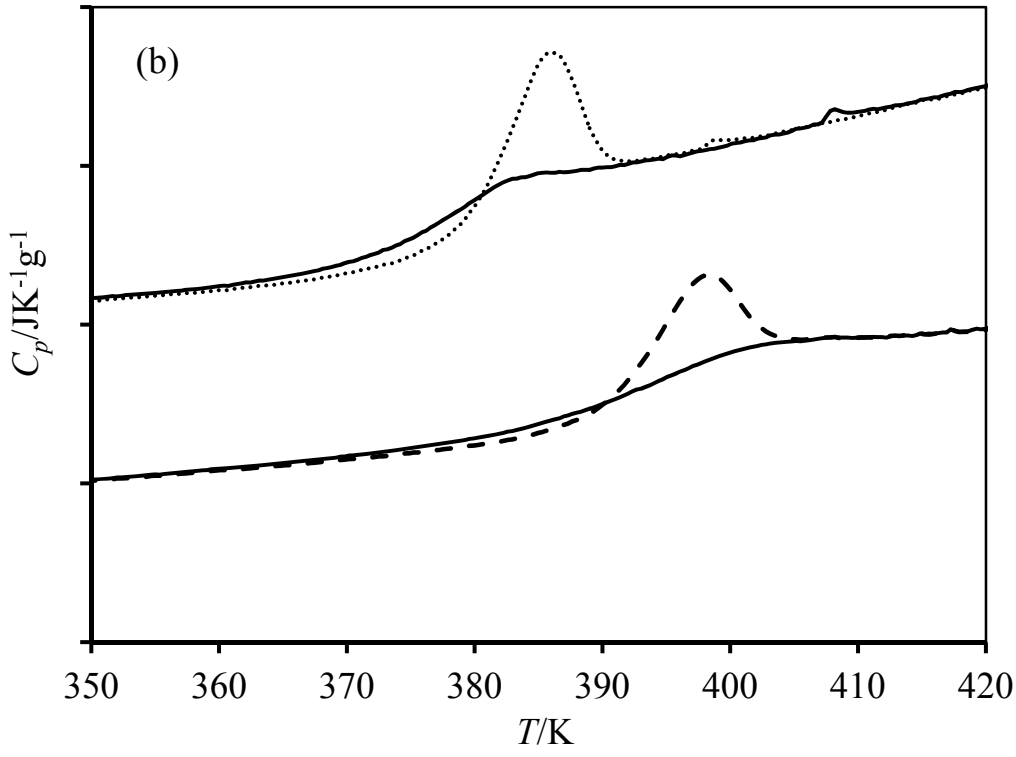
(b)
C_p/JK^{-1}g^{-1}
350
360
370
380
390
400
410
420
T/K

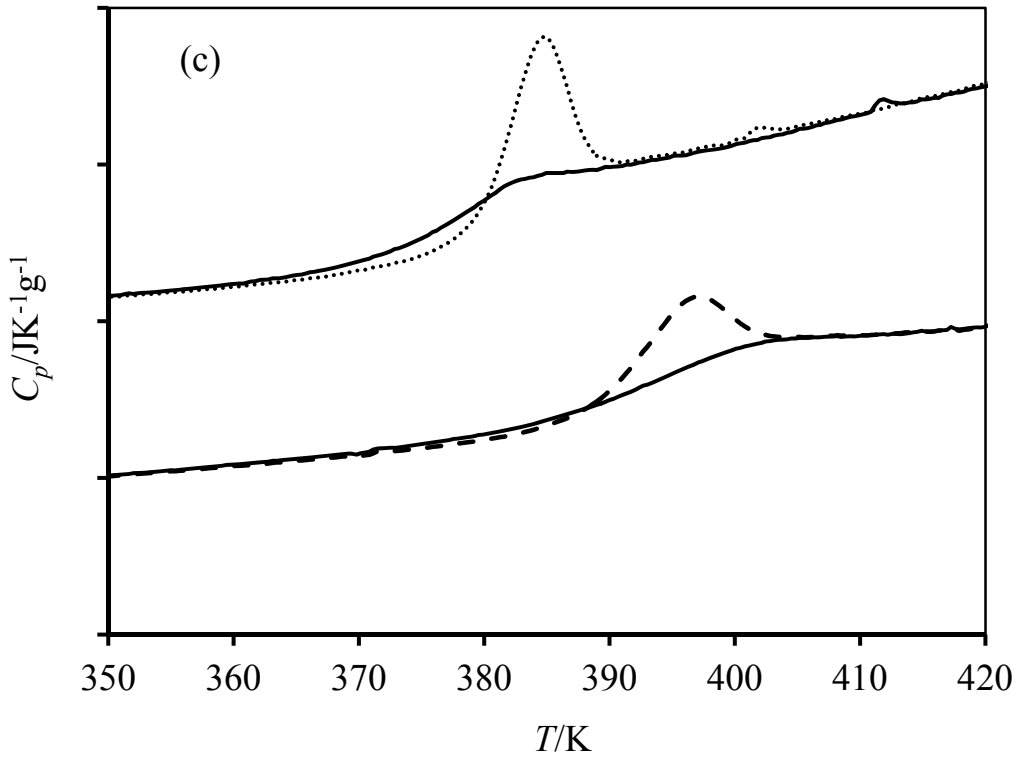

Figure 5.29 Heat capacity curves (aged and unaged) for t_a = 2000 minutes. From bottom to top 49/51 P4HS/PEMA, 59/41 SHS50/PEMA: (a) T_g – 5, (b) T_g – 10 and (c) T_g - 15.

Enthalpy relaxation data $\Delta H(T_a, t_a)$, for three aging temperatures (i.e. T_g-15, T_g-10 and T_g-15) are plotted in Figure 5.30. Also plotted are the theoretical curves obtained from a fit to the CF model. It can be noted from Figure 5.29 that at aging temperature closed to T_g the enthalpy relaxation data of SSH50/PEMA reach plateau faster than other temperature as in SHS50/PMMA (Figure 5.25 b).

CF parameters are reported in Table 5.6. $\Delta H_\infty(T_a)$ and the relaxation time (Log(t_c)) increase as aging temperature decreases, as expected.

Figure 5.31 displays all ΔH_∞ data as function of distance from T_g. As expected $\Delta H_\infty(T_a)$ data for SHS50/PEMA are intermediate between those of the SHS50 copolymer and PEMA as result of intermediate hydrogen bonding interactions in SHS50/PEMA. The similarity of $\Delta H_\infty(T_a)$ results of SHS50/PEMA (Table 5.6) with those of SHS50/PMMA (Table 5.5) confirms that the addition of methylene groups does not affect aging.

The kinetics of aging of SHS50/PEMA was measured by monitoring the $\log(\langle t_C \rangle)$ against $(T_g - T_a)$. The increase of $\log(\langle t_C \rangle)$ values of SHS50/PEMA blend with compared of SHS50 copolymer revealed that the blend relaxed slower than the copolymer. Moreover, at T_a near T_g (i.e. T_g-5) the relaxation of the blend becomes more fast than other aging temperatures because the hydrogen bonding of hydroxyl groups in the copolymer may have ordered together to create more favourable domains hindering the styrene units less able move, and then make blends to relax more faster in this temperature.

Table 5.6 CF Parameters for 59/41 SHS50/PEMA blend

T_a / K	$T_g - T_a$ / K	$\Delta H_\infty(T_a)$ / Jg^{-1}	$\log(t_c)$ / min)	β
384	15	1.81	2.18	0.29
389	10	1.42	1.91	0.29
394	5	1.11	1.33	0.29

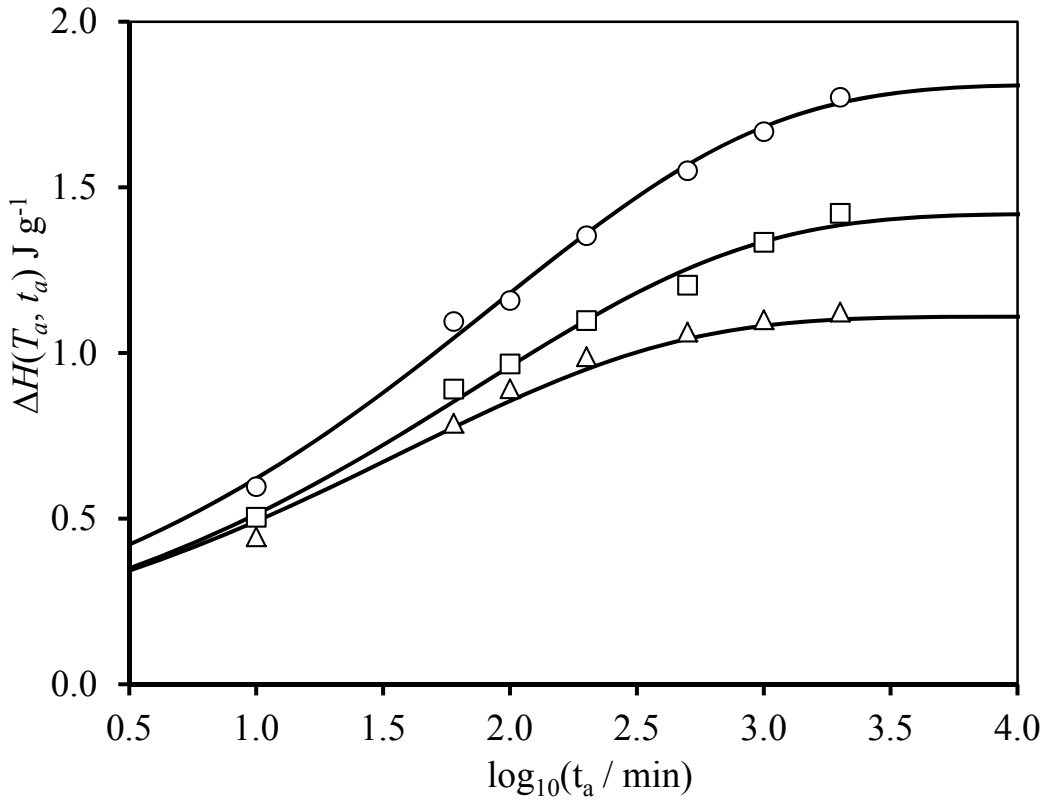

Figure 5.30 Enthalpy relaxation data for 59/41 SHS50/PEMA blend at T_a = 384 K (○), 389 K (□) and 394 K (Δ). Solid lines are fits to the experimental data using the CF equation.

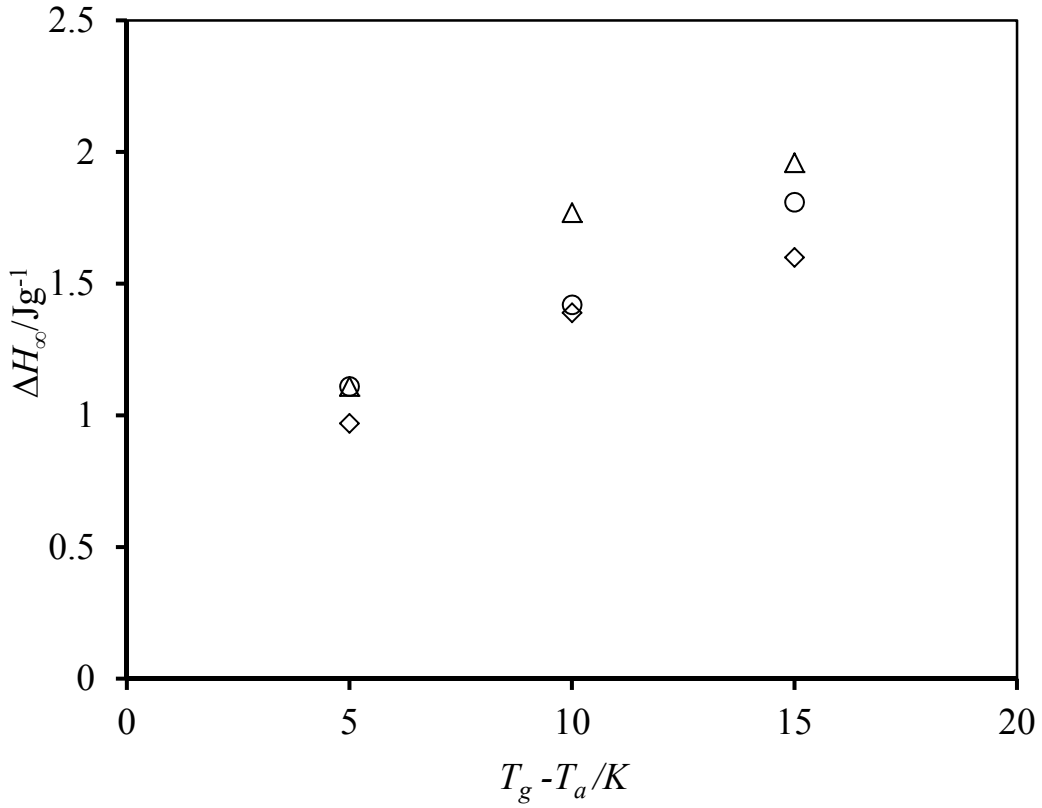

Figure 5.31 Enthalpy relaxation for 59/41 SHS50/PEMA (O), 49/51 PHS/PEMA (Δ) and SHS50 copolymer (◊).

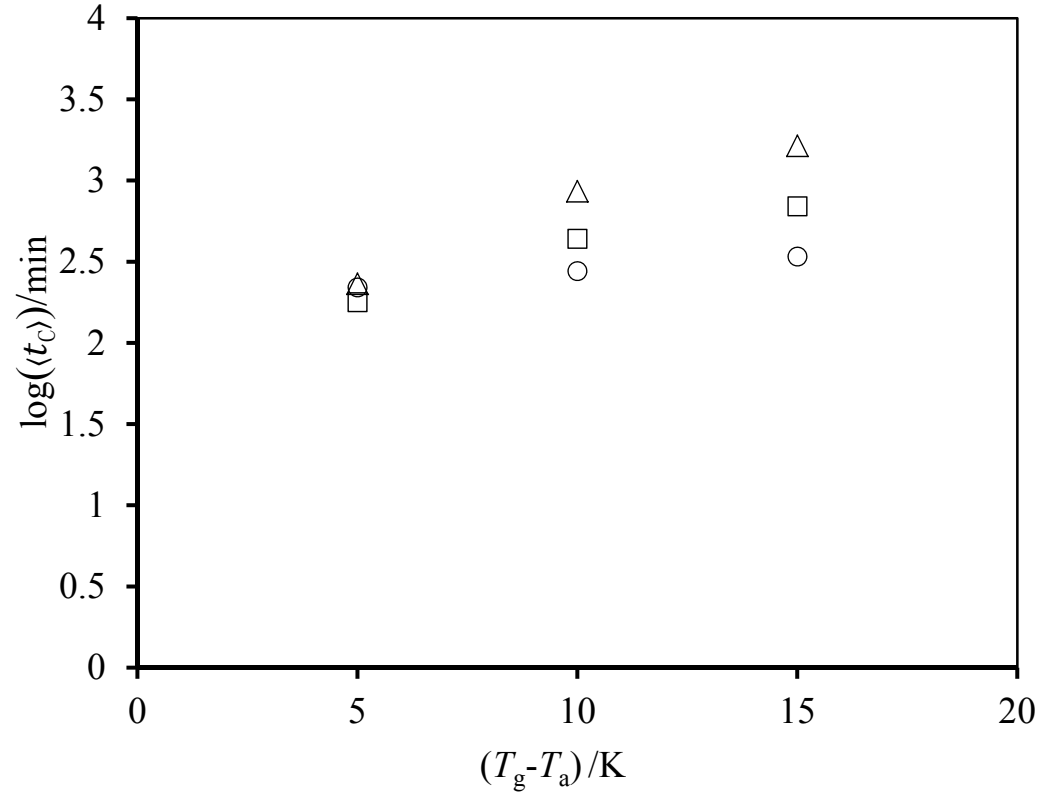

Figure 5.32 Average relaxation time as a function of (T_g-T_a) for 59/41 SHS50/PEMA (Δ).For comparison data for SHS50 copolymer (O); and PEMA (□) are included.

5.3.2 Styrene-4-hydroxystyrene/polyethers blends

In section 5.2.2 from this chapter we have examined the effects of dilutions and copolymer compositions of SHS copolymers on the strength of their intra- and inter-association interaction with PEO and PVME. Here, we try to explore same effects on the enthalpies relaxations of SHS/PEO and SHS/PVME blends as functions of physical aging.

5.3.2.1 SHS/PEO blends

Figures 5.33 and 5.34 display typical C_p data for 59/41 SHS50/PEO and 59/41 SHS70/PEO samples aged at 15K below T_g. The presence of styrene in the copolymer causes that the width of the glass transition has narrowed but not as much as SHS copolymers, suggesting that the distributions of hydrogen bonds should be intermediate between P4HS/PEO blend and SHS.

With respect to the effect of the strength of hydrogen bonds in SHS50/PEO blends on the shape of C_p data, Figure 5.35 shows that as hydrogen bonds increase the width of T_g becomes broader as result of intermolecular hydrogen bonding interactions that have been reported to be stronger than self-associations interactions in SHS copolymers [113, 163]. Thus, the enthalpy relaxation peaks of all SHS/PEO blends under study are more broads and shorts comparison with SHS copolymers (Figures 5.35 and 5.36). The intermolecular hydrogen bonding interactions in SHS50/PEO blends are also reason to make the energy releases over a much wider range of temperature.

Enthalpy relaxation data $\Delta H(T_a, t_a)$ for the three aging temperatures studied (i.e. T_g-5, T_g-10, and T_g-15) at various aging times up to 125 hours are plotted in Figures 5.37 and 5.38. Also plotted are the theoretical curves obtained from a fit to CF model. The three parameters $\Delta H_\infty(T_a)$, log (t_c) and β are determined by using a non-linear least squares curves fitting algorithm as we have explained in the introduction. Table 5.7 lists the values of the three parameters for each aging temperature. As expected $\Delta H_\infty(T_a)$ increase with decreasing T_a. $\Delta H(T_a, t_a)$ values also appear that the distance from the equilibrium enthalpy curve increases as the departure from T_g to T_a increases.

Figure 5.39 shows ΔH_∞ (T_a) against the distance from T_g of 59/41 blends composition: SHS50/PEO, SHS70/PEO blends and P4HS/PEO (note: ΔH_∞ (T_a) data of 59/41 P4HS/PEO blend have been taken for comparison from Chapter 4). It appears that 59/41 SHS/PEO blends is a complex function of hydrogen bonding, and its enthalpy relaxation parameters, can be justified by taking these interactions into account. Recalling from Chapter 3 that hydrogen bonding can be seen as equilibrium, it follows that in the blends there are basically two competitive equlibria, the hydroxyl self-association and hydroxyl-ether interactions. Since there is a 2:1 excess of hydroxyl groups at high T_a (i.e. close to T_g region), the complete intermolecular bonding interactions between hydroxyl groups and ether in SHS/PEO blends are impeded by self-association interactions. Moreover, the enthalpy released of SHS/PEO blends is higher than the copolymers (Figure 5.40) as a result of that the numbers of intermolecular hydrogen bonds in SHS/PEO blends are stronger than self-association once in SHS copolymers.

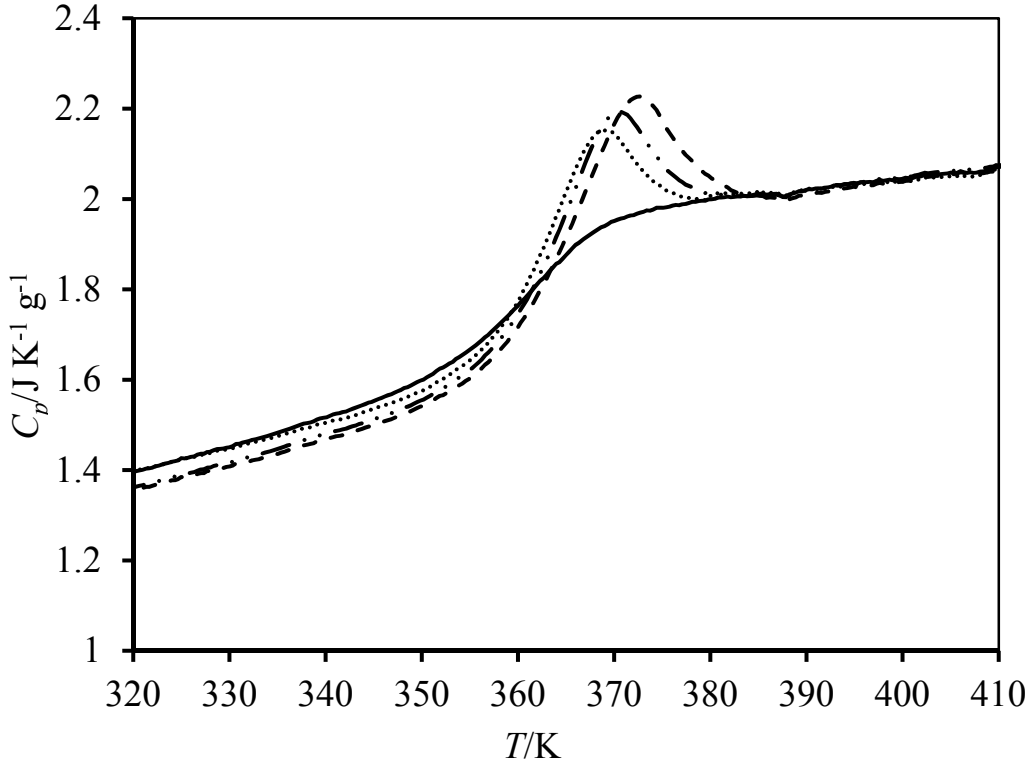

Figure 5.33 Heat capacity curves for 59/41 SHS50/PEO at T_g -T_a = 15 K for 200(……..), 500(—••—••—) and 2000 (— — —) minutes

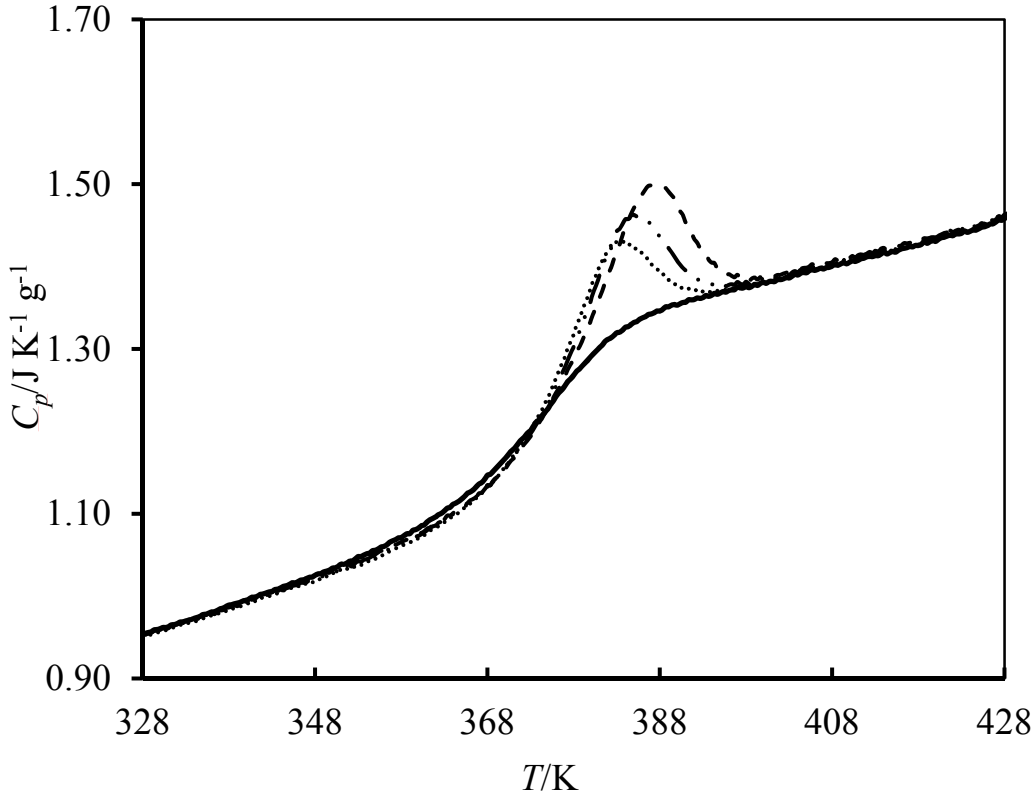

Figure 5.34 Heat capacity curves for 59/41 SHS70/PEO at T_g -T_a = 15 K for 200 (……..), 500 (—••—••—) and 2000 (— — —) minutes.

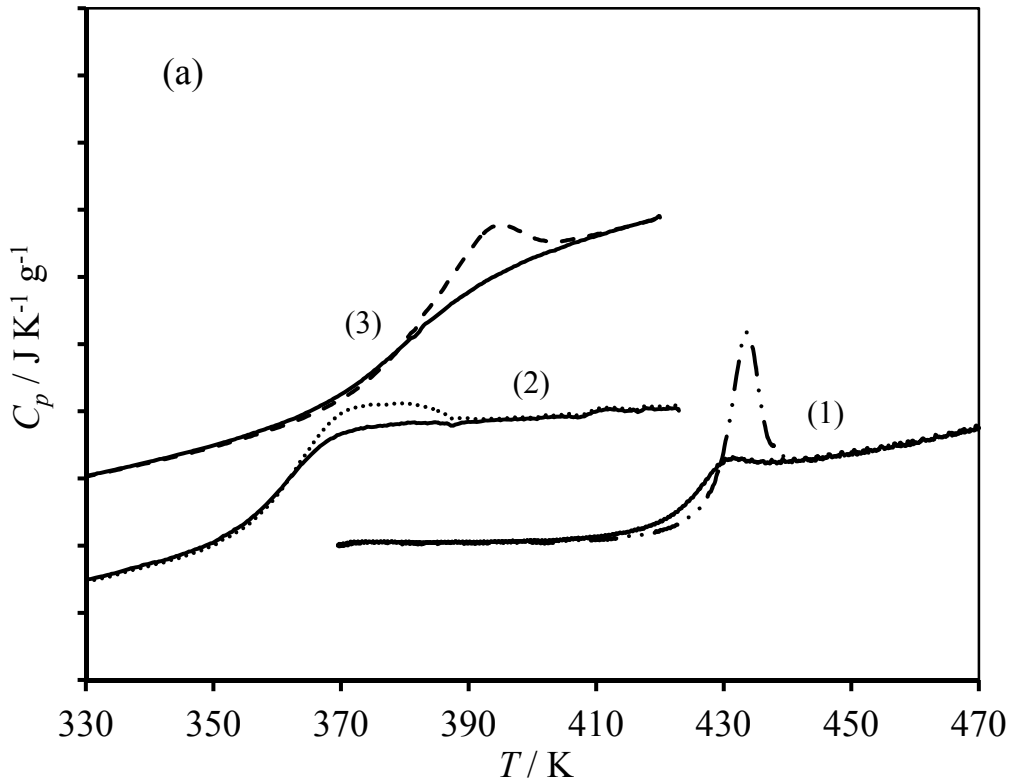

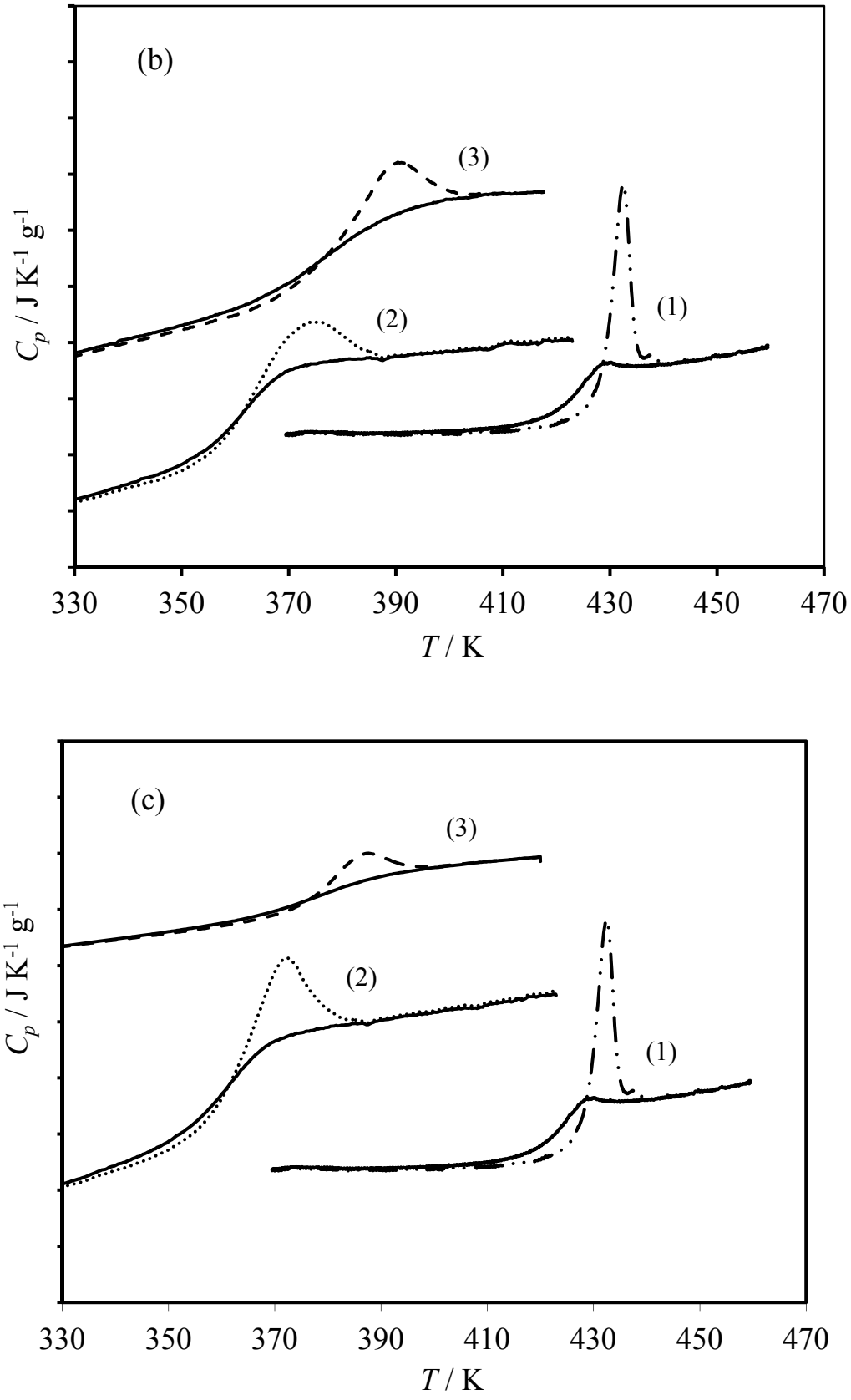

Figure 5.35 Heat capacity curves (aged and unaged) for t_a = 2000 minutes. (1) SHS50, (2) SHS50/PEO, and (3) P4HS/PEO: (a)T_g – 5, (b) T_g – 10 and (c) T_g - 15.

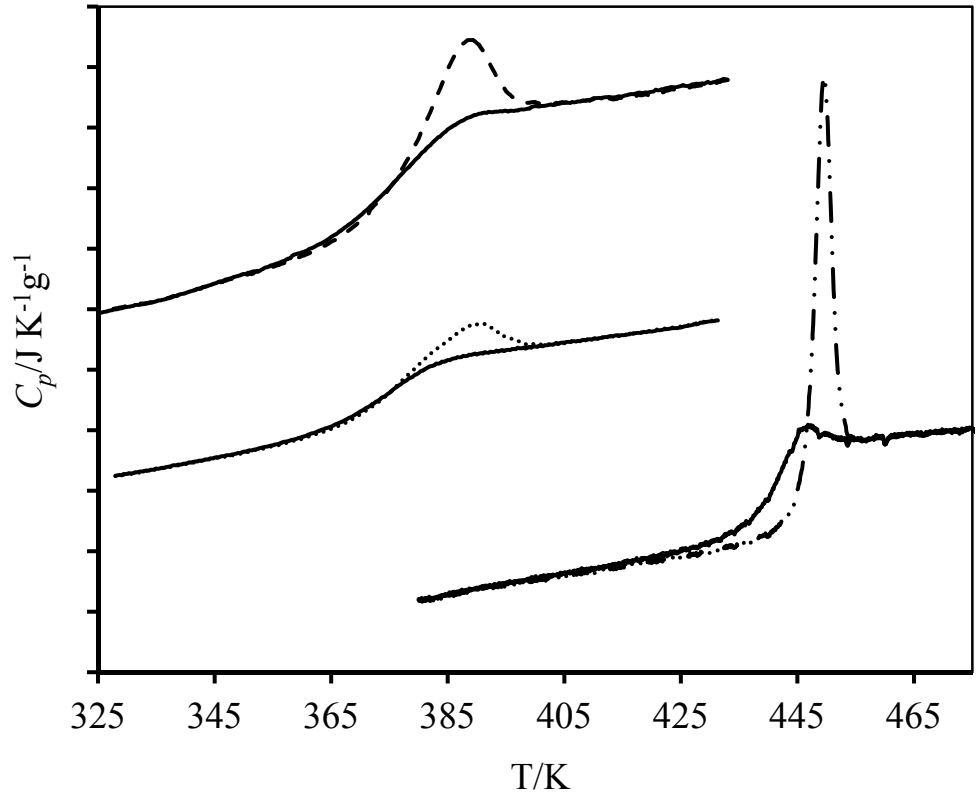

Figure 5.36 Heat capacity curves (aged and unaged) for t_a = 2000 minutes. From bottom to top SHS70, 59/41 SHS70/PEO, and 59/41 P4HS/PEO at T_g – 10.

Table 5.7 CF Parameters for 59/41 SHS/PEO

blends	T_a *(K)*	T_g- T_a *(K)*	$\Delta H_\infty(T_a)$ *(J g^{-1})*	log t_c (min)	β
SHS50/PEO	345	15	2.66	2.28	0.35
	350	10	1.90	2.09	0.35
	355	5	1.41	1.84	0.35
SHS70/PEO	359	15	2.71	2.46	0.33
	364	10	2.36	2.37	0.33
	369	5	1.63	1.97	0.33

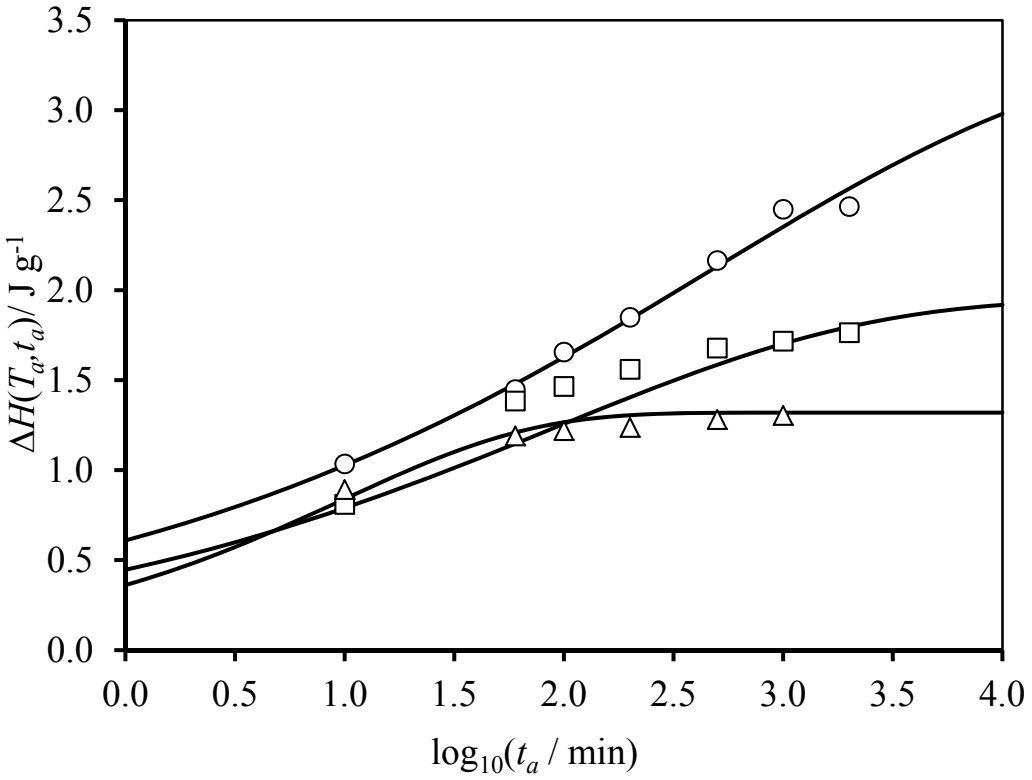

Figure 5.37 Enthalpy relaxation data for 59/41 SHS50/PEO blend at T_a = 345 K (○), 350 K (□) and 355 K (Δ). Solid lines are fits to the experimental data using the CF equation.

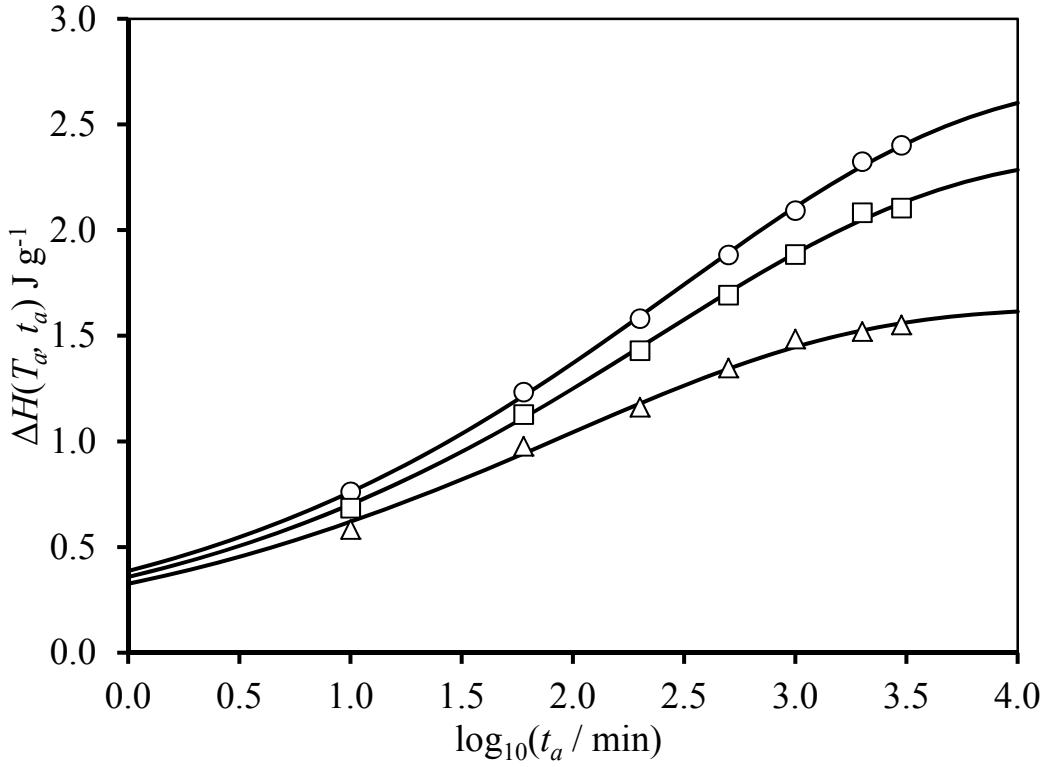

Figure 5.38 Enthalpy relaxation data for 59/41 SHS70/PEO blend at T_a = 360 K (○), 365 K (□) and 370 K (Δ). Solid lines are fits to the experimental data using the CF equation.

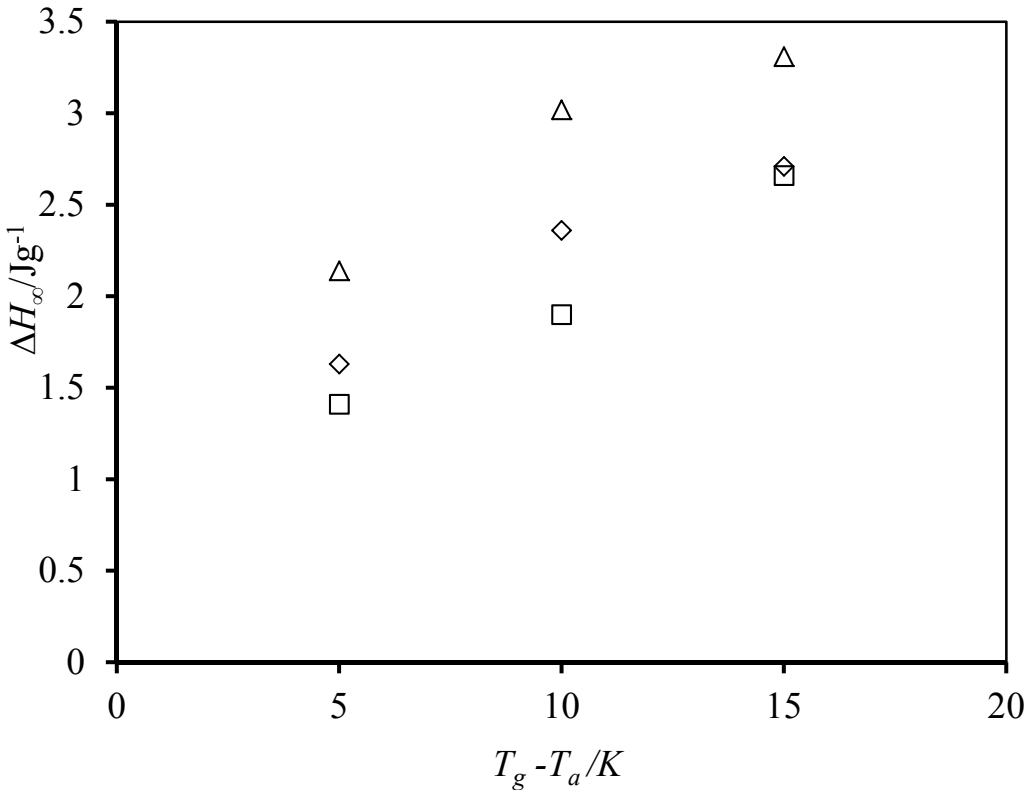

Figure 5.39 Enthalpy relaxation for the 59/41 SHS50/PEO (□) and 59/41 SHS70/PEO (◊); for the comparison the data has plotted with 59/41 PHS/PEO (Δ). ΔH_∞ data are extracted from fits.

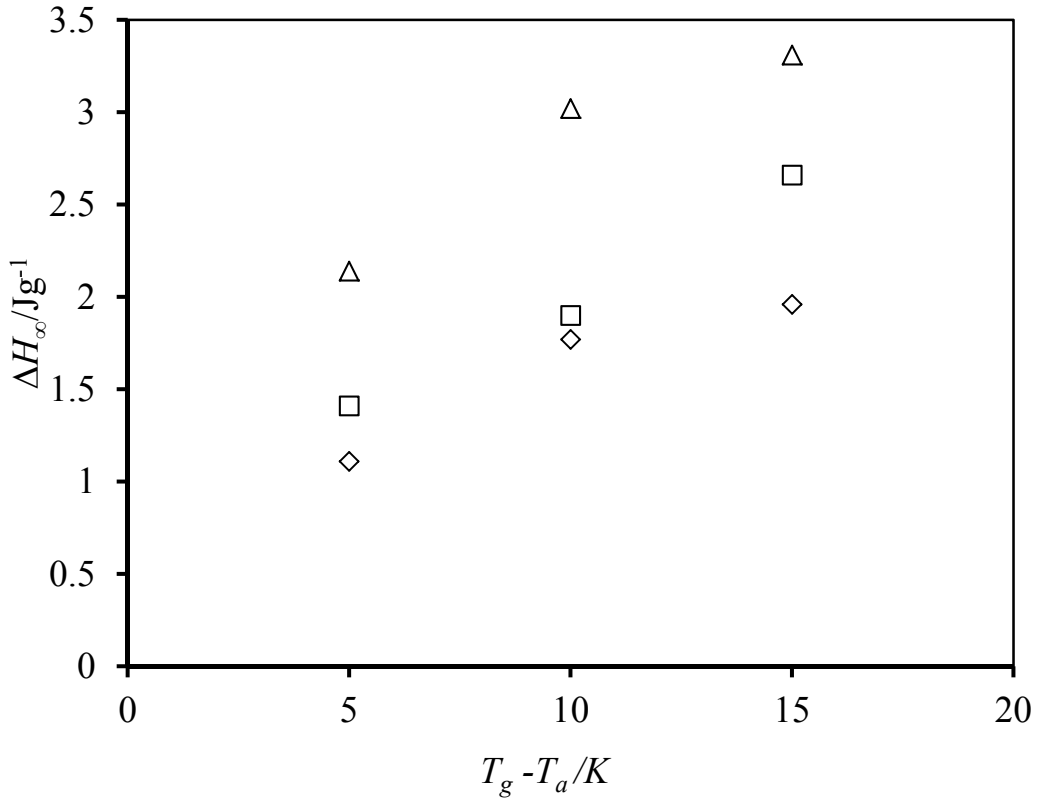

Figure 5.40 Enthalpy relaxation for the 59/41 SHS50/PEO (□); for the comparison the data has plotted with 59/41 PHS/PEO blend (Δ) and SHS50 copolymer (◊). ΔH_∞ data are extracted from fits.

The hydrogen bonding interactions of P4HS/PVME have been reported to hinder relaxation [55, 110], favour co-operativity and increase the friction coefficient [55]. Our aging results of P4HS/PEO blends (Chapter 4) also indicated that the intermolecular hydrogen bonding retarded the relaxation. Thus, depending on the fact that only the interacting fraction can relax we expected that the average relaxation time $\langle t_C \rangle$ of SHS50/PEO blend as a function of aging kinetics increases as intermolecular hydrogen bonds interactions between hydroxyl groups of P4HS and ether oxygen in PEO increase. Moreover, self-association interactions in the SHS copolymers are bigger than those in its blends with PEO and this should make copolymers relax more slowly than the blends. However, log(t_c) data (Table 5.7) indicate that the 59/41 SHS50/PEO blend relaxes more slowly than SHS50 copolymer. These results confirm that as the self-association interactions between hydroxyl groups increase the rigidity in the copolymer or blend increase; thus any attempt to motion of the segments will lead to destroy hydrogen bonds and this increases the relaxation rate. This phenomenon (i.e. hydrogen bonds destruction) is missed in SHS50/PEO blend as result of that hydrogen

bonds in SHS50/PEO is more flexible; consequently, the motion will not be accompanied by the destructions of hydrogen bonds. However, SHS50/PEO blend will undergo segments rearrangement that is needed long time, which means that SHS/PEO blends relax more slowly than SHS copolymers (Figure 5.41). Moreover, the effect of repulsion forces between styrene units on the SHS copolymer and PEO unites will leads the blend lost its motion forces, which means slow relaxation. On the other hand the increasing of styrene units in SHS/PEO blends leads to increase in un-associated PEO units that will make SHS/PEO blends to relax faster than P4HS/PEO blends (Figure 5.42).

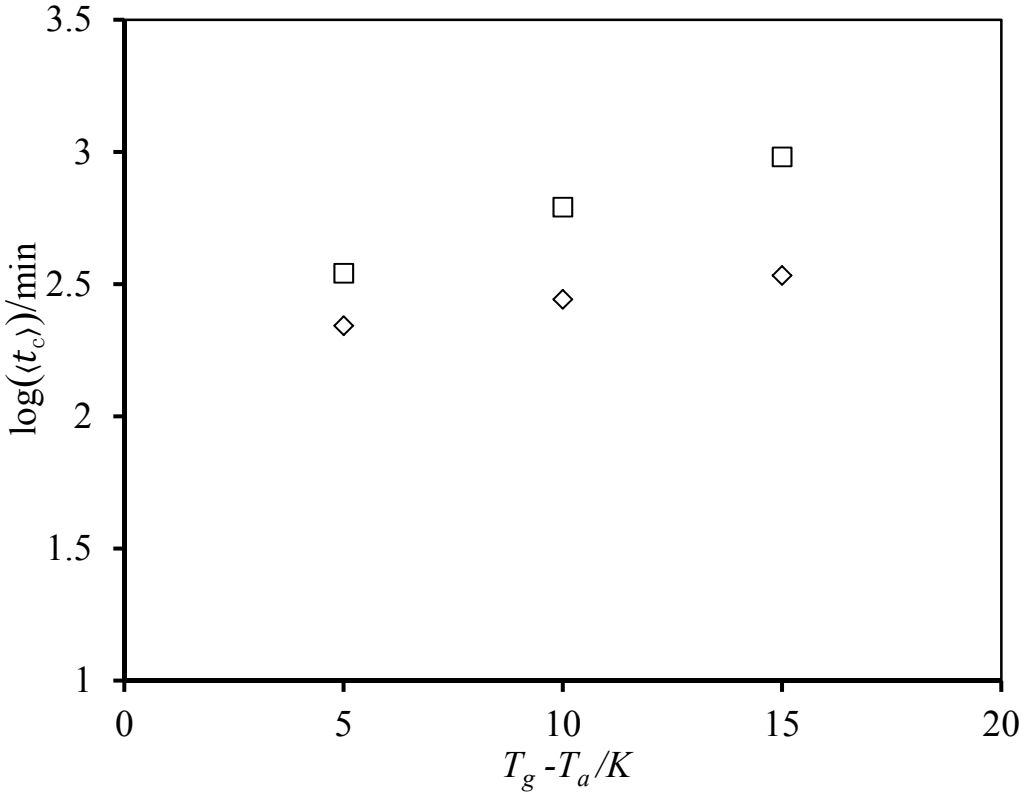

Figure 5.41 Average relaxation time as a function of (T_g-T_a) for the 59/41 SHS50/PEO blends (□); for the comparison the data has plotted with SHS50 copolymer (◊). Data are based on the CF equation calculations.

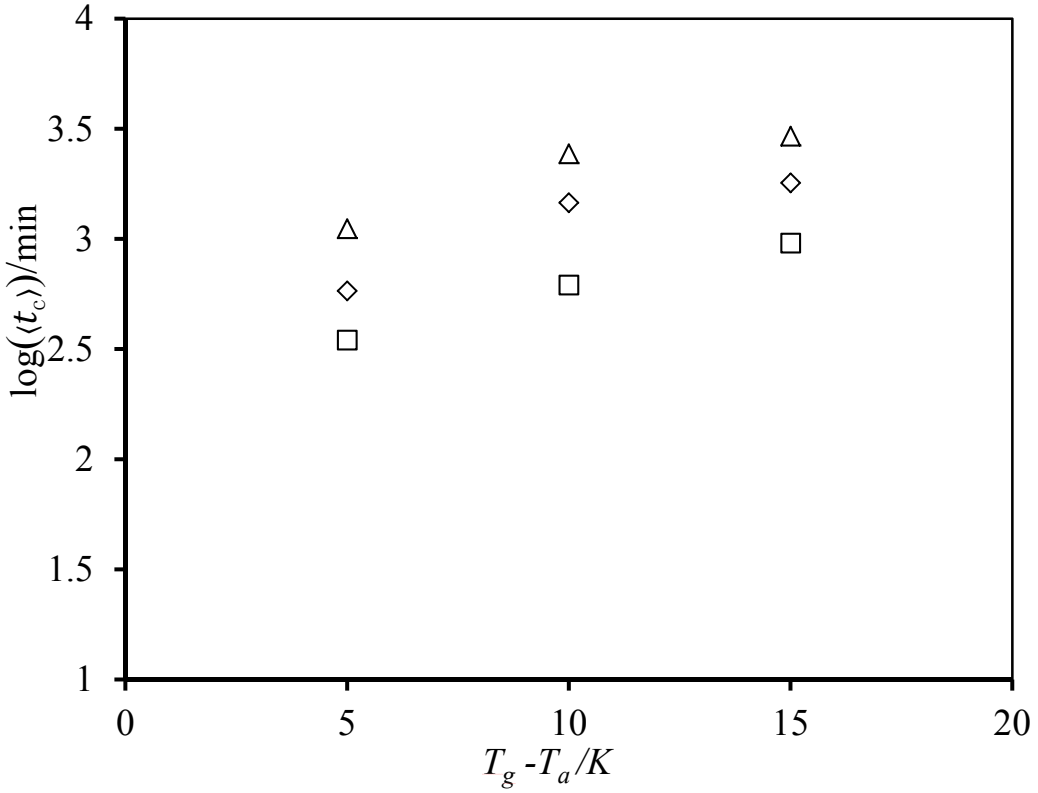

Figure 5.42 Average relaxation time as a function of (T_g-T_a) for the 59/41 SHS50/PEO (□) and 59/41 SHS70/PEO (◊); for the comparison the data has plotted with 59/41 PHS/PEO blend (Δ). Data are based on the CF equation calculations.

5.3.2.2 SHS/PVME blends

Enthalpy relaxation experiments were carried out on a 59/41 SHS50/PVME blend. The choice of this composition was motivated primarily by desirability to compare its aging behaviour with that of a P4HS/PVME blend having the same PVME content, as reported by Arrighi and co-workers [110].

Figures 5.43 (a) and (b) display an isothermal set of aged C_p curves at different t_a of 59/41 SHS50/PVME at 15 and 10K below $T_{g,}$ respectively. The shifting of C_p curves increases as aging times increase at T_a far from T_g (i.e. T_a= T_g-15 or more), however, at aging temperature that are near to T_g (i.e. T_g-10 or less) the upward shift of the transition onset with t_a is absent (Figure 5.43 (b)) that suggests that not all of the segments undergo aging. It follows that there is a fraction of polymer segments that does not contribute to the overall $\Delta H(T_a, t_a)$ when are free to move. This would be also explaining the appearance of enthalpic peak near the middle of the transition. Moreover,

in Figure 5.44 the effect of ether-hydroxyl hydrogen bonding interactions clearly appears with C_p peaks of SHS50/PEO blend. The width of glass transition appears to be more broad comparison with SHS50 copolymer that has self-association interactions that have been reported to be weaker than ether-hydroxyl intermolecular interactions. However, at T_g-15 or less, C_p peaks of SHS50/PEO blend appear to be high and narrow (Figure 5.44). This behaviour could be attributed to the mobility increasing of styrene unites that lead to hindering the ordering of hydrogen bonds.

Figure 5.45 shows $\Delta H(T_a, t_a)$ versus $\log_{10}(t_a)$ for all three aging temperatures. The data collected at T_g-5 (i.e. 374 K (Δ)) reached a limiting value after a relatively short aging time (~ 10 minutes). The CF parameters obtained from these data and the other aging temperatures studied are listed in Table 5.8.

The enthalpy relaxation at 374K is almost too fast to be accurately measured by DSC. It is not feasible to collect enthalpy relaxation data below an aging time of five minutes due to the thermal lag effects within the sample. Data points at short aging times are therefore restricted at this temperature. However, the data shown in Figure 5.44 for T_a=374K for aging times ranging from 10 minutes to 2000 minutes were reproducible, therefore this rapid relaxation is real phenomenon for this particular sample of 59/41 SHS50/PVME blend. This suggested that, at this temperature the restricted molecular motions occurring in the glass are of longer range. Thus, the sample might not be behaving like a 'true' glass at this aging temperature. Although, other workers [135] have reported enthalpy relaxation data of PS at temperatures of less than 2 degrees below T_g. However, the validity of data collected under these conditions could be questioned.

FTIR measurements of SHS/PVME blends (sec. 5.2.2.2) and the effect of hydrogen bonding strength in these types of blends (i.e. polyether/P4HS based blends) on the enthalpy relaxation[110], one would expect that the distance between non- equilibrium state to thermodynamic equilibrium state ($\Delta H_\infty (T_a)$) would increase with increasing the interaction strength in the blend.

Figure 5.46 displays enthalpy relaxation $\Delta H_\infty(T_a)$ against the T_g-T_a of 59/41 SHS50/PVME, 59/41 P4HS/PVME and SHS50 copolymer (note: $\Delta H_\infty (T_a)$ data for 59/41 P4HS/PVME SHS50 have taken for comparison from ref. [110] and section 3.2.2.2 of Chapter 3, respectively). It appears that $\Delta H_\infty(T_a)$ values of 59/41

SHS50/PVME blend are close to those of SHS50 copolymer (sec. 5.2.2.2). On the other hand $\Delta H_\infty(T_a)$ values of 59/41 SHS50/PVME are lower than 59/41 P4HS/PVME blend. The reason of low $\Delta H_\infty(T_a)$ values of SHS50/PVME could be attributed also to the present of styrene units that have been found have very weakly interacting with PVME ether oxygen [158, 164, 165] in comparison with strong interaction of P4HS/PVME blend.

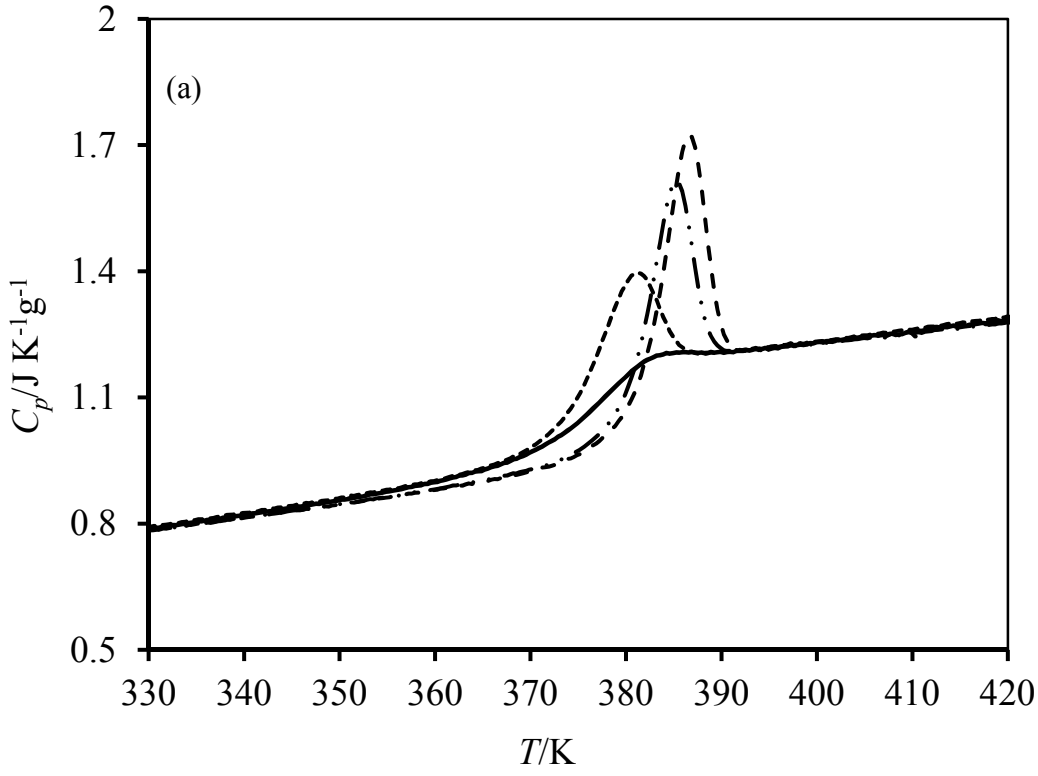

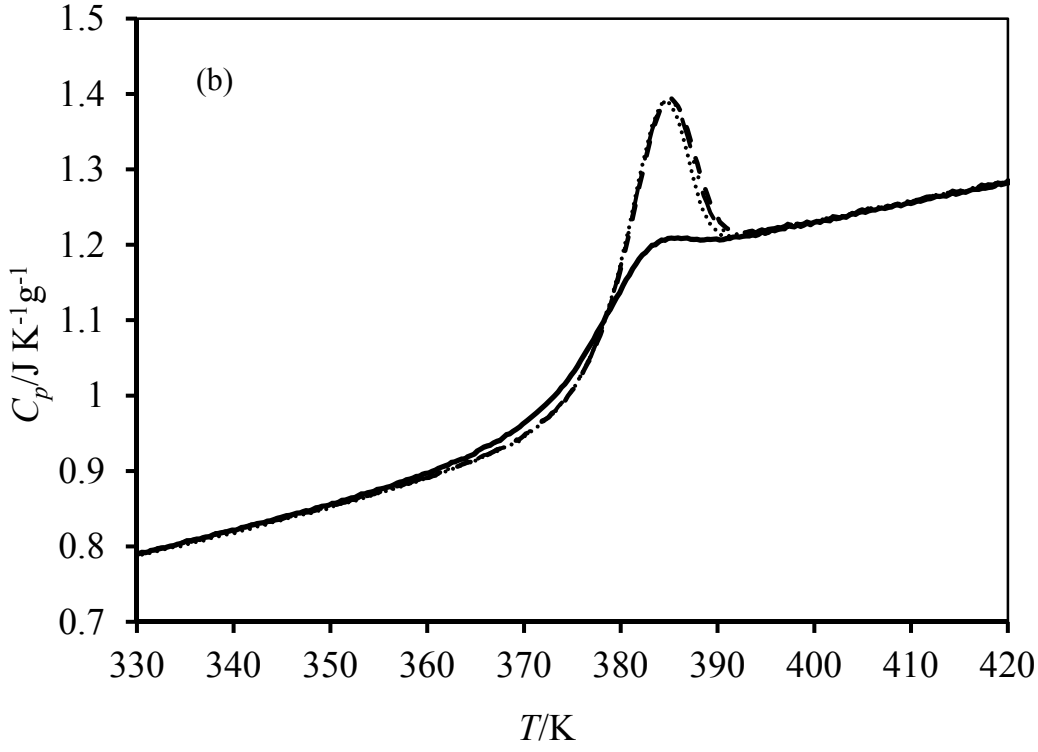

Figure 5.43 Heat capacity curves for 59/41 SHS50/PVME at T_g -T_a = 15 K (a), and T_g -T_a = 10 K (b) for 200 (……..), 500 (—●●—●●—) and 2000 (— — —) minute

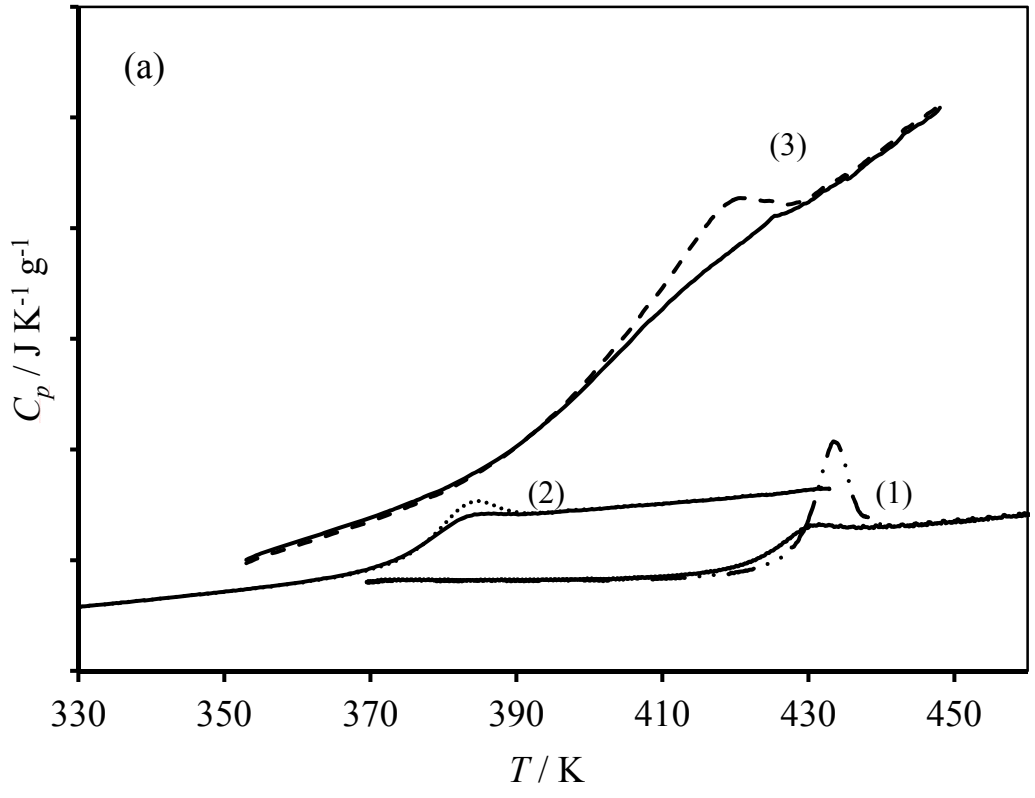

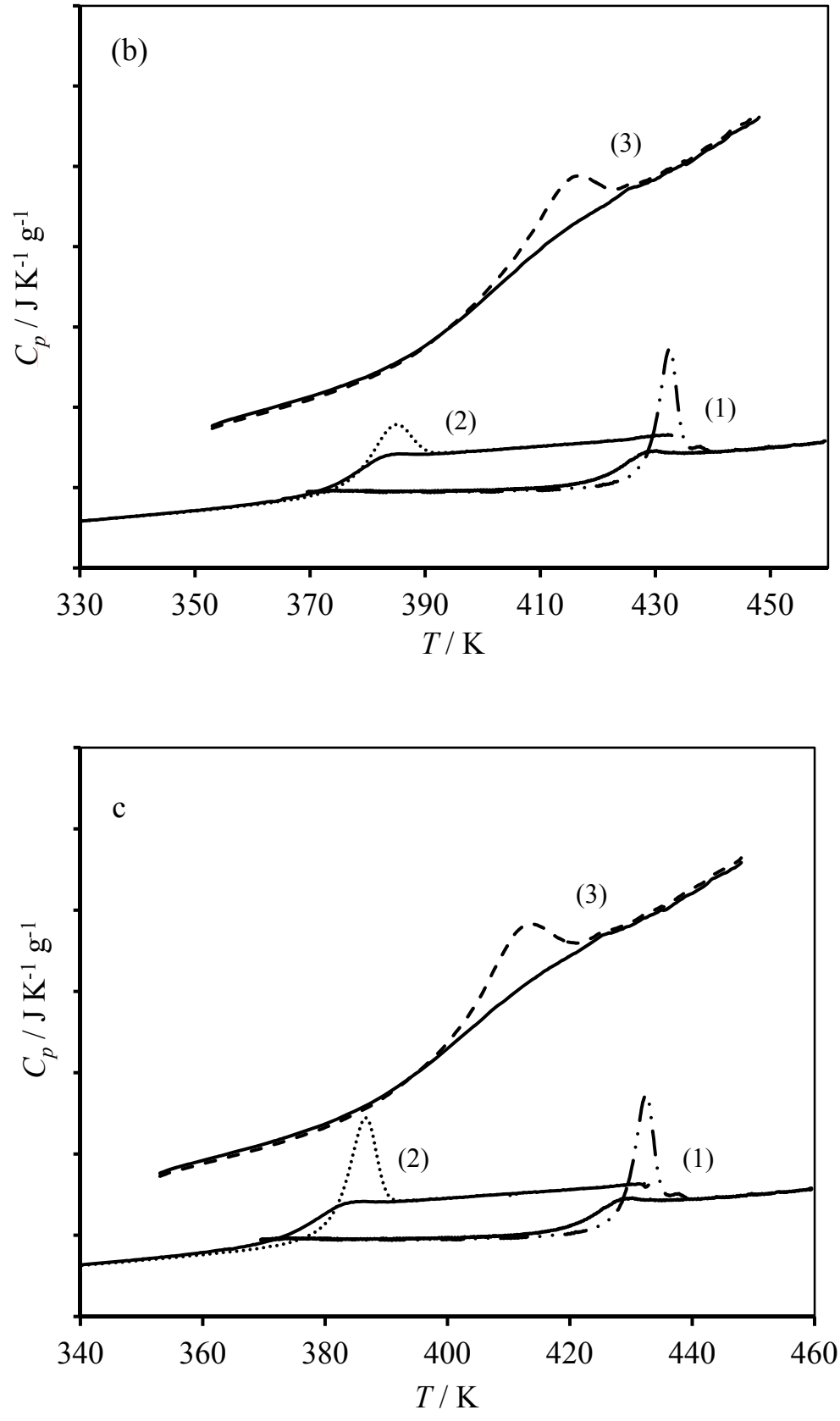

Figure 5.44 Heat capacity curves (aged and unaged) for t_a = 2000 minutes. From bottom to top (1) SHS50, (2) SHS50/PVME, and (3) P4HS/PVME: (a)T_g – 5, (b) T_g – 10 and (c) T_g - 15.

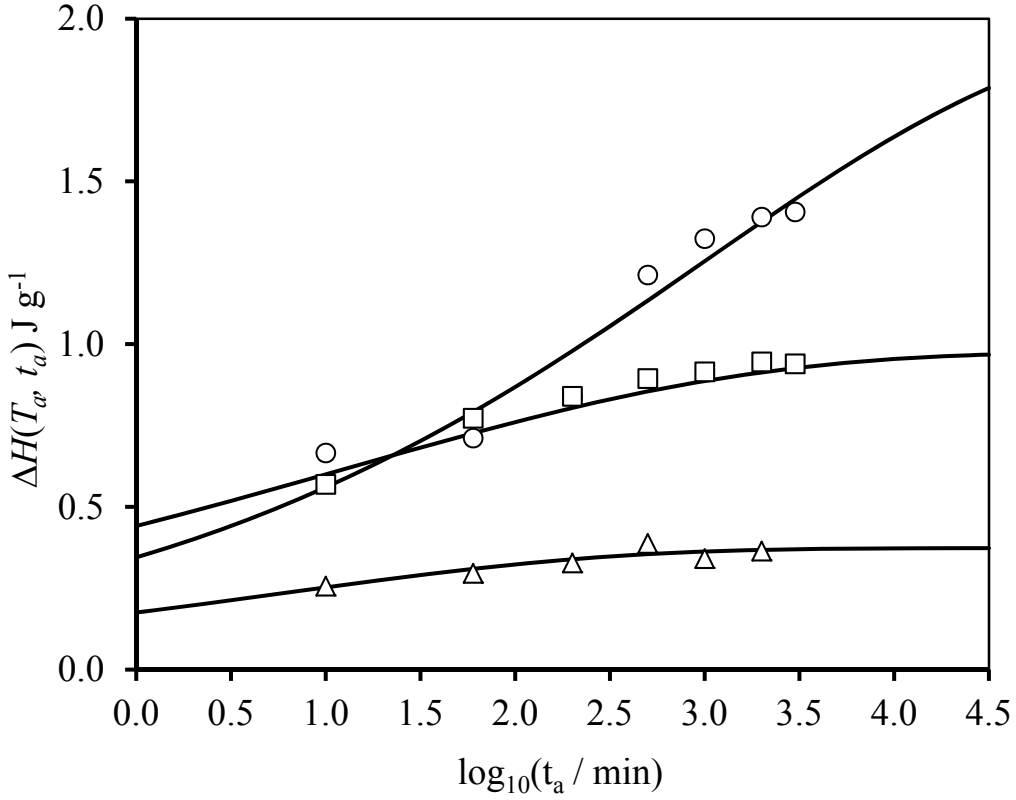

Figure 5.45 Enthalpy relaxation data for 59/41 SHS50/PVME blend at T_a = 364 K (○), 369 K (□) and 374 K (Δ). Solid lines are fits to the experimental data using the CF equation.

Table 5.8 CF Parameters for 59/41 SHS50/PVME

T_a / K	$T_g - T_a$ / K	$\Delta H_\infty(T_a)$ / Jg^{-1}	$\log(t_c)$ / min)	β
364	15	1.90	2.23	0.49
369	10	1.39	1.97	0.49
374	5	0.91	1.10	0.49

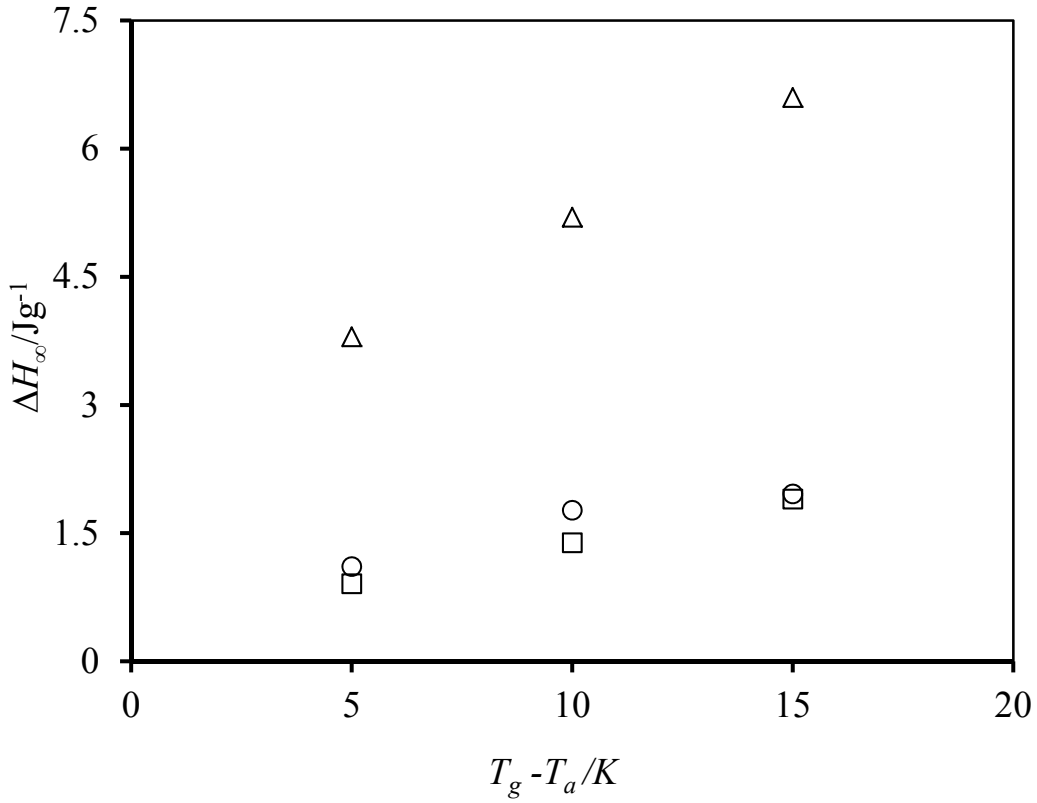

Figure 5.46 Enthalpy relaxation for the (□) 59/41 SHS50/PVME. For the comparison the data has plotted with (O) SHS50 copolymer (Chapter 3) and (Δ) 59/41 P4HS/PVME blend (Ref. [110]) . Data are based on the CF equation calculations

Figure 5.47 shows values of log($\langle t_C \rangle$) against (T_g - T_a) for 59/41 SHS50/PVME. Generally, the aging process appears to become faster with as aging temperature be closed to T_g and the opposite is true, which is to be expected given that the motion of relaxing elements will be slow and that will hinder the favourable rearrangements. For SHS50/PVME blends the behaviour of log($\langle t_C \rangle$) data are identical to ΔH_∞ (T_a) behaviour, where the reasons of the increase or decrease in log($\langle t_C \rangle$) values itself causes the increase or decrease of ΔH_∞ (T_a).

Addition point, for 59/41 SHS50/PVME blend at T_a far from T_g (i.e. T_g-15) log($\langle t_C \rangle$) value is close to SHS50 copolymer (sec. 3.2.2.2) . The reason of this special case could be related to that first the present of styrene units, where with increase the distance from T_g the styrene unites may be somewhat less free to move, second reason

would be related to hydrogen bonds segments rearrangements that become more slow with lower aging temperatures [134].

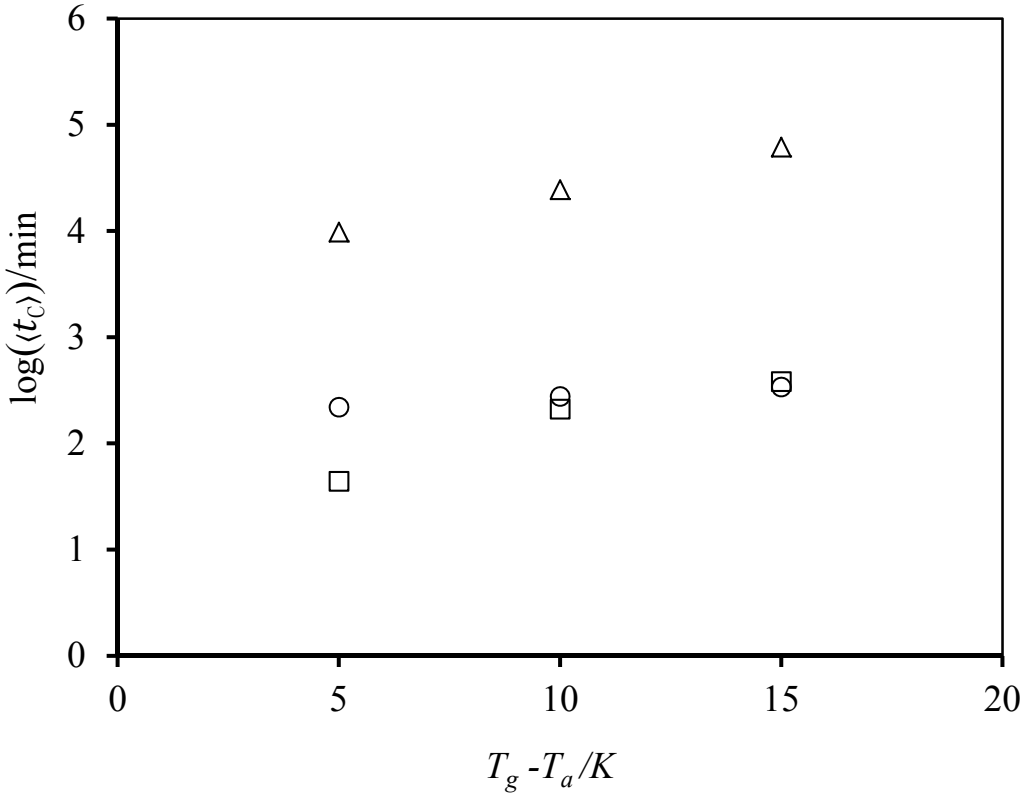

Figure 5.47 Average relaxation time as a function of (T_g-T_a) for the (□) 59/41 SHS50/PVME. For comparison data have been plotted with (O) SHS50 copolymer (Chapter 3) and (Δ) 59/41 P4HS/PVME blend (Ref. [110]) . Data are based on the CF equation calculations

5.3.3 Average segmental activation energies <Ea> from enthalpic aging parameters for SHS blends

It was explained early the importance of calculating the activation energy of polymer blends. Here, we will discuss the effect of dilution by styrene units on strong hydrogen bonds of SHS blends with carbonyl and ether polymers.

To discussing the activation energy results of SHS blends we should first calculate the activation energies of neat copolymers. Thus, average segmental activation energies have been calculated from C-F parameters (Chapter 3) and the results are listed in Table

5.9. $<E_a>$ values of SHS copolymers are usually lying between the values of neat polymers. Moreover, the increasing of hydroxyl groups in the copolymer leads to higher $<E_a>$ values as a result of hydrogen bonding interactions that appear to impede the localised segmental relaxation and slow down the aging process. Thus, the activation energy of SHS copolymers is greater than that of PS. However, the $<E_a>$ values of SHS70 (i.e. 70 mole-% HS) are higher than that of P4HS. This could be related to the T_g of P4HS that was found to be lower than SHS70 as a result of the extreme hygroscopic nature of P4HS as mentioned previously.

In regard to SHS/PMMA and SHS/PEMA blends, the average segmental activation energies have been calculated for four blends of SHS/PMMA and one blend of SHS/PEMA. Values of $<E_a>$ are relatively large for SHS copolymers (Tables 5.8) compared to those measured for SHS/(PMMA or PEMA) blends and neat polymers (i.e. PMMA and PEMA) (Tables 5.9 and 5.10). Moreover, as hydroxyl groups increases in the copolymer the activation energy of the blend increases as a result of the increase in hydroxyl-carbonyl hydrogen bonds. Furthermore, the increase of hydroxyl groups in SHS copolymer is likely decrease the repulsion forces between styrene units on the SHS copolymer and PMMA or PEMA. Consequently, the presence of hydrogen bonding interactions has produced a close packed blend with strong inter-chain H-bonding. This also affects average segmental activation energies.

Table 5.9 the average activation energies for SHS copolymers at several aging temperatures

mol% HS in SHS	T_a (K)	$T_g - T_a$ (K)	log t_c (min)	β	$\langle E_a \rangle$ (kJ mole^{-1})	$\langle E_a \rangle^{(a)}$ (kJ mole^{-1})
P4HS	412	15.0	2.40	0.35	89.3	87.5
	417	10.0	1.92	0.35	89.7	
	422	5.0	1.03	0.35	83.6	
70% HS	426	15.0	1.87	0.37	91.5	92.1
	431	10.0	1.81	0.37	92.1	
	436	5.0	1.75	0.37	92.7	
50% HS	403	15.0	1.98	0.39	87.7	88.0
	408	10.0	1.89	0.39	88.1	
	413	5.0	1.79	0.39	88.4	
30% HS	398	15.0	1.91	0.37	85.9	85.5
	403	10.0	1.78	0.37	86.0	
	408	5.0	1.45	0.37	84.5	
PS	358	15.0	2.30	0.38	80.0	76.4
	363	10.0	2.04	0.40	79.5	
	368	5.0	0.48	0.40	69.6	

[(a)] average values

Table 5.10 the average activation energies for 59/41 SHS/PMMA blends at several aging temperatures

Blends or polymer	T_a (K)	$T_g - T_a$ (K)	log t_c (min)	β	$\langle E_a \rangle$ (kJ mole^{-1})	$\langle E_a \rangle^{(a)}$ (kJ mole^{-1})
PMMA (Data from ref. [22])	380	15.0	2.43	0.43	86.4	84.8
	385	10.0	2.10	0.35	84.1	
	387	7.4	2.15	0.30	84.0	
SHS30/PMMA	386	15.0	2.20	0.32	84.6	83.0
	391	10.0	2.12	0.32	85.1	
	396	5.0	1.23	0.32	79.4	
SHS50/PMMA	394	15.0	2.59	0.24	87.3	85.4
	399	10.0	2.51	0.24	87.8	
	404	5.0	1.48	0.24	80.9	
SHS70/PMMA	398	15.0	2.25	0.47	89.5	89.8
	403	10.0	2.06	0.47	89.1	
	408	5.0	2.12	0.47	90.7	
P4HS/PMMA	396	15.0	2.58	0.39	90.7	90.3
	401	10.0	2.53	0.39	91.5	
	406	5.0	2.03	0.39	88.7	

Table 5.11 the average activation energies for 59/41 SHS/PEMA blend at several aging temperatures

Blends	T_a (K)	T_g- T_a (K)	log t_c (min)	β	$<E_a>$ (kJ mole^{-1})	$<E_a>^{(a)}$ (kJ mole^{-1})
SHS50/PEMA	384	15.0	2.18	0.29	83.4	81.7
	389	10.0	1.91	0.29	82.5	
	394	5.0	1.33	0.29	79.2	

With respect of SHS/polyether (i.e. SHS/PEO and SHS/PVME) blends their average segmental activation energies are listed in Table 5.12 and Table 5.13, respectively. In these types of blends our attention has focused on the effect of copolymer compositions of SHS on activation energy.

Figure 5.48 displays $<E_a>$ of 59/41 SHS/PEO blends with different copolymer compositions. From Figure 5.48, it can clearly be seen that the increase of styrene units in the copolymer leads to decreasing in the average segmental activation energy of SHS/PEO blends in comparison with P4HS/PEO blends as result of effect the repulsion forces between styrene units on the SHS copolymer and PEO units (see sec. 5.3.2.1) that make unassociated PEO segments in SHS blends relax faster than in P4HS blends as we have reported that previously (sec. 5.3.2.1). Since the relaxation time is a linear function of $<E_a>$; thus, the increase in the relaxation rate of the segments in SHS/PEO blends means a weak interaction between those segments compared with P4HS/PEO blends, which also mean that minimum energy is required starting segmental relaxation in SHS/PEO blends compared to P4HS/PEO blends.

Regarding SHS50/PVME blends, their average segmental activation energies are also less than those of P4HS/PVME (Table 5.12) like SHS/PEO. However, the reason of that lack is different, where PVME is miscible with P4HS, so, there is not repulsion forces effect. However, as well known that the interactions between ether oxygen of PVME with styrene units are weaker than those between PVME ether oxygen and hydroxyl groups; consequently, the increase in styrene units in SHS copolymers leads to

increase the interactions of PVME ether oxygen units with styrene units on expanse of their interactions with hydroxyl groups. Thus, SHS/PVME blends relax faster than P4HS/PVME blends that means that $<E_a>$ of SHS/PVME blends are less than $<E_a>$ of P4HS /PVME blends.

Table 5.12 the average activation energies for 59/41 SHS/PEO blends at several aging temperatures

Blends	T_a (K)	$T_g - T_a$ (K)	log t_c (min)	β	$<E_a>$ (kJ mole^{-1})	$<E_a>^{(a)}$ (kJ mole^{-1})
SHS50/PEO	345	15.0	2.28	0.35	76.6	76.3
	350	10.0	2.09	0.35	76.4	
	355	5.0	1.84	0.35	75.8	
SHS70/PEO	357	15.0	2.46	0.33	80.8	80.6
	362	10.0	2.37	0.33	81.3	
	367	5.0	1.97	0.33	79.3	
P4HS/PEO	360	15.0	2.62	0.32	81.8	81.7
	365	10.0	2.54	0.32	82.4	
	370	5.0	2.20	0.32	81.1	

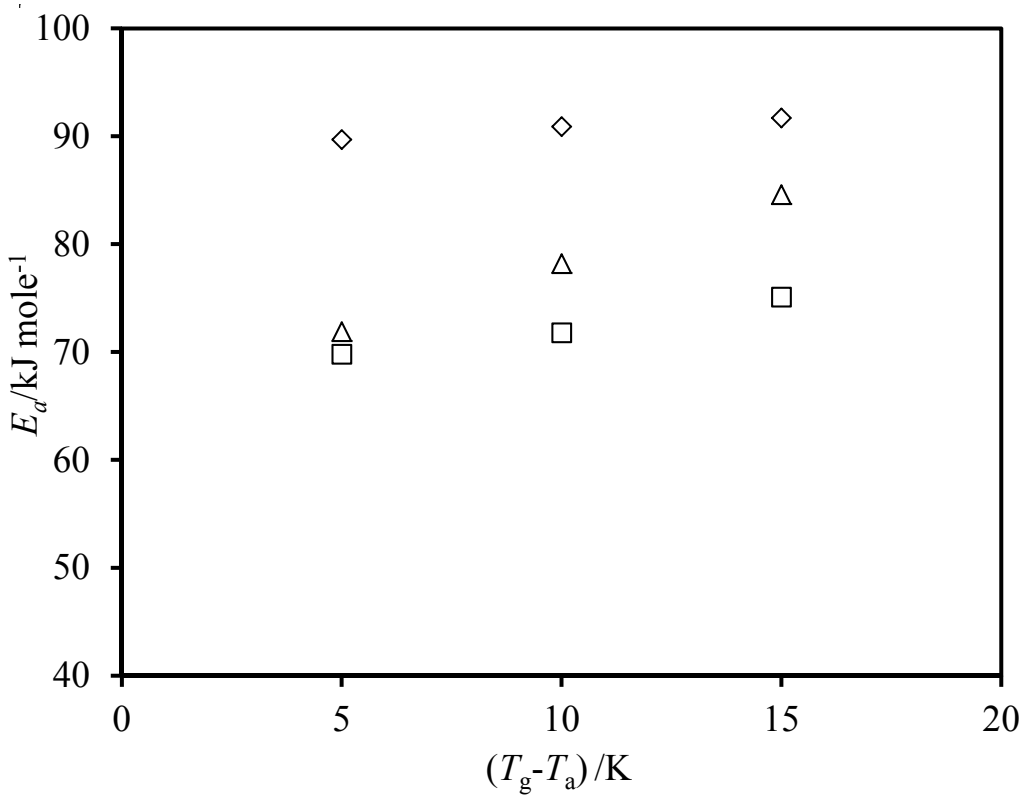

Figure 5.48 Average activation energy as a function of $(T_g - T_a)$ for 59/41 SHS/PEO blends: (◊) 100; (Δ) 70; and (□) 50mole-% HS in the copolymer.

Table 5.13 the average activation energies for SHS/PVME (59/41 mole-%) blends at several aging temperatures

Blends	T_a (K)	T_g - T_a (K)	log t_c (min)	β	$<E_a>$ (kJ mole^{-1})	$<E_a>^{(a)}$ (kJ mole^{-1})
SHS50/PVME	364	15.0	2.95	0.24	83.2	74.8
	369	10.0	1.10	0.24	71.2	
	374	5.0	0.79	0.24	70.0	
P4HS/PVME [ж]	381	15.0	3.30	0.24	89.6	87.8
	386	10.0	2.90	0.24	87.8	
	391	5.0	2.50	0.24	86.0	

[ж] data have been used from ref [2] for comparison

Chapter 6 Conclusion

6.1 Conclusions on FTIR results

Infrared spectroscopy revealed that, in P4HS, the hydroxyl groups participate in the formation of self-associated hydrogen bonds, with some free hydroxyls remaining. However, the dilution of self-association interactions through the introduction of styrene units (i.e. SHS copolymers) does not affect their strength compared to pure P4HS. For pure P4HS, it was noted that, with increasing temperature, the intra-molecular peak shifts towards higher wavenumbers and the intermolecular band disappears when the temperature reaches 100^{o}C or higher. In contrast, the intensity of the free hydroxyl band increases as the temperature increases. Consequently, at higher temperature, the intra-molecular interactions in P4HS are dominant, at the expense of intermolecular bonds.

With respect to SHS copolymers, a temperature increase leads to a large increase in free hydroxyl groups, in comparison with P4HS, as a result of the presence of styrene units, which induce a kind of segregation between SHS chains, increasing the distance between hydroxyl groups. Thus, the hydroxyl groups of any SHS chain are unable to interact with other hydroxyl groups on other chains, causing an increase of free hydroxyl groups at the expense of intermolecular hydrogen bonds.

FTIR spectra of P4HS blends with PEO, PEMA, and P4VPy confirm that this polymer forms self-associating hydrogen bonds which are disrupted by blending with an interacting polymer component. For example, when P4HS is blended with PEO, most of the hydroxyl groups are bonded to the ether oxygens of the PEO units, in intermolecular association.

The FTIR results in this study have confirmed that the hydroxyl groups in P4HS form strong hydrogen bonds with ether or vinyl pyridine groups. The strength and temperature stability of the hydrogen bonds increases as the ether or pyridine content in the blend increases. In P4HS/PEMA, the hydrogen bonding between hydroxyl and carbonyl groups is weaker.

FTIR spectra of SHS/poly (n-alkyl methacrylate) (PMMA or PEMA) blends indicate that the strength of interaction between hydroxyl and carbonyl groups decreases with increasing number of styrene units. Moreover, the FTIR measurements indicate

that the hydroxyl-carbonyl interactions in the blends are weaker than the self-association interactions between SHS chains.

For SHS/polyether (PEO or PVME) blends, FTIR results show that hydrogen bonding is weaker than for P4HS blends and this effect increases with increasing styrene content in the copolymers. Furthermore, it is interesting to mention that although hydrogen bonds in P4HS/PEO blends are stronger than those in P4HS/PVME, SHS copolymers interact more strongly with PVME than PEO. This is likely to be due to repulsion forces between styrene units in SHS copolymers and PEO and their competition with hydrogen bonding interactions, while in SHS/PVME blends, the styrene units interact with the ether oxygen of PVME.

6.2 Conclusions on enthalpy relaxation results

It is extremely difficult to explain the enthalpy relaxation behaviour of highly self-associated systems such as P4HS and SHS copolymers. Values of enthalpy lost on annealing to equilibrium, $\Delta H_\infty(T_a)$, of P4HS and SHS were high. A possible reason is that during aging, the dynamic equilibrium of un-bonded groups is not completely achieved and during that segmental rearrangement, the hydrogen bonds are disrupted, but because of high hydroxyl group density, some of the hydrogen bonds are re-formed.

The experimental results for $\log\langle t_c \rangle$ indicate that P4HS relaxes faster than PS, deep in the glass region (i.e. $T_a = T_g$-15 or less). Supposing that the relaxation rate increases with the increasing of the chains' rigidity, this would explain the faster relaxation rate in the case of a stronger interaction.

As shown by data for the SHS copolymers, the relaxation time is affected by dilution. For example, at 30 mole% HS, although the interactions are stronger compared with PS, the system relaxes more slowly near T_g. The hydroxyl groups may have ordered together to create more favourable domains, rendering the styrene units less able to move. However, SHS50 and SHS70 samples show faster relaxations, as indicated by the $\log\langle t_c \rangle$ values, presumably as a result of the increase in H-bonding concentration.

Aging experiments on PEMA were also carried out at different aging temperature below glass enthalpic transition. $\Delta H_\infty(T_a)$ values coincide with those of PMMA, which suggests that the interaction strengths in these polymers are similar. log t_c values indicate that PEMA relaxes slower than PMMA at T_a far from T_g and faster than PMMA at T_a close to T_g.

It was difficult to carry out enthalpy relaxation measurements on neat PEO, as experiments had to be conducted at low temperature and also due to the high crystallinity of the sample. Aging data could only be collected at T_g-5, as a result of the low amorphous content in PEO and the inability of the DSC instrument to detect a small change in heat capacity deep in the glassy region (i.e. T_g-10 or less).

ΔH_∞ (T_a) and Log$\langle t_c \rangle$ values at T_g-5 for PEO were very low in comparison to values reported for other homopolymers and copolymers. This supports the fact that the increase in the fraction of amorphous chains in semi-crystalline polymer would result in the shift of the relaxation spectrum to longer times [140].

Aging experiments on P4HS blends were also performed at different aging temperatures below the enthalpic glass transition. The average relaxation time $\langle t_c \rangle$ versus T_g -T_a data indicates that the aging process is hindered in the P4HS/PEO and P4HS/PEMA blends when compared with the blends' components, as a result of intermolecular interactions. However, P4HS/P4VPy blends relax faster than P4HS and P4VPy, as result of very strong hydrogen bonds in these blends that suppress the motion of the segments to the minimum motion[156]. Thus, any attempt at molecular motion will lead to considerable destruction of hydrogen bonding interaction, which will cause faster relaxation. Thus, it can be concluded that that the average relaxation time, $\langle t_c \rangle$, increases in the order

P4HS/P4VPy < P4HS < P4HS/PEMA < P4HS/PEO < P4HS/PVME.

This order reflects the fact that the average relaxation time, $\langle t_c \rangle$, increases as the rigidity of the chains in the blend decreases.

The ΔH_∞ (T_a) values of SHS/PMMA or SHS/PEMA blends were found to be less than for P4HS and higher than those of PMMA or PEMA. This observation is

consistent with reports that hydroxyl-carbonyl group interactions are weaker than self-association between OH of P4HS [62].

For SHS/PEO blends, the enthalpy released upon aging is higher than that for SHS copolymers, as expected. $\Delta H_\infty\ (T_a)$ values decrease with increasing styrene content in the copolymer, which causes a restriction of complete intermolecular interactions between hydroxyl groups and ether oxygen. Moreover, the presence of styrene units in SHS/PEO blends leads to an increase in unassociated PEO segments, which causes a faster relaxation of SHS/PEO in comparison with P4HS/PEO.

Enthalpy relaxation experiments were carried out on 33/67 and 59/41 mole% SHS50/PVME blends. $\Delta H_\infty\ (T_a)$ *and* $\log\langle t_c \rangle$ values of the SHS50/PVME blends clearly confirmed that the relaxation time increases as PVME content increases in the blend, as a result of the increase in the intermolecular hydrogen bonding interactions between hydroxyl groups and the ether oxygen of the blend.

6.3 Conclusions on average segmental activation energy results

In this thesis, the average segmental activation energies $\langle E_a \rangle$ were calculated using the equation below. Thus, $<E_a>$ is dependent on both the aging temperature, which is, in turn, dependent on T_g, and the distribution of the relaxation time, which is calculated from CF model.

$$\langle E_a \rangle = RT_a[\langle ln\tau \rangle - lnt_0]$$

The $\langle E_a \rangle$ values of P4HS/PEMA were higher compared to PEMA, as a result of the glass transition temperature effect, which increases with increasing P4HS content. Moreover, the relaxation time distributions of P4HS/PEMA were wider than that of PEMA, which also caused an increase in $\langle E_a \rangle$.

The trend of $\langle E_a \rangle$ for P4HS/PEO blends was similar to that observed for PEMA blends. Moreover, $\langle E_a \rangle$ values were much closer to those of P4HS than PEO, suggesting that P4HS dominates the glass transitions. Thus, the values of $\langle E_a \rangle$ of strongly

interacting blends (i.e. P4HS/PEMA, P4HS/PEO) increase with increase P4HS in the blend composition.

The activation energies of P4HS/P4VPy blends were higher than those of P4HS/polyether and P4HS/PEMA, as a result of their high T_g.

On average segmental activation energies, $\langle E_a \rangle$**,** of SHS/PMMA and SHS/PEMA were intermediate between the activation energies of the neat polymers and the copolymers, which added more support to the idea that hydroxyl-carbonyl group interactions in SHS/poly(n-alkyl methacrylate) samples are weaker than self-association interactions between P4HS units, but stronger than dipole-dipole interactions of PMMA or PEMA neat polymers [62].

The $\langle E_a \rangle$ values of all the SHS/polyether (PEO and PVME) blends were lower than those of the copolymers, as a result of the domains of PEO and PVME, which have low T_g.

6.4 Future work

In the experimental chapter, the synthesis of deuterated P4HS was described. The plan was to use neutron scattering to investigate the dynamic behaviour of H-bonded P4HS-d/PEO blends, particularly changes in PEO dynamics in blends with P4HS. Physical aging studies of P4HS/PEO show that the relaxation in the blends is very slow, depending on blend composition. Based on these results it is expected that motion of the individual components, particularly the low T_g polymer, could be strongly affected. Due to time limitations, these measurements could not be done in this project. Thus, it would be worth undertaking further experiments to investigate the dynamics of this blend.

Appendix A-Convention for Storing Data

A directory was created for each polymer system (P4HS, SHS, P4HS/PEO, P4HS/PEMA… etc) and subdirectories were then created for each aging temperature (422K, 417K, 412K etc.).

Data were saved as deflection files in a directory called 'Defl'. They were converted to heat capacity (Cp) files using the !Cp_Calc program on the Compaq workstation. Once converted the data were saved as Cp data files in a directory called 'Cp'. This file format is necessary for the data processing stage, which is described below.

Appendix B- FTIR spectra at different aging times of P4HS

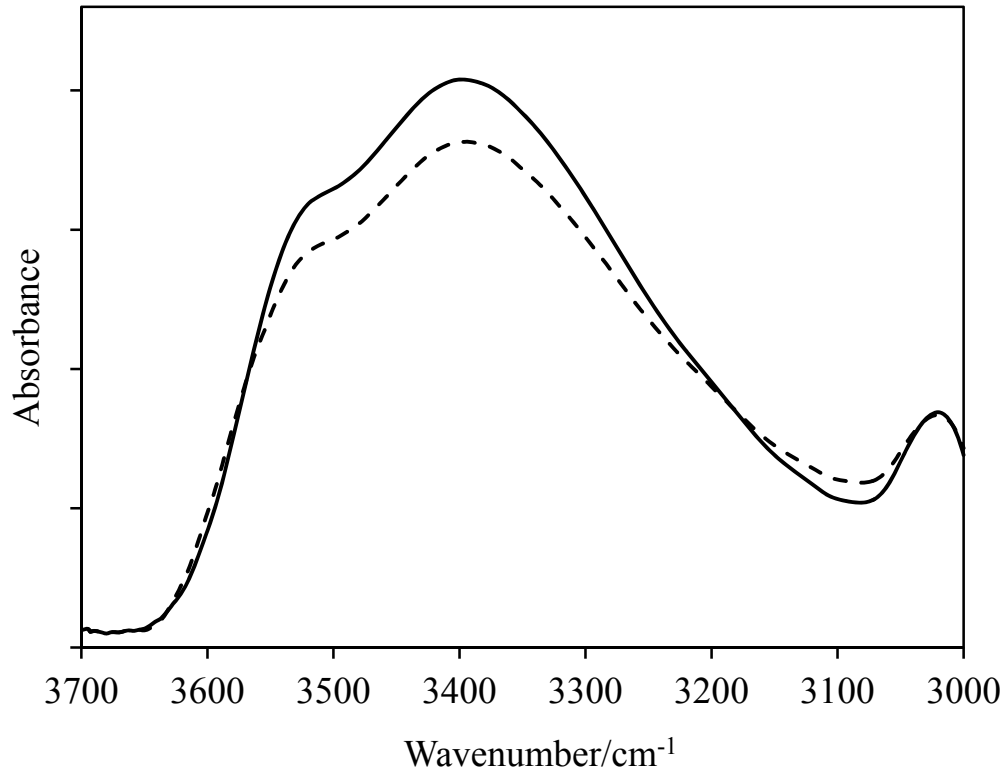

FTIR - Spectra recorded at different aging times at 139°C in the 3700-3000 cm^{-1} region for P4HS: (——) 10min, (– – –) 1000min.

Appendix C- Compositions of copolymers

An NMR spectrum has been run for each sample. An example of an NMR spectrum is given in Figure 3.1:

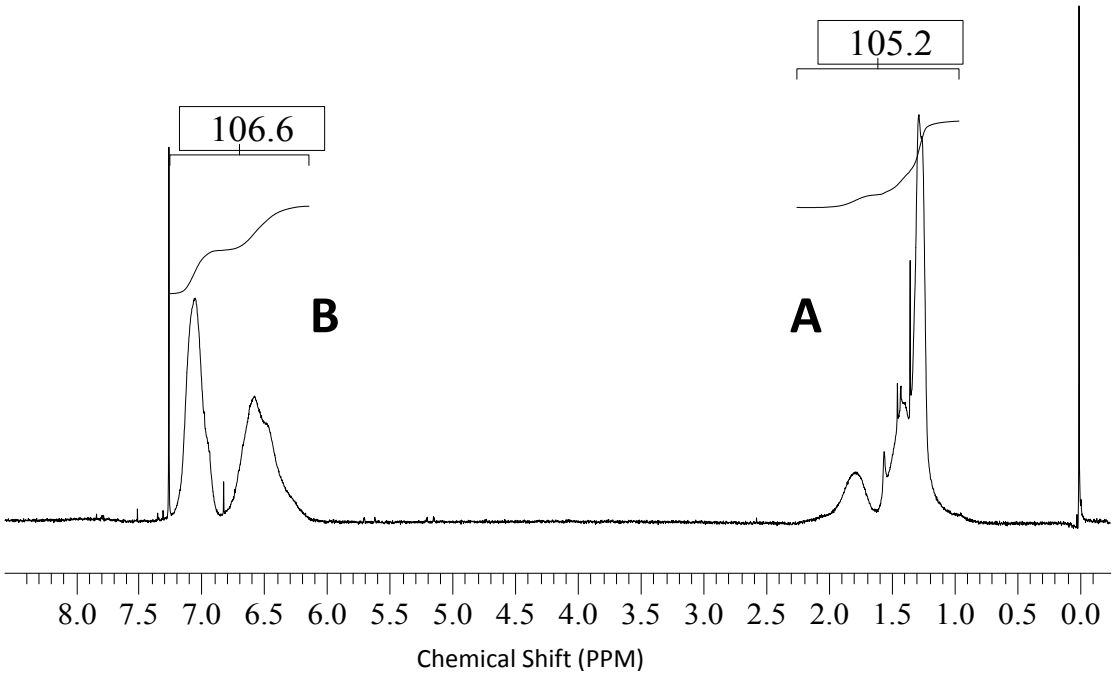

Figure 3.2: Proton NMR spectrum of PStBuS with a composition of 20% mole of tBuS

Where **A** corresponds to **aliphatic protons**: and **B** corresponds to **aromatic protons**:

The following equation was used to determine the copolymer composition from the proton NMR spectra.

$$R = \frac{I(aliphatic)}{I(aromatic)}$$

R is the ratio between integral in the aliphatic region over the aromatic one. After that the mole fraction is found by using this equation:

$$R = \frac{F_1 h_1^{al} + (1 - F_1) h_2^{al}}{F_1 h_1^{ar} + (1 - F_1) h_2^{ar}}$$

Here, h corresponds to the number of protons present in each monomer and contributing to either the aliphatic h^{al} or aromatic h^{ar} of the spectrum.

The reliability of this method depends on the quality of the NMR spectra, for example if solvent or monomers are still in the sample, it changes considerably the results obtained.

If styrene is taken as 1 and tertio-butoxystyrene as 2 in the formula (15), values of h can be found using the Figure 3.3:

$$h_{TBS}^{al} = 12 \qquad h_{S}^{al} = 3 \qquad h_{TBS}^{ar} = 4 \qquad h_{S}^{ar} = 5$$

The formula (15) can be arranged in order to isolate F:

$$F_S = \frac{12 - 4R}{9 + R}$$

By using the values collected on the NMR spectrum of the Figure 3.2, we can determine the experimental copolymer composition:

$$R = \frac{105.2}{106.6} = 0.987$$

$$F_S = \frac{12 - (4 \times 0.987)}{9 + 0.987} = 0.806 \qquad F_{TBS} = 1 - F_s = 1 - 0.806 = 0.194$$

References

1. Cowie, J.M.G., and V. Arrighi, *Physical aging of polymer blends*, in *Encyclopedia of polymer blends*, A.I. Isayev, Editor. 2010, Wiley-VCH. p. 199-232.
2. Cowie, J.M.G., and V. Arrighi, *PHYSICAL AGING*, in *Polymer Physics: From Suspensions to Nanocomposites and Beyond*, L.A. Utracki, and Jamieson, A. M., Editor. 2010: Hoboken, New Jersey. p. 357.
3. Cowie, J.M.G., and R. Ferguson, *Physical aging studies in poly (vinylmethyl ether). I. Enthalpy relaxation as a function of aging temperature.* Macromolecules, 1989. **22**(5): p. 2307-2312.
4. Struik, L.C.E., *Physical aging in amorphous polymers and other materials*. Vol. 106. 1978: Elsevier Amsterdam.
5. McCrum, N.G., B.E. Read, and G. Williams, *Anelastic and dielectric effects in polymeric solids.* 1967.
6. Ferry, J.D., *Viscoelastic properties of polymers*. 1980: John Wiley & Sons Inc.
7. Hutchinson, J.M., *Physical aging of polymers.* Progress in Polymer Science, 1995. **20**(4): p. 703-760.
8. Lagasse, R., *Improved calorimetric procedure for monitoring the approach to thermodynamic equilibrium in glassy polymers.* Journal of Polymer Science: Polymer Physics Edition, 1982. **20**(2): p. 279-295.
9. Cowie, J., I. J. McEwen, and R. McIntyre, *Aging and degradation of polymer blends*, in *Polymer blends handbook*, L.A. Utracki, Editor. 2002, Kluwer Academic Pub: Dordrecht, The Netherlands.
10. Bueche, F., *Rate and Pressure Effects in Polymers and Other Glass-Forming Substances.* The Journal of Chemical Physics, 1962. **36**: p. 2940.
11. Aklonis, J. and A. Kovacs, *A New Nook at the Glass Transition*, in *Contemporary Topics in Polymer Science*, E. M. Shen, Editor. 1979, Plenum: New York. p. 267.
12. Narayanaswamy, O.S., *A model of structural relaxation in glass.* Journal of the American Ceramic Society, 1971. **54**(10): p. 491-498.
13. Kovacs, A.J., J. J. Aklonis, J. M. Hutchinson, and A. R. Ramos, *Isobaric volume and enthalpy recovery of glasses. II. A transparent multiparameter theory.* Journal of Polymer Science: Polymer Physics Edition, 1979. **17**(7): p. 1097-1162.
14. DeBolt, M.A., A. J. Easteal, P. B. Macedo, and C. T. Moynihan, *Analysis of structural relaxation in glass using rate heating data.* Journal of the American Ceramic Society, 1976. **59**(1-2): p. 16-21.
15. Jean, Y. and Q. Deng, *Direct measurement of free-volume hole distributions in polymers by using a positronium probe.* Journal of Polymer Science Part B: Polymer Physics, 1992. **30**(12): p. 1359-1364.
16. Cowie, J.M.G., I. McEwan, I. J. McEwen, and R. A. Pethrick, *Investigation of hydrogen-bonding structure in blends of poly (N-vinylpyrrolidone) with poly (vinyl acetate-co-vinyl alcohol) using positron annihilation.* Macromolecules, 2001. **34**(20): p. 7071-7075.
17. Mcgonigle, E.A., J. M. G. Cowie, V. Arrighi, and R. A. Pethrick, *Enthalpy relaxation and free volume changes in aged styrene copolymers containing a hydrogen bonding co-monomer.* Journal of materials science, 2005. **40**(8): p. 1869-1881.
18. Brunacci, A., Cowie, J. M. G., Ferguson, R., and McEwen, I. J., *Enthalpy relaxation in glassy polystyrenes: 1.* Polymer, 1997. **38**(4): p. 865-870.
19. Cowie, J., S. Harris, and I. McEwen, *Physical ageing in poly (vinyl acetate) 1. Enthalpy relaxation.* Journal of Polymer Science Part B: Polymer Physics, 1997. **35**(7): p. 1107-1116.
20. Hodge, I., J. O'REILLY, and S. CHENG, *COMMENT ON'STRUCTURE AND THERMAL HISTORY DEPENDENT ENTHALPY RELAXATION ATTHE GLASS TRANSITION OF SEMICRYSTALLINE POLYMERS'BY SZD CHENG ET AL. RE SPONSE.* Polymer, 1992. **33**(22): p. 4883-4884.
21. Ribelles, J.L., R. Diaz-Calleja, R. Ferguson, and J. M. G. Cowie, *Glass transition and physical ageing in plasticized poly (vinyl chloride).* Polymer, 1987. **28**(13): p. 2262-2266.

22. Cowie, J. and R. Ferguson, *Physical ageing of poly (methyl methacrylate) from enthalpy relaxation measurements.* Polymer, 1993. **34**(10): p. 2135-2141.
23. Olabisi, O., L. M. Robeson , and M. T. Shaw, *Polymer–polymer miscibility*. 1979, New York: Academic Press.
24. Ten Brinke, G. and F.E. Karasz, *Lower critical solution temperature behavior in polymer blends: compressibility and directional-specific interactions.* Macromolecules, 1984. **17**(4): p. 815-820.
25. Woo, E.M., I.C. Cho, and L.T. Lee, *Experimental verification on upper critical solution temperature (UCST) behavior in blend of poly (2, 6-dimethyl< i> p</i>-phenylene oxide) with poly (4-methyl styrene).* Polymer, 2002. **43**(15): p. 4225-4230.
26. Cong, G., Y. Huang, W. J. MacKnight, and F. E. Karasz, *Upper and lower critical solution temperature behavior in thermoplastic polymer blends.* Macromolecules, 1986. **19**(11): p. 2765-2770.
27. Arrighi, V., and Cowie, J. M. G., *Miscibility*, in *Encyclopedia of Polymer Science and Technology*. 2003, John Wiley & Sons, Inc.
28. Robeson, L.M., *Polymer blends: a comprehensive review*. 2007, Munich: Hanser Verlag.
29. Utracki, L.A., *Polymer blends and alloys.* Hanser, New York, 1989.
30. Arrighi, V., J. M. G. Cowie, S. Fuhrmann, and A. Youssef *Miscibility Criterion in Polymer Blends and its Determination*, in *Encyclopedia of polymer blends*, A.I. Isayev, Editor. 2010, Wiley-VCH. p. 153-197.
31. Cowie, J.M.G., *Polymers: Chemistry & Physics of modern materials*. 1991: CRC PressI Llc.
32. Wang, J., M. Cheung, and Y. Mi, *Miscibility of poly (ethyl oxazoline)/poly (4-vinylphenol) blends as investigated by the high-resolution solid-state< sup> 13</sup> C NMR.* Polymer, 2001. **42**(5): p. 2077-2083.
33. Lodge, T.P. and T.C. McLeish, *Self-concentrations and effective glass transition temperatures in polymer blends.* Macromolecules, 2000. **33**(14): p. 5278-5284.
34. Coleman, M.M., J.F. Graf, and P.C. Painter, *Specific interactions and the miscibility of polymer blends: practical guides for predicting & designing miscible polymer mixtures*. 1991: CRC.
35. He, Y., B. Zhu, and Y. Inoue, *Hydrogen bonds in polymer blends.* Progress in Polymer Science, 2004. **29**(10): p. 1021-1051.
36. Coleman, M.M. and P.C. Painter, *Hydrogen bonded polymer blends.* Progress in polymer science, 1995. **20**(1): p. 1-59.
37. Coleman, M.M.a.P.C.P., *Fourier Transform Infrared Spectroscopy: Probing the Structure of Multicomponent Polymer Blends.* Applied Spectroscopy Reviews, 1984. **20**(3-4): p. 255-346.
38. Ryou, J.H., C.S. Ha, and W.J. Cho, *Miscibility of poly (vinyl methyl ether) and poly (styrene-co-2-vinylnaphthalene) blends by FT-IR spectroscopy and Tg measurements.* Journal of Polymer Science Part A: Polymer Chemistry, 1993. **31**(2): p. 325-333.
39. Garcia, D., *High-temperature fourier transform infrared study of polystyrene/poly (vinyl methyl ether) blends.* Journal of Polymer Science: Polymer Physics Edition, 1984. **22**(10): p. 1773-1779.
40. Coleman, M.M., Y. Xu, P. C. Painter, and J. P. Harrell *Miscibility maps for copolymer-copolymer blends: A comparison of theoretical predictions to experimental studies of poly (styrene-co-vinyl phenol) blends with poly (ethylene-co-methyl acrylate)*. in *Makromolekulare Chemie. Macromolecular Symposia*. 1991: Wiley Online Library.
41. Li, D., and J. Brisson, *Hydrogen bonds in poly (methyl methacrylate)-poly (4-vinyl phenol) blends: 2. Quantification near the glass transition temperature.* Polymer, 1998. **39**(4): p. 801.

42. Li, D., and J. Brisson, *Hydrogen bonds in poly (methyl methacrylate)-poly (4-vinyl phenol) blends: 1. Quantitative analysis using< i> FT</i> ir spectroscopy.* Polymer, 1998. **39**(4): p. 793-800.
43. Serman, C.J., P. C. Painter, and M. M. Coleman, *Studies of the phase behaviour of poly (vinyl phenol)-poly (n-alkyl methacrylate) blends.* Polymer, 1991. **32**(6): p. 1049-1058.
44. Pomposo, J., A. Etxeberria, and M. Cortazar, *Group contribution method for predicting polymer-polymer miscibility: binary blends of poly (p-vinylphenol) and ester-containing polymers.* Macromolecules, 1992. **25**(25): p. 6909-6914.
45. Meaurio, E., E. Zuza, and J-R. Sarasua *Direct measurement of the enthalpy of mixing in miscible blends of poly (DL-lactide) with poly (vinylphenol).* Macromolecules, 2005. **38**(22): p. 9221-9228.
46. Serman, C.J., Y. Xu, P. C. Painter, and M. M. Coleman *Poly (vinyl phenol)--polyether blends.* Polymer, 1991. **32**(3): p. 516-522.
47. Coleman, M.M., A. M. Lichkus, and P. C. Painter, *Thermodynamics of hydrogen bonding in polymer blends. 3. Experimental studies of blends involving poly (4-vinylphenol).* Macromolecules, 1989. **22**(2): p. 586-595.
48. Mirau, P.A., H. Tanaka, and F.A. Bovey, *Two-dimensional NMR studies of polymer mixtures.* Macromolecules, 1988. **21**(10): p. 2929-2933.
49. Mirau, P.A. and F.A. Bovey, *Two-dimensional NMR studies of molecular weight and concentration effects on polymer-polymer interactions.* Macromolecules, 1990. **23**(21): p. 4548-4552.
50. Mirau, P. and J. White, *Solid-state NMR studies of intermolecular interactions in solid polymer blends.* Magnetic Resonance in Chemistry, 1994. **32**: p. 23.
51. Beaucage, G., R. S. Stein, T. Hashimoto, and H. Hasegawa *Tacticity effects on polymer blend miscibility.* Macromolecules, 1991. **24**(11): p. 3443-3448.
52. Gestoso, P. and J. Brisson, *Orientation of uniaxially stretched poly (vinyl phenol)/poly (vinyl methyl ether) blends.* Polymer, 2001. **42**(20): p. 8415-8424.
53. Zhang, S.H., X. Jin, P. C. Painter, and J. Runt *Dynamical Heterogeneity in the Thermodynamically Miscible Polymer Blend of Poly (vinyl ethyl ether) and Styrene-co-p-hydroxystyrene Copolymer.* Macromolecules, 2003. **36**(15): p. 5710-5718.
54. Pedrosa, P., J. A. Pomposo, E. Calahorra, and M. Cortazar *On the glass transition behavior, interaction energies, and hydrogen-bonding strengths of binary poly (p-vinylphenol)/polyether blends.* Macromolecules, 1994. **27**(1): p. 102-109.
55. Gestoso, P. and J. Brisson, *Towards the simulation of poly (vinyl phenol)/poly (vinyl methyl ether) blends by atomistic molecular modelling.* Polymer, 2003. **44**(8): p. 2321-2329.
56. Zhang, S., P.C. Painter, and J. Runt, *Coupling of component segmental relaxations in a polymer blend containing intermolecular hydrogen bonds.* Macromolecules, 2002. **35**(25): p. 9403-9413.
57. Zhang, X., A. Natansohn, and A. Eisenberg, *Intermolecular cross-polarization studies of the miscibility enhancement of PS/PMMA blends through ionic interactions.* Macromolecules, 1990. **23**(2): p. 412-416.
58. Serman, C.J., Y. Xu, P. C. Painter, and M. M. Coleman *On the phase behavior and the limits of miscibility of styrene-co-vinylphenol blends with poly (alkyl methacrylates).* Macromolecules, 1989. **22**(4): p. 2015-2019.
59. Chen, C.T. and H. Morawetz, *Characterization of polymer miscibility by fluorescence techniques. Blends of styrene copolymers carrying hydrogen bond donors with polymethacrylates.* Macromolecules, 1989. **22**(1): p. 159-164.
60. Yilmaz, E., O. Yilmaz, and H. Caner, *Miscibility studies on polystyrene/poly (ethylene oxide) and polybutadiene-< i> graft</i>-polystyrene/poly (ethylene oxide) blends by dilute solution viscometry.* European polymer journal, 1996. **32**(8): p. 927-933.
61. Sotele, J.J., V. Soldi, and A.T. Nunes Pires, *Characterization and morphology of Novolak or poly (vinyl phenol)/poly (ethylene oxide) blends.* Polymer, 1997. **38**(5): p. 1179-1185.

62. Kuo, S.W. and F.C. Chang, *Miscibility and hydrogen bonding in blends of poly (vinylphenol-co-methyl methacrylate) with poly (ethylene oxide).* Macromolecules, 2001. **34**(12): p. 4089-4097.
63. Cai, H., A. Ait-Kadi, and J. Brisson, *Dynamic rheological analysis of a miscible blend showing strong interactions.* Polymer, 2003. **44**(5): p. 1481-1489.
64. Rocco, A.M., C. Bielschowsky, and R.P. Pereira, *Blends of poly (ethylene oxide) and poly (4-vinylphenol-< i> co</i>-2-hydroxyethyl methacrylate): thermal analysis, morphological behaviour and specific interactions.* Polymer, 2003. **44**(2): p. 361-368.
65. Huang, X.D., S.H. Goh, and S.Y. Lee, *Miscibility of C60-end-capped poly (ethylene oxide) with poly (p-vinylphenol).* Macromolecular Chemistry and Physics, 2000. **201**(18): p. 2660-2665.
66. Rinderknecht, S. and J. Brisson, *Orientation of a miscible polymer blend with strong interchain hydrogen bonds: Poly (vinylphenol)-poly (ethylene oxide).* Macromolecules, 1999. **32**(25): p. 8509-8516.
67. Zhang, X., K. Takegoshi, and K. Hikichi, *Composition dependence of the miscibility and phase structure of amorphous/crystalline polymer blends as studied by high-resolution solid-state carbon-13 NMR spectroscopy.* Macromolecules, 1992. **25**(9): p. 2336-2340.
68. Jin, X., S. Zhang, and J. Runt, *Dielectric Studies of Poly (ethylene oxide)/Poly (styrene-co-p-hydroxystyrene) Blends: Influence of Hydrogen Bonding on the Dynamics of Amorphous Blends.* Macromolecules, 2003. **36**(21): p. 8033-8039.
69. Paul, D.R. and C. Bucknall, *Polymer blends*. 2000: Wiley New York.
70. Shonaike, G.O. and G.P. Simon, *Polymer blends and alloys*. Vol. 52. 1999: CRC.
71. Pearce, E.M., T. Kwei, and B. Min, *Polymer compatibilization through hydrogen bonding.* Journal of Macromolecular Science—Chemistry, 1984. **21**(8-9): p. 1181-1216.
72. Coleman, M. and J. Zarian, *Fourier-transform infrared studies of polymer blends. II. Poly (ϵ-caprolactone)–poly (vinyl chloride) system.* Journal of Polymer Science: Polymer Physics Edition, 1979. **17**(5): p. 837-850.
73. Rostami, S.S. and D.J. Walsh, *Miscibility of ethylene-vinyl acetate copolymers with chlorinated polyethylenes. 3. Simulation of the spinodal using the equation of state theory.* Macromolecules, 1984. **17**(3): p. 315-320.
74. Zhang, H., D. E. Bhagwagar, J. F. Graf, P. C. Painter, and M. M. Coleman, *The effect of hydrogen bonding on the phase behaviour of ternary polymer blends.* Polymer, 1994. **35**(25): p. 5379-5397.
75. Wu, C., Y. Wu, and R. Zhang, *Miscibility of phenoxy polymer/poly (methyl acrylate-co-methyl methacrylate) blends.* European polymer journal, 1998. **34**(9): p. 1261-1263.
76. Li, G., J. Cowie, and V. Arrighi, *Miscibility of polymer blends of poly (styrene-co-4-hydroxystyrene) with bisphenol-A polycarbonate.* Journal of applied polymer science, 1999. **74**(3): p. 639-646.
77. Hsu, W.P., *Achieving miscible ternary polymer blends with hydrogen bonding.* Journal of applied polymer science, 2006. **101**(1): p. 643-652.
78. Li, G., S. Mong, S. Jiang, L. Ragupathy, J. M. G. Cowie, F. Ferguson, and V. Arrighi *Miscibility of blends of bisphenol-A-polycarbonate and poly (styrene-co-acrylonitrile-co-hydroxystyrene) terpolymer.* Journal of applied polymer science, 2007. **106**(2): p. 944-949.
79. Bada, R., M. A. Jubindo, M. R. De La Fuente, and I. Katime *Low frequency dielectric relaxation study in PMMA/PS blends.* Materials chemistry and physics, 1987. **18**(4): p. 359-373.
80. Lee, J.K., and C. D. Han, *Evolution of polymer blend morphology during compounding in an internal mixer.* Polymer, 1999. **40**(23): p. 6277-6296.
81. Xanthos, M. and S. Dagli, *Compatibilization of polymer blends by reactive processing.* Polymer Engineering & Science, 1991. **31**(13): p. 929-935.
82. Atkins, P.W., *Physical Chemistry*. 3rd Ed ed. 1986: Oxford University Press.

83. Pimentel, G.C., and A. L. McClellan *The Hydrogen bond*. 1960, San Francisco and London: W. H. Freeman& Co.
84. Shamblin, S.L., L.S. Taylor, and G. Zografi, *Mixing behavior of colyophilized binary systems.* Journal of pharmaceutical sciences, 1998. **87**(6): p. 694-701.
85. Fuller, C.S., R. J. MacRae, M. Walther, and R. E. Cameron *Interactions in poly (ethylene oxide)–hydroxypropyl methylcellulose blends.* Polymer, 2001. **42**(23): p. 9583-9592.
86. Joesten, M.D., *Hydrogen bonding and proton transfer.* Journal of Chemical Education, 1982. **59**(5): p. 362.
87. Zhang, X., K. Takegoshi, and K. Hikichi, *High-resolution solid-state< sup> 13</sup> C nuclear magnetic resonance study on poly (vinyl alcohol)/poly (vinylpyrrolidone) blends.* Polymer, 1992. **33**(4): p. 712-717.
88. Coleman, M.M., E. J. Moskala, P. C. Painter, D. J. Walsh, and S. Rostami *A Fourier transform infra-red study of the phase behaviour of polymer blends. Ethylene-vinyl acetate copolymer blends with poly (vinyl chloride) and chlorinated polyethylene.* Polymer, 1983. **24**(11): p. 1410-1414.
89. Murray, T.J. and S.C. Zimmerman, *New triply hydrogen bonded complexes with highly variable stabilities.* Journal of the American Chemical Society, 1992. **114**(10): p. 4010-4011.
90. Li, D. and J. Brisson, *DMTA and FTIR Investigation of the Phase Behavior of Poly (methyl methacrylate)-Poly (4-vinylphenol) Blends.* Macromolecules, 1996. **29**(3): p. 868-874.
91. Zhang, S.H., X. Jin, P. C. Painter, and J. Runt *Composition-dependent dynamics in miscible polymer blends: influence of intermolecular hydrogen bonding.* Polymer, 2004. **45**(11): p. 3933-3942.
92. Wang, J., M. K. Cheung, and Y. Mi, *Miscibility in blends of poly (4-vinylpyridine)/poly (4-vinylphenol) as studied by< sup> 13</sup> C solid-state NMR.* Polymer, 2001. **42**(7): p. 3087-3093.
93. Tang, M. and W.-R. Liau, *Solvent effect on the miscibility of poly (4-hydroxystyrene)–poly (ethylene oxide) blends.* European polymer journal, 2000. **36**(12): p. 2597-2603.
94. Lim, K.G., M. R. Choi, H. B. Kim, J. H. Park, and T. W. Lee *High-efficiency polymer photovoltaic cells using a solution-processable insulating interfacial nanolayer: the role of the insulating nanolayer.* Journal of Materials Chemistry, 2012. **22**(48): p. 25148-25153.
95. Yoshida, H., K. Nakamura, and Y. Kobayashi, *Differential scanning calorimetric study of enthalpy relaxation in polystyrene, poly (4-hydroxystyrene), and their copolymers.* Polymer Journal, 1982. **14**(11): p. 855-859.
96. Hubbe, M.A., H. Nanko, and M.R. McNeal, *Retention aid polymer interactions with cellulosic surfaces and suspensions: a review.* BioResources, 2009. **4**(2): p. 850-906.
97. Schmitt, R.L., *Polyethylene oxide*, in *Handbook of pharmaceutical excipients*, R.C. Rowe, Sheskey, P. J., and Waller, P. J, Editor. 2003, Pharmaceutical Press and American Pharmaceutical Association: London UK. p. 460-461.
98. Vernel, J., R. W. Rychwalski, V. Pelíšek, P. Sáha, M. Schmidt, and F. H. J. Maurer *Physical aging in poly (ethylene oxide)/< i> atactic</i>-poly (methyl methacrylate) blends.* Thermochimica acta, 1999. **342**(1): p. 115-137.
99. Zhao, Y., B. Jasse, and L. Monnerie, *Orientation and relaxation in uniaxially stretched poly (methyl methacrylate)-poly (ethylene oxide) blends.* Polymer, 1989. **30**(9): p. 1643-1650.
100. Jin, X., S. Zhang, and J. Runt, *Broadband dielectric investigation of amorphous poly (methyl methacrylate)/poly (ethylene oxide) blends.* Macromolecules, 2004. **37**(21): p. 8110-8115.
101. Slobodian, P., P. Říha, R. W. Rychwalski, I. Emri, P. Sáha, and J. Kubát *The relation between relaxed enthalpy and volume during physical aging of amorphous polymers and selenium.* European polymer journal, 2006. **42**(10): p. 2824-2837.

102. Jin, X., S. Zhang, and J. Runt, *Observation of a fast dielectric relaxation in semi-crystalline poly (ethylene oxide).* Polymer, 2002. **43**(23): p. 6247-6254.
103. Kiss, D., K. Süvegh, T. Marek, L. Dévényi, C. Novák, and R. Zelkó *Tracking the physical aging of poly (ethylene oxide): A technical note.* AAPS PharmSciTech, 2006. **7**(4): p. 95-98.
104. Beiner, M., F. Garwe, K. Schröter, and E. Donth *Ageing effects on dynamic shear moduli at the onset of the dynamic glass transition in two poly (alkyl methacrylate) s.* Polymer, 1994. **35**(19): p. 4127-4132.
105. Grooten, R. and G. Ten Brinke, *Enthalpy relaxations in blends of polystyrene and poly (2-vinylpyridine).* Macromolecules, 1989. **22**(4): p. 1761-1766.
106. Cowie, J.M.G., and R. Ferguson, *Physical aging studies in polymer blends. 2. Enthalpy relaxation as a function of aging temperature in a poly (vinyl methyl ether)/polystyrene blend.* Macromolecules, 1989. **22**(5): p. 2312-2317.
107. Bosma, M., G. Ten Brinke, and T.S. Ellis, *Polymer-polymer miscibility and enthalpy relaxations.* Macromolecules, 1988. **21**(5): p. 1465-1470.
108. Ten Brinke, G. and R. Grooten, *Enthalpy relaxations in polymer blends and block copolymers: Influence of domain size.* Colloid and Polymer Science, 1989. **267**(11): p. 992-1001.
109. Cowie, J.M.G., V. Arrighi, and E. A. McGonigle *Enthalpy Relaxation in Poly (4-hydroxystyrene)/Poly (methyl methacrylate) Blends.* Macromolecular Chemistry and Physics, 2005. **206**(7): p. 767-776.
110. Arrighi, V., J. M. G. Cowie, R. Ferguson, I. J. McEwen, E. A. McGonigle, R. A. Pethrick, and E. Princi *Physical ageing in poly (4-hydroxy styrene)/poly (vinyl methyl ether) blends.* Polymer international, 2006. **55**(7): p. 749-756.
111. Pomposo, J.A., I. Eguiazabal, E. Calahorra, and M. Cortazar *Glass transition behaviour and interactions in blends.* Polymer, 1993. **34**(1): p. 95-102.
112. Zhang, S., X. Jin, P. C. Painter, and J. Runt *Broad-band dielectric study on poly (4-vinylphenol)/poly (ethyl methacrylate) blends.* Macromolecules, 2002. **35**(9): p. 3636-3646.
113. Moskala, E., D. Varnell, and M. Coleman, *Concerning the miscibility of poly (vinyl phenol) blends--FTi. r. study.* Polymer, 1985. **26**(2): p. 228-234.
114. QIN, C., T. Pires, and L. Belfiore, *Morphological and physicochemical interactions in semicrystalline polymer-polymer blends.* Polymer communications, 1990. **31**(5): p. 177-182.
115. de Meftahi, M.V. and J.M.J. Fréchet, *Study of the compatibility of blends of polymers and copolymers containing styrene, 4-hydroxystyrene and 4-vinylpyridine.* Polymer, 1988. **29**(3): p. 477-482.
116. Zhou, X., S. H. Goh, S. Y. Lee, and K. L. Tan *X-ray photoelectron spectroscopic studies of interactions between poly (p-vinylphenol) and poly (vinylpyridine) s.* Applied surface science, 1997. **119**(1): p. 60-66.
117. Wang, L., E.M. Pearce, and T. Kwei, *Glass transitions in hydrogen-bonded polymer complexes.* Journal of Polymer Science Part B: Polymer Physics, 1991. **29**(5): p. 619-626.
118. Nasrullah, J.M., S. Raja, K. Vijayakumaran, and R. Dhamodharan *A practical route for the preparation of poly (4-hydroxystyrene), a useful photoresist material.* Journal of Polymer Science Part A: Polymer Chemistry, 2000. **38**(3): p. 453-461.
119. Deokar, S., R. S. Ghadage, C. R. Rajan, and S. Ponrathnam *Facile synthesis of poly (4-hydroxy styrene) from polystyrene.* Journal of applied polymer science, 2004. **91**(5): p. 3192-3201.
120. Richardson, M.J. and N. Savill, *Derivation of accurate glass transition temperatures by differential scanning calorimetry.* Polymer, 1975. **16**(10): p. 753-757.

121. Xu, Y., P.C. Painter, and M.M. Coleman, *Miscibility windows for poly (styrene-co-vinyl phenol) blends with poly (alkyl methacrylate) s: Further comparisons of theoretical predictions to FTIR experimental data.* Polymer, 1991. **32**(17): p. 3103-3118.
122. Daugaard, A.E. and S. Hvilsted, *The Influence of Pendant Carboxylic Acid Loading on Surfaces of Statistical Poly [(4-hydroxystyrene)-co-styrene] s.* Macromolecular Rapid Communications, 2008. **29**(12-13): p. 1119-1125.
123. Tanaka, S., H. Nishida, and T. Endo, *Miscibility of Polynorbornene/Poly (styrene-co-hydroxystyrene) Binary Blend Based on Hydrogen-Bonding Interaction.* Macromolecular Chemistry and Physics, 2009. **210**(15): p. 1235-1240.
124. Willenberg, B., *Proton-deuteron exchange in polystyrene–A new simple method for rapid deuteration of polymers with aromatic substituents.* Die Makromolekulare Chemie, 1976. **177**(12): p. 3625-3628.
125. Kuo, S.W. and F.C. Chang, *Effect of inert diluent segment on the miscibility behavior of poly (vinylphenol) with poly (acetoxystyrene) blends.* Journal of Polymer Science Part B: Polymer Physics, 2002. **40**(15): p. 1661-1672.
126. Dobrosielska, K., Wakao, S., Takano, A., and Matsushita, Y., *Nanophase-separated structures of AB block copolymer/C homopolymer blends with complementary hydrogen-bonding interactions.* Macromolecules, 2008. **41**(20): p. 7695-7698.
127. Dobrosielska, K., Wakao, S., Suzuki, J., Noda, K., Takano, A., and Matsushita, Y., *Effect of homopolymer molecular weight on nanophase-separated structures of AB block copolymer/C homopolymer blends with hydrogen-bonding interactions.* Macromolecules, 2009. **42**(18): p. 7098-7102.
128. Devlin, B.G., *Investigations of Surface Enrichment in Mixed Polymer Films, PhD. Thesis,* . November 1991, Heriot-Watt University.
129. Garton, A., *Infrared Spectroscopy of Polymer Blends, Composites and Surfaces*. 1992, Munich: Hanser Publishers.
130. Paul, D.R., and C. B. Bucknall, *Polymer blends: formulation and performance*. 2000, Wiley: New York.
131. Savitzky, A. and M.J. Golay, *Smoothing and differentiation of data by simplified least squares procedures.* Analytical chemistry, 1964. **36**(8): p. 1627-1639.
132. Steinier, J., Y. Termonia, and J. Deltour, *Smoothing and differentiation of data by simplified least square procedure.* Analytical Chemistry, 1972. **44**(11): p. 1906-1909.
133. De Levie, R., *Advanced ExcelR for Excientific Data Analysis*. 2004: Oxford University Press.
134. Brunacci, A., *Physical Aging in Polymers, Copolymers and Blends of Polystyrene Derivatives, PhD. Thesis,*. January 1995, Heriot-Watt University.
135. Agrawal, A., *Effect of temperature and molecular weight on enthalpy relaxation in polystyrene.* Journal of Polymer Science Part B: Polymer Physics, 1989. **27**(7): p. 1449-1461.
136. Moskala, E.J., S. E. Howe, P. C. Painter, and M. M. Coleman *On the role of intermolecular hydrogen bonding in miscible polymer blends.* Macromolecules, 1984. **17**(9): p. 1671-1678.
137. Yoshida, H. and Y. Kobayashi, *Sen-i Gakkaishi, 37.* T-458, 1981.
138. Lindsey, C. and G. Patterson, *Detailed comparison of the Williams–Watts and Cole–Davidson functions.* The Journal of Chemical Physics, 1980. **73**: p. 3348.
139. Schroeder, M., C. Roland, and T. Kwei, *Segmental relaxation of poly (styrene-co-vinylphenol).* Macromolecules, 1999. **32**(19): p. 6249-6253.
140. Velikov, V. and H. Marand, *Studies of the enthalpy relaxation and the "multiple melting" behavior of semicrystalline poly (arylene ether ether ketone)(PEEk).* Journal of Thermal Analysis and Calorimetry, 1997. **49**(1): p. 375-383.

141. Pedrosa, P., J. A. Pomposo, E. Calahorra, and M. Cortazar *Crystallization of poly (ethylene oxide) in binary blends containing poly (< i> p</i>-vinyl phenol).* Polymer, 1995. **36**(20): p. 3889-3897.
142. Yang, Z. and C.D. Han, *Rheology of miscible polymer blends with hydrogen bonding.* Macromolecules, 2008. **41**(6): p. 2104-2118.
143. Dai, J., S. H. Goh, S. Y. Lee, and K. S. Siow *Interpolymer Complexation between Poly (p-vinylphenol) and Pyridine-Containing Polymers.* Polymer journal, 1994. **26**(8): p. 905-911.
144. Cui, L., J. T. Yeh, K. Wang, and Q. Fu *Miscibility and isothermal crystallization behavior of polyamide 6/poly (vinyl alcohol) blend.* Journal of Polymer Science Part B: Polymer Physics, 2008. **46**(13): p. 1360-1368.
145. Lee, H.F., S. W. Kuo, C. F. Huang, J. S. Lu, S. C. Chan, C. F. Wang, and F. C. Chang *Hydrogen-bonding interactions mediate the phase behavior of an AB/C block copolymer/homopolymer blend comprising poly (methyl methacrylate-b-vinylpyrrolidone) and poly (vinylphenol).* Macromolecules, 2006. **39**(16): p. 5458-5465.
146. Painter, P.C., S. L. Shenoy, D. E. Bhagwagar, J. Fishburn, and M. M. Coleman *Effect of hydrogen bonding on the melting point depression in polymer blends where one component crystallizes.* Macromolecules, 1991. **24**(20): p. 5623-5629.
147. Zhang, X., K. Takegoshi, and K. Hikichi, *Poly (vinylphenol)/poly (methyl acrylate) and poly (vinylphenol)/poly (methyl methacrylate) blends: hydrogen bonding, miscibility, and blending effects on molecular motions as studied by carbon-13 CP/MAS NMR.* Macromolecules, 1991. **24**(21): p. 5756-5762.
148. Bhagwagar, D.E., P.C. Painter, and M.M. Coleman, *Mapping the phase diagram of polymer-polymer blends using infrared spectroscopy. 2. The poly (4-vinylphenol)-EVA [45] system.* Macromolecules, 1992. **25**(4): p. 1361-1365.
149. Cai, H. and J. Brisson, *Quantitative analysis of hydrogen bonding in poly (4-vinylphenol) blends using near infrared spectroscopy.* Journal of near infrared spectroscopy, 2003. **11**(3): p. 183-192.
150. Brisson, J., *Blends, hydrogen bonds, and orientation: Understanding the role of interactions.* Polymer Engineering & Science, 2004. **44**(2): p. 241-251.
151. Le Menestrel, C., D. E. Bhagwagar, P. C. Painter, M. M. Coleman, and J. F. Graf *Hydrogen bonding in ternary polymer blend systems: determination of association parameters.* Macromolecules, 1992. **25**(26): p. 7101-7106.
152. Kwei, T.K., *The effect of hydrogen bonding on the glass transition temperatures of polymer mixtures.* J. Polym. Sci., Polym. Lett. Ed, 1984. **22**: p. 307-313.
153. Painter, P.C., J.F. Graf, and M.M. Coleman, *Effect of hydrogen bonding on the enthalpy of mixing and the composition dependence of the glass transition temperature in polymer blends.* Macromolecules, 1991. **24**(20): p. 5630-5638.
154. Hsu, W.P., *Reexamination of the miscibility of stereoregular poly (methyl methacrylate) with poly (vinyl phenol).* Journal of applied polymer science, 2002. **83**(7): p. 1425-1431.
155. Kuo, S.W. and F.C. Chang, *Studies of miscibility behavior and hydrogen bonding in blends of poly (vinylphenol) and poly (vinylpyrrolidone).* Macromolecules, 2001. **34**(15): p. 5224-5228.
156. Masser, K.A. and J. Runt, *Dynamics of Polymer Blends of a Strongly Interassociating Homopolymer with Poly (vinyl methyl ether) and Poly (2-vinylpyridine).* Macromolecules, 2010. **43**(15): p. 6414-6421.
157. Zhang, S., P.C. Painter, and J. Runt, *Suppression of the dielectric secondary relaxation of poly (2-vinylpyridine) by strong intermolecular hydrogen bonding.* Macromolecules, 2004. **37**(7): p. 2636-2642.
158. Pathak, J.A., R. H. Colby, G. Floudas, and R. Jérôme *Dynamics in miscible blends of polystyrene and poly (vinyl methyl ether).* Macromolecules, 1999. **32**(8): p. 2553-2561.

159. Xiang, M., M. Jiang, Y. Zhang, and C. Wu *Intermacromolecular complexation due to specific interactions. 5. The hydrogen-bonding complex of poly (styrene-co-4-vinylphenol) and poly (ethyl methacrylate).* Macromolecules, 1997. **30**(18): p. 5339-5344.
160. Hsu, W.P., R. J. Li, A. S. Myerson, and T. K. Kwei *Sorption and diffusion of water vapour in hydrogen-bonded polymer blends.* Polymer, 1993. **34**(3): p. 597-603.
161. Radmard, B. and M. Dadmun, *The accessibility of functional groups to intermolecular hydrogen bonding in polymer blends containing a liquid crystalline polymer.* Polymer, 2001. **42**(4): p. 1591-1600.
162. Cassu, S.N. and M.I. Felisberti, *Poly (vinyl alcohol) and poly (vinyl pyrrolidone) blends: miscibility, microheterogeneity and free volume change.* Polymer, 1997. **38**(15): p. 3907-3911.
163. Ting, S.P., B. J. Bulkin, E. M. Pearce, and T. K. Kwei *Compatibility studies of styrene and hydroxyl containing styrene copolymers with poly (ethylene oxide).* Journal of Polymer Science: Polymer Chemistry Edition, 1981. **19**(6): p. 1451-1473.
164. Takeno, H., S. Koizumi, H. Hasegawa, and T. Hashimoto *Small-angle neutron scattering study of anomalous mixing behaviors in deuterated polystyrene/poly (vinyl methyl ether) mixtures near the glass transition temperature.* Macromolecules, 1996. **29**(7): p. 2440-2448.
165. Cendoya, I., A. Alegria, J. M. Alberdi, J. Colmenero, H. Grimm, D. Richter, and B. Frick *Effect of blending on the PVME dynamics. A dielectric, NMR, and QENS investigation.* Macromolecules, 1999. **32**(12): p. 4065-4078.